5-503.31. 1768

DEVELOPMENT AND VERIFICATION OF VAM3DF: A NUMERICAL CODE FOR MODELING FLOW AND TRANSPORT IN GROUNDWATER

Documentation and User's Guide

Prepared for:

Fluor Daniel Fernald
7400 Willey Road
Hamilton, OH 45013-9402

July 1998

HydroGeoLogic, Inc.
1155 Herndon Parkway
Suite 900
Herndon, Virginia 20170
(703) 478-5186

0000001

DEVELOPMENT AND VERIFICATION OF VAM3DF: A NUMERICAL CODE FOR MODELING FLOW AND TRANSPORT IN GROUNDWATER

Documentation and User's Guide

Prepared for:

Fluor Daniel Fernald
7400 Willey Road
Hamilton, OH 45013-9402

Prepared by:

HydroGeoLogic, Inc.
Herndon, VA 20170

July 1998

TABLE OF CONTENTS

		Page
1.0	INTRODUCTION	1-1
1.1	BACKGROUND	1-1
1.2	OBJECTIVES	1-2
2.0	FORMULATION	2-1
2.1	BACKGROUND - PROCESS AND GEOMETRY	2-1
2.2	GOVERNING FLOW EQUATIONS	2-1
2.2.1	Treatment of Hysteresis and Anisotropy	2-4
2.2.2	Treatment of Variable Unsaturated Anisotropy	2-7
2.2.3	Pseudo-Soil Functions for Predicting Water-Table Levels	2-9
2.2.4	Atmospheric Boundary Conditions	2-12
2.3	GOVERNING TRANSPORT EQUATIONS	2-12
2.3.1	Equilibrium Mass Transfer Between the Aqueous and Solid Phases	2-13
2.3.2	Kinetic Mass Transfer	2-14
2.3.3	Hydrodynamic Dispersion Coefficients	2-14
2.3.4	Boundary Conditions	2-15
2.4	ASSUMPTIONS	2-16
2.5	LIMITATIONS	2-16
3.0	MULTI-DISPERSIVITY MODULE	3-1
3.1	PURPOSE	3-1
3.2	GOVERNING EQUATIONS	3-1
3.2.1	Generalized Dispersion Coefficients	3-1
3.2.2	Two-Parameter Dispersion Coefficients	3-1
3.2.3	Multi-Parameter Dispersion Coefficients	3-2
3.3	NUMERICAL TREATMENT	3-3
3.4	VERIFICATION	3-3
3.4.1	Case 1 - 1-D Horizontal Flow	3-3
3.4.2	Case 2 - 1-D Vertical Flow	3-6
3.4.3	Case 3 - 3-D Flow with Partially Penetrating Wells	3-10
3.5	PARAMETER ESTIMATION GUIDELINES	3-15
3.6	DISCUSSION	3-16
4.0	KINETIC CONTAMINANT MASS TRANSFER BETWEEN LIQUID AND SOLID PHASES	4-1
4.1	PURPOSE	4-1
4.2	GOVERNING EQUATIONS FOR KINETIC MASS TRANSFER AMONG PHASES	4-1
4.3	NUMERICAL TREATMENT	4-4
4.4	VERIFICATION PROBLEMS	4-6
4.4.1	Verification Problem 1. Verification of Mass Transfer with Dissolution and Precipitation	4-6

TABLE OF CONTENTS

Page

4.4.2 Verification Problem 2. Verification of Mass Transfer with Chemisorption 4-8
4.5 BEHAVIOR OF KINETIC MASS TRANSFER BETWEEN LIQUID AND SOLID PHASE 4-8
4.6 PARAMETER ESTIMATION GUIDELINES 4-20

5.0 TVD SOLUTION SCHEME 5-1
5.1 PURPOSE 5-1
5.2 NUMERICAL TREATMENT 5-1
5.2.1 Implementation of Boundary Conditions 5-3
5.2.2 Solution Procedures 5-3
5.3 VERIFICATION 5-4
5.3.1 Verification Case 1 - One-Dimensional, Single-Species Transport . 5-4
5.3.2 Verification Case 2 - Two-Dimensional Transport from a Point Source in a Steady Uniform Flow Field 5-4
5.4 SUMMARY 5-5

6.0 GENERAL MODEL APPLICATION PROCESS 6-1
6.1 MODEL BOUNDARY AND GRID 6-1
6.1.1 Specification of Mesh Parameters For Rectangular Grid 6-1
6.1.2 Specification of Mesh Parameters For Curvilinear Grid 6-1
6.1.3 Initial and Boundary Condition Specifications 6-4
6.2 PARAMETER ESTIMATION 6-8
6.3 INPUT FILE DEVELOPMENT 6-8
6.3.1 Required Input Data 6-10
6.4 CALIBRATION 6-13
6.5 MODEL OUTPUT 6-14
6.5.1 Output Control 6-14

7.0 SITE SIMULATION 7-1
7.1 BACKGROUND INFORMATION 7-1
7.2 MODEL SCENARIOS SCENARIOS 7-1
7.3 VERIFICATION BASED ON THE EXISTING MODEL 7-7
7.4 SENSITIVITY ANALYSIS BASED ON THE NEW KINETIC MODULES 7-29
7.4.1 Fully Reversible Sorption 7-29
7.4.2 Simulations with Chemisorption 7-34

8.0 SUMMARY, CONCLUSIONS, AND RECOMMENDATIONS 8-1
8.1 SUMMARY AND CONCLUSIONS 8-1

9.0 REFERENCES 9-1

Appendix A User's Guide

LIST OF TABLES

		Page
Table 1.1	The Advantages of VAM3DF over MODFLOW-SURFACT, MT3D96 and MODFLOWT	1-3
Table 3.1	Parameters Used	3-14
Table 4.1	Summary of Study Cases for Behavior of Kinetic Mass Transfer	4-21
Table 5.1	Model Parameters for Simulation of Two-Dimensional Transport From a Point Source in a Steady, Uniform Flow Field	5-12
Table 7.1	Pumping stress and boundary conditions used in the flow simulations	7-5
Table 7.2	Parameters used in the transport simulations	7-5
Table 7.3	Estimate of the computer run time for the 10-year scenario	7-7
Table 7.4	Comparison between VAM3DF GMA Model Simulation and Water Levels	7-22
Table 7.5	Values of Sorption Parameters used for the Simulations with the Kinetic Module	7-34
Table 7.6	Values of Sorption Parameters Used for the Simulations with the Kinetic Module	7-56

LIST OF FIGURES

		Page
Figure 1.1	Solid Phase Contamination Versus Solute Concentration	1-4
Figure 2.1	Example of hysteretic $S_w(\psi)$ relation showing the boundary wetting and drying curves.	2-6
Figure 2.2	Typical scanning curves produced by the hysteresis model in VAM3DF. Curve (1) denotes primary wetting scanning curve, curve (2) denotes secondary drying scanning curve.	2-8
Figure 2.3	Example of anisotropic $k_{rw}(\psi)$ relation as modeled by VAM3DF.	2-10
Figure 3.1	Definition Sketch, Verification Case 1.	3-4
Figure 3.2	Concentration Profile Along the x-direction, at 2,000 days, Verification Case 1	3-7
Figure 3.3	Concentration Profile Along the y- and z-directions at 2,000 Days, Verification Case 1.	3-8
Figure 3.4	Definition Sketch, Verification Case 2.	3-9
Figure 3.5	Concentration Profile Along the z-direction, at 2,000 Days, Verification Case 2	3-11
Figure 3.6	Concentration Profiles Along the x- and y-directions, at 2,000 Days, Verification Case 2.	3-12
Figure 3.7	Definition Sketch, Verification Case 3.	3-13
Figure 3.8	Concentration Distribution on a Vertical Plane Traversing the Extraction Well and the Midpoint of the Source, at 5,000 Days.	3-17
Figure 4.1	C_s vs Time for Verification Problem	4-7
Figure 4.2	C_s vs Time Verification Problem 2 Mass Transfer with (Chemisorption).	4-9
Figure 4.3	Problem Setup and Domain Geometry.	4-11
Figure 4.4	C_s vs C_w for the First Study Case	4-12
Figure 4.5	C_s vs C_w for the Second Study Case. (Linear adsorption desorption at high groundwater velocity).	4-13
Figure 4.6	C_s vs C_w for the Third Study Case. (Non-linear adsorption/desorption at low groundwater velocity).	4-14
Figure 4.7	C_s vs C_w for the Fourth Study Case (Non-linear adsorption/desorption high groundwater velocity, n = 0.5)	4-15
Figure 4.8	C_s vs C_w for the Fifth Study Case (Non-linear adsorption/desorption at low groundwater velocity, n = 0.2)	4-16
Figure 4.9	C_s vs C_w for the Sixth Study Case (Non-linear adsorption/desorption with chemisorption at high groundwater velocity, n = 0.5)	4-17
Figure 4.10	C_s vs C_w for the Seventh Study Case. (Non-linear adsorption/desorption with chemisorption at high groundwater velocity, n = 0.5, contamination period = 4,000 days).	4-18
Figure 4.11	C_s vs C_w for the Eighth Study Case. (Non-linear adsorption/desorption with chemisorption at high groundwater velocity, n = 0.2, contamination period = 4,000 days).	4-19
Figure 4.12	C_s vs C_w for the Ninth Study Case. (Non-linear adsorption/desorption with precipitation and dissolution).	4-22

000006

LIST OF FIGURES

		Page
Figure 4.13	C_s vs C_w for the Tenth Study Case. (Non- linear adsorption/desorption with chemisorption).	4-23
Figure 4.14	C_s vs C_w for the Eleventh Study Case. (Non-linear adsorption/desorption with precipitation and dissolution).	4-24
Figure 5.1	One-Dimensional Transport of a Conservative Species.	5-6
Figure 5.2	Finite Difference Results for α_L=2 m.	5-7
Figure 5.3	Finite Element Results for α_L=2 m.	5-8
Figure 5.4	Finite Difference Results for α_L=0.	5-9
Figure 5.5	Finite Element Results for α_L=0.	5-10
Figure 5.6	Two-Dimensional Transport from a Point Source in a Uniform Flow Field: (a) Problem Description, and (b) Model Discretization.	5-11
Figure 5.7	Finite Difference Results (parallel flow).	5-13
Figure 5.8	Finite Element Results (parallel flow).	5-14
Figure 5.9	Finite Difference Results (diagonal flow).	5-15
Figure 5.10	Finite Element Results (diagonal flow).	5-16
Figure 6.1	Automatic discretization of flow region using the vertical slicing approach (y-axis vertically upward), and ISWAP=0.	6-2
Figure 6.2	Automatic discretion of flow region using the horizontal sectioning approach, with ISWAP=1.	6-3
Figure 6.3	Discretization of a domain using a curvilinear grid and transition elements	6-6
Figure 6.4	Example illustrating calculation of integrated nodal fluxes for a two-dimensional cross-sectional analysis. Closed dots represent nodes along boundary segment receiving flux. Open dots represent remaining nodes	6-7
Figure 7.1	VAM3DF GMA Model Mesh with Respect to Fernald Site	7-2
Figure 7.2	Discretization of the Hydrogeologic Layers in SWIFT and VAM3DF GMA Models.	7-4
Figure 7.3	VAM3DF GMA Model Steady State Head Contours Prior to on-site Pumping Wells (Lower Node of Layer 1) (Run: A1).	7-9
Figure 7.4	Modeled Ground Water Elevations for 1997, for the 10-Year Scenario. Comparison between SWIFT (Layer 1) and VAM3DF (Lower Node of Layer 1) GMA Model (Run: A2).	7-10
Figure 7.5	Modeled Ground Water Elevations for 1998, for the 10-Year Scenario. Comparison between SWIFT (Layer 1) and VAM3DF (Lower Node of Layer 1) GMA Model (Run: A2).	7-11
Figure 7.6	Modeled Ground Water Elevations for 1999 through 2003, for the 10-Year Scenario. Comparison between SWIFT (Layer 1) and VAM3DF (Lower Node of Layer 1) GMA Model (Run: A2).	7-12
Figure 7.7	Modeled Ground Water Elevations for 2004 through 2006, for the 10-Year Scenario. Comparison between SWIFT (Layer 1) and VAM3DF (Lower Node of Layer 1) GMA Model (Run: A2).	7-13

LIST OF FIGURES

		Page
Figure 7.8	Ground Water Drawdown Contours for 1997 (Lower Node of Layer 1 in VAM3DF) (Run: A2).	7-14
Figure 7.9	Ground Water Drawdown Contours for 1998 (Lower Node of Layer 1 in VAM3DF) (Run: A2).	7-15
Figure 7.10	Ground Water Drawdown Contours for 1999 through 2003 (Lower Node of Layer 1 in VAM3DF) (Run: A2).	7-16
Figure 7.11	Ground Water Drawdown Contours for 2005 through 2007 (Lower Node of Layer 1 in VAM3DF) (Run: A2).	7-17
Figure 7.12	Ground Water Elevations under Different Pumping Rates at the SOWC Collector Wells for 1997 (VAM3DF GMA Model Results for the Lower Node of Layer 1) (Run: A3).	7-18
Figure 7.13	Ground Water Elevations under Different Pumping Rates at the SOWC Collector Wells for 1998 (VAM3DF GMA Model Results for the Lower Node of Layer 1) (Run: A3).	7-19
Figure 7.14	Ground Water Elevations under Different Pumping Rates at the SOWC Collector Wells for 1999 through 2003 (VAM3DF GMA Model Results for the Lower Node of Layer 1) (Run: A3).	7-20
Figure 7.15	Ground Water Elevations under Different Pumping Rates at the SOWC Collector Wells for 2003 through 2006 (VAM3DF GMA Model Results for the Lower Node of Layer 1) (Run: A3).	7-21
Figure 7.16	Projected Uranium Concentration Contours for 1997 (Run: B1).	7-30
Figure 7.17	Projected Uranium Concentration Contours for 1998 (Run: B1).	7-31
Figure 7.18	Projected Uranium Concentration Contours for 2003 (Run: B1).	7-32
Figure 7.19	Projected Uranium Concentration Contours for 2006 (Run: B1).	7-33
Figure 7.20	Initial Uranium Concentration Contours.	7-35
Figure 7.21	Projected Uranium Concentration Contours for 1997, Using the Kinetic Model (Run: C1).	7-36
Figure 7.22	Projected Uranium Concentration Contours for 1998, Using the Kinetic Model (Run: C1).	7-37
Figure 7.23	Projected Uranium Concentration Contours for 2003, Using the Kinetic Model (Run: C1).	7-38
Figure 7.24	Projected Uranium Concentration Contours for 2006, Using the Kinetic Model (Run: C1).	7-39
Figure 7.25	Projected Uranium Concentration Contours for 1997, Using the Kinetic Model (Run: C2).	7-40
Figure 7.26	Projected Uranium Concentration Contours for 1998, Using the Kinetic Model (Run: C2).	7-41
Figure 7.27	Projected Uranium Concentration Contours for 2003, Using the Kinetic Model (Run: C2).	7-42
Figure 7.28	Projected Uranium Concentration Contours for 2006, Using the Kinetic Model (Run: C2).	7-43
Figure 7.29	Projected Uranium Concentration Contours for 1997, Using the Kinetic Model (Run: C3).	7-44

LIST OF FIGURES

		Page
Figure 7.30	Projected Uranium Concentration Contours for 1998, Using the Kinetic Model (Run: C3).	7-45
Figure 7.31	Projected Uranium Concentration Contours for 2003, Using the Kinetic Model (Run: C3).	7-46
Figure 7.32	Projected Uranium Concentration Contours for 2006, Using the Kinetic Model (Run: C3).	7-47
Figure 7.33	Projected Uranium Concentration Contours for 1997, Using the Kinetic Model (Run: C4).	7-48
Figure 7.34	Projected Uranium Concentration Contours for 1998, Using the Kinetic Model (Run: C4).	7-49
Figure 7.35	Projected Uranium Concentration Contours for 2003, Using the Kinetic Model (Run: C4).	7-50
Figure 7.36	Projected Uranium Concentration Contours for 2006, Using the Kinetic Model (Run: C4).	7-51
Figure 7.37	Projected Uranium Concentration Contours for 1997, Using the Kinetic Model (Run: C5).	7-52
Figure 7.38	Projected Uranium Concentration Contours for 1998, Using the Kinetic Model (Run: C5).	7-53
Figure 7.39	Projected Uranium Concentration Contours for 2003, Using the Kinetic Model (Run: C5).	7-54
Figure 7.40	Projected Uranium Concentration Contours for 2006, Using the Kinetic Model (Run: C5).	7-55
Figure 7.41	Projected Uranium Concentration Contours for 1997, Using the Kinetic Model (Run: D1).	7-57
Figure 7.42	Projected Uranium Concentration Contours for 1998, Using the Kinetic Model (Run: D1).	7-58
Figure 7.43	Projected Uranium Concentration Contours for 2003, Using the Kinetic Model (Run: D1).	7-59
Figure 7.44	Projected Uranium Concentration Contours for 2006, Using the Kinetic Model (Run: D1).	7-60
Figure 7.45	Mass Distribution at a Location with High Initial Aqueous Concentration	7-61
Figure 7.46	Mass Distribution at a Pumping Well RW-2.	7-62
Figure 7.47	Distribution of the Total Uranium Mass over the Site (Run: D1).	7-64
Figure 7.48	Projected Uranium Concentration Contours for 1997, Using the Kinetic Model (Run: D2).	7-65
Figure 7.49	Projected Uranium Concentration Contours for 1998, Using the Kinetic Model (Run: D2).	7-66
Figure 7.50	Projected Uranium Concentration Contours for 2003, Using the Kinetic Model (Run: D2).	7-67
Figure 7.51	Projected Uranium Concentration Contours for 2006, Using the Kinetic Model (Run: D2).	7-68
Figure 7.52	Distribution of the Total Uranium Mass over the Site (Run: D2).	7-69

LIST OF FIGURES

		Page
Figure 7.53	Equilibrium Isotherm Used for Run D3.	7-70
Figure 7.54	Projected Uranium Concentration Contours for 1997, Using the Kinetic Model (Run: D3).	7-71
Figure 7.55	Projected Uranium Concentration Contours for 1998, Using the Kinetic Model (Run: D3).	7-72
Figure 7.56	Projected Uranium Concentration Contours for 2003, Using the Kinetic Model (Run: D3).	7-73
Figure 7.57	Projected Uranium Concentration Contours for 2006, Using the Kinetic Model (Run: D3).	7-74

000010

1.0 INTRODUCTION

1.1 BACKGROUND

HydroGeoLogic has developed and verified a robust numerical flow and transport modeling code for Fernald Environmental Management Project (FEMP) as Phase 1 of work for the development of aquifer restoration management support tools. The work of Phase 1 involved customizing a HydroGeoLogic code to provide specific simulation capabilities for the simulation of groundwater flow and mass transport in the Great Miami Aquifer (GMA) at the Fernald Environmental Management Project (FEMP). Specific customization included: kinetic contaminant mass transfer between liquid and solid phases, a multi-dispersivity model, and the Total Variation Diminishing (TVD) solution to accommodate high groundwater velocity in the vicinity of the extraction/injection wells.

The HydroGeoLogic code that was customized was the Variably Saturated Analysis Model in 3-Dimensions for the Data Fusion System (VAM3DF) (HydroGeoLogic, 1995). The goal was to provide a transport simulator that can handle Fernald Environmental Management Project (FEMP) specific conditions and is efficient enough for Data Fusion Modeling (DFM). The customized code has the following features:

a) Reversible/non-reversible uniform/non-uniform contaminant mass transfer between liquid and solid phases.
b) Groundwater flow simulation.
c) Capability to simulate high groundwater velocity in the vicinity of the extraction/injection wells.
d) Realistic dispersion tensor.
e) Mass balance analysis.
f) Efficient solution algorithm.

DOE invested in a Data Fusion Workstation (DFW) for the purpose of providing a software platform that could be customized to handle the wide range of problems encountered at waste sites such as the Fernald site (Coleman Research Corporation, 1994; DOE, 1997). VAM3DF is believed to be the most appropriate flow and transport model to use in this instance because it has already been implemented with DFM; and it has the basic features needed to meet the DFM project objectives. Table 1.1 shows a comparison of the advantages of VAM3DF with MODFLOW-SURFACT, MT3D96, and MODFLOWT. Further, VAM3DF has been benchmarked, documented, and peer reviewed (Huyakorn et al., 1991; Huyakorn and Panday, 1990; Huyakorn et al., 1989; Huyakorn et al., 1986; Huyakorn et al., 1985; Huyakorn et al., 1984; HydroGeoLogic, 1995; Panday et al., 1993; Kool and Wu, 1991; Kool et al., 1990; Porter et al., 1996; HydroGeoLogic, 1996) and applied at the following sites (with DFM where indicated):

- DOE Savannah River Site, SC (HydroGeoLogic, 1995; Huyakorn and Panday, 1990)
  - TNX-Area
  - Z-Area

000011

- OBG-Area with DFM
- A&M-Area with DFM

- DOE Hanford Site, WA (Law et al., 1997; Chiaramonte et al., 1997)
  - Site-wide model
  - 200 West Area
  - Tank Farm Area
- NRC-Licensed Low-Level West Valley Site, NY (Kool and Wu, 1991a and 1991b)
- Los Alamos Lab Site, NM (Huyakorn, et al., 1986)
- Several Superfund Sites (Unpublished litigation studies)

It is envisioned that, following the completion of Phase 1, work for the development of aquifer restoration management support tools will be completed in the following phases: Phase 2 for calibration and prediction using DFM, Phase 3 for remediation optimization, and Phase 4 for technology transfer.

In Phase 2, DFM code would be customized to calibrate VAM3DF parameters and perform transport prediction. DFM uses Kalman filter methods to quantify prediction uncertainties by computing the statistical prediction error variances. Consequently, DFM can be used to optimize monitoring well locations and sampling frequencies to provide the best tradeoff between plume prediction confidence and monitoring cost. In Phase 3, the optimization code would be customized to help make remediation decisions. The optimization code can be used to provide the best tradeoff between remediation cost and decisions relative to extraction/injection rates, installation of new wells, and shutdown of existing wells.

1.2 OBJECTIVES

The overall objective of the work was to provide a customized contaminant transport simulator that can handle FEMP-specific conditions and be efficient enough to be used with DFM. Specific objectives were to have the following capabilities and features in VAM3DF:

- **Reversible/non-reversible uniform/non-uniform contaminant mass transfer between liquid and solid phases**. Equilibrium sorption mode cannot simulate the expected hysteretic behavior when switching from source loading to aquifer restoration as shown in Figure 1.1. The adsorption-desorption module has been enhanced by extending VAM3DF to include kinetic mass transfer between liquid and solid phases. Mass transfer processes included are: adsorption, desorption, chemisorption, precipitation, and dissolution.

- **Groundwater flow simulation**. Advanced numerical methods were used to produce efficient flow simulation code. Both finite element and finite difference formulations are provided. The finite element form provides the most accuracy, and the finite difference form provides the most computational speed for use with DFM. Automatic adaptive time- stepping algorithms are used for efficient transient solution, and robust efficient solution schemes are used to solve the large sparse system of equations.

000012

Table 1.1
The Advantages of VAM3DF over MODFLOW-SURFACT, MT3D96 and MODFLOWT

CODE	MODFLOW SURFACT	VAM3DF	MT3D96	MODFLOWT
Numerical Implementation	Finite-Difference	Finite-Difference and Finite-Element Options	Finite-Difference and MOC	Finite-Difference
Temporal discretization	Finite-Difference	Finite-Difference	Finite-Difference	Finite-Difference
Spatial transport solution scheme	Mass Conserved TVD	Mass Conserved TVD	MOC (non-mass conserved)	Mass Conserved upstream weighting may give excessive front smearing.
Dispersivity	3-component. Cross dispersion terms iteratively updated.	3-component (4-component to be implemented). All cross-terms are fully implicit.	3-component. Cross-terms are time lagged.	3-component. Cross-terms are time lagged.
Data Fusion	Available for the flow equation limited functionality	Available for the flow equation and for transport prediction with quantified uncertainty	Not available	Not available
Sorption	K_d	K_d Rate-limited sorption	K_d	K_d
User-Interface	Groundwater Vistas with a separate interface for data fusion	Integrated Graphical User Interface (GIS) with Gridmaker for model and data fusion	GMS	Groundwater Vistas
Commercial distribution	Yes	Yes	Yes	Yes
Developed by	HydroGeoLogic, Inc.	HydroGeoLogic, Inc.	S.S. Papadopulos & Associates	Hydro Solve

000013

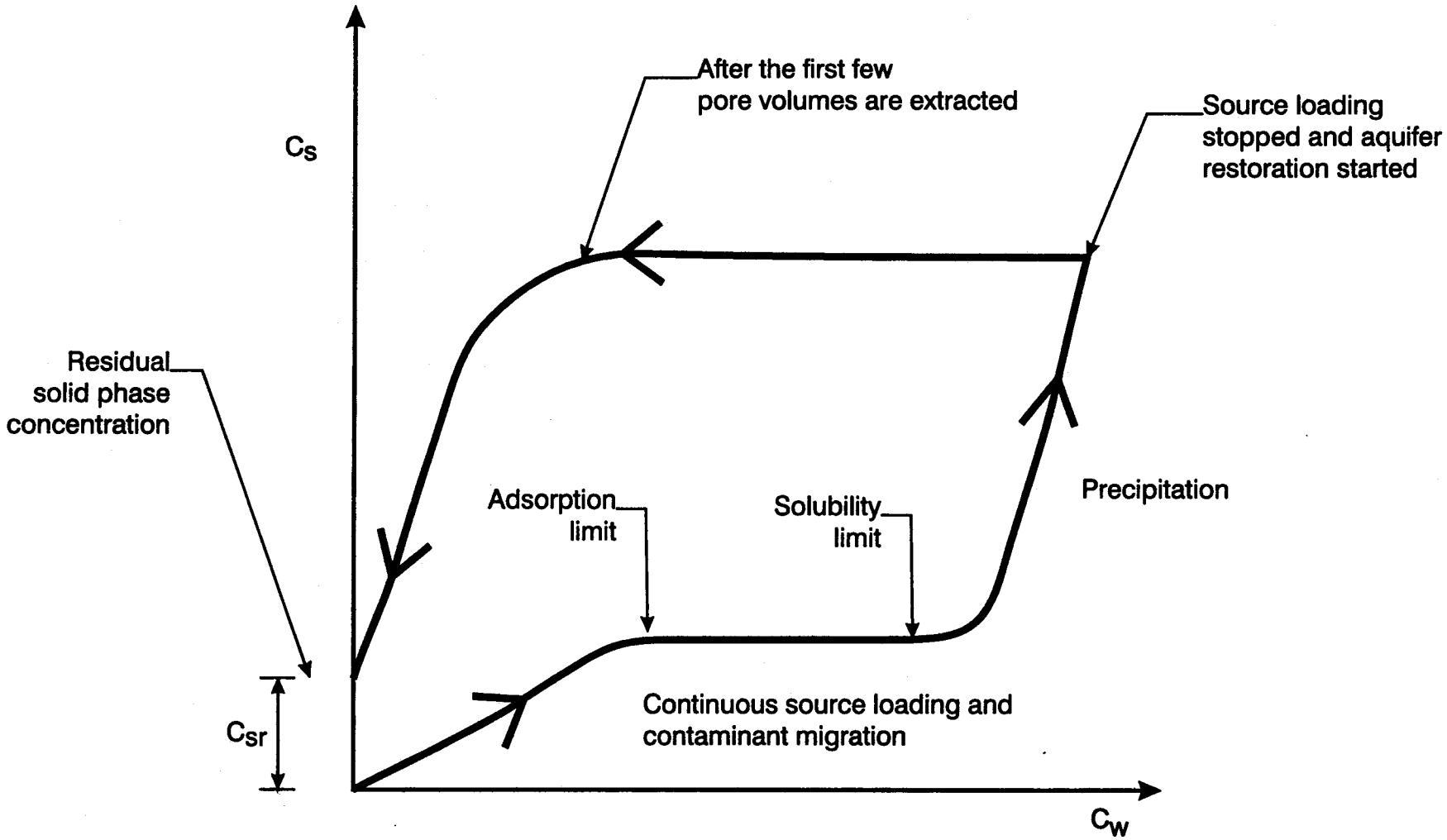

Figure 1.1 Solid Phase Contamination Versus Solute Concentration.

000014

- **High groundwater velocity in the vicinity of the extraction/injection wells.** When using pump-and-treat where hydraulic conductivity is high, it is often necessary to use high extraction and injection rates that produce high groundwater velocity. This can lead to grid sizes and time steps that are too small for efficient computation. In addition, large sources or sinks can lead to numerical oscillation and poor mass balance. In order to accommodate high groundwater velocity, the Total Variation Diminishing (TVD) solution is incorporated fully implicitly in VAM3DF.

- **Realistic dispersion tensor.** A dispersion coefficient tensor based on two longitudinal and transverse dispersivity parameters results in unrealistic dispersion in the vertical direction when there is vertical anisotropy and pronounced vertical velocity. Vertical velocity can be significant in the vicinity of partially-penetrating extraction/injection wells and can produce unrealistic dispersion with the two parameter model. To solve this problem, a new four parameter model has been incorporated into VAM3DF to minimize unrealistic dispersion in the vertical direction.

- **Mass balance analysis.** VAM3DF performs a mass balance analysis for both flow and transport. These routines were modified to provide a complete water and mass budget report of the individual components of the system.

All capabilities and features were individually tested and verified using analytical solutions, and solutions from other numerical codes. Further, site simulation based on the enhanced VAM3DF code were conducted and compared against results from the existing GMA groundwater flow and mass transport model.

The basic flow and transport formulation is provided in the next section. This is followed by sections describing multi-dispersivity, kinetic mass transfer between liquid and solid phases, and the TVD solution. Then sections are provided for the general model application process and site simulation results. The final section presents recommendations, summary, and conclusions.

2.0 FORMULATION

This section describes the formulation of the original VAM3DF code. Details relating to the customization of the original code to include multidispersivity, kinetics, and addition of the TVD solution scheme, are presented in Sections 3, 4, and 5.

2.1 BACKGROUND - PROCESS AND GEOMETRY

VAM3DF performs three-dimensional, two-dimensional or axisymmetric finite-element and finite-difference simulations of water flow and/or solute transport in variably saturated and fully saturated porous media. The code employs the state-of-the-art numerical technology to provide efficient steady-state and transient solutions of practical problems encountered in the investigation, mitigation and remediation of soil and groundwater contamination due to disposal of chemical and/or nuclear wastes. The steady-state analysis is performed by disregarding all storage terms of the governing equations thus avoiding the necessity of time marching. The transient analysis is performed by time marching (or time stepping) until the prescribed number of time steps is reached. For water flow simulations, VAM3DF can handle a variety of boundary conditions including infiltration, evaporation, and plant root extraction. The code is designed to accommodate severely nonlinear soil moisture characteristics. Pseudo-soil relations are also provided for cases where the soil retention and relative permeability functions are unknown, and unsaturated zone behavior is unimportant. For solute transport simulations, VAM3DF accounts for advection, hydrodynamic dispersion, equilibrium sorption, and first-order decay. Single component transport of conservative and non-conservative solutes can be handled.

VAM3DF employs a right-handed Cartesian or an Orthogonal Curvilinear coordinate system (x,y,z) to generate a three-dimensional grid for finite element analysis. If a fully three-dimensional analysis is required, the grid may be oriented such that either y- or z-axis points in the vertical upward direction. For a two-dimensional (cross-section or areal) analysis, the grid needs to be oriented such that the x-y plane corresponds to the (vertical or horizontal) plane where spatial variation of the unknown variable (head or concentration) occurs. In the case of an axisymmetric analysis, the grid is oriented such that the x and y axes correspond to the radial and vertical coordinates of the cylindrical coordinate system, respectively.

2.2 GOVERNING FLOW EQUATIONS

To perform a variably saturated flow analysis, the VAM3DF code uses the pressure head or the hydraulic head as the dependent variable if a rectangular grid is used. For an orthogonal curvilinear grid, the dependent variable is the hydraulic head. This is advantageous because it precludes the necessity of computing gradients in the elevation potential term. The governing equation for water flow in a variably saturated soil is written as:

$$\frac{\partial}{\partial x_i}\left[\rho_w K_{ij} k_{rw} \left(\frac{\partial \psi}{\partial x_j} + e_j\right)\right] = \frac{\partial}{\partial t}\left(\rho_w \phi S_w\right) - \rho_w q \qquad (2.1)$$

where ρ_w is the density of water, ψ is the pressure head, K_{ij} is the saturated hydraulic conductivity tensor, k_{rw} is the relative permeability with respect to the water phase, x_i $(i = 1, 2, 3)$ are a set of

orthogonal spatial coordinates, t is time, e_j is the unit vector assumed to be vertically upward, S_w is water phase saturation, ϕ is the effective porosity, and q is the volumetric flow rate via sources (or sinks) per unit volume of the porous medium. The pressure head and hydraulic head h are related as $h = \psi + z$ where z is the vertically upward direction.

For a slightly compressible fluid, equation (2.1) can be written in the form (Cooley, 1971):

$$\frac{\partial}{\partial x_i}\left[K_{ij} k_{rw} \left(\frac{\partial \psi}{\partial x_j} + e_j\right)\right] = \left(S_w S_s + \phi \frac{dS_w}{d\psi}\right) \frac{\partial \psi}{\partial t} - q \tag{2.2}$$

or

$$\frac{\partial}{\partial x_i}\left[K_{ij} k_{rw} \left(\frac{\partial \psi}{\partial x_j} + e_j\right)\right] = \eta \frac{\partial \psi}{\partial t} - q \tag{2.3}$$

where η is a coefficient defined as

$$\eta = S_w S_s + \phi \frac{dS_w}{d\psi} \tag{2.4}$$

The coefficient S_s is the specific storage defined as (Bear, 1979)

$$S_s = \rho_w g \left(\phi \beta_w + \alpha_s\right) \tag{2.5}$$

where g is the gravitational constant and α_s and β_w are coefficients of compressibility of the porous medium and water, respectively. The off-diagonal components of the saturated conductivity tensor will be zero if the coordinate system coincides with the principal axes of anisotropy of the hydraulic conductivity (e.g., the x_1 and x_3 directions are parallel to the plane of stratification, and x_2 direction is normal to the plane of stratification).

The initial and boundary conditions of the variably saturated flow problem are

$$\psi(x_i, 0) = \psi_o(x_i) \tag{2.6}$$

$$\psi(x_i, t) = \tilde{\psi} \quad on\ B_1 \tag{2.7}$$

and

$$V_i n_i = -V_n \text{ on } B_2 \tag{2.8}$$

where ψ_0 is the initial head value, B_1 is the portion of the flow boundary where ψ is prescribed as $\bar{\psi}$, V_i is the Darcy velocity vector, B_2 is the portion of the flow boundary where the outward normal velocity is prescribed as $-V_n$, and n_i is the outward unit normal vector. The boundary and initial conditions are provided in terms of hydraulic head h instead of the pressure head ψ when the hydraulic head is the dependent variable.

In order to solve the variably saturated flow problem, it is also necessary to specify the relationships of relative permeability versus water phase saturation, and pressure head versus water phase saturation. Two alternative functional expressions are used to describe the relationship of relative permeability versus water saturation. These functions are given by (Brooks and Corey, 1966):

$$k_{rw} = S_e^n \tag{2.9}$$

and (van Genuchten, 1976):

$$k_{rw} = S_e^{1/2}[1-(1-S_e^{1/\gamma})^\gamma]^2 \tag{2.10}$$

where n and γ are empirical parameters and S_e is the effective water saturation defined as $S_e = (S_w - S_{wr})/(1-S_{wr})$ with S_{wr} being referred to as the residual water saturation.

The relationship of pressure head versus water saturation is described by the following function (van Genuchten, 1976; Mualem, 1976):

$$\frac{S_w - S_{wr}}{1 - S_{wr}} = \begin{cases} \dfrac{1}{[1+(\alpha|\psi-\psi_a|)^\beta]^\gamma} & \text{for } \psi < \psi_a \\ 1 & \text{for } \psi \geq \psi_a \end{cases} \tag{2.11}$$

where α and β are empirical parameters, ψ_a is the air entry pressure head value, and S_{wr} is the residual water phase saturation. The parameters β and γ are usually related by $\gamma = 1-1/\beta$. The Brooks-Corey and van Genuchten functions for the moisture retention and relative permeability characteristics can be measured in the laboratory for a given soil.

Equation (2.3) is solved numerically using the Galerkin finite element method subject to the initial and boundary conditions given in (2.5) through (2.7). After the distributions of ψ (or h) and S_w have been determined, Darcy velocity components are calculated from

$$V_i = -K_{ij} k_{rw} \left(\frac{\partial \psi}{\partial x_j} + e_j\right) = -K_{ij} k_{rw} \frac{\partial h}{\partial x_j} \tag{2.12}$$

2.2.1 Treatment of Hysteresis and Anisotropy

To simulate the effect of hysteresis in soil moisture properties in a variably saturated flow simulation, VAM3DF incorporates the procedure described by Kool and Parker (1987). This procedure requires that the boundary wetting and drying curves in the $S_w(\psi)$ relation are known. In VAM3DF it is assumed that these boundary curves are described by expressions that have the same form as (2.11), but with different parameter values for the wetting and drying boundary curves. Using superscripts w and d to distinguish between wetting and drying, respectively, the boundary $S_w(\psi)$ curves are described by the following relationships:

$$\frac{S_w^w - S_{wr}}{S_{ws} - S_{wr}} = \begin{cases} \dfrac{1}{[1 + (\alpha^w |\psi - \psi_a|)^{\beta^w}]^{\gamma^w}} & \psi < \psi_a \\ 1 & \psi \geq \psi_a \end{cases} \tag{2.13}$$

$$\frac{S_w^d - S_{wr}}{1 - S_{wr}} = \begin{cases} \dfrac{1}{[1 + (\alpha^d |\psi - \psi_a|)^{\beta^d}]^{\gamma^d}} & \psi < \psi_a \\ 1 & \psi \geq \psi_a \end{cases} \tag{2.14}$$

In equation (2.13) S_{ws} represents the maximum saturation value upon rewetting of an initially air-dry soil. If no air-entrapment occurs, $S_{ws} = 1.0$. However, if air-entrapment occurs, S_{ws} will be less than one. Parameters α, β and γ are the van Genuchten curve shape parameters, with different values for wetting and drying. Note that α^w cannot be less than α^d, *i.e.*

$$\alpha^w \geq \alpha^d$$

often, the following simplifications can be used (Kool and Parker, 1987):

$$\beta^w = \beta^d = \beta$$

$$\gamma^w = \gamma^d = 1 - 1/\beta$$

000019

With these simplifications, only four parameters are required to characterize the hysteretic saturation-pressure head relation. The parameters are the residual saturation, S_{wr}, and the shape parameters α^w, α^d and β. Lacking data, one may use $\alpha^w = 2\alpha^d$ as a first approximation (Kool and Parker, 1987). A typical hysteretic $S_w(\psi)$ relation is shown in Figure 2.1. This figure illustrates the correspondence of the parameters in (2.13) and (2.14) to the boundary wetting and drying curves.

In a hysteretic flow simulation, VAM3DF automatically computes scanning curves in the $S_w(\psi)$ relation to determine the appropriate saturation path for every element in the modeled domain when reversals from wetting to drying, or vice versa occur. This is achieved by defining "pseudo" values of the residual and saturated values of S_w. In the simulation, these pseudo-values are substituted into Eqs. (2.13) and (2.14). This has the effect of scaling the boundary wetting and drying curves to make them pass through the reversal points. For a reversal from wetting to drying, the nominal value of 1.0 for S_w at saturation is replaced by

$$S'_{ss} = \frac{S_w^{rev} - S_{wr}\,[1 - S_e^d\,(\psi^{rev})]}{S_e^d\,(\psi^{rev})} \tag{2.15}$$

where S_w^{rev} and ψ^{rev} are the saturation and pressure head at the reversal point respectively, and $S_e^d\,(\psi^{rev})$ is the effective drying saturation given by the left hand side of (2.14) for $\psi = \psi^{rev}$. Analogously, for a reversal from drying to wetting, a pseudo-value for S_{wr} is used, which is given by

$$S'_{wr} = \frac{S_w^{rev} - S_e^w\,(\psi^{rev})}{1 - S_e^w\,(\psi^{rev})} \tag{2.16}$$

where S_e^w is the effective wetting saturation corresponding to the left hand side of (2.13). The hysteresis subroutine in VAM3DF checks whether each element is wetting or drying and computes the appropriate values of S'_{ss} and S'_{wr} for each element. This is achieved by means of an index variable, κ_i, which is set to $\kappa_i = +1$ if the *i-th* element is wetting and $\kappa_i = -1$ if the *i-th* element is drying. At the end of every time step a check is made for every element to determine whether a reversal in the saturation path has occurred. A reversal occurs if:

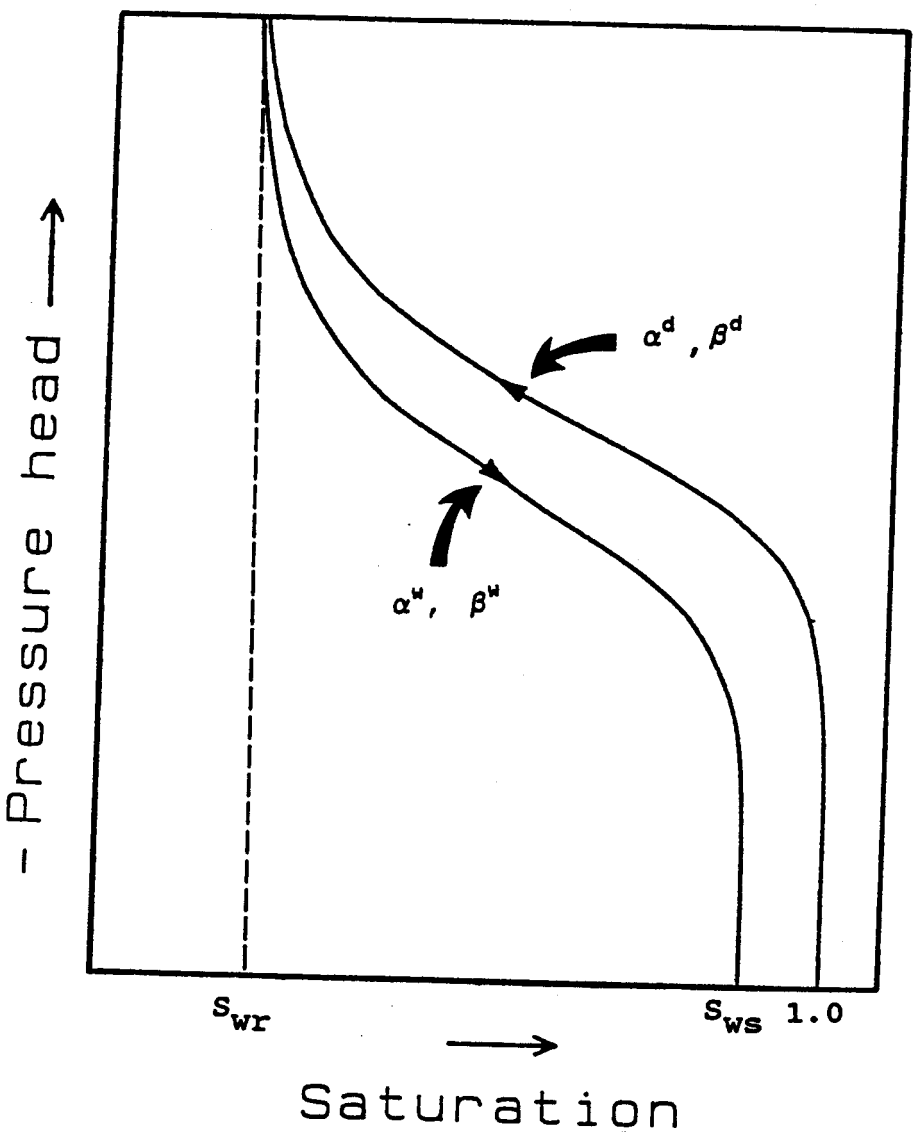

Figure 2.1 **Example of hysteretic $S_w(\psi)$ relation showing the boundary wetting and drying curves.**

000021

$$\frac{\bar{\psi}_i^{t-\Delta t} - \bar{\psi}_i^t}{\kappa_i} > \delta_\psi \tag{2.17}$$

where δ_ψ is the pressure head iteration convergence tolerance, and $\bar{\psi}_i$ is the average nodal pressure head for the *i-th* element

$$\bar{\psi}_i = \frac{1}{n_i} \sum_{j=1}^{n_i} \psi_{ij} \tag{2.18}$$

with n_i the number of nodes for the element. When a reversal occurs, the code determines the new scanning curve for the element which is subsequently used to calculate $S_w(\psi)$. An example of such scanning curves is shown in Figure 2.2. In this example the boundary hysteresis loop is closed at saturation, i.e., $S_{ws} = 1.0$. The figure shows a primary wetting scanning curve (1) and a secondary drying scanning curve (2). In order to completely specify the initial conditions for a hysteretic simulation, the user must specify not only the initial nodal values of ψ, but also the initial saturation values for each element, and whether the element is initially wetting or drying.

2.2.2 Treatment of Variable Unsaturated Anisotropy

Many natural soils and other geologic media exhibit some degree of stratification leading to anisotropy of hydraulic conductivity, with higher conductivity in the direction parallel to stratification than perpendicular to stratification. This anisotropy is usually expressed as a ratio.

$$r = \frac{K_{11}}{K_{33}} = \frac{K_{22}}{K_{33}} \tag{2.19a}$$

where the indices 1 and 2 indicate the directions parallel to stratification and 3 corresponds to the perpendicular direction. As expressed by (2.19a), the anisotropy ratio is constant and independent of saturation. Recent research (e.g., Yeh et al., 1985; Mantoglou and Gelhar, 1987; McCord et al., 1988) suggests that in reality, the relative permeability k_{rw} may be subject to strong anisotropy. This research indicates that for unsaturated conditions, the hydraulic conductivity anisotropy is inversely related to the degree of water saturation. Assuming an exponential $k_{rw}(\psi)$ relation and using stochastic theory, Yeh et al. (1985) have developed the following expression for anisotropy as a function of pressure head for layered soils with a mean unit downward hydraulic gradient

$$r(\psi) = \frac{(Kk_{rw})_{11}}{(Kk_{rw})_{33}} = \frac{(Kk_{rw})_{22}}{(Kk_{rw})_{33}} = \exp\left[\frac{\sigma_f^2 + \sigma_a^2 \bar{\psi}^2}{1 + \mu\, \bar{a} \cos\omega}\right] \tag{2.19b}$$

where σ_f^2 is the variance of the log saturated conductivity (lnK), a is the slope of the $ln(k_{rw})$ versus ψ curve, $\bar{a}$ is the mean value of a, σ_a^2 is the variance of a, $\bar{\psi}$ is the mean value of ψ, μ is the spatial correlation length, and ω is the angle between the soil layer stratification and the horizontal.

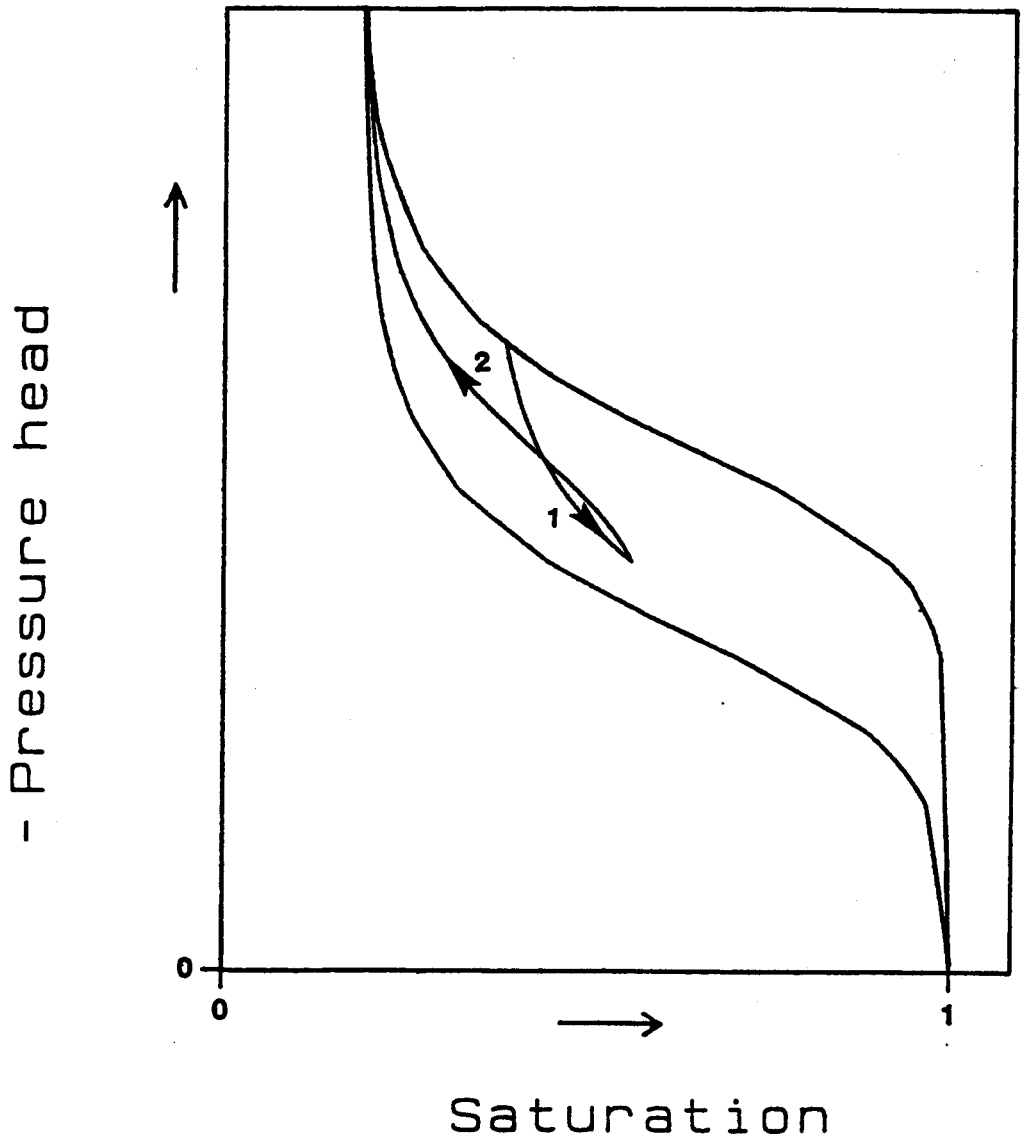

Figure 2.2 **Typical scanning curves produced by the hysteresis model in VAM3DF. Curve (1) denotes primary wetting scanning curve, curve (2) denotes secondary drying scanning curve.**

000023

Equation (2.19b) indicates that anisotropy increases as an exponential function of the second power of pressure head. According to (2.19b) anisotropy will also be more pronounced when the spatial variability of hydraulic conductivity increases and the correlation length, μ, decreases. The concept of variable anisotropy is based on mainly theoretical considerations and the predictive value of (2.19b) has not been extensively tested. Nevertheless, McCord et al. (1988) have experimentally observed patterns of water and solute plume migration in a hill slope infiltration study that are similar to results obtained by computer simulation which incorporated (2.19b) to model variable anisotropy.

VAM3DF can simulate the effect of saturation dependent anisotropy on unsaturated flow by using Equation (2.19b) to evaluate anisotropy as a function of pressure head. This requires input values of the variables σ_f^2, σ_a^2, μ and ω. The parameter $\bar{a}$ can be treated either as an input variable or be evaluated by VAM3DF as the derivative of the $ln[k_{rw}(\psi)]$ relation. When the latter option is used with Brooks and Corey (1966), van Genuchten (1980) or pseudo-soil relative permeability functions to describe the $k_r(S_w)$ relation, the value of $\bar{a}$ will tend to decrease with decreasing saturation. This will magnify the predicted anisotropy compared to the case of a user-specified constant value for $\bar{a}$. In order to obtain an operational algorithm, two additional criteria were implemented:

First, a maximum bound must be imposed on the anisotropy ratio. Inspection of Equation (2.19b) shows that otherwise the computed anisotropy ratio will easily become unrealistically large, even for moderate values of ψ. The upper bound, r_{max}, for $r(\psi)$ is a user-specified value in VAM3DF. A value of $r_{max} = 10^7$ has been found to give satisfactory results in many cases. Secondly, Equation (2.19b) gives the conductivity ratio, but not the actual values of conductivities parallel and perpendicular to stratification. In order to obtain the desired, monotonically decreasing $k_{rw}(\psi)$ relations, VAM3DF uses an empirical logarithmic interpolation procedure to ensure that $(Kk_{rw})_{11}$, $(Kk_{rw})_{22}$, and $(Kk_{rw})_{33}$ decrease with decreasing pressure head and that the correct anisotropy ratio is maintained for any ψ value. An example anisotropic $k_{rw}(\psi)$ relation as modeled by VAM3DF is shown in Figure 2.3. This figure shows relative conductivity as a function of soil water pressure head. The solid curve represents the isotropic case in which conductivity is given by the van Genuchten function. The dashed lines represent the anisotropic case with anisotropy ratio computed from Equation (2.19b). The following anisotropy parameters were used here: $\sigma_f^2 = 0.82$, $\sigma_a^2 = 0.0005$, $\mu = 40$ cm and $\omega = 0.0$. The figure clearly illustrates the dramatic effect of tension (pressure head) variations on the magnitude of anisotropy.

2.2.3 Pseudo-Soil Functions for Predicting Water-Table Levels

When the soil retention and relative permeability functions of a soil are unknown, and the unsaturated zone moisture behavior is unimportant to the simulated scenario, VAM3DF uses pseudo-relations to predict the water-table levels. With this option, the code utilizes simple linear relations to account for changes in element saturated thickness and relative permeability due to the transient movement of the water table in the aquifer.

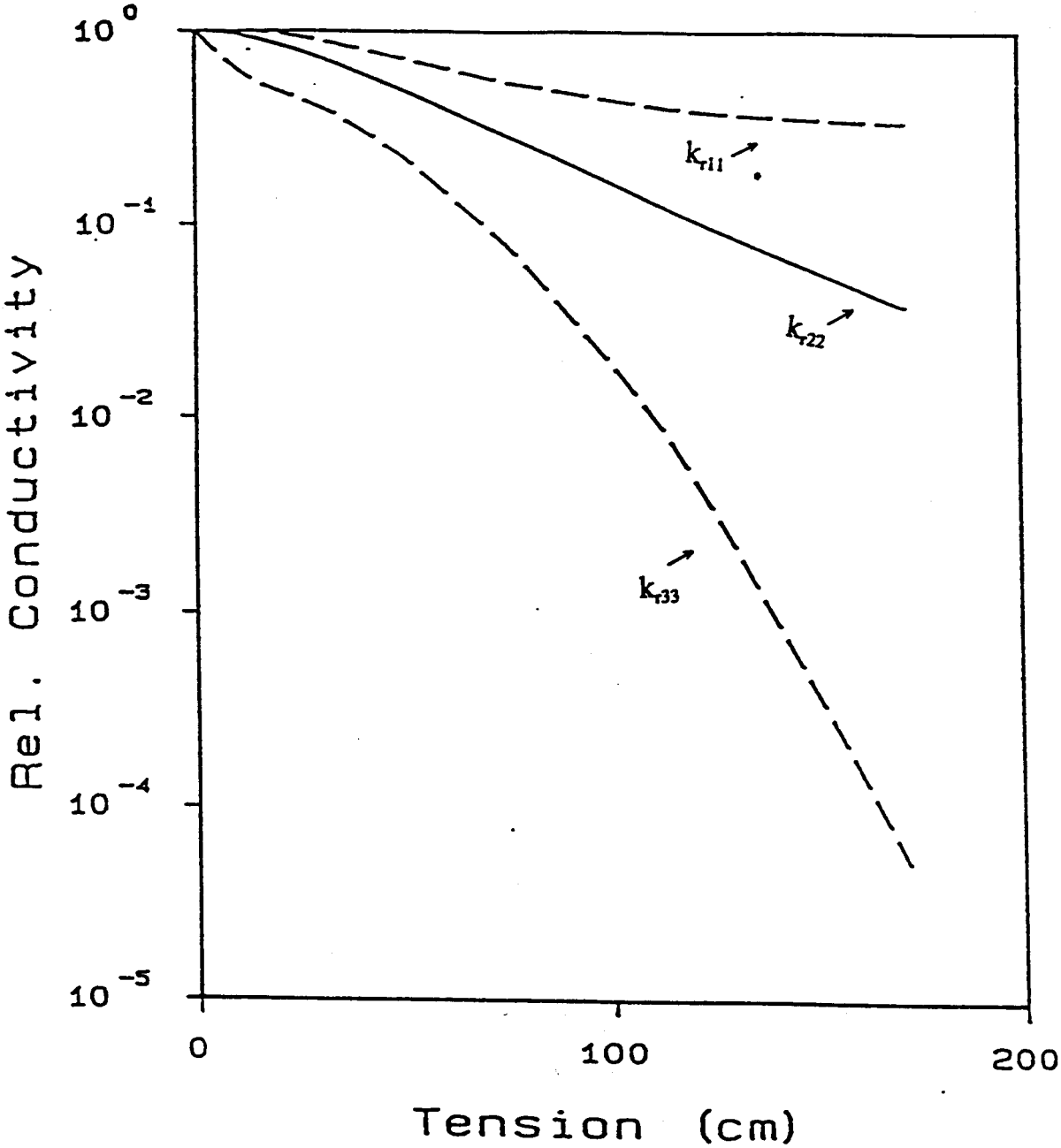

Figure 2.3 **Example of anisotropic $k_{rw}(\psi)$ relation as modeled by VAM3DF.**

000025

These linear pseudo-soil moisture relations are given by

$$S_w = 1 - \left(\frac{|\bar{\psi} - \psi_s|}{b} \right) \geq 0.01$$

and

$$k_{rw} = S_w$$

where S_w is the saturation of the element defined such that $S_w = 1$ when the water table is above the top of the element, and $S_w \approx 0$ when the water table is below the bottom of the element. $\bar{\psi}$, is the pressure head at the element centroid, which governs the pseudo-relation, b is the average elemental thickness and ψ_s = b/2 is the pressure head scaling parameter. The pseudo-relative permeability function ensures that the vertically integrated transmissivity of the element is adjusted to its saturated thickness as is done in the solution to the vertically integrated areal 2-D aquifer flow equations.

The above pseudo-constitutive relations are simple linear functions which are not dependent on any unsaturated-zone soil properties. This is advantageous in that data on unsaturated properties of the soil is often unavailable. Neither is the use of such data warranted when one is mainly concerned with groundwater flow in the saturated zone of the aquifer system. The variably saturated pseudo soil (VSPS) modeling approach to unconfined flow problems is not only effective but also advantageous as compared to conventional fully saturated modeling approaches to unconfined systems. The multi-layered areal modeling approach using the vertically integrated Boussinesque equation with leakance between layers neglects vertical components of flow, assuming instant vertical equilibrium within each layer. Further, the quasi-three dimensional coupling creates convergence difficulties for large leakances across layers, and re-saturation of a de-saturated cell is not possible. The fixed grid 2-D cross-sectional or 3-D modeling approach accounts for the vertical flow but neglects the effects of desaturation of a grid block on its conductivity. The adjustable finite element or finite difference grid scheme to accommodate the water table or free surface movement of an unconfined aquifer system is complex to implement especially in three-dimensions.

The main advantages of the VSPS modeling approach are summarized as follows:

- The VSPS approach is general, robust and able to handle complex multilayer problems involving desaturation and resaturation of grid blocks (or drastic changes in the water table position).

- The VSPS approach is efficient and practical to use because of its fixed grid formulation and linearized constitutive relations. No additional user input is required.

- The VSPS approach is a flexible modeling approach that can be simplified to that equivalent to the areal modeling approach by using a 3-D grid with two nodes on each vertical grid line or a single element covering the entire aquifer thickness. In such a case, vertical flow components are essentially neglected. On the other hand, the VSPS approach can be made rigorous by using a 3-D grid with multiple element subdivisions in the vertical direction, thus allowing proper account of vertical flow components, as well as accommodating the presence of seepage faces if desirable.

2.2.4 Atmospheric Boundary Conditions

Atmospheric boundaries may correspond to soil-air interfaces where evaporation or infiltration occurs. They may also correspond to seepage faces through which water seeps from the saturated portion of the flow domain.

Along infiltration and evaporation boundaries, conditions may change from the Dirichlet (prescribed head) to the Neuman (prescribed flux) type. In the absence of surface ponding, a numerical solution must be obtained by maximizing the absolute value of the flux (while maintaining the appropriate sign) subject to the following requirements (Hanks et al., 1969; Neuman et al., 1974):

$$|v_i n_i| \leq |E_s^*|$$

and

$$\psi_L \leq \psi \leq 0 \tag{2.20}$$

where E_s^* is the maximum potential surface flux under the prevailing atmospheric conditions, and ψ_L is the minimum pressure head allowed under the prevailing soil conditions.

For cases involving plant root uptake, the sink term in the governing equation (2.3) is represented by the following equation (Feddes et al., 1974):

$$q = K_{33}\, k_{rw}\, (\psi - \psi_r) b'$$

where ψ_r is the root pressure head, and b′ is the root effectiveness function.

2.3 GOVERNING TRANSPORT EQUATIONS

The governing equation for three-dimensional transport of a non-conservative component in a variably saturated soil takes the form (Bear, 1979)

000027

$$\frac{\partial}{\partial x_i}\left(D_{ij}\frac{\partial C_w}{\partial x_j}\right) - \frac{\partial}{\partial x_i}(v_i C_w) = \frac{\partial}{\partial t}\left[\phi S_w C_w + \rho_s (1-\phi) C_s\right] - qC^* + \lambda\left[\phi S_w C_w + \rho_s (1-\phi) C_s\right], \quad i \text{ or } j = 1,2,3 \tag{2.21}$$

where D_{ij} is the apparent hydrodynamic dispersion tensor, C_w is solute concentration in the fluid, v_i is the Darcy velocity, ρ_s is the density of solid grains, C_s is the adsorbed concentration, λ is the first-order decay coefficient, and C^* is the solute concentration in the injected fluid.

2.3.1 Equilibrium Mass Transfer Between the Aqueous and Solid Phases

Assuming that the relation between adsorbed and solution concentration is described by a linear equilibrium isotherm, Equation (2.21) can be expressed as

$$\frac{\partial}{\partial x_i}\left(D_{ij}\frac{\partial C_w}{\partial x_j}\right) - \frac{\partial}{\partial x_i}(v_i C_w) = \frac{\partial}{\partial t}\left[\phi S_w \left(1 + \frac{\rho_s (1-\phi) k_d}{\phi S_w}\right) C_w\right] - qC^* + \lambda \phi S_w \left[1 + \frac{\rho_s (1-\phi) k_d}{\phi S_w}\right] C_w \tag{2.22}$$

where k_d is the distribution coefficient.

Equation (2.22) reduces to

$$\frac{\partial}{\partial x_i}\left(D_{ij}\frac{\partial C_w}{\partial x_j}\right) - \frac{\partial}{\partial x_i}(v_i C_w) = \frac{\partial}{\partial t}(\phi S_w R C_w) + \lambda \phi S_w R C_w - qC^* \tag{2.23}$$

where R is the retardation factor defined as

$$R = 1 + \frac{\rho_s (1-\phi) k_d}{\phi S_w} = 1 + \frac{\rho_B k_d}{\phi S_w} \tag{2.24}$$

000028

with the bulk density ρ_B being defined as $(1-\phi)\rho_s$. Expanding the convective and mass accumulation terms of Equation (2.23) and using the continuity equation of fluid flow, one obtains

$$\frac{\partial}{\partial x_i}\left(D_{ij}\frac{\partial C_w}{\partial x_j}\right) \quad v_i\frac{\partial C_w}{\partial x_i} \quad \phi S_w R\frac{\partial C_w}{\partial t} \quad C_w\frac{\partial}{\partial t}(\phi S_w) \quad C_w\frac{\partial}{\partial t}(\rho_B k_d)$$
$$C_w\frac{\partial}{\partial t}(\phi S_w) \quad q(C_w \quad C) \quad \lambda\phi S_w R C_w \tag{2.25}$$

which, assuming that the time derivative of $(\rho_B k_d)$ is negligible, reduces to

$$\frac{\partial}{\partial x_i}\left(D_{ij}\frac{\partial C_w}{\partial x_j}\right) \quad v_i\frac{\partial C_w}{\partial x_i} \quad \phi S_w R\left(\frac{\partial C_w}{\partial t} \quad \lambda C_w\right) \quad q(C_w \quad C) \tag{2.26}$$

Note that the term $q(C-C^*)$ is zero for the case where q corresponds to the specific discharge of a pumped well, because $C \equiv C^*$.

2.3.2 Kinetic Mass Transfer

VAM3DF has been enhanced to handle kinetic mass transfer between the aqueous and solid phases. Details are given in Section 4.

2.3.3 Hydrodynamic Dispersion Coefficients

The hydrodynamic dispersion tensorial components are computed using the following constitutive relations for homogeneous systems (Scheidegger, 1961):

$$D_{ij} \quad \alpha_T |v| \delta_{ij} \quad (\alpha_L \quad \alpha_T)\frac{v_i v_j}{|v|} \quad \tau D^o \delta_{ij} \tag{2.27a}$$

where α_L and α_T are longitudinal and transverse dispersivities, respectively, δ_{ij} is the Kronecker delta, D^o is the bulk molecular diffusion coefficient, and τ is the tortuosity given by the Millington-Quirk (1961) equation as $\tau = S_w^{10/3}\phi^{4/3}$. The two-dispersivity model was employed in the previous version of VAM3DF.

Alternatively, the hydrodynamic dispersion may be computed from the relations provided by Burnett and Frind (1987) for stratified porous media, as

$$D_{xx} \quad \alpha_L\frac{v_x^2}{|v|} \quad \alpha_T\frac{v_y^2}{|v|} \quad \alpha_v\frac{v_z^2}{|v|} \quad \tau D_o \tag{2.27b}$$

000029

$$D_{yy} = \alpha_T \frac{v_x^2}{|v|} + \alpha_L \frac{v_y^2}{|v|} + \alpha_v \frac{v_z^2}{|v|} + \tau D_o \tag{2.27c}$$

$$D_{zz} = \alpha_v \frac{v_x^2}{|v|} + \alpha_v \frac{v_y^2}{|v|} + \alpha_L \frac{v_z^2}{|v|} + \tau D_o \tag{2.27d}$$

$$D_{xy} = D_{yx} = (\alpha_L - \alpha_T)\, v_x v_y / |v| \tag{2.27e}$$

$$D_{yz} = D_{zy} = (\alpha_L - \alpha_v)\, v_y v_z / |v| \tag{2.27f}$$

$$D_{zx} = D_{xz} = (\alpha_L - \alpha_v)\, v_z v_x / |v| \tag{2.27g}$$

where z is the index for the vertical direction. Note that equations (2.27b) through (2.27g) collapse to equation (2.27a) when $\alpha_v = \alpha_T$.

Dispersion coefficients with flow dispersivity components are presented in Section 3.

2.3.4 Boundary Conditions

Equation (2.26) is the required form of the transport equation and will be approximated using the upstream weighted residual finite element technique of Huyakorn and Nilkuha (1979). The initial and boundary conditions associated with Equation (2.26) are as follows:

$$c(x_i, 0) = c_o \tag{2.28a}$$

$$c(x_i, t) = \tilde{c} \ on \ B_1' \tag{2.28b}$$

$$D_{ij} \frac{\partial c}{\partial x_j} n_i = q_c^D \quad on \ B_2' \tag{2.28c}$$

$$D_{ij} \frac{\partial c}{\partial x_j} n_i - v_i n_i c = q_c^T \quad on \quad B_3' \tag{2.28d}$$

where B_1' is the portion of the boundary where concentration is prescribed as $\tilde{c}$, and B_2' and B_3' are portions of the boundary where the dispersive and the total solute mass fluxes are prescribed as q_c^D and q_c^T, respectively.

2.4 ASSUMPTIONS

VAM3DF contains both flow and solute transport models. Major assumptions of the flow model are as follows:

- Water is the only flowing fluid phase (i.e., the air phase is assumed to be inactive).
- Flow of the fluid phase is considered isothermal and governed by Darcy's law.
- The fluid considered is slightly compressible and homogeneous.
- The soil or rock medium may be represented by a single continuum porous medium.

Major assumptions of the solute transport model are as follows:

- Dispersion in the porous medium system is governed by Fick's law. The hydrodynamic dispersion coefficient is defined as the sum of the coefficients of mechanical dispersion and molecular diffusion.
- Decay of the solute may be described by a first order decay rate respectively.
- Mass transfer between the aqueous and solid phases is described by either a linear equilibrium isotherm or kinetic mass transfer processes which include adsorption, desorption, precipitation, chemisorption, and dissolution.

2.5 LIMITATIONS

- In performing a variably saturated flow analysis, the code handles only single-phase flow (i.e., water) and ignores the flow of a second phase (i.e., air or other nonaqueous phase) which, in some instances, can be significant.
- Flow and transport in fractures are not taken into account.

3.0 MULTI-DISPERSIVITY MODULE

3.1 PURPOSE

In the transport component of the previous version of the VAM3DF code, the dispersion coefficients are based on two parameters: the longitudinal dispersivity; and the transverse dispersivity (see section 2.3.3). The availability of only two dispersivities may be inappropriate for some situations (see discussion in Sections 3.2.3 and 3.6). To circumvent the dispersivity-related limitations, a new dispersion coefficient module has been added to the VAM3DF. The theoretical basis of the new hydrodynamic dispersion coefficient model, and verification results are presented in the following subsections.

3.2 GOVERNING EQUATIONS

3.2.1 Generalized Dispersion Coefficients

The generalized dispersion coefficients may be tensorially written as (Bear, 1972):

$$D_{ij} = a_{ijkm} \frac{u_k u_m}{|U|} + T_{ij} D_d \tag{3.1}$$

where

D_{ij}	=	Hydrodynamic dispersion coefficient tensor
T_{ij}	=	Tortuosity tensor
D_d	=	Molecular diffusion coefficient
a_{ijkm}	=	Dispersivity tensor
u_i	=	Velocity component in the i-th direction
$\|U\|$	=	Magnitude of velocity

3.2.2 Two-Parameter Dispersion Coefficients

According to Bear (1979), the dispersivity tensor in Equation (3.1) for isotropic media is shown below:

$$a_{ijkm} = a_T \delta_{ij} \delta_{km} + \left(\frac{a_L - a_T}{2} \right) (\delta_{ik} \delta_{jm} + \delta_{im} \delta_{jk}) \tag{3.2}$$

where

a_L	=	Longitudinal dispersivity

000032

a_T	=	Transverse dispersivity
δ_{ij}	=	Kronecker's delta

In the original VAM 3DF code, the above dispersivity tensor was used.

3.2.3 Multi-Parameter Dispersion Coefficients

The availability of only two dispersivity constants in Equation (3.2) may be inappropriate for the simulations of the following scenarios:

(1) Different magnitudes of transverse hydrodynamic dispersion in the vertical and horizontal directions

(2) Different magnitudes of longitudinal hydrodynamic dispersion in the vertical and horizontal directions

The above two scenarios may arise at sites with anisotropic hydrostratigraphic units. Simulations of these scenarios using the current VAM3DF code with two dispersivity constants usually result in unrealistic downward migration of contaminant concentration. To circumvent the dispersivity-related limitations, an additional dispersion coefficient module has been developed and incorporated into the VAM3DF code. This module is based on an assumption of transverse anisotropy (anisotropy with axial symmetry) of the geologic materials being simulated. This type of anisotropy is not uncommon in sedimentary aquifers.

For an anisotropic material with axial symmetry, the dispersivity tensor is given by (Bear, 1979):

$$\begin{aligned} a_{ijkm} = {} & \alpha_I \delta_{ij} \delta_{km} + \alpha_{II} (\delta_{ik}\delta_{jm} + \delta_{im}\delta_{jk}) \\ & + \alpha_{III} (\delta_{ij} h_k h_m + \delta_{km} h_i h_j) \\ & + \alpha_{IV} (\delta_{ik} h_j h_m + \delta_{jk} h_i h_m + \delta_{im} h_j h_k + \delta_{jm} h_i h_k) \\ & + \alpha_V h_i h_j h_k h_m \end{aligned} \tag{3.3}$$

where

α_I, α_{II}, α_{III}, α_{IV}, *and* α_V	=	Five independent dispersivity constants
h	=	Unit vector directed along the axis of symmetry

Assuming that: (1) the axis of symmetry points vertically upward, (2) α_V may be arbitrarily set to zero because it operates exclusively in the vertical direction, and (3) dispersion in the vertical direction is adequately described by the remaining four constants, the four remaining parameters are given below (Guvanasen, 1998):

$$
\begin{aligned}
\alpha_I &= \alpha_{TH} \\
\alpha_{II} &= \frac{1}{2}(\alpha_{LH} - \alpha_{TH}) \\
\alpha_{III} &= \alpha_{TV} - \alpha_{TH} \\
a_{IV} &= \frac{1}{4}((\alpha_{LV} - 2\alpha_{TV}) - (\alpha_{LH} - 2\alpha_{TH}))
\end{aligned}
\tag{3.4}
$$

where

α_{LH}	=	Longitudinal dispersivity in the horizontal direction
α_{LV}	=	Longitudinal dispersivity in the vertical direction
α_{TH}	=	Transverse dispersivity in the horizontal direction
α_{TV}	=	Transverse dispersivity in the vertical direction

The dispersion coefficient tensor may be generated using Equations (3.1), (3.3), and (3.4). For a perfectly horizontal flow along the horizontal plane, α_{LH} operates along the flow direction, α_{TH} operates normally to the flow direction in the horizontal plane, and α_{TV} operates normally to the flow direction in the vertical direction. For a perfectly vertical flow along the vertical axis, α_{LV} operates along the flow direction and α_{TV} operates normally to the flow direction. In this report, dispersion coefficients based on the above four parameters are verified using two flow directions: horizontal and vertical. Details of the verification are presented in Section 3.4.

3.3 NUMERICAL TREATMENT

There is no special numerical treatment for the new dispersion coefficients. The general equation for dispersion coefficient tensor, Equation (3.1) is used in conjunction with Equations (3.3) and (3.4) to generate all the elements in the tensor. With the use of the Total Variation Diminishing (TVD) solution scheme for the transport equation, there is no limitation on grid Péclet number. However, if the central differencing scheme is used without TVD, the grid Péclet number should be below 2.

3.4 VERIFICATION

3.4.1 Case 1 - 1-D Horizontal Flow

A definition sketch of Verification Case 1 is presented in Figure 3.1. This verification case involves one-dimensional flow in the horizontal direction along the x-direction, and three-dimensional transport.

Discretization details and parameter values used in all the verification runs are presented in Table 3.1. Because of symmetry, only one-quarter of the domain was discretized. To minimize the potential errors due to numerical dispersion and diffusion, the grid Péclet number (α_{LH}/Δ_x) along the flow direction was set to two.

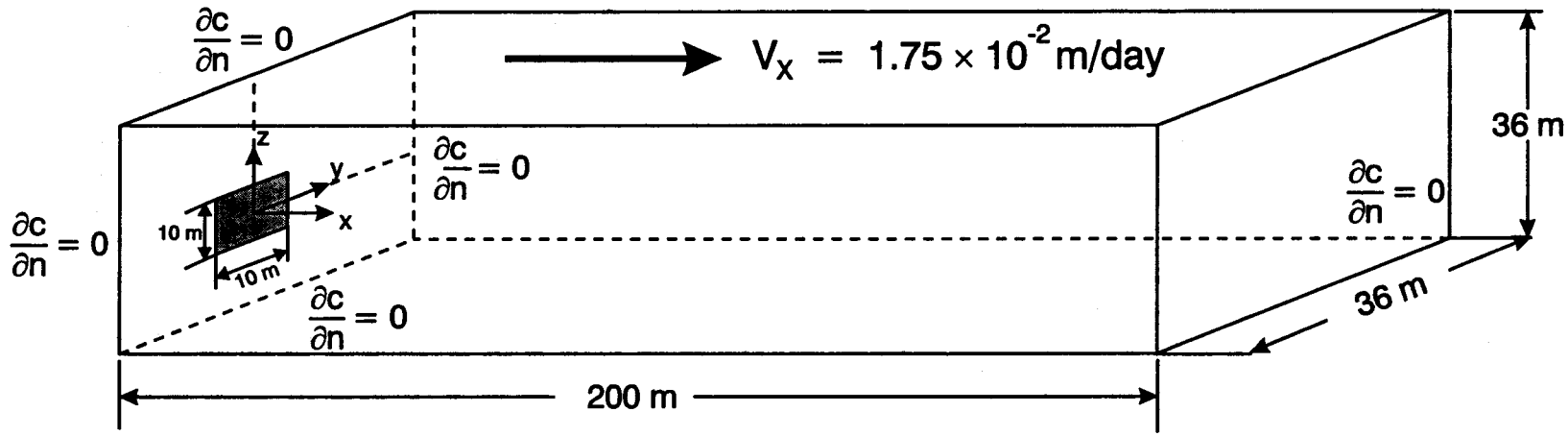

Figure 3.1 Definition Sketch, Verification Case 1.

000035

As shown in Figure 3.1, the following initial and boundary conditions apply.

Initial Condition

$$C(x,y,z,0) = 0 \tag{3.5}$$

where

$C(x,y,z,0)$	=	Initial contaminant concentration at $t=0$, and location x, y, z.
t	=	Time

Boundary Condition

Hydraulic heads at the upgradient and downgradient boundaries were prescribed such that the groundwater velocity in the x direction was 1.75 x 10^2 m/day and spatially uniform.

Concentration at the nodes representing the source area was fixed at 0.1 mg/ℓ. At other boundary nodes, zero concentration gradient was prescribed.

The new code was verified by comparing it against an analytical solution. An approximate analytical solution by Domenico and Robbins (1985) was used to verify VAM3DF. This analytical solution is shown below.

$$\frac{C}{C_o} = \frac{1}{8}\left[erfc\left(\frac{x-vt}{2\sqrt{\alpha_{LH}vt}}\right)\right]\cdot\left[erf\left(\frac{y+0.5W_y}{2\sqrt{\alpha_{TH}x}}\right) - erf\left(\frac{y-0.5W_y}{2\sqrt{\alpha_{TH}x}}\right)\right]\cdot\left[erf\left(\frac{z+0.5W_z}{2\sqrt{\alpha_{TV}x}}\right) - erf\left(\frac{z-0.5W_z}{2\sqrt{\alpha_{TV}x}}\right)\right] \tag{3.6}$$

where

C_o	=	concentration at the source
C	=	concentration
α_{LH}	=	Longitudinal dispersivity in the flow direction in the horizontal plane
α_{TH}	=	Transverse dispersivity normal to the flow direction in the horizontal plane
α_{TV}	=	Transverse dispersivity normal to the flow direction in the vertical plane
t	=	time
v	=	velocity along the x-directon
W_y	=	source dimension in the y-direction
W_z	=	source dimension in the z-direction

As shown in Figure 3.1, because of symmetry in the y- and z-directions, only one-quarter of the source in the y and z-directions was simulated. In the same figure, W_y = 10 m, W_z = 10 m.

Results

A comparison between the analytical solution and VAM3DF concentration profiles along the x- direction, and y- and z-directions, is presented in Figures 3.2 and 3.3, respectively. In the two figures, it may be observed that the agreement between VAM3DF and the analytical solution is very favorable.

3.4.2 Case 2 - 1-D Vertical Flow

A definition sketch of Verification Case 2 is presented in the attached Figure 3.4. This verification case involves one-dimensional flow in the vertical plane along the z-direction, and three-dimensional transport.

Discretization details and parameter values used in all the verification runs are presented in Table 3.1. To minimize the potential errors due to numerical dispersion and diffusion, the grid Péclet number ($\alpha_{LV}/\Delta z$) along the flow direction was set to two.

As shown in Figure 3.4, the following initial and boundary conditions apply.

Initial Condition

$$C(x,y,z,0)=0 \tag{3.7}$$

where

$C(x, y, z, 0)$	=	Initial contaminant concentration at $t=0$, and location x, y, z.
t	=	Time

Boundary Condition

Hydraulic heads at the top and bottom boundaries were prescribed such that the darcy velocity in the z-direction was 1.75×10^{-2} m/day.

Concentration at the nodes representing the source area was fixed at 0.1 mg/ℓ. At other boundary nodes, zero concentration gradient was prescribed.

VAM3DF was verified by comparing it against an approximate analytical solution by Domenico and Robbins (1985). This analytical solution is shown below.

$$\frac{C}{C_{max}} = \frac{1}{8}\left[erfc\left(\frac{z'-vt}{2\sqrt{\alpha_{LV}vt}}\right)\right]\cdot\left[erf\left(\frac{y'+0.5W_y}{2\sqrt{\alpha_{TV}z'}}\right)-erf\left(\frac{y'-0.5W_y}{2\sqrt{\alpha_{TV}z'}}\right)\right]\cdot\left[erf\left(\frac{x'+0.5W_x}{2\sqrt{\alpha_{TV}z'}}\right)-erf\left(\frac{x'-0.5W_x}{2\sqrt{\alpha_{TV}z'}}\right)\right] \tag{3.8}$$

000037

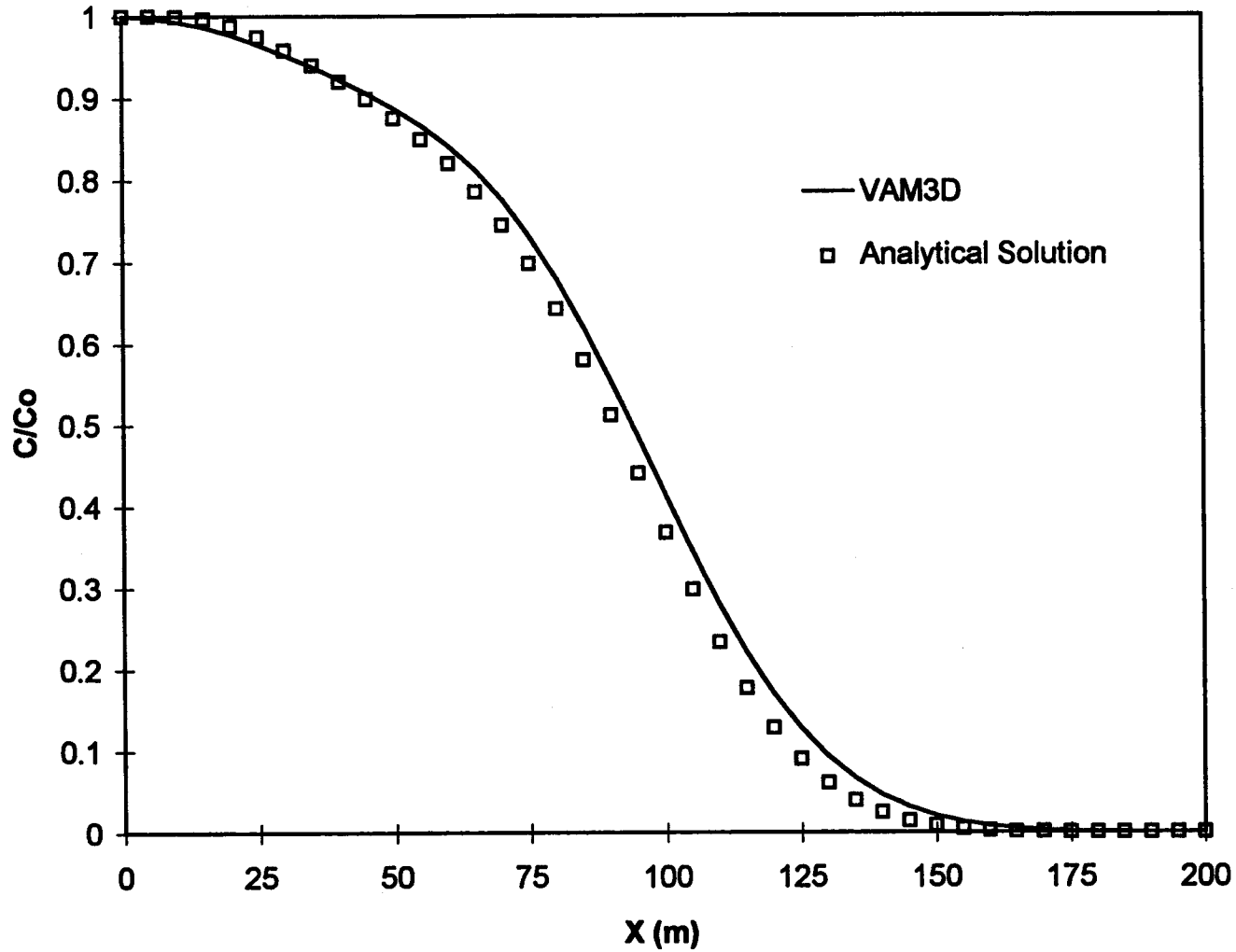

Figure 3.2 Concentration Profile Along the x-direction, at 2,000 days, Verification Case 1.

000038

1768

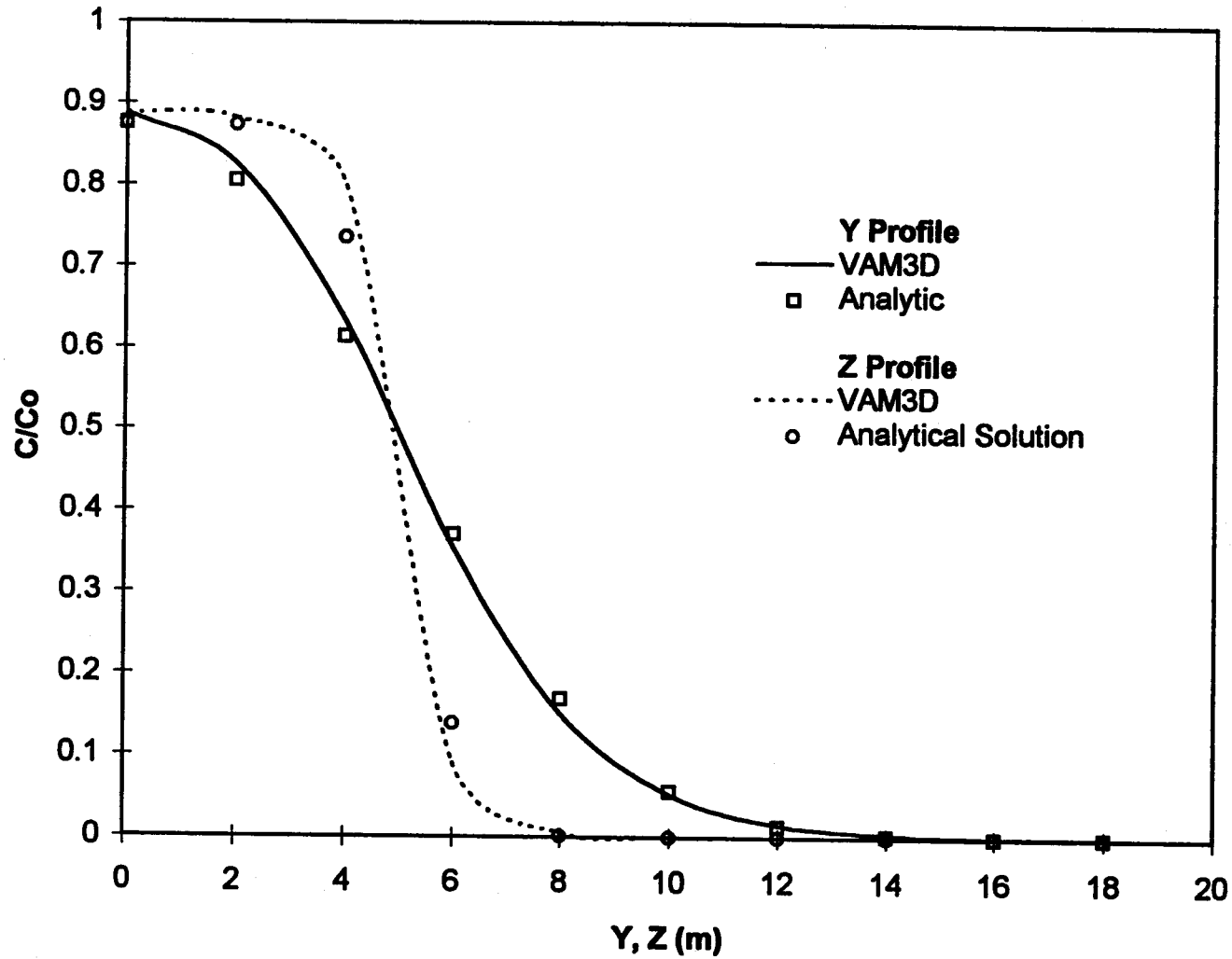

Figure 3.3 Concentration Profile Along the y- and z-directions at 2,000 Days, Verification Case 1.

000039

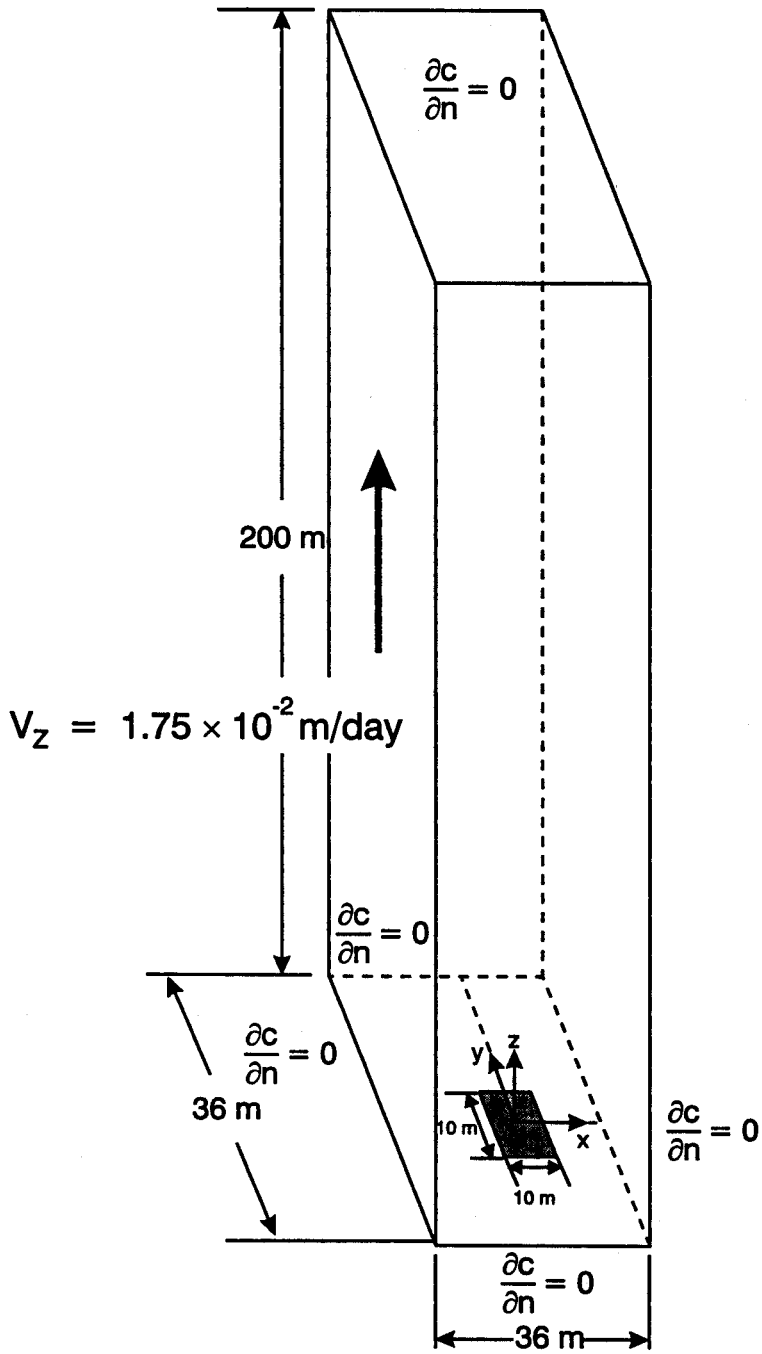

Figure 3.4 Definition Sketch, Verification Case 2.

where

v	=	Velocity along the z-direction
α_{LV}	=	Longitudinal dispersivity in the flow direction in the vertical plane
α_{TV}	=	Transverse dispersivity normal to the flow direction in the vertical plane
W_x	=	Source dimension in the x-direction
W_y	=	Source dimension in the y-direction

In Figure 3.4, W_x = 10 m, W_y = 10 m.

Results

A comparison between the analytical solution and VAM3DF concentration profiles along the z- direction, and x- and y-directions, is presented in Figures 3.5 and 3.6, respectively. In the two figures, it may be observed that the agreement between VAM3DF and the analytical solution is very favorable. Note that the concentration profiles in the x- and y-directions are identical.

3.4.3 Case 3 - 3-D Flow with Partially Penetrating Wells

A definition sketch of Verification Case 3 is presented in Figure 3.7. As shown, a partially penetrating well, in a confined aquifer, is located at some distance from a source. Because of symmetry, only one-half of the flow domain was discretized. Details of discretization and parameter values are given in Table 3.1. The maximum grid Péclet number in the x- and y-directions is two.

Because of symmetry, only one-half of the domain was discretized and simulated.

Case 3 is divided into three subcases with different dispersivity values. As shown in Table 3.1, the three subcases are categorically summarized below.

(i)	Case 3A	=	Four-dispersivity-based dispersion coefficients
(ii)	Case 3B	=	Three-dispersivity-based dispersion and coefficients ($\alpha_{LH} = \alpha_{LV}$)
(iii)	Case 3C	=	Two-dispersivity-based dispersion coefficients ($\alpha_{LH} = \alpha_{LV}$, $\alpha_{TH} = \alpha_{TV}$)

Initial Condition

$$C(x, y, z, 0) = 0$$

Boundary Conditions

No-flow and zero concentration gradient conditions were imposed on all boundaries. However, along the boundary on the right hand side (Figure 3.7), hydraulic heads were kept constant and concentration at the nodes representing the source area was maintained at 1 mg/ℓ. The flow field was generated by extracting groundwater at the well located 90 m from the source at the rate of 15 m^3/day. The well depth was set at 5 m as shown in Figure 3.7.

000041

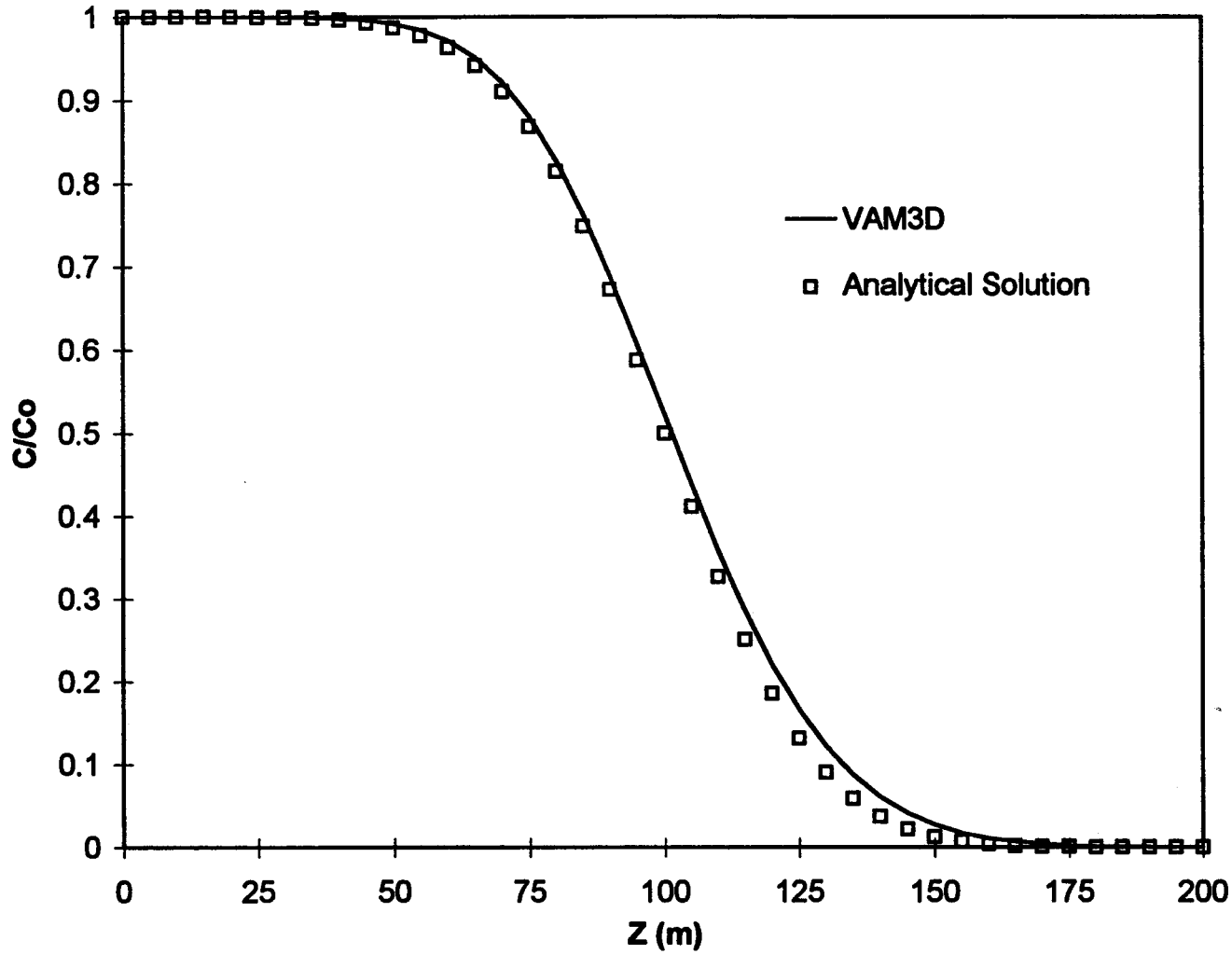

Figure 3.5 Concentration Profile Along the z-direction, at 2,000 Days, Verification Case 2.

000042

1768

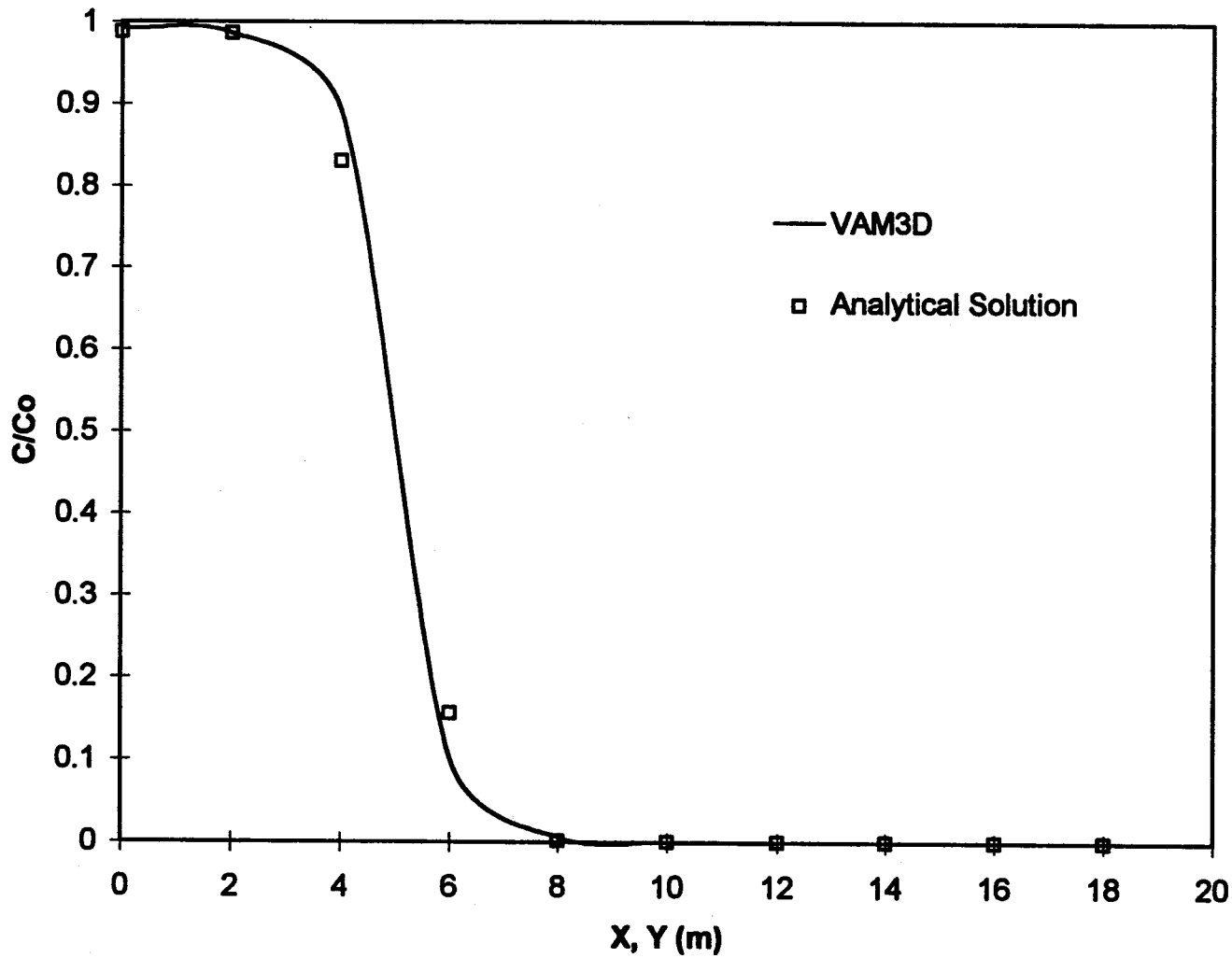

Figure 3.6 Concentration Profiles Along the x- and y-directions, at 2,000 Days, Verification Case 2.

000043

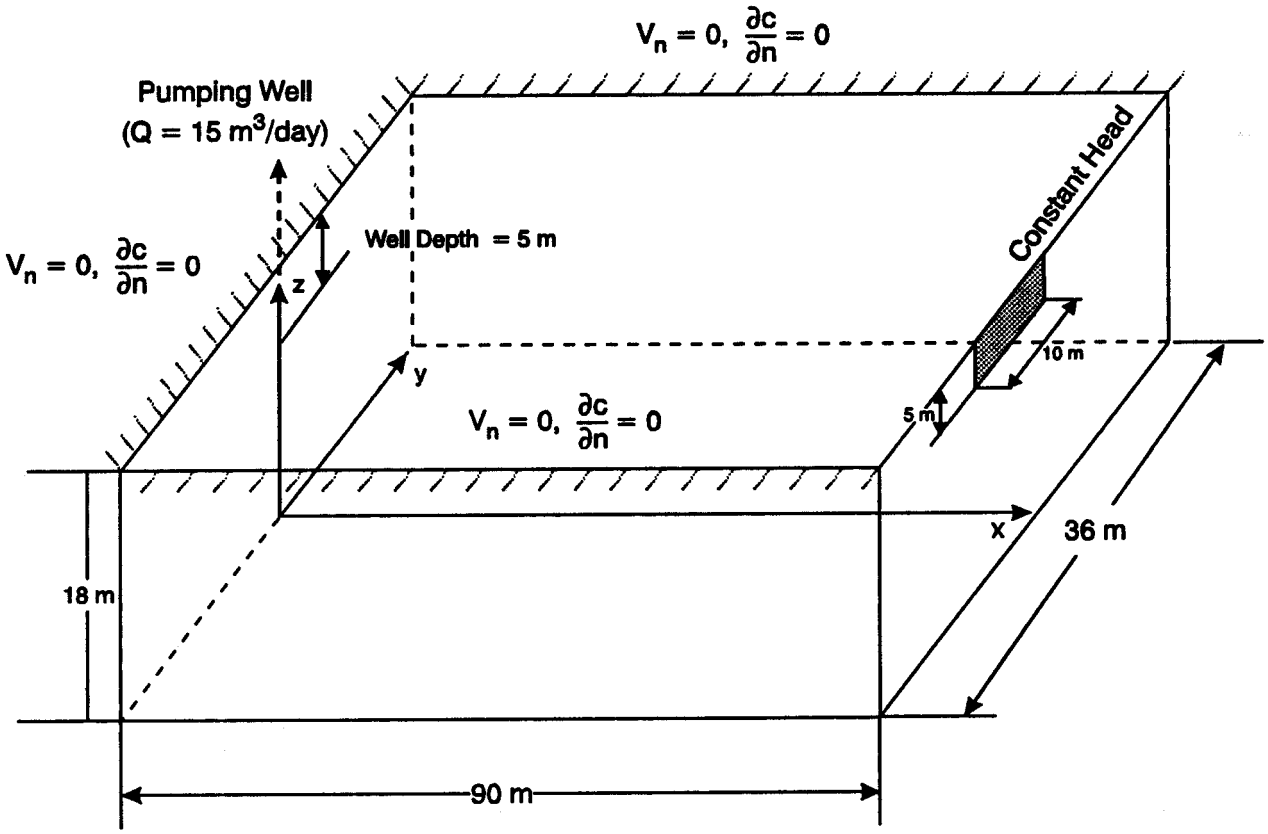

Figure 3.7

Figure 3.7 Definition Sketch, Verification Case 3.

Table 3.1
Parameters Used

PARAMETERS					
K (m/day)	1.0	1.0	8.0	8.0	8.0
Porosity	0.35	0.35	0.35	0.35	0.35
Velocity (m/day)	0.05	0.05 (V)	(*)	(*)	(*)
Δx (m)	5	2	10	10	10
Δy (m)	2	2	2	2	2
Δz (m)	2	5	2	2	2
Δt (m)	10	10	50	50	50
α_{LH} (m)	2.5	10	10	10	10
α_{TH} (m)	0.1	0.1	1	1	1
α_{LV} (m)	0.00	2.5	1	10	10
α_{TV} (m)	0.01	0.01	0.1	0.1	1

Note:
(V) Vertical velocity
(*) Spatially non-uniform

Results

Normalized concentration (C/C_{source}) contours for Cases 3A, 3B, and 3C, at 5,000 days on a vertical plane traversing the extraction well and the midpoint of the source are shown in Figure 3.8. An inspection of the three concentration distributions reveals that the degree of dispersion, especially in the vertical direction is dependent on the nature of dispersion coefficients. The coefficients based on two dispersivities resulted in the most dispersion especially near the extraction well where the vertical flow direction is prevalent. The least dispersion occurred when the four dispersivities were utilized.

3.5 PARAMETER ESTIMATION GUIDELINES

Owing to vertical anisotropy, dispersion coefficients are based on up to four dispersivity parameters: horizontal longitudinal and transverse dispersivities, and vertical longitudinal and transverse dispersivities. The four-parameter model may be required to avoid excessive vertical dispersion that can occur with a lower-order (fewer-dispersivity) model.

Parameters estimation may be performed using DFM, which has the flexibility to view dispersivity parameters as constants over the model domain, constants within zones, or as heterogeneous parameters having geostatistical variation. Geostatistical variation can be viewed as a polynomial trend plus a spatially correlated process with a correlation distance and a standard deviation. Calibration parameters are a combination of constants, zonal constants, trend coefficients, and values of the spatially correlated process. Guidance for determining prior information about calibration parameter estimates and uncertainties can be obtained from previous data, data analysis, and the literature.

Initial values for the horizontal longitudinal and transverse dispersivities can be obtained from preliminary model calibration and the literature. Because of the backward collapsibility of the muliple-dispersivity model, guidance for the initial values of the dispersivities can be based on a lower-order model. It is known that the vertical transverse dispersivity of Burnett and Frind (1987) is a fraction of the horizontal transverse dispersivity. Similarly, based on field observations close to pumping wells, it is anticipated that the vertical longitudinal dispersivity is a fraction of the horizontal longitudinal dispersivity. These observations may be incorporated as constraints in the DFM. DFM can calibrate both horizontal and vertical parameters based on the constraint that the vertical parameters are fractions of the horizontal parameters.

It is believed that there are enough data for unique calibration when the number of data points over time, that are available for calibration targets, are considered. Consequently, DFM will allow for the determination of realistic dispersivities while still achieving a reasonably unique model. DFM will determine the dispersivities by minimizing data fit residuals subject to physical model and prior information constraints. The dispersivities will be realistic because DFM has the flexibility to incorporate the realistic four-parameter model. The model will be reasonably unique because DFM can incorporate prior information and data over time. It should be noted that the four-dispersivity model (and DFM) can always be degraded to a lower-order (two- or three-dispersivity) model (if considered appropriate) by prescribing the following constraints:

$$\alpha_{LV} = \alpha_{LH} \quad \text{(for the three-dispersivity model)}$$

and

$$\left.\begin{aligned} \alpha_{TV} &= \alpha_{TH} \\ \alpha_{LV} &= \alpha_{TH} \end{aligned}\right\} \text{(for the three-dispersivity model)}$$

3.6 DISCUSSION

Some of the dispersivity-related problems include:

- Excessive dispersion in the vertical direction where the vertical flow direction is significant; and
- Excessive horizontal dispersion in the vadose zone.

Because of the vertical anisotropy, the existing two-dispersivity model is not adequate for either of the two problems. Neither is the three-dispersivity model. The latter is appropriate only when the vertical velocity is absent. In our experience, the problems could be very much alleviated, if not eradicated, by the four-dispersivity model.

All the multiple-dispersivity models are related in the sense of backward compatibility and collapsibility. The four-dispersivity model becomes the three-dispersivity model when the two longitudinal dispersivities are set equal. The three-dispersivity model becomes the two-dispersivity model when the two lateral dispersivities are set equal. Each multiple-dispersivity model represents an incremental improvement and realism over the immediately lower multiple-dispersivity model.

Models are normally less unique or overparameterized when parameters which cannot be substantiated are used. In the case of additional dispersivities in the multiple-dispersivity models, each dispersivity is a subset of the five-dispersivity model for transversely anisotropic materials which represent most of sedimentary materials in aquifers. The vertical lateral dispersivity and the vertical longitudinal dispersivity are based on a firm theoretical basis which is consistent with field observations. The four parameters will be determined based on physical constraints (e.g., α_{LV} is a fraction of α_{LH}, and α_{TV} is a fraction of α_{TH}), prior information of the dispersivity values, and observed concentration data over time. When the physical flow and transport models are used in DFM to relate the physical constraints, prior information, and data overtime, it is believed that there is adequate information to identify spatial distribution of the four dispersivities.

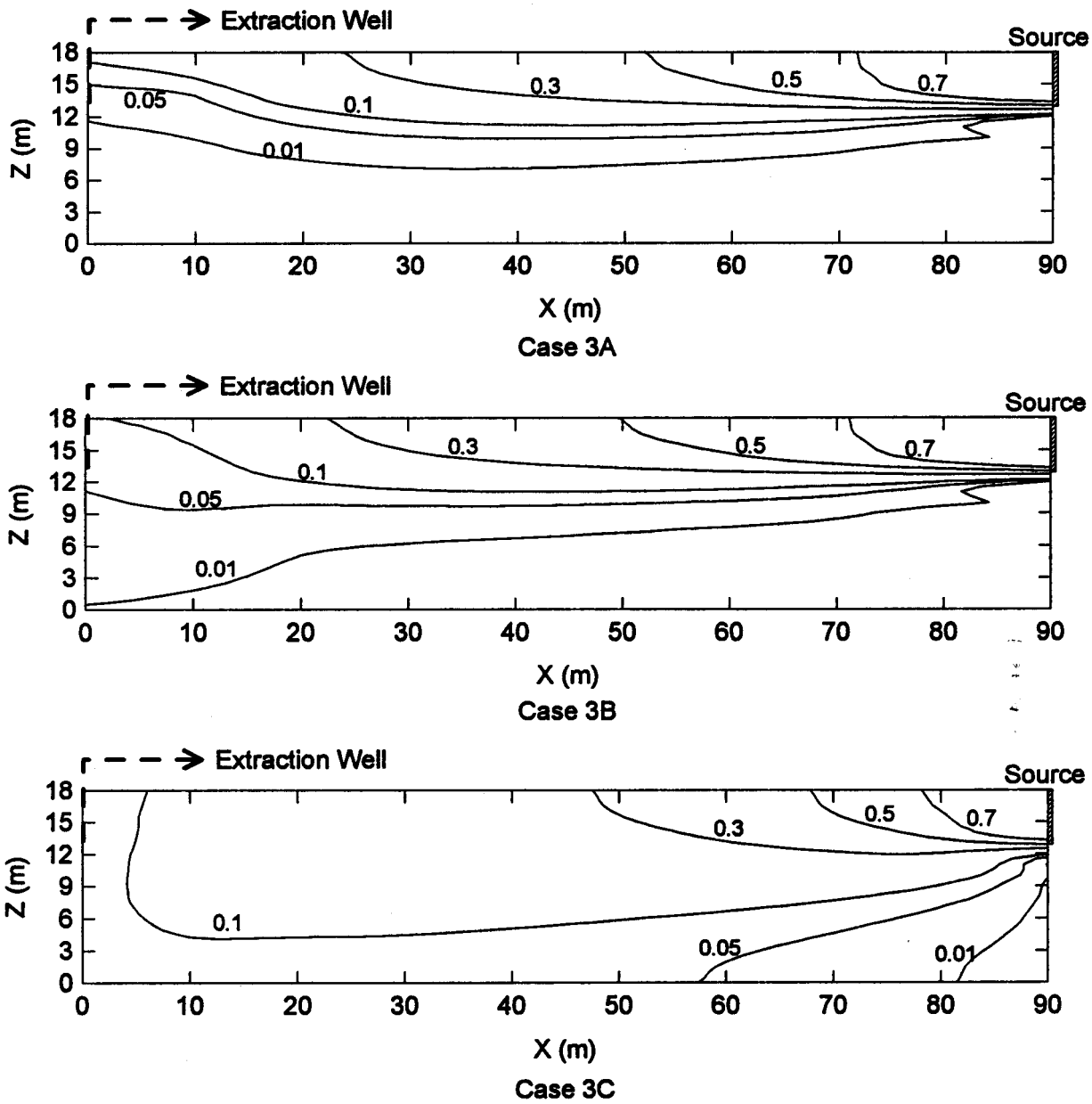

Figure 3.8 **Concentration Distribution on a Vertical Plane Traversing the Extraction Well and the Midpoint of the Source, at 5,000 Days.**

4.0 KINETIC CONTAMINANT MASS TRANSFER BETWEEN LIQUID AND SOLID PHASES

4.1 PURPOSE

The general VAM3DF model discussed earlier has been extended here to include kinetic mass transfer between liquid and solid phases, to incorporate conditions occurring at several contaminated sites where equilibrium assumptions would be in error. Mass transfer processes discussed here include adsorption, desorption, chemisorption, precipitation, and dissolution. Adsorption refers to mass transfer from water to soil grains, with the reverse process being referred to as desorption. Precipitation and dissolution are similarly, reversible processes. Chemisorption refers to an irreversible process whereby adsorbed material is transformed into a bonded state from which it cannot be released. This section discusses the respective governing equations, mass transfer assumptions, numerical procedures, and verification problems for kinetic mass transfer reactions. Finally, the behavior of the kinetic mass transfer reactions is examined with respect to the various rate parameters.

4.2 GOVERNING EQUATIONS FOR KINETIC MASS TRANSFER AMONG PHASES

The contaminant transport equation for a partially saturated porous medium with kinetic mass transfer for adsorption and precipitation may be written in the primitive form for the water phase as

$$\frac{\partial}{\partial t}(\phi S_w C_w) - qC_w^* + R_{ws} - R_{sw} + R_p - R_d = \frac{\partial}{\partial x_j}\left[D_{ij}\frac{\partial C_w}{\partial x_j}\right] - \frac{\partial}{\partial x_i}\left(v_i C_w\right) \tag{4.1}$$

where t is time, ϕ is the effective porosity, S_w is the water saturation, C_w is solute concentration in terms of mass of solute per volume of solution, q is the volumetric flow rate via sources (or sinks) per unit volume of porous medium, C_w^* is the solute concentration of the sources (or sinks). R_{ws} is the rate of mass transfer of solute from water to solid phase (adsorption), R_{sw} is the rate of mass transfer of contaminant from solid to water phase (desorption), R_p is the rate of precipitation of contaminant, R_d is the rate of dissolution, x_i are the three principal coordinate directions, D_{ij} is the apparent hydrodynamic dispersion tensor, and v_i is the Darcy velocity. Mass transfer to the air phase is neglected, and decay terms are omitted from Equation (4.1).

The mass balance equation for contaminant on the solid phase may be written as

$$\frac{\partial}{\partial t}\left(\rho_B C_s\right) - R_{ws} + R_{sw} + R_c = 0 \tag{4.2}$$

where ρ_B is the bulk density, C_s is the mass fraction of contaminant on soil, and R_c is the rate at which contaminant moves from the adsorbed state to a bonded chemisorbed state.

The continuity equation for mass of contaminant in the chemisorbed state may be written as

$$\frac{\partial}{\partial t}\left(\rho_B C_{sr}\right) - R_c = 0 \tag{4.3}$$

where C_{sr} is the mass fraction of contaminant in the chemisorbed state on soil (i.e., mass of contaminant in chemisorbed state/mass of soil).

Finally, the mass conservation equation of the precipitated phase may be written as

$$\frac{\partial}{\partial t}\left(M_p\right) - R_p + R_d = 0 \tag{4.4}$$

where M_p is the mass of precipitated phase per unit volume of porous medium.

The mass transfer rates between the solution and adsorbed state may be expressed as

$$R_{ws} = \alpha_a \phi S_w C_w \tag{4.5}$$

and

$$R_{sw} = \alpha_d \ \rho_B \ C_s \tag{4.6}$$

where α_a is the adsorption rate coefficient (t^1) and α_d is the desorption rate coefficient (t^1). Note that under equilibrium conditions, mass transfer across the interface between water and soil solid phases is equal in both directions, and $R_{ws}=R_{sw}$. Therefore, combining Equations (4.5) and (4.6) we have

$$\frac{C_s}{C_w} = \frac{\alpha_a \phi S_w}{\alpha_d \rho_B} \tag{4.7}$$

where C_s/C_w is the slope on a linear equilibrium isotherm, K. Now α_a is modeled as a function of solid concentration, C_s, depicting a change in available adsorption sites with a change in the mass already adsorbed. The Freundlich isotherm may be written to model this as

$$C_s = k_d C_w^n \tag{4.8}$$

000050

which gives

$$\frac{C_s}{C_w} = \frac{k_d^{1/n}}{C_s^{\left(\frac{1-n}{n}\right)}} \tag{4.9}$$

where n is the Freundlich isotherm exponent.

Incorporating Equation (4.9) into (4.7) gives

$$\alpha_a = \frac{k_d^{1/n} \alpha_d \rho_B}{C_s^{\left(\frac{1-n}{n}\right)} \phi S_w} \tag{4.10}$$

The mass transfer rate for contaminant from the adsorbed state to a bonded chemisorbed state may be expressed as

$$R_c = \alpha_c \rho_B C_s \tag{4.11}$$

where α_c is the chemisorption rate constant (t^{1}). Mass transfer rates for precipitation and dissolution are expressed as

$$R_p = \begin{cases} \alpha_p \phi S_w C_w & \text{if } C_w \geq C_{SL} \\ 0 & \text{if } C_w < C_{SL} \end{cases} \tag{4.12}$$

and

$$R_d = \begin{cases} \alpha_s & \text{if } M_p > 0 \\ 0 & \text{if } M_p = 0 \end{cases} \tag{4.13}$$

where α_p is the precipitation rate constant (t^{1}), C_{SL} is the solubility limit ($M\ L^{-3}$) and α_s is the zero-th solubilization rate ($ML^{-3}t^{-1}$)assumed to be a constant. These equations fully describe reversible/non-reversible contaminant mass transfer conditions between solid and liquid phases.

The mass transfer terms, R_{ws}, R_{sw}, R_p and R_d are incorporated into the water phase mass balance equation of VAM3DF and the mass balance Equations (4.2), (4.3), and (4.4) for adsorbed, chemisorbed, and precipitated states respectively are solved using the Galerkin finite element method subject to initial conditions for C_w, C_s,C_{sr}, and M_p, and boundary conditions for the water phase equations as prescribed by VAM3DF. Note that Equations (4.2), (4.3), and (4.4) do not contain mass transport terms between nodes.

4.3 NUMERICAL TREATMENT

Equations (4.1), (4.2), (4.3). and (4.4) are solved in an iterative sequential solution fashion for C_w, C_s, C_{sr}, and M_p, respectively. The Cooley (1983) algorithm is applied to each equation to dampen flip-flop behavior between iterations. Automatic time step reduction and marching procedures used to handle convergence difficulties are discussed in the VAM3DF document (HydroGeoLogic, 1995) in relation to nonlinearities of the unsaturated flow equation.

The water phase mass balance equation requires the terms R_{ws}, $-R_{sw}$, R_p, and $-R_d$ (as expressed by Equations (4.5), (4.6), (4.12), and (4.13)) to be added to the transport matrix assembled by VAM3DF. R_{ws} and R_p contain C_w as a variable, which may be updated via the global equation matrix (LHS) or via the right-hand-side (RHS) vector, while R_{sw} and R_d are assembled into the RHS vector. Thus, for θ_2 being a general updating factor varying between 0 (for RHS vector update) and 1 (for LHS matrix update), the additional terms required on the LHS matrix of the transport equation for each node are

$$\theta_2\left[\alpha_a \phi S_w + \alpha_p \phi S_w H\left(C - C_{SL}\right)\right]\forall \tag{4.14}$$

where $\forall$ is the nodal volume and H is the Heavyside step function. The additional terms required on the RHS vector of the transport equation for each node assembled by VAM3DF are

$$\left(\theta_2 - 1\right)\left(\alpha_a \phi S_w C_w + R_p\right) + \alpha_d \rho_B C_s + R_d \tag{4.15}$$

where equation (4.15) is computed using the latest iterate values for C_w, C_s, and M_p. The mass balance equation for the adsorbed solute, Equation (4.2), is assembled for C_s with the terms R_{sw} and R_c being updated either on the LHS matrix or on the RHS vector, and the term R_{ws} being assembled on the RHS vector. The LHS matrix for he adsorbed contaminant may be written as

$$\text{LHS} = \left[\frac{\rho_B}{\Delta t} + \alpha_d \rho_B + \alpha_c \rho_B\right]\forall \tag{4.16}$$

where $\forall$ is the nodal volume and Δt is the time-step size. The RHS vector for adsorbed contaminant may be written as

$$\text{RHS} = \left[\frac{\rho_B}{\Delta t} C_s^{\circ} + \alpha_a \, \phi \, S_w \, C_w \right] \forall \tag{4.17}$$

where C_s° is the adsorbed concentration at the previous time step and C_w is the latest iterate value of water phase concentration.

The mass balance equation for chemisorbed contaminant, Equation (4.3), is assembled for C_{sr} as

$$\text{LHS} = \frac{\rho_B}{\Delta t} \forall \tag{4.18}$$

and

$$\text{RHS} = \left[\frac{\rho_B}{\Delta t} C_{sr}^{\circ} + \alpha_c \, \rho_B \right] \forall \tag{4.19}$$

Finally, the mass balance equation for precipitated mass, Equation (4.4), is assembled for M_p as

$$\text{LHS} = \left[\frac{1}{\Delta t} + \alpha_p \, \phi \, S_w \, H \left(C_w - C_{SL}\right)\right] \forall \tag{4.20}$$

and

$$\text{RHS} = \left[\frac{M_p^o}{\Delta t} + R_d\right] \forall \tag{4.21}$$

Each equation is solved for its respective variable with application of Cooley's (1983) underrelaxation factor before proceeding to the next iteration. Convergence is achieved when all variables are below their respective tolerance limits. Note that the chemisorbed equation (4.3) and its discretized form (4.19) and (4.20) is a linear equation; however, it is retained in the iteration loop.

000053

4.4 VERIFICATION PROBLEMS

The additional modules incorporated into VAM3DF to model kinetic mass transfer of contaminant between liquid and solid phases, are individually verified against a series of analytical solutions. The examples below demonstrate proper operation of all aspects of the code pertaining to the kinetic mass transfer modules.

4.4.1 Verification Problem 1. Verification of Mass Transfer with Dissolution and Precipitation

The terms R_{ws}, - R_{sw}, R_p, and - R_d in equation (4.1) may be expanded using (4.5), (4.6), (4.12), and (4.13) with $C_{SL} = 0$ to give

$$R_{ws} - R_{sw} + R_p - R_d = -\alpha_d \rho_B C_s + \alpha_s + (\alpha_a \phi S_w + \alpha_p \phi S_w) C_w$$

Further, with the Freundlich exponent $n=1$ we have

$$\alpha_a = \frac{k_d \alpha_d \rho_B}{\phi S_w}$$

Assuming steady state one-dimensional flow, Equation (4.1) can be expressed as

$$A\frac{\partial C_w}{\partial t} + B + CC_w = D\frac{\partial^2 C_w}{\partial x^2} - v\frac{\partial C_w}{\partial x}$$

where $A = \phi S_w$; $B = \alpha_s - \alpha_d \rho_B C_s$; $C = k_d \alpha_d \rho_B + \alpha_p \phi S_w$; D is the diffusion coefficient and v is the velocity along the x direction. This equation has an analytical solution (Van Genuchten and Alves, 1982). Figure 4.1 shows C_w vs time for the analytical and numerical solutions at $x = 1.0$ m with $\phi = 0.45$, $S_w = 1$, $\alpha_s = 0.05$, $\alpha_d = 0.0$, $\rho_B = 1.46$, $k_d = 1.0$, $\alpha_p = 0.25$, and $v = 0.25$ m/d. The numerical solution is obtained for a 2.0 m horizontal soil column with initial conditions $C_w = C_s = C_{sr} = M_p = 0$ and the left boundary being a Dirichlet condition of $C_w = 100$ mg/L. Δx was 0.1 m and Δt was determined automatically by the code. Comparison of the two solutions shows good agreement, thus the kinetic mass transfer terms in the water phase mass balance equation are behaving appropriately. Note that α_d was set to zero to prevent the nonlinearity of C_s from entering the solution (B is a constant), thus precipitation and dissolution only were tested without considering adsorption and desorption for this example. The excellent mass balance (error $= 10^{-6}$) indicates that the precipitated phase mass balance equation is accumulating mass appropriately.

000054

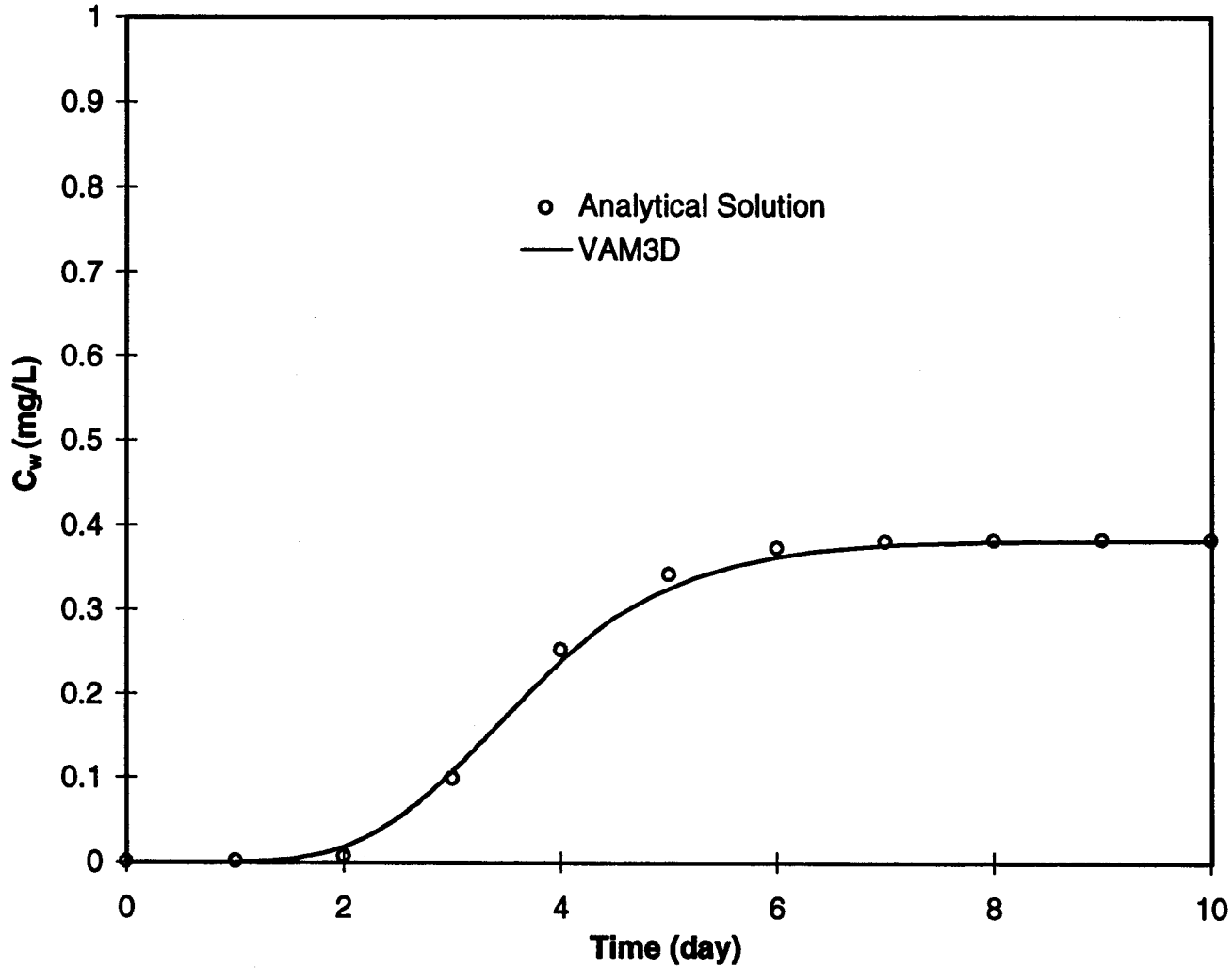

Figure 4.1 C_s vs Time for Verification Problem 1 (Mass Transfer with Dissolution and Precipitation).

000055

17698

4.4.2 Verification Problem 2. Verification of Mass Transfer with Chemisorption

Mass transfer with Chemisorption was verified using the equation for decay of a contaminant,

$$\frac{\partial C}{\partial t} + AC + B = 0$$

which has an analytical solution given by (van Genuchten and Alvis, 1982)

$$C = \frac{B(e^{-At} - 1)}{A}$$

where C is the concentration and A and B are coefficients of first-order and zeroeth-order terms. The solid phase mass balance equation (4.2) is analogous to this if the Freundlich isotherm exponent $n=1$, $C_{SL}=0$, and

$$B = -k_d \alpha_d C_w$$

and

$$A = \alpha_d + \alpha_c$$

A one-element (8 node) problem was setup for this verification problem with initial conditions $C_w=1$ mg/L, $C_s=C_{sr}=M_p=0$, and all 8 nodes maintaining $C_w=1$ as a first type boundary condition. Figure 4.2 shows C_s versus time for the analytical and numerical solutions with values of $k_d=1$, $\alpha_d=0.1$ and $\alpha_c=0.0$. The comparison of the two solutions is excellent, showing that the solid phase mass balance equation is behaving appropriately. Further, with a mass balance error of 10^{-6} the desorption term appearing in the water phase equation is behaving appropriately therefore ensuring that this term is correctly solved in the water phase equation. Figure 4.2 also shows C_s versus time for the analytical and numerical solutions, with $\alpha_c=0.01$, showing good comparison. Further, with a mass balance error of 10^{-6}, this shows that chemisorbed mass is being generated correctly; therefore, the chemisorbed phase equation is also behaving appropriately.

4.5 BEHAVIOR OF KINETIC MASS TRANSFER BETWEEN LIQUID AND SOLID PHASE

This section discusses the C_s versus C_w behavior simulated by the kinetic mass transfer equations discussed earlier. The intent here is to examine this behavior for various combinations of the kinetic rate parameters, fluid fluxes, contamination duration, and flushing duration. A systematic examination of this behavior also provides an understanding of the effects of these parameters and the processes they represent.

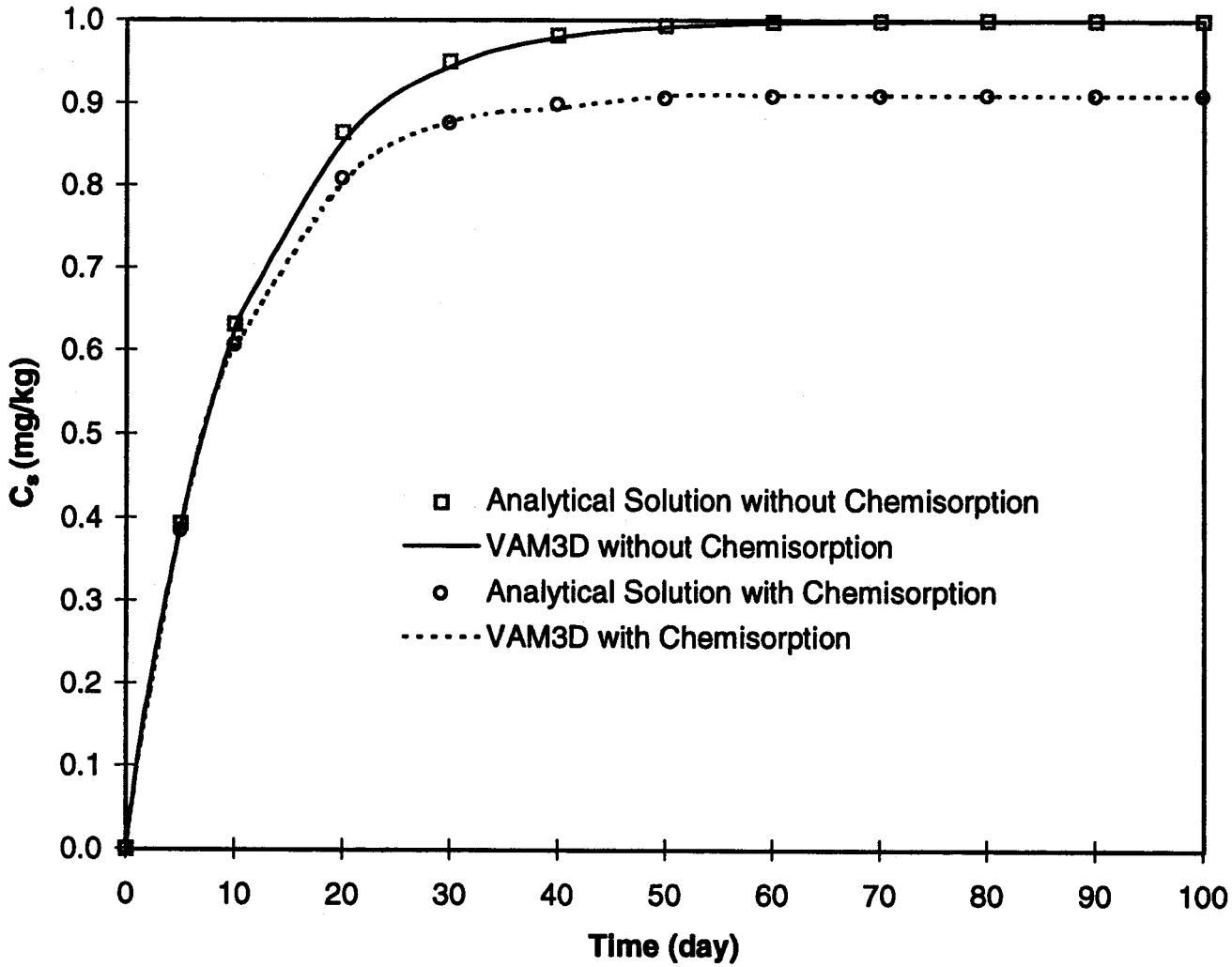

Figure 4.2 C_s vs Time Verification Problem 2 Mass Transfer with (Chemisorption).

0000557

1768

The problem configuration and domain geometry are depicted in Figure 4.3. Initially, the domain is free of all contaminants (i.e., $C_w=C_s=C_{sr}=M_p=0$), and flow is from left to right with Darcy velocity V. A Dirichlet boundary condition of $C_w=1$ mg/ℓ is provided on the left boundary for the first stress period of duration t_1, after which this boundary becomes $C_w=0$ mg/ℓ for the second stress period to allow flushing of the system for duration t_2.

The first study case examined considers linear adsorption and desorption only (i.e., Freundlich exponent $n=1$, $\alpha_c=\alpha_p=\alpha_s=0$). Further, for this case $V=1$ *m/d*, $t_1=1{,}000$ d, $t_2=5{,}000$ d, and the remaining parameters are noted on Figure 4.3. Figure 4.4 shows the C_s versus C_w curve for this case. It is noted that for this small velocity, the liquid and absorbed phase concentrations are very close to the equilibrium concentration line.

For the second study case, V was increased to 10 m/d. Figure 4.5 shows the C_s versus C_w curve for this case, which further deviates from the equilibrium curve than those in Figure 4.4, but maintains its rotational symmetry. Smaller V with its long residence times for water is therefore noted to have curves closer to equilibrium than larger V.

For the third and fourth study cases, a nonlinearity is introduced to the first and second cases respectively, by changing the Freundlich exponent from 1 to 0.5. Figure 4.6 shows the C_s versus C_w curve for the third case with $V=1$ m/d and Figure 4.7 shows the C_s versus C_w curve for the fourth case with $V=10$ m/d. Again, the longer residence times of Figure 4.6 allow for the curves to show smaller hysteretic behavior than for the higher velocities of Figure 4.7. The effect of the nonlinearity is noted to follow that of the equilibrium curves for both cases; however, neither case achieved equilibrium before the flushing period began.

The fifth study case was modified from the fourth by decreasing the Freundlich exponent to 0.2. Figure 4.8 shows that the C_w-C_s paths also follow the equilibrium curve, with the hysteresis less than the case with larger Freundlich exponent (the fourth study case).

The sixth study case includes chemisorption, with $\alpha_c = 0.0001$. The remaining parameters are the same as those in the fourth case discussed earlier. Figure 4.9 shows that for this case, the C_w - C_{stotal} curve closely follows that of the fourth case (Figure 4.7); however, the flushing curve retains the chemisorbed component after the completion of flushing. Note that C_{stotal} is the sum of absorbed and chemisorbed concentrations.

Figure 4.10 shows C_s versus C_w for the seventh study case which differs from the sixth case in that the contamination duration t_i, was extended to 4,000 *d*. The larger residence time is noted to increase the residual (chemisorbed) concentration in the solids after flushing. The eighth study case mimics the seventh, with the Freundlich exponent decreased to 0.2 (from 0.5). Figure 4.11 shows the C_s versus C_w curve for the eighth case.

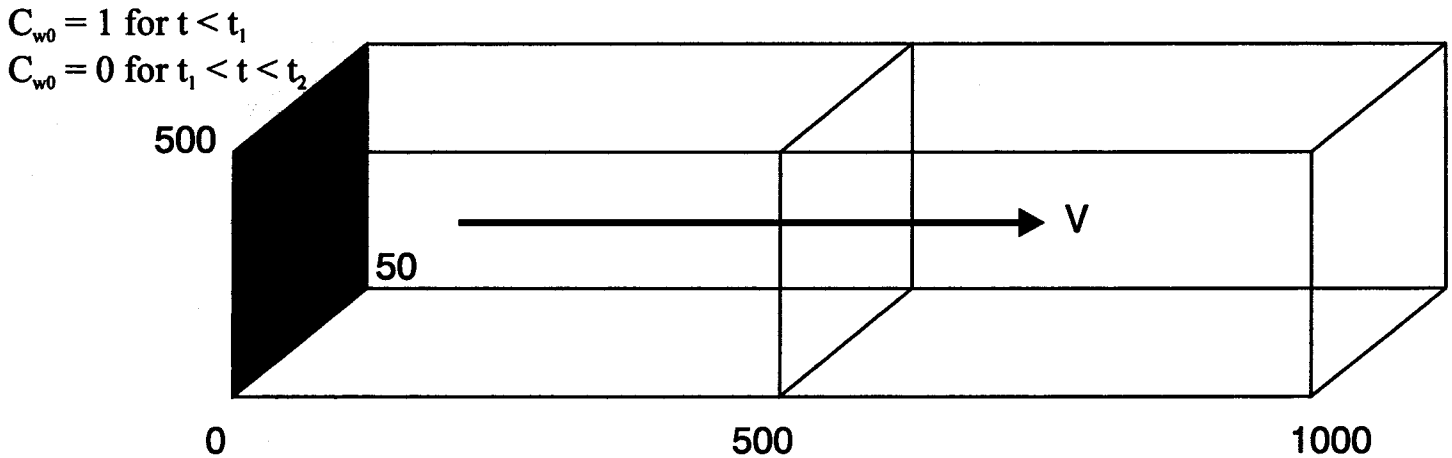

α_L = longitudinal dispersivity = 1
α_T = transverse dispersivity = 1
ϕ = effective porosity = 0.3
$\int_B$ = bulk density = 0.3

Figure 4.3 Problem Setup and Domain Geometry.

000059

1768

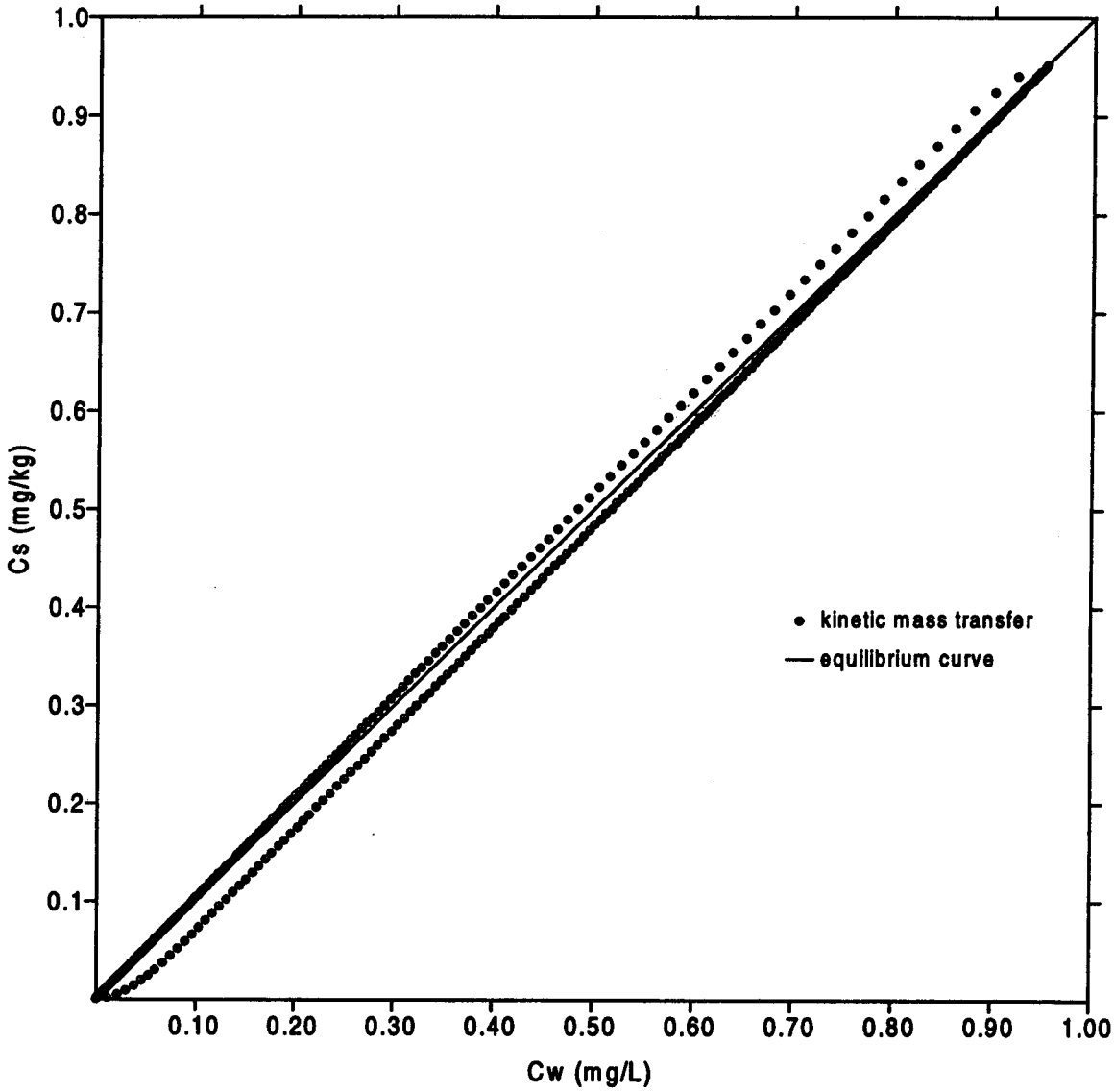

Figure 4.4 C_s vs C_w for the First Study Case (Linear Desorption/Adsorption at low groundwater velocity).

000060

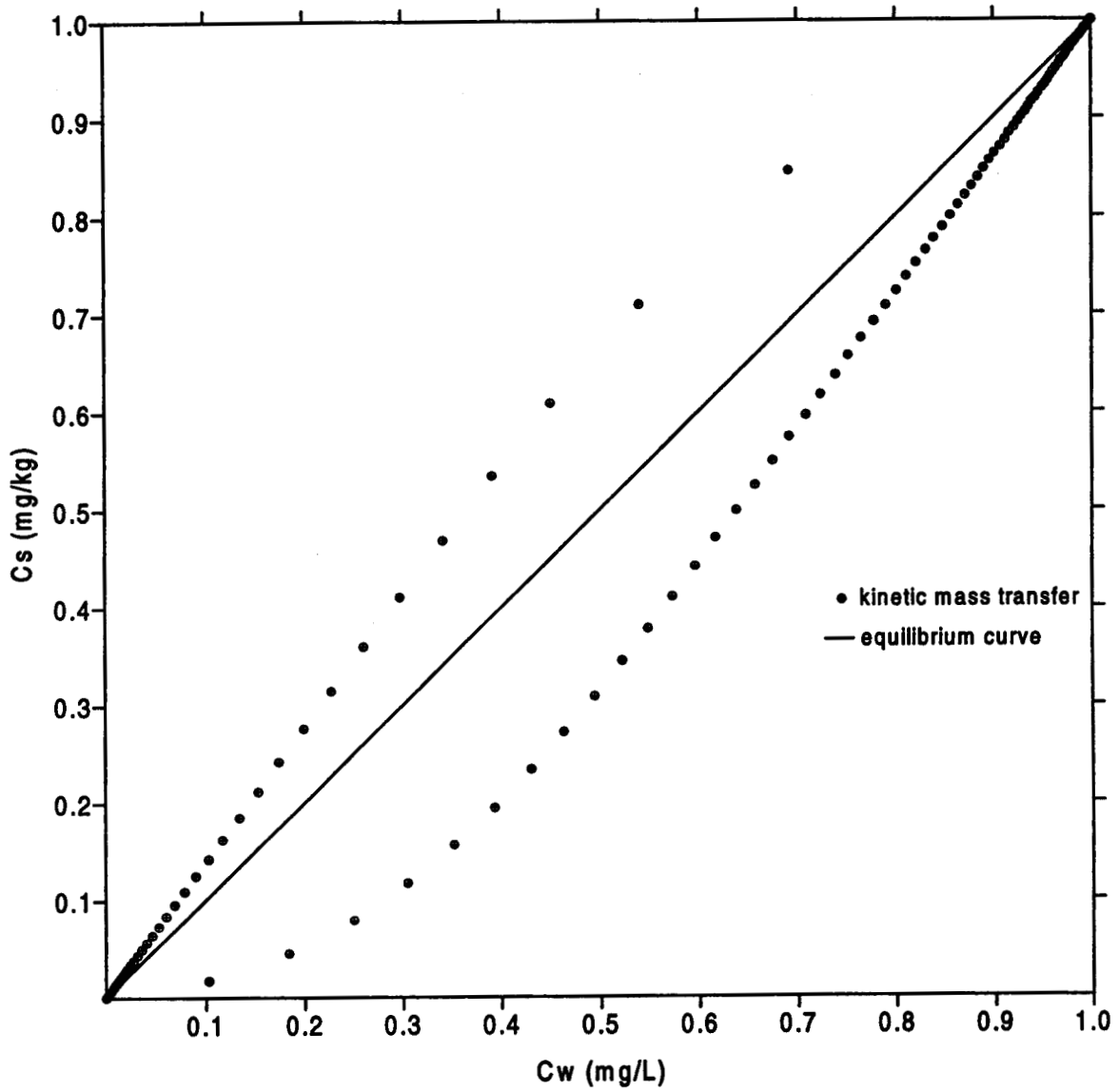

Figure 4.5 C_s vs C_w for the Second Study Case. (Linear adsorption desorption at high groundwater velocity).

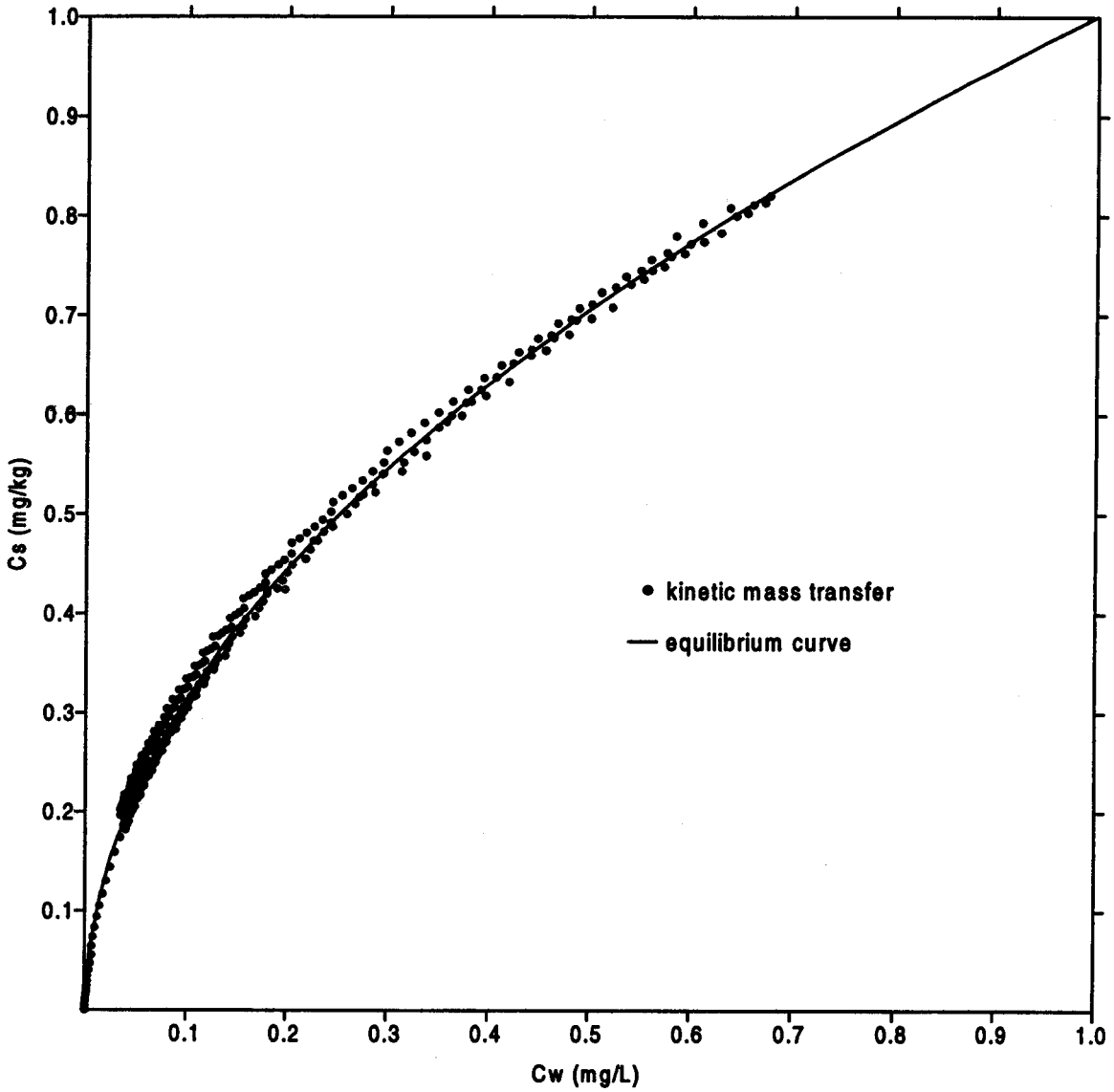

Figure 4.6 C_s vs C_w for the Third Study Case. (Non-linear adsorption/desorption at low groundwater velocity).

000062

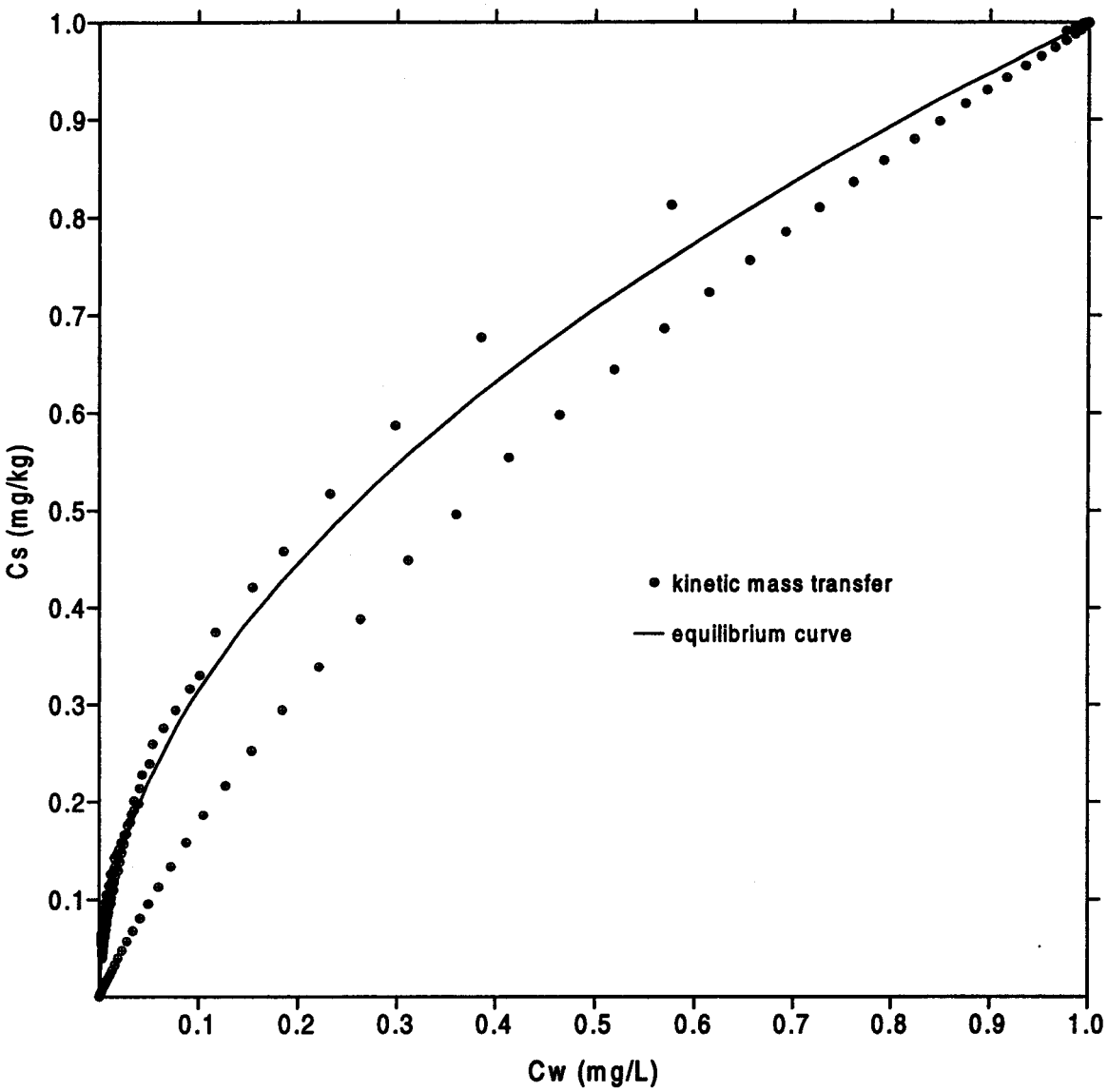

Figure 4.7 **C_s vs C_w for the Fourth Study Case. (Non-linear adsorption/desorption at high groundwater velocity, n = 0.5).**

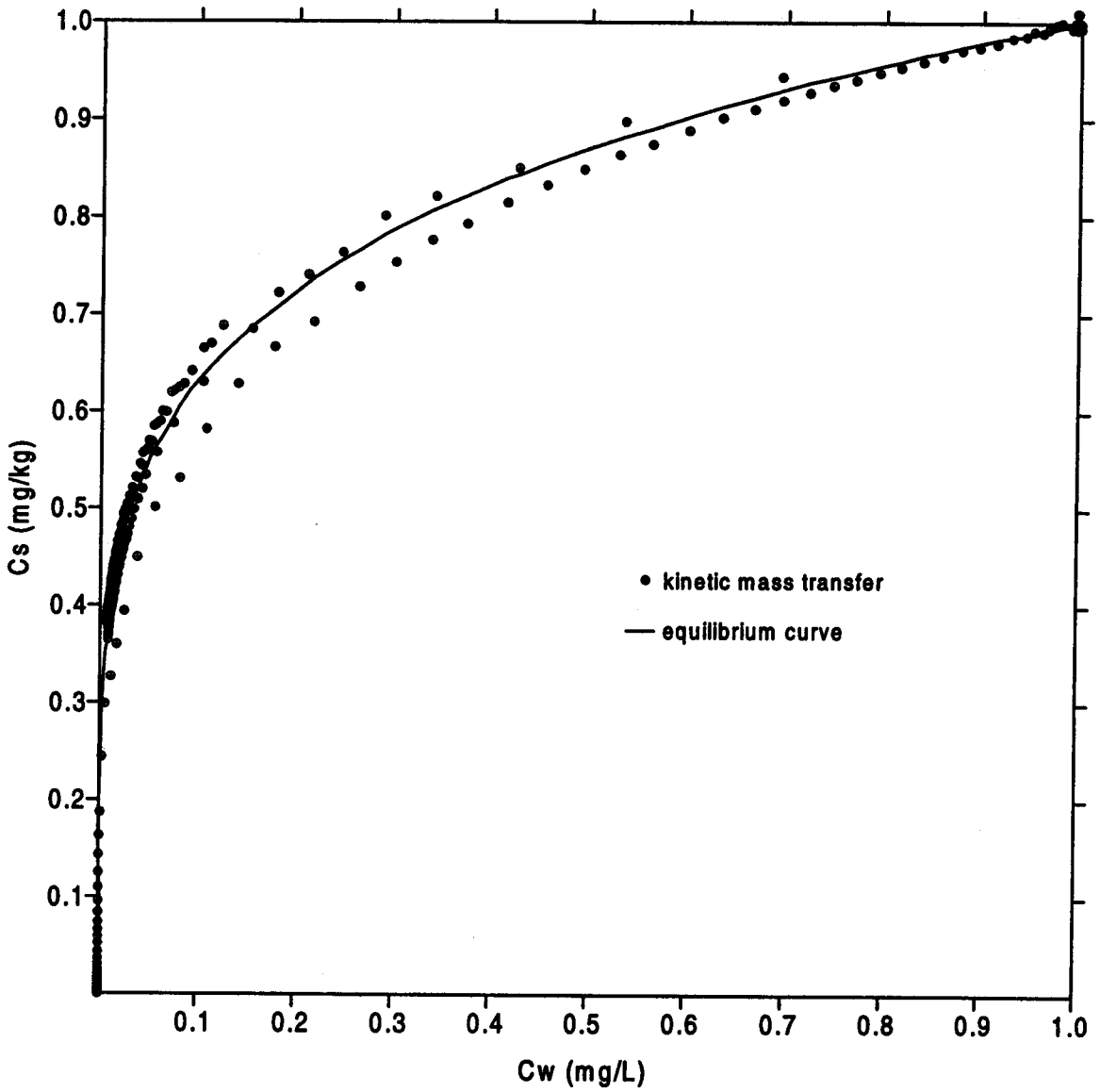

Figure 4.8 **C_s vs C_w for the Fifth Study Case. (Non-linear adsorption/desorption at low groundwater velocity, n = 0.2).**

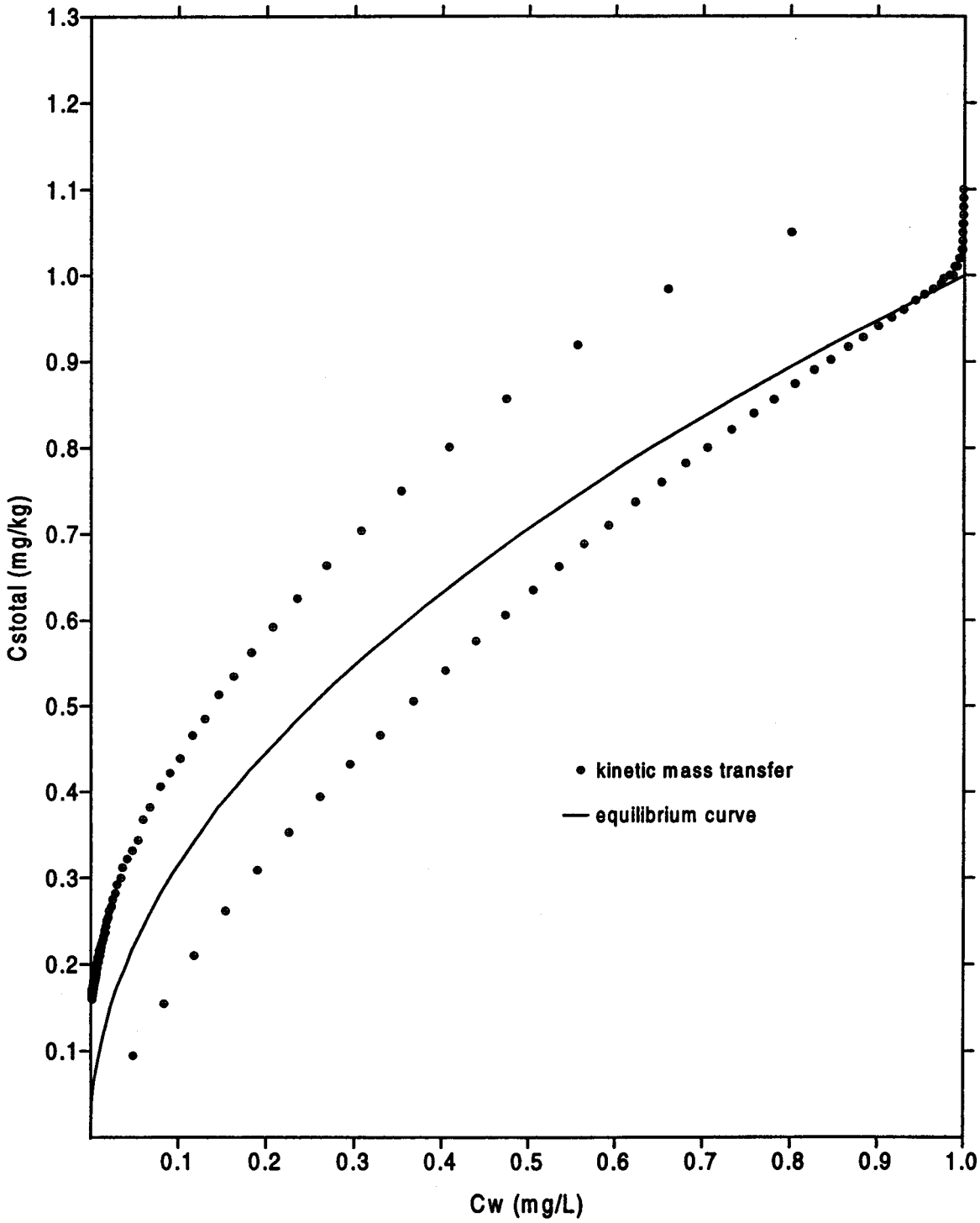

Figure 4.9 C_s vs C_w for the Sixth Study Case. (Non-linear adsorption desorption with chemisorption at high groundwater velocity, n = 0.5).

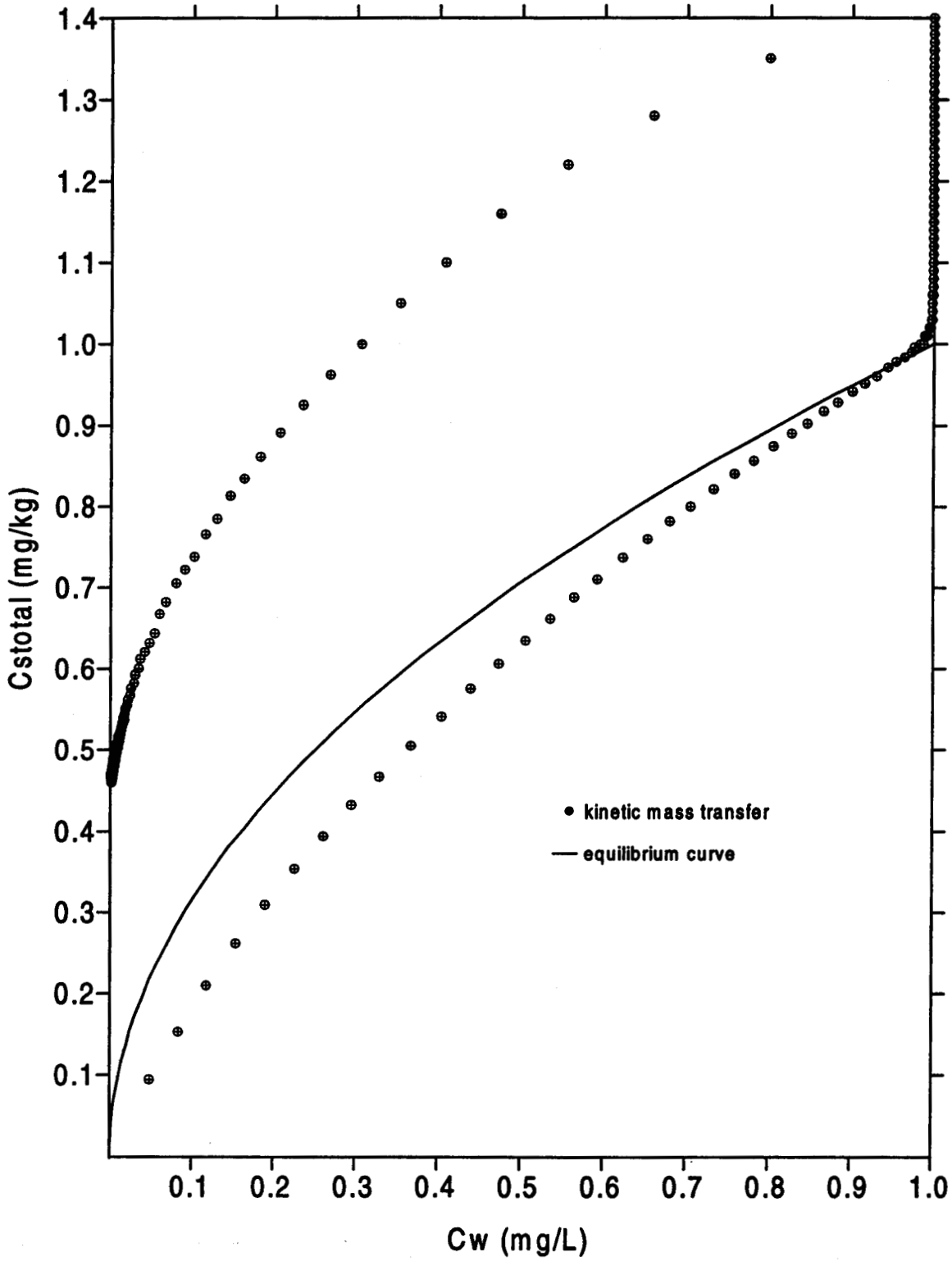

Figure 4.10 **C_s vs C_w for the Seventh Study Case. (Non-linear adsorption/desorption with chemisorption at high groundwater velocity, n = 0.5, contamination period = 4,000 days).**

000066

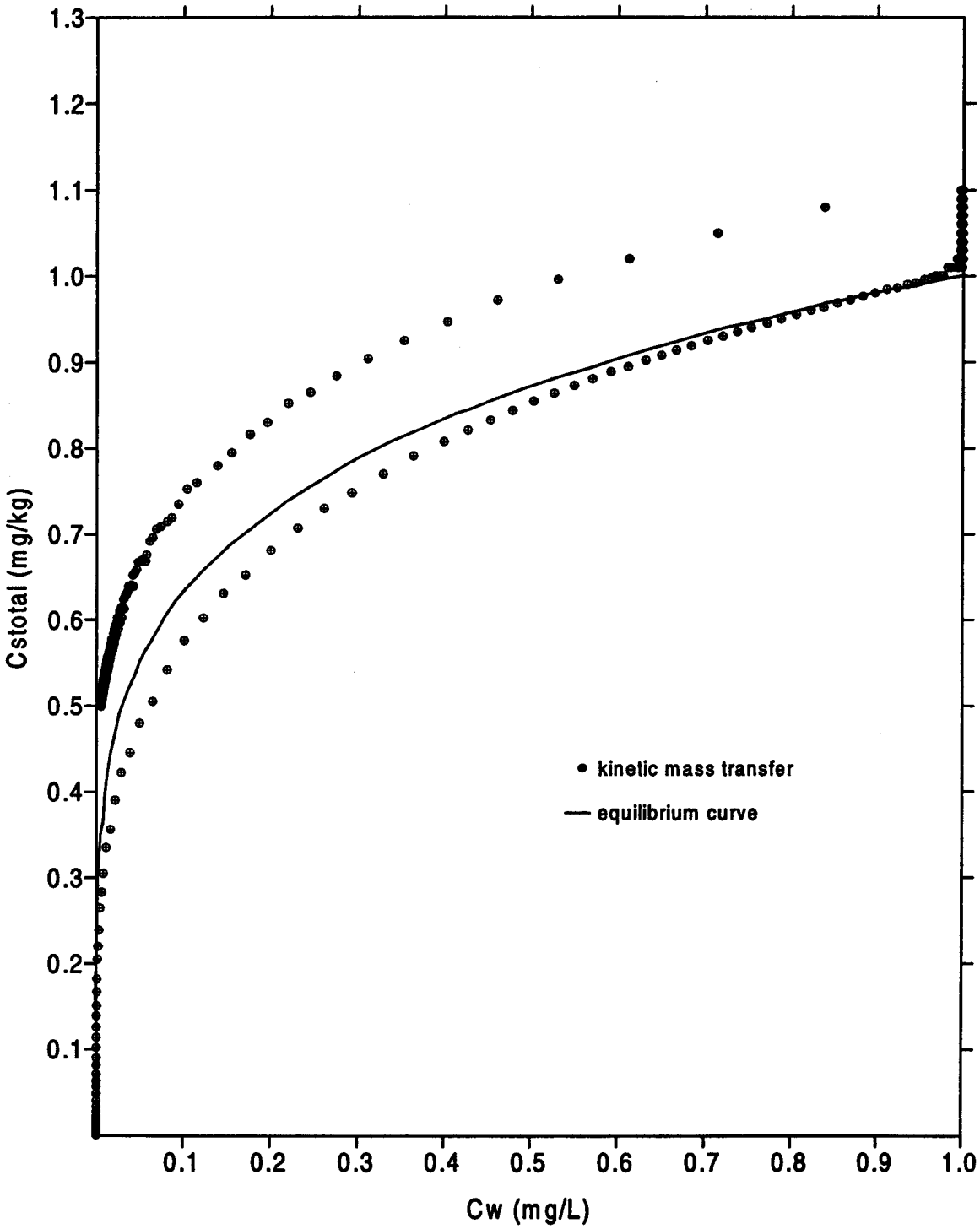

Figure 4.11 **C_s vs C_w for the Eighth Study Case. (Non-linear adsorption/desorption with chemisorption at high groundwater velocity, n = 0.2, contamination period = 4,000 days).**

The ninth study case includes precipitation and dissolution, with $\alpha_p=0.002$ and $\alpha_s=0.0001$. The remaining parameters are the same as for the sixth case discussed earlier. Figure 4.12 shows that for this case, the C_w- C_{stotal} curve exactly follows that of the sixth case (Figure 4.7) when C_w is lower than the solubility limit, 0.6 mg/L; however, as C_w increases beyond the solubility limit, precipitation occurs, resulting in higher C_{stotal} than without precipitation. During the flushing period, the precipitated component dissolves. At the end of the flushing period, the flushing curve retains the chemisorbed component only. Note that for cases in which chemisorption and precipitation/dissolution are active, the solid concentration C_{stotal} is defined as the sum of adsorbed, chemisorbed, and precipitated concentrations. Precipitated concentration is divided by bulk density for unit conversion.

For the tenth and eleventh study cases, the cycle of contamination and flushing for the sixth and ninth cases, respectively, was repeated to examine possible history effects in the second cycle. Following the first flushing period (second stress period), the left boundary was reassigned with $C_w=1$ mg/L to recontaminate the system for 1,000 d during the third stress period, after which this boundary reverted to $C_w=0$ during the fourth stress period to flush the system for 5,000 d. Figures 4.13 and 4.14 show C_s versus C_w for the tenth and eleventh cases, respectively. For both cases, the initial C_s value for the second cycle is noted to be the chemisorbed concentration retained from the first contamination and flushing cycle. The shapes of the contamination and flushing curves for the second cycle for the tenth and eleventh cases are similar to the curves of the first cycle, however, the second cycle is noted to have higher solid concentrations than the first cycle.

All of the above study cases are summarized in Table 4.1.

4.6 PARAMETER ESTIMATION GUIDELINES

Kinetic mass transfer parameters need to be estimated to simulate the hysteresis behavior of solid phase contamination versus solute concentration when switching from source loading to restoration. Parameters are needed for desorption, chemisorption, and precipitation.

Calibration parameters for adsorption are the desorption rate coefficient α_d and the Freundlich isotherm parameters k_d and n. The actual adsorption rate coefficient α_a does not need to be separately calibrated since it is a function of other variables. For chemisorption, the calibration parameter is the chemisorption rate constant α_c. The calibration parameters for precipitation are the precipitation rate constant α_p and the solubilization rate α_s.

DFM has the flexibility to view kinetic mass transfer parameters as constants over the model domain, constants within zones, or as heterogeneous parameters having geostatistical variation. Geostatistical variation can be viewed as a polynomial trend plus a spatially correlated process with a correlation distance and a standard deviation. Calibration parameters are a combination of constants, zonal constants, trend coefficients, and values of the spatially correlated process. Guidance for determining prior information about calibration parameter estimates and uncertainties can be obtained from previous data, data analysis, and the literature.

There are enough data for unique calibration when the number of data points over time that are available for calibration targets are considered. Consequently, DFM will allow for realistic

hysteretic behavior while still achieving a unique model. Realistic hysteretic behavior will be provided because DFM has the flexibility to incorporate realistic contaminant mass transfer models. The model will be unique because DFM can incorporate the prior information and data over time. DFM will determine the kinetic mass transfer parameters by minimizing the data fit residuals subject to physical model and prior information constraints.

Table 4.1
Summary of Study Cases for Behavior of Kinetic Mass Transfer

Case	n	v (m/d)	α_1 (1/d)	α_2 (1/d)	α_3 (mg/L/d)	t_1 (d)	t_2 (d)	Brief Description
1.	1	1	0	0	0	1,000	5,000	Linear adsorption and desorption
2.	1	10	0	0	0	1,000	5,000	Groundwater velocity is increased to 10 m/d
3.	0.5	1	0	0	0	1,000	5,000	Nonlinear adsorption and desorption
4.	1	10	0	0	0	1,000	5,000	Groundwater velocity is increased to 10 m/d
5.	0	1	0	0	0	1,000	5,000	n is reduced to 0.2
6.	1	10	0.0001	0	0	1,000	5,000	Chemisorption is included
7.	1	10	0.0001	0	0	4,000	5,000	Extended contamination duration
8.	0	10	0.0001	0	0	4,000	5,000	Extended contamination duration
9.	1	10	0.0001	0.002	0.0001	1,000	5,000	Precipitation/dissolution is included
10.	1	10	0.0001	0	0	1,000	5,000	Two-cycle chemisorption
11.	1	10	0.0001	0.002	0.0001	1,000	5,000	Two-cycle precipitation and dissolution

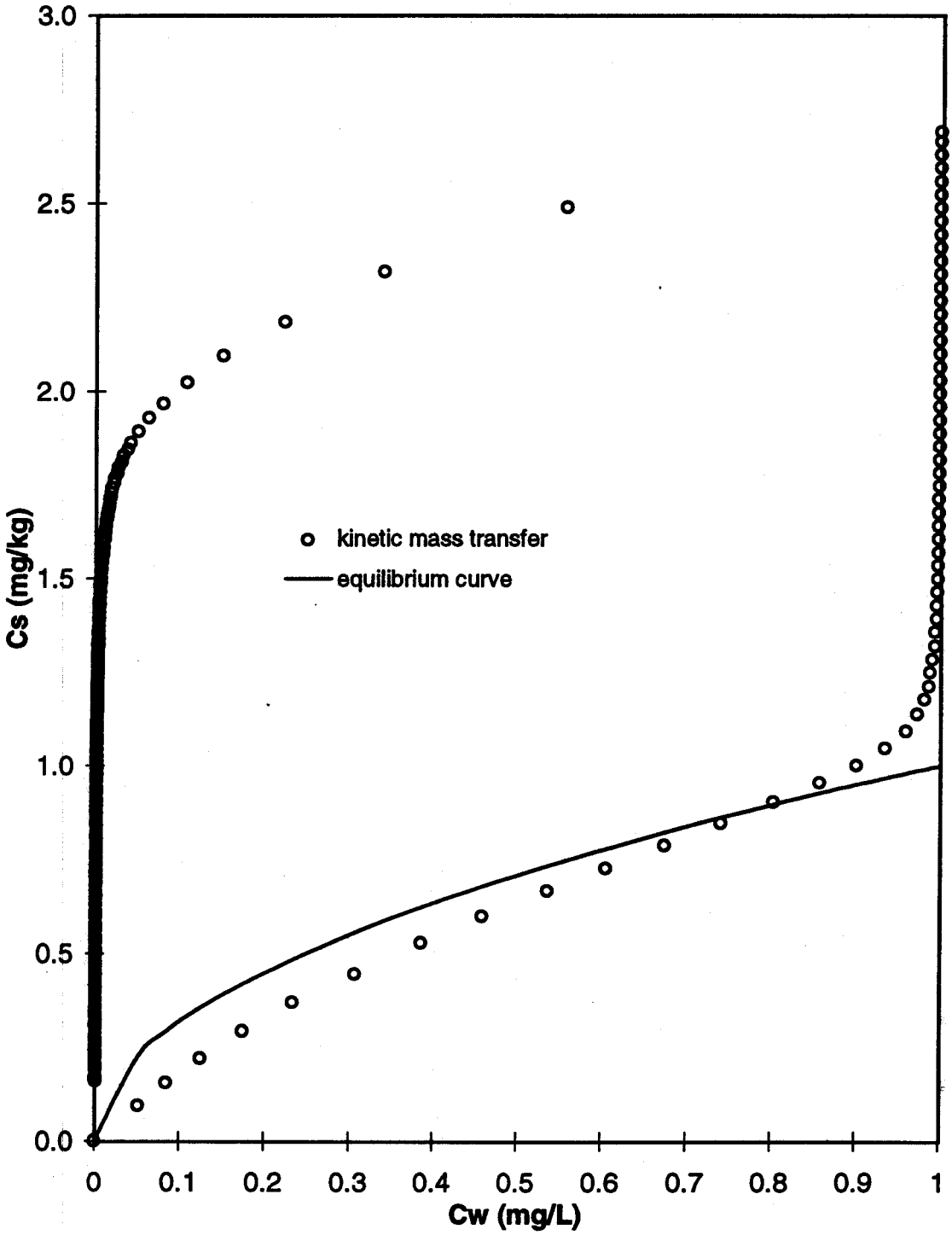

Figure 4.12 **C_s vs C_w for the Ninth Study Case. (Non-linear adsorption/desorption with precipitation and dissolution).**

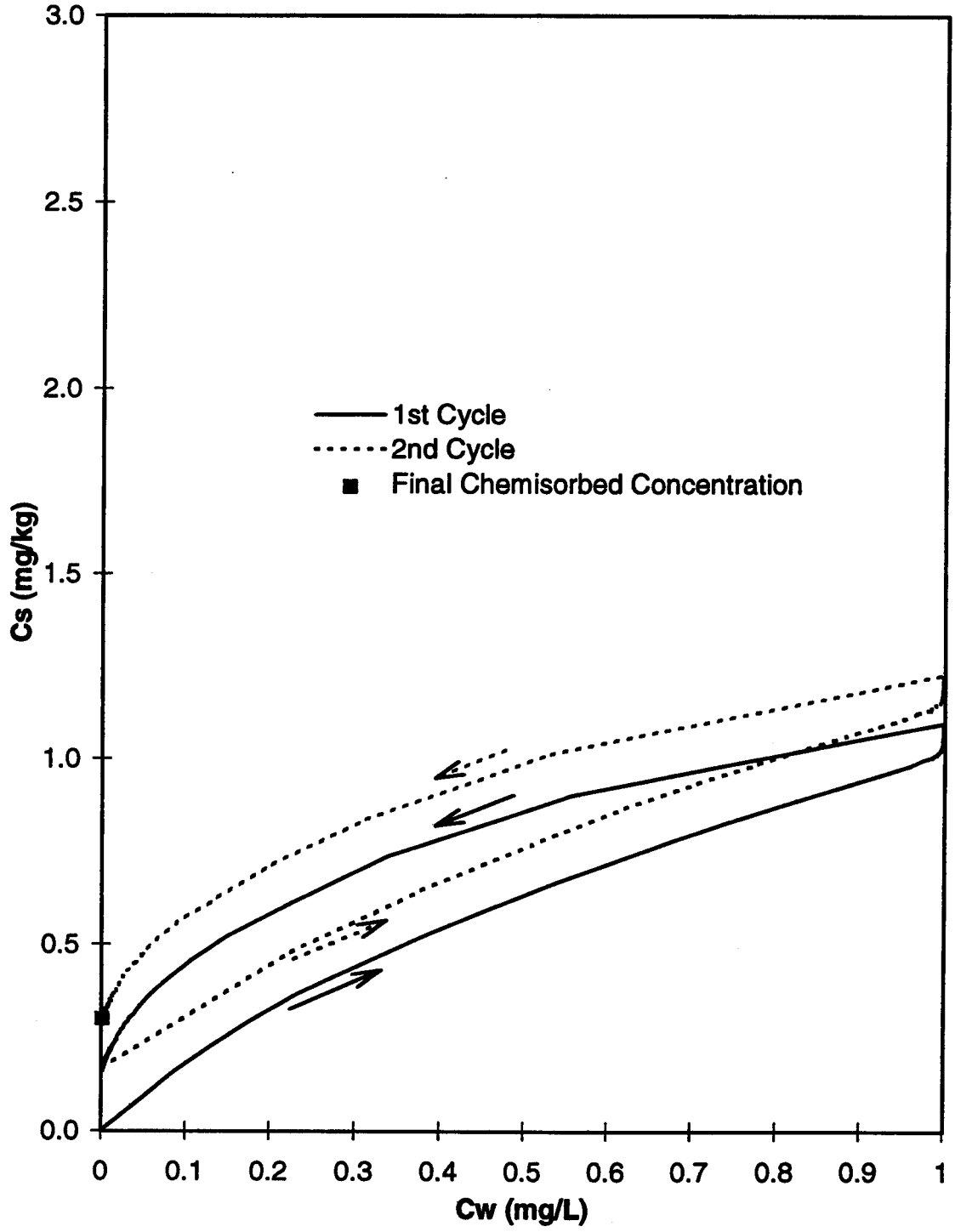

Figure 4.13 **C_s vs C_w for the Tenth Study Case. (Non- linear adsorption/desorption with chemisorption).**

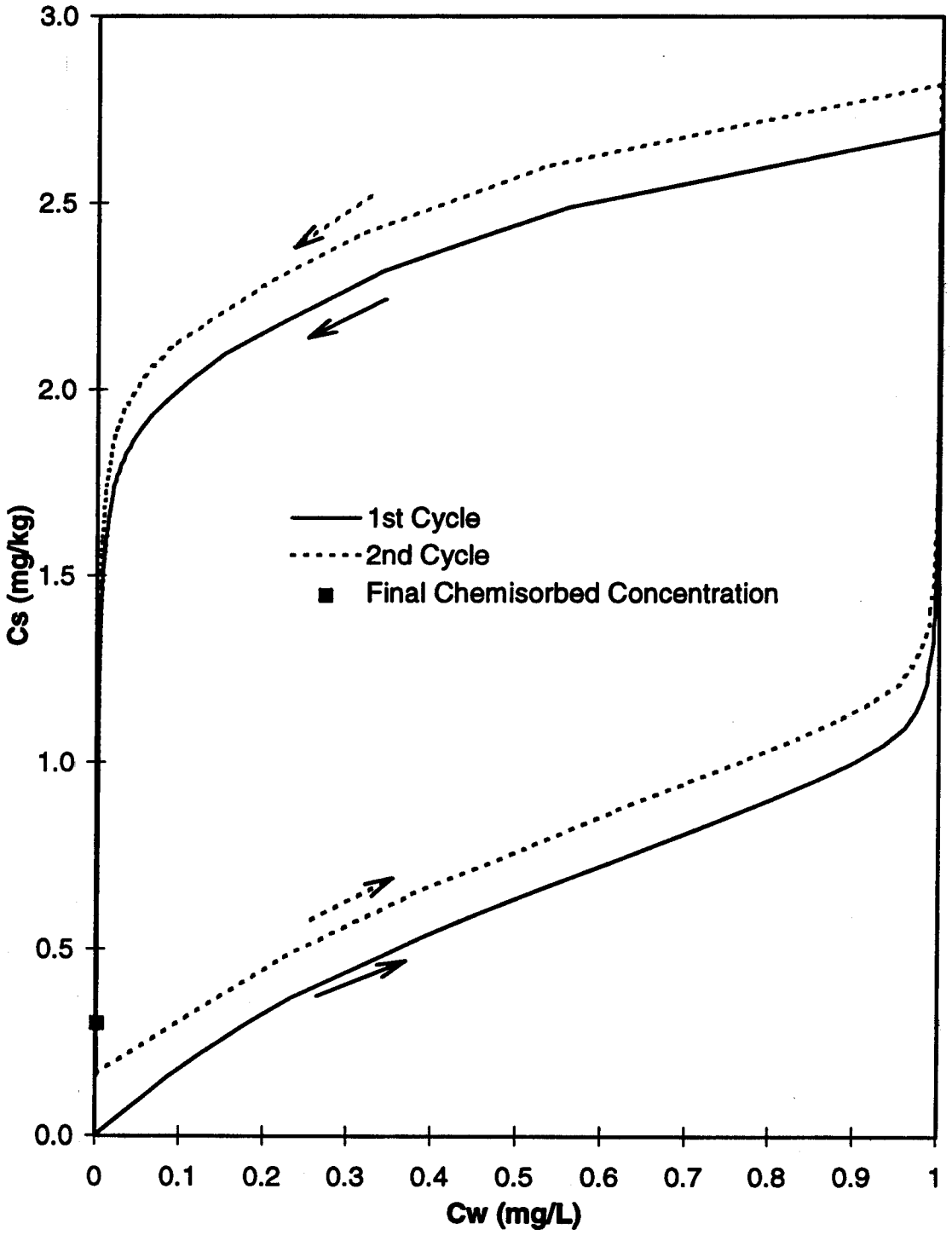

Figure 4.14 C_s vs C_w for the Eleventh Study Case. (Non-linear adsorption/desorption with precipitation and dissolution).

000072

5.0 TVD SOLUTION SCHEME

5.1 PURPOSE

In performing groundwater remediation using the pump-and-treat method in areas with high hydraulic conductivity, it is often necessary to utilize wells with high extraction or injection rates to realize large areal coverage with a minimum number of wells. In the immediate vicinity of these wells, groundwater velocity is accordingly high. In terms of practical numerical simulation of chemical transport, it often means that the grid Péclet number must be kept relatively large, often much greater than 2, which is normally the upper bound of allowable grid Péclet number. In addition, the grid Courant number is likely to exceed unity in these areas. To keep the grid Péclet and Courant numbers below 2 and 1, respectively, the grid size and time step must be impractically small. In addition, the inclusion of large sources or sinks often lead to numerical oscillation and poor mass balance. In order to accommodate the existence of high groundwater velocity near extraction/injection wells, the Total Variation Diminishing (TVD) scheme (Harten, 1983), shown to overcome the problems of oscillatory or dispersed solutions for high Péclet and Courant numbers and poor mass balance, has been incorporated fully implicit into the VAM3DF code. Details of the TVD scheme and the incorporation of the scheme to the VAM3DF code are presented below.

5.2 NUMERICAL TREATMENT

The interblock concentrations in the advection terms on the left-hand-side of the discrete transport equation (Equation 5.1) are calculated using a mass conservative second-order TVD scheme (Roe, 1981; Harten, 1983; Sweby, 1984; Yee, 1987; Cox and Nishikawa, 1991; Blunt and Rubin, 1992; Arminjon, and Dervieux, 1994; Forsyth, 1994; Liu et al., 1994; and Unger, et al. 1996) with the van Leer flux limiter (van Leer, 1977, 1979):

$$\begin{aligned}
&\nabla_x(\tau_{xx}\nabla_x\bar{c}) + \nabla_y(\tau_{yy}\nabla_y\bar{c}) + \nabla_z(\tau_{zz}\nabla_z\bar{c}) - Q_x\nabla_x\bar{c} - Q_y\nabla_y\bar{c} - Q_z\nabla_z\bar{c} \\
&= (\Delta x_j \Delta y_i \Delta z_k)\left\{\nabla_t(\phi S_w Rc) + (\lambda\phi S_w Rc)\right\} - Q(c-c^*)^{n+1} \\
&+\nabla_x(\tau_{xy}\nabla_y\bar{c}) + \nabla_x(\tau_{xz}\nabla_z\bar{c}) + \nabla_y(\tau_{yx}\nabla_x\bar{c}) + \nabla_y(\tau_{yz}\nabla_z\bar{c}) + \nabla_z(\tau_{zx}\nabla_x\bar{c}) + \nabla_z(\tau_{zy}\nabla_y\bar{c})
\end{aligned} \tag{5.1}$$

An assumption is made that x, y, and z correspond to x_1, x_2, and x_3, respectively in (2.26) where $\bar{c}^k$ is the time-weighted concentration for component k; ∇_x, ∇_y, and ∇_z finite- difference gradient operators in the x, y, and z directions, respectively; ∇_t is the temporal difference operator; $n+1$ denotes the current time level; τ_{xx}, τ_{yy}, τ_{zz} are the discretized dispersive terms; and Q_x, Q_y, Q_z are volumetric fluxes in the principal coordinate directions. Q is the volumetric, flux from sources and sinks. The discretized cross dispersion terms, τ_{xy}, τ_{xz}, τ_{yx}, τ_{yz}, τ_{zx}, and τ_{zy}, are optionally taken into account by the code if requested.

Expansion of the interblock advective flux term may be written as

$$Q_i\,\nabla_i\,\bar{c} = Q_i\,\bar{c}_{i+½} - Q_i\,\bar{c}_{i-½} \tag{5.2}$$

where i is any coordinate direction (i=1,2,3), $i+½$ is the forward face of the grid block, and i-½ is the backward face of the gridblock in the ith coordinate direction. The concentration at the face $\bar{c}_{i+½}$ may be expressed in a TVD form as

$$\bar{c}_{i+½} = \bar{c}_{ups} + \sigma(\gamma_{ij}) \left[\bar{c}_{dwn} - \frac{\bar{c}_{ups}}{2} \right] \tag{5.3}$$

where *ups* is the upstream point and *dwn* is the downstream point of the nodal pair i and $i+1$, and σ is the flux limiter term, which is a function of γ_{ij}, the smoothness sensor. Concentration at the face $\bar{c}_{i-½}$ is expressed in a similar fashion. The TVD scheme minimizes numerical dispersion and preserves monotonicity properties of the exact solution and appears in Equation (5.3) as a correction to the upstream solution. The smoothness sensor is calculated from concentrations at the downstream, upstream, and second point upstream nodes and detects rapid changes in concentration. The van Leer flux limiter weights the solution from fully upstream to fully downstream. When the degree of implicitness of the solution varies, the Crank-Nicolson factor is chosen as close to ½ as possible, without violating the TVD property of the solution (Blunt and Rubin, 1992).

The TVD property, when applied to the advective term, ensures physically correct solutions without spurious oscillations even for totally advective transport. As stated by Harten (1983), the TVD property guarantees that for a nonlinear, scalar equation or a linear system of equations, the total variation (TV) of the solution will not increase as the solution advances in time, i.e.,

$$TV\,(c^{n+1}) \leq TV\,(c^{n}) \tag{5.4}$$

where $n+1$ and n denote the current and previous time levels, and the total variation of a quantity c is defined as

$$TV\,(c) = \sum_{i=-\infty}^{\infty} |c_i - c_{i-1}| \tag{5.5}$$

in which i and i–1 denote adjacent grid points. The van Leer limiter used in VAM3DF is capable of capturing a shock within three nodes, under optimal time stepping conditions, thus providing accurate, physically correct mass conserved solutions. For TVD schemes with automatic control over implicitness, the time weighting factor is adaptively adjusted for optimal accuracy of temporal discretization, while still maintaining the TVD property. Options for upstream, midstream, and mixed spatial weighting of the advective terms also are provided for quick initial simulations toward calibration.

000074

5.2.1 Implementation of Boundary Conditions

All external and internal flow boundaries of the domain (including injection/withdrawal wells) are treated as third-type boundaries for transport. The concentrations of contaminant species, input by the user at all possible inflow boundaries, are multiplied by the fluid flux and implemented into the right-hand side vector. Outflow boundaries to the system do not require user supplied concentration values, which are ignored if provided. For outflow boundaries, the fluid flux is added to the diagonal term of the left-hand-side matrix and outflow concentrations are computed by the code. All third-type (fluid/contaminant flux) boundaries act in an additive fashion, so a user may implement, for example, recharge, evapotranspiration, and drain conditions, all on one node. For this case, recharge water with prescribed concentrations enters the cell, fresh water (without contaminants) leaves due to evapotranspiration thus further affecting the cell concentration, and water with calculated resultant concentration for that cell leaves it through the drain boundary. Note that evapotranspiration is treated by allowing only water but no contaminant efflux. Prescribed concentration (first-type) conditions may be implemented anywhere in the domain, including at flow boundaries. Numerical implementation is performed by multiplying the diagonal by a large number and replacing the right-hand-side by the large number times the prescribed concentration value for the respective node. Note that first-type boundary conditions supersede all other third-type conditions prescribed at the same node.

5.2.2 Solution Procedures

Nonlinearities in adsorption or of implicit TVD schemes used to solve the transport equation are treated using Picard iterations. The Cooley (1983) under-relaxation scheme is used to dampen flip-flop behavior during iterations. The system of matrix equations is solved using the Orthomin scheme (Anderson, 1983a, b; Behie and Vinsome, 1982; Panday et al., 1994). Cross-dispersion terms are included for the mixed and upstream weighted schemes, if desired, and are implemented through the right-hand-side vector. For Courant numbers not much greater than unity, the user may choose to apply the cross-dispersion term or the TVD flux limiter as a flux correction with two iterations, as is done in Flux Corrected Transport (FCT) schemes (Boris and Book, 1973). Time-lagging these terms is common practice by modelers, and this option may be invoked by requesting only one iteration. However, iterations are relatively inexpensive, and time-lagging is not advised.

When an implicit TVD solution or a nonlinear transport problem does not converge within the prescribed number of iterations for a particular flow time step, the time-step size is reduced by a factor of 2 and the solution is reattempted for the reduced time-step size. This process is repeated until convergence is achieved or a user-defined number of sub-steps is exceeded, whereby the computations are aborted. Successful computations for all sub-steps are performed before proceeding to the next flow time step. When an explicit TVD scheme encounters stability problems, the target time-step is divided into a number of stable sub-steps for which computations are performed before proceeding to the next flow time step, if a user defined maximum is not exceeded.

5.3 VERIFICATION

5.3.1 Verification Case 1 - One-Dimensional, Single-Species Transport

This problem concerns one-dimensional advective-dispersion of a conservative solute species through a semi-infinite porous medium (Figure 5.1). As illustrated, the contaminant is released from a channel fully penetrating a shallow confined aquifer. An analytical solution of the problem was developed by Ogata and Banks (1961). This solution also can be found in Bear (1979). For the cases documented herein, the inlet was a first-type boundary with prescribed relative concentration of 1.0 g/m^3. The values of Darcy velocity and effective porosity were specified as 1 m/d and 0.25, respectively. The modeled length of the aquifer domain was specified as 400 m. A uniform rectangular mesh was used consisting of 40 elements, each with Δx = 10 m. Two cases were studied with different values of longitudinal dispersivity (α_L). The first case had a dispersivity value of 2 m and the second case had a dispersivity of zero. For the two cases, the simulation was performed for 50 time steps with Δt kept constant and equal to 1.0 days. Simulated concentration distributions using the flux limiter scheme used automatic time stepping. Figure 5.2 presents the simulated and analytical concentration distributions at $t=50d$ with grid Péclet number $P_e=\Delta x/\alpha_L=5$ and Courant number $C_o=V\Delta t/\Delta x=0.4$. The following simulations are compared in Figure 5.2:

- Finite difference with central weighting
- Finite difference with upstream weighting
- Finite difference with the explicit flux limiter
- Finite difference with the implicit flux limiter

All simulations used a central difference time stepping scheme. Figure 5.3 shows the comparisons when using the finite element method. Both the finite difference and finite element results show that the flux limiter produces a sharper front without oscillations. The upstream scheme produces smeared concentration fronts.

Figure 5.4 presents the simulated and analytical concentrations distributions at $t=50d$ with grid Péclet number $P_e=\infty$. Figure 5.5 shows the finite element results. The central difference scheme produced oscillations while the upstream scheme produced a smeared front. Again, the flux limiter produced a sharper concentration front with a small under shoot in the finite element results.

5.3.2 Verification Case 2 - Two-Dimensional Transport from a Point Source in a Steady Uniform Flow Field

This problem concerns two-dimensional dispersion of solute in a uniform and steady groundwater flow field. In practice, the situation may correspond to that involving the areal migration of contaminants continually released into an extensive aquifer from an injection well treated as a point source in the areal plane (Figure 5.6a). Assuming that the injected rate is small

so that the natural groundwater flow is virtually undisturbed, the analytical solution of the problem can be found in Wilson and Miller (1978). The model parameters, shown in Table 5.1, are taken from Huyakorn et al. (1984). The selected parameter values were based on data from the field study of the hexavalent chromium contamination problem reported by Perlmutter and Lieber (1970). Numerical simulations were performed using a rectangular grid that represents the domain shown in Figure 5.6b. The grid consists of 684 elements, each with $\Delta x=30$ m, and $\Delta y=30$ m. The simulations were performed for 14 time steps with Δt kept constant and equal to 100 days. This problem has a grid Péclet number $P_e=\Delta x/\alpha_L=1.4$ and Courant number $C_o=V\Delta t/\Delta x=1.5$. Simulated concentration distributions using the flux limiter scheme used automatic time stepping. Concentration profiles along the x-axis centerline at $t=1400$ *d* are plotted in Figure 5.7. The four finite difference simulations gave similar results. All simulations used a central difference time stepping scheme. Figure 5.8 shows the finite element results. The upstream weighted and flux limited simulations are smeared transverse to the flow direction while the central weighted simulation exhibits slight oscillatory behavior near the source, transverse to the flow direction.

In order to investigate grid orientation effects, the same problem was simulated on a square grid with $\Delta x=\Delta y=30$ m and a diagonal uniform flow field. Figure 5.9 shows the finite difference simulated concentrations along the centerline of $t=1400$ *d*. Comparing Figures 5.7 and 5.9, reveals the grid orientation effects of the finite difference approximation. Figure 5.10 shows the finite element results which exhibit very little grid orientation effects. The upstream weighted and flux limited simulations are smeared transverse to the flow direction and the central weighted simulation has no oscillation.

5.4 SUMMARY

Verification Case 1 showed that the TVD scheme overcomes problems of oscillatory or dispersed solutions for high Péclet numbers. Verification Case 2 showed that the central weighted scheme should be used when the Péclet number is low. Grid orientation effects of the finite difference approximation were also revealed.

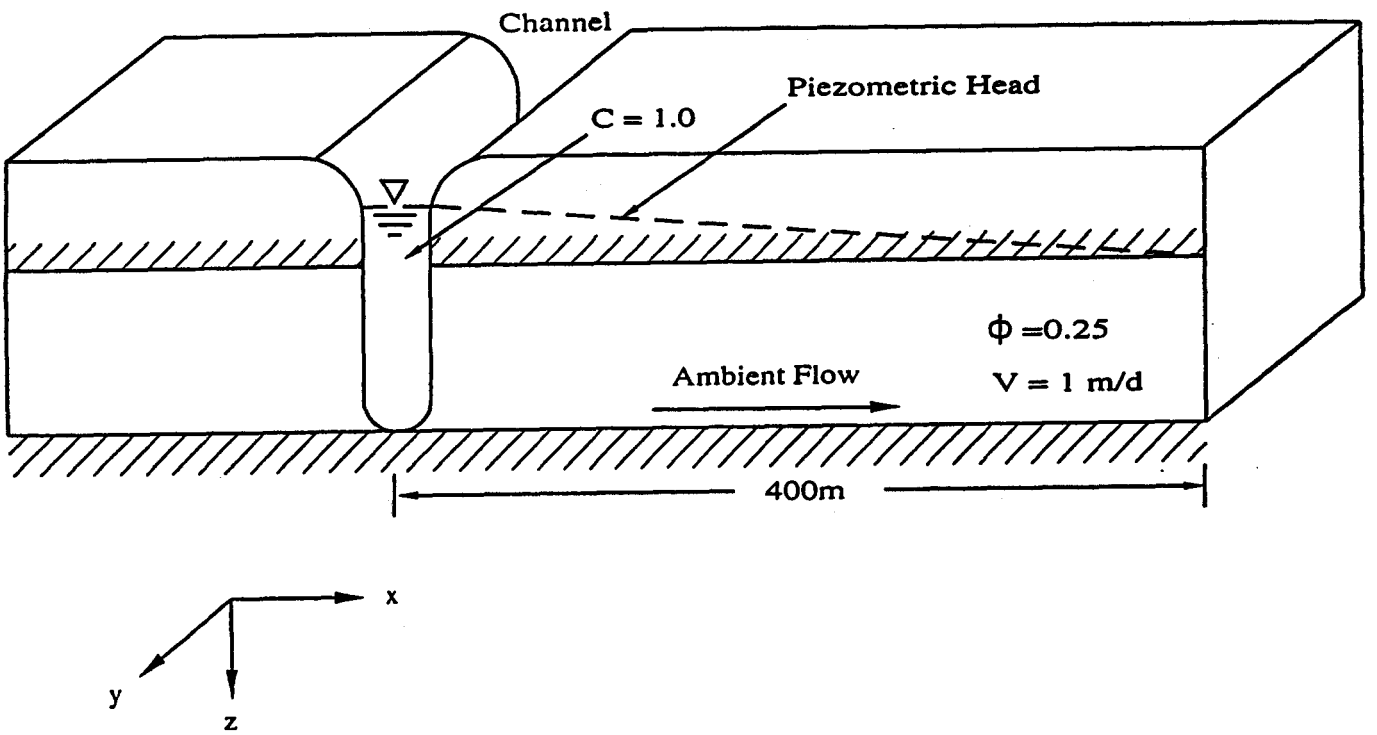

Figure 5.1 One-Dimensional Transport of a Conservative Species.

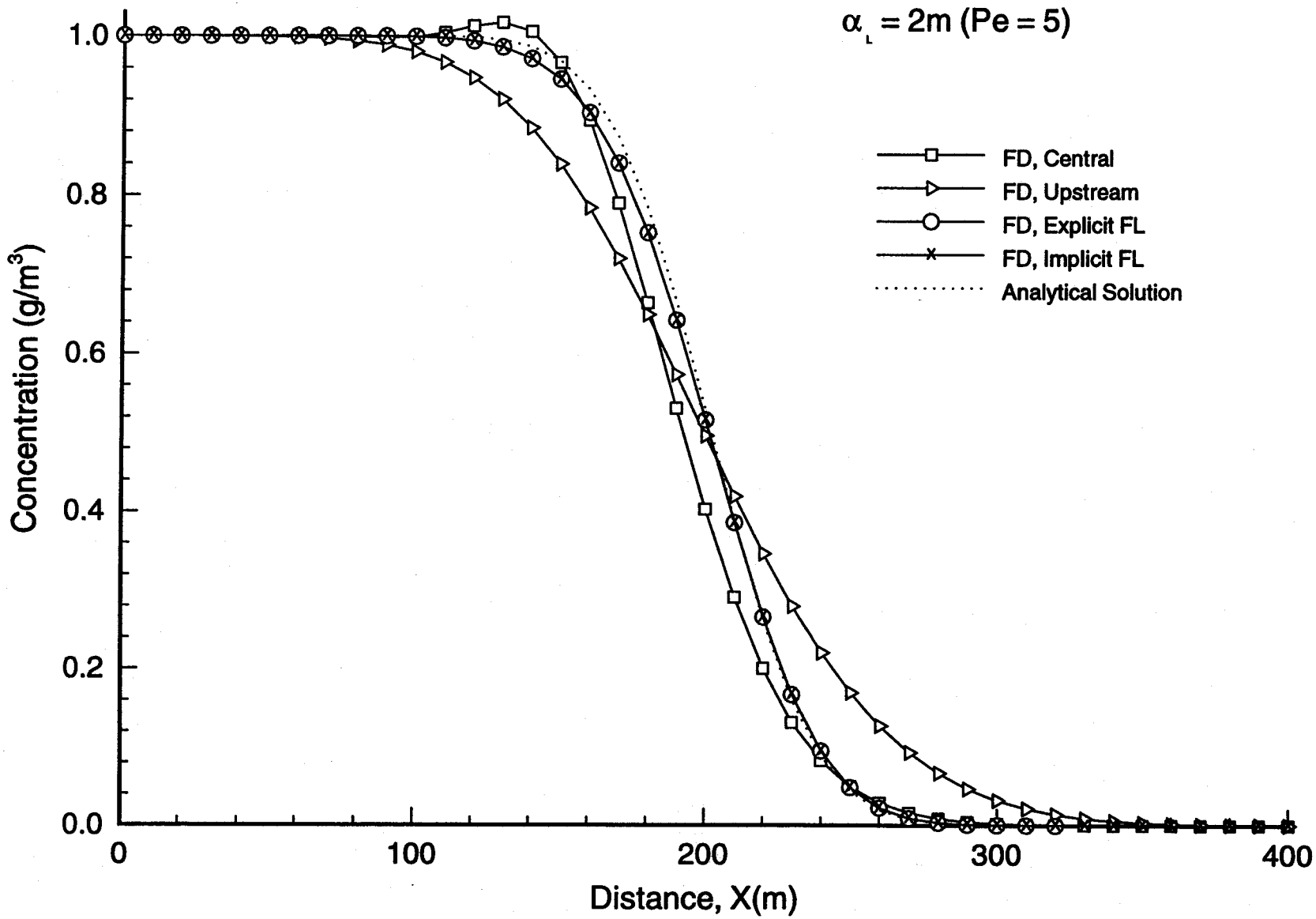

Figure 5.2 Finite Difference Results for α_L=2 m.

620000

1768

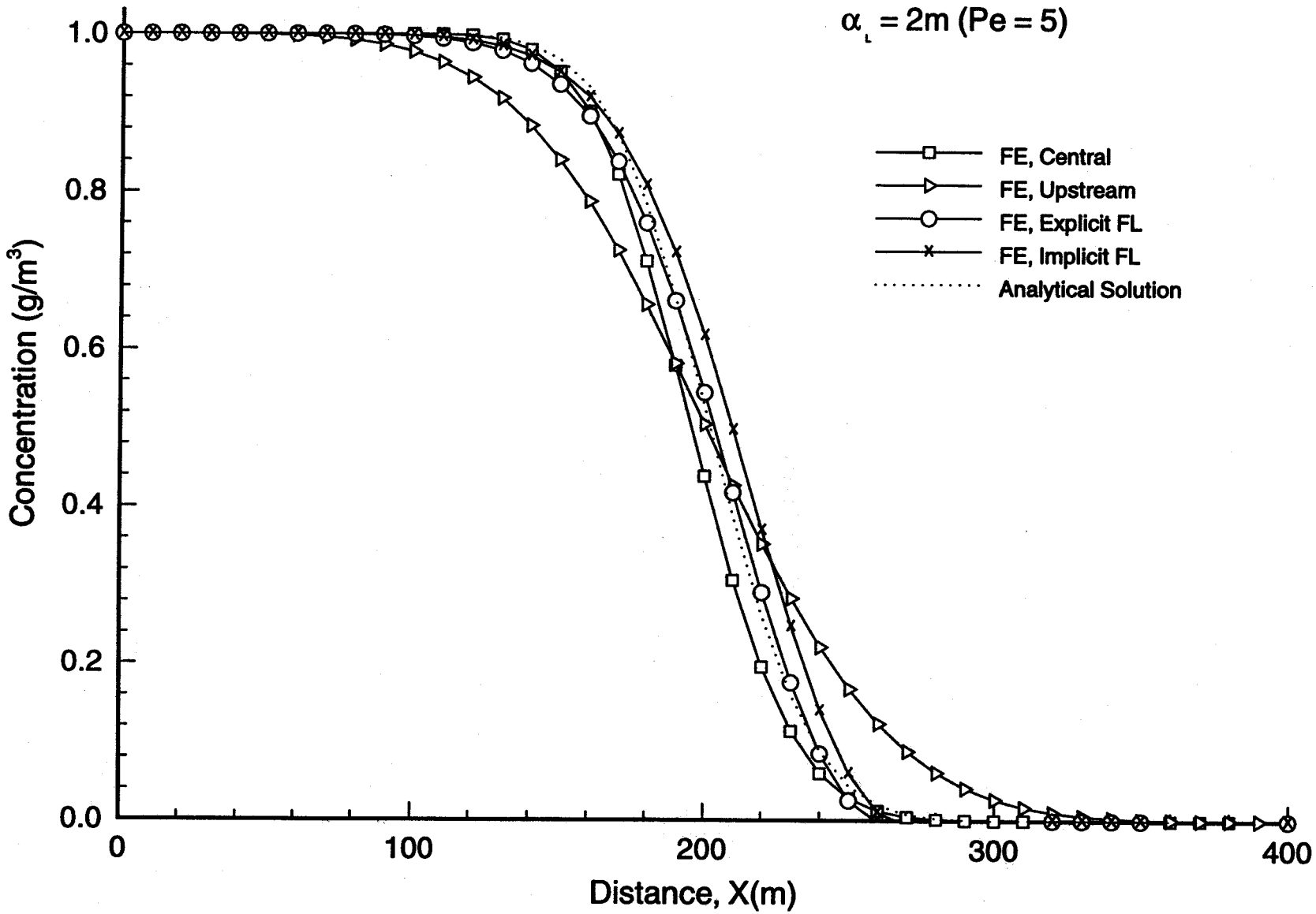

Figure 5.3 Finite Element Results for α_L=2 m.

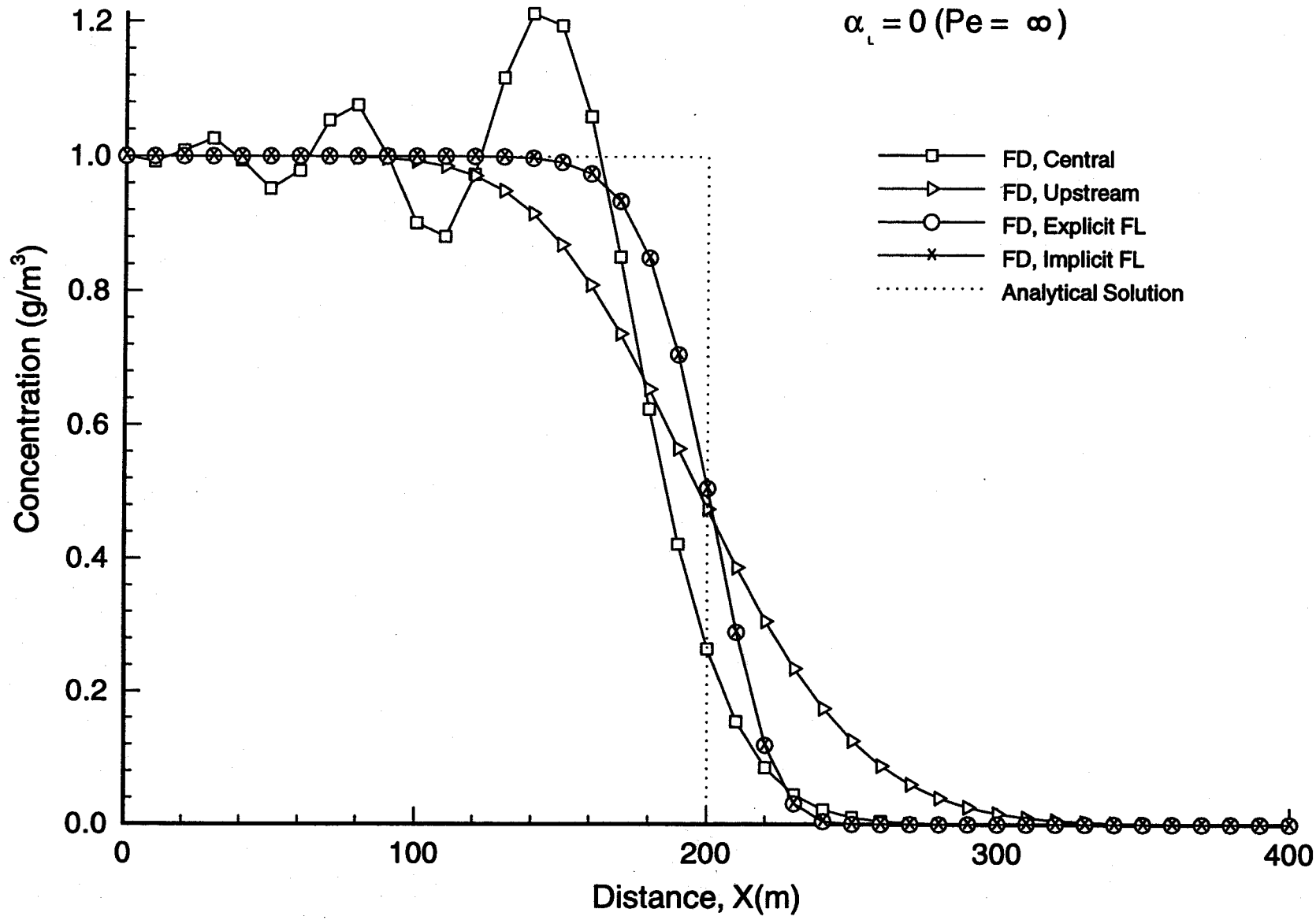

Figure 5.4 Finite Difference Results for $\alpha_L = 0$.

000081

176 8

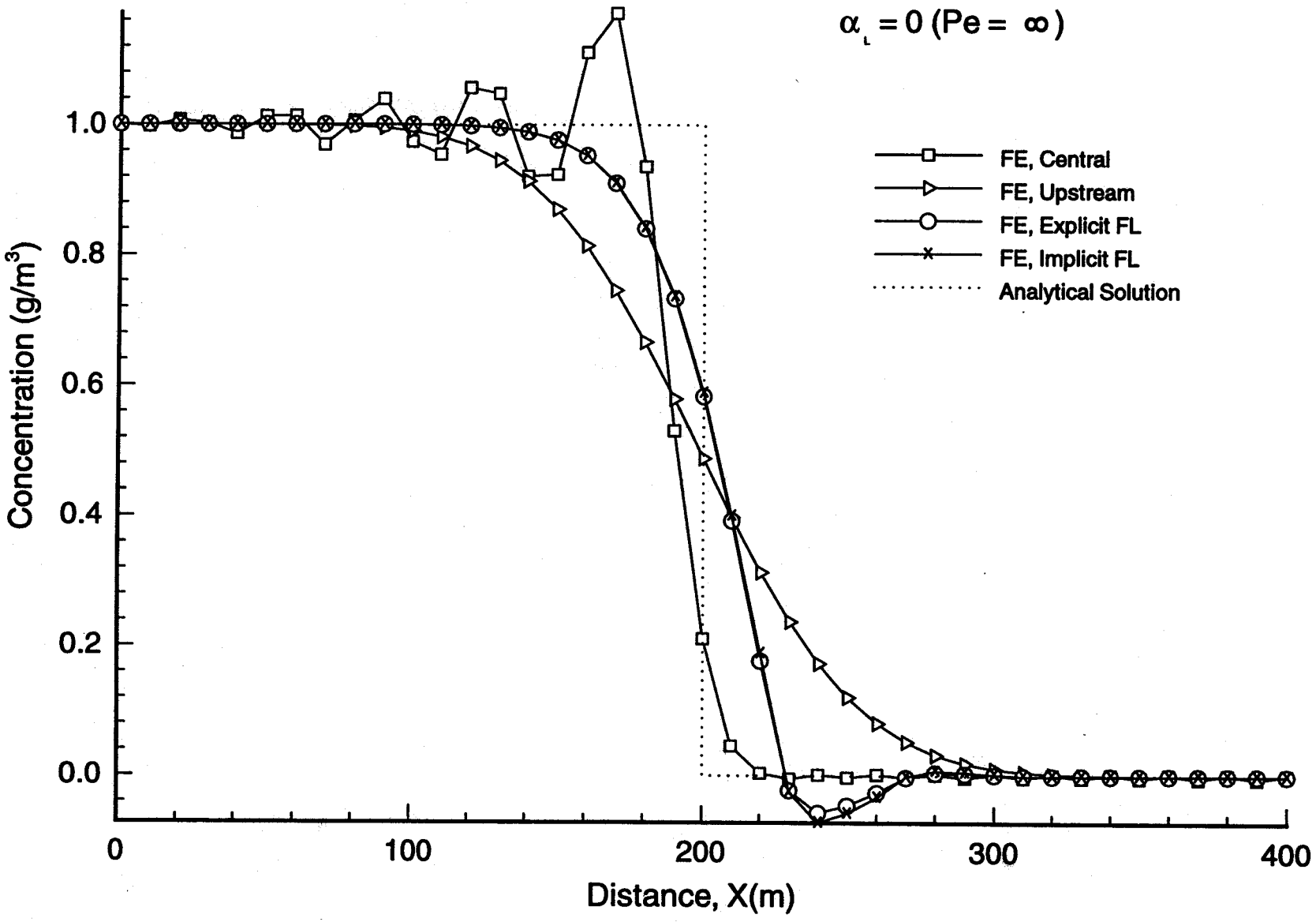

Figure 5.5 Finite Element Results for $\alpha_L = 0$.

280000 000082

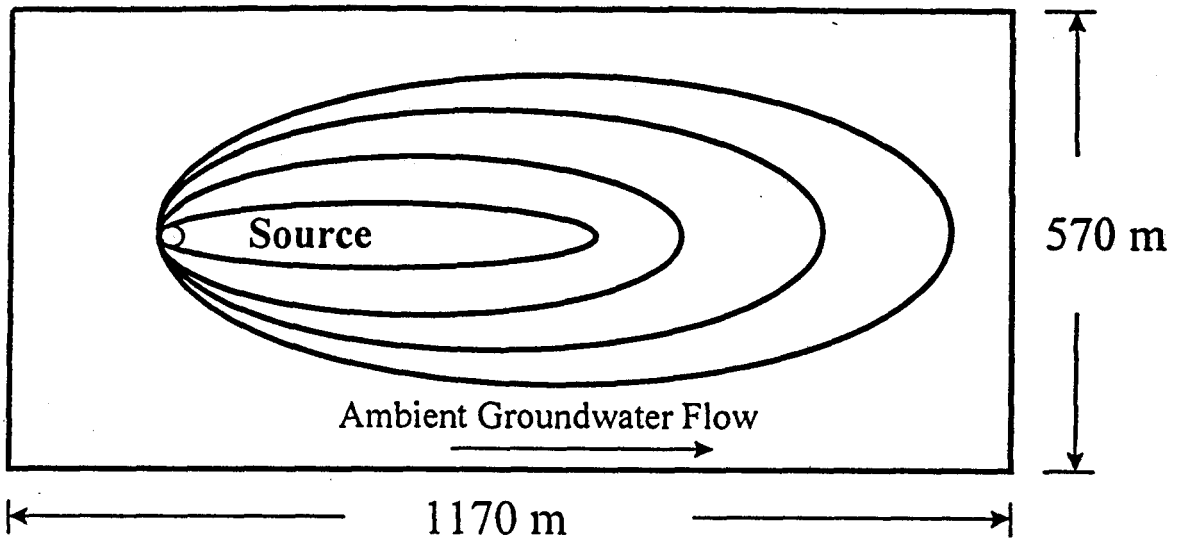

(a)

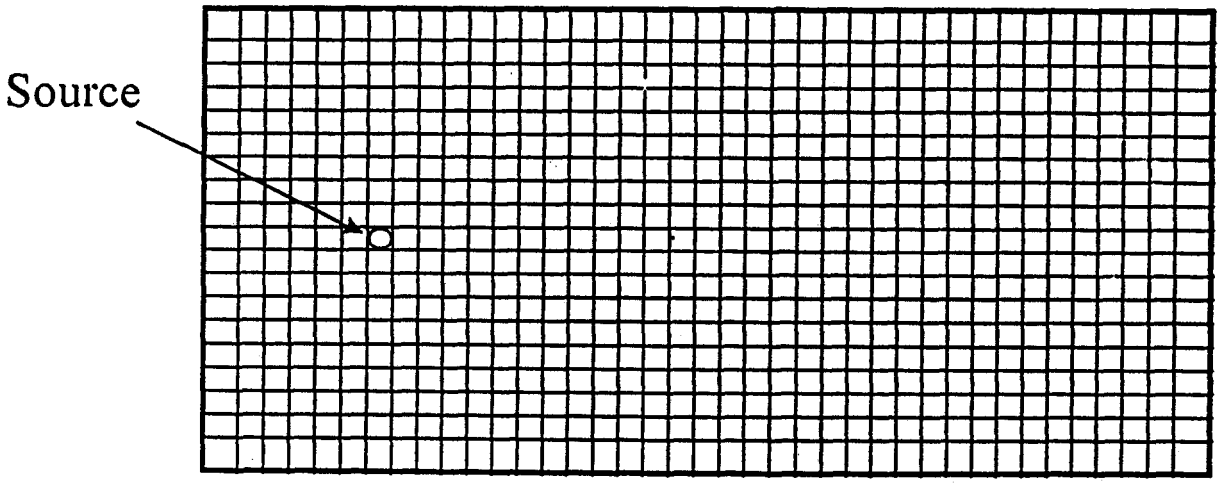

(b)

Figure 5.6 Two-Dimensional Transport from a Point Source in a Uniform Flow Field: (a) Problem Description, and (b) Model Discretization.

Table 5.1
Model Parameters for Simulation of Two-Dimensional Transport From a Point Source in a Steady, Uniform Flow Field

Parameter	Value
Darcy velocity, V	0.161 m/d
Porosity, ϕ	0.35
Longitudinal dispersivity, α_L	21.3 m
Transverse dispersivity, α_T	4.3 m
Aquifer saturated thickness, b	33.5 m
Contaminant mass flux, Qc_o (per unit thickness of aquifer)	704 g/(m.d)
Case 1:	
Linear adsorption coefficient, K_d	0.0
Retardation Coefficient, $R = 1 + \frac{\alpha_B K_d}{\phi}$	1.0
Decay constant, λ	0.0
Case 2:	
Linear adsorption coefficient, K_d	0.14 m^3/Kg
Bulk density of soil, ρ_B	2.5 Kg/m^3
Retardation coefficient, $R = 1 + \frac{\rho_B K_d}{\phi}$	2.0
Decay constant, λ	0.00019/d
Selected grid Δx = 30 m, Δy = 30 m, 19 x 39 grid Source location = Row 10, Column 7	
Time steps Δt = 100 d (used 14 time steps)	

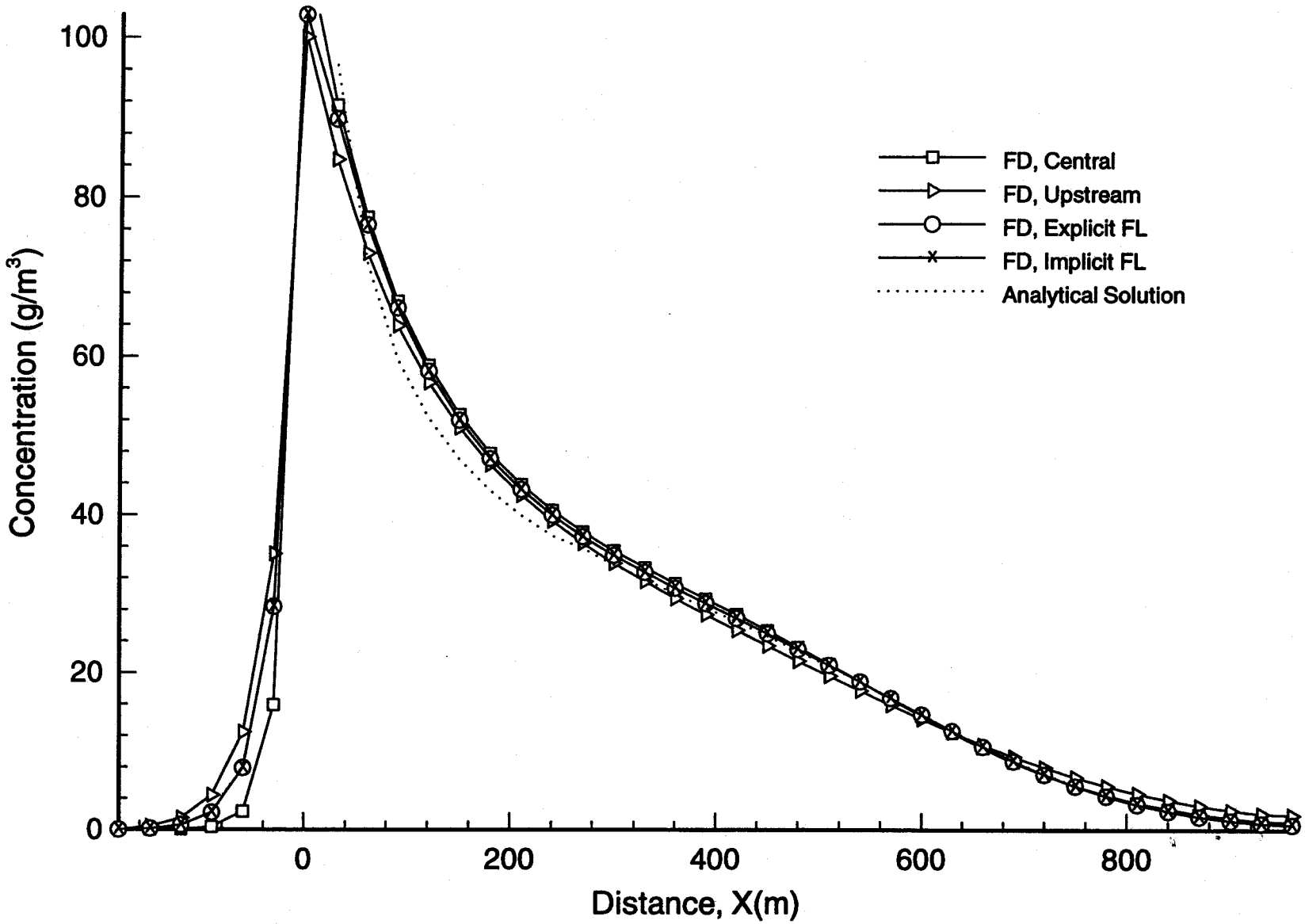

Figure 5.7 Finite Difference Results (parallel flow).

000085

1768

000086

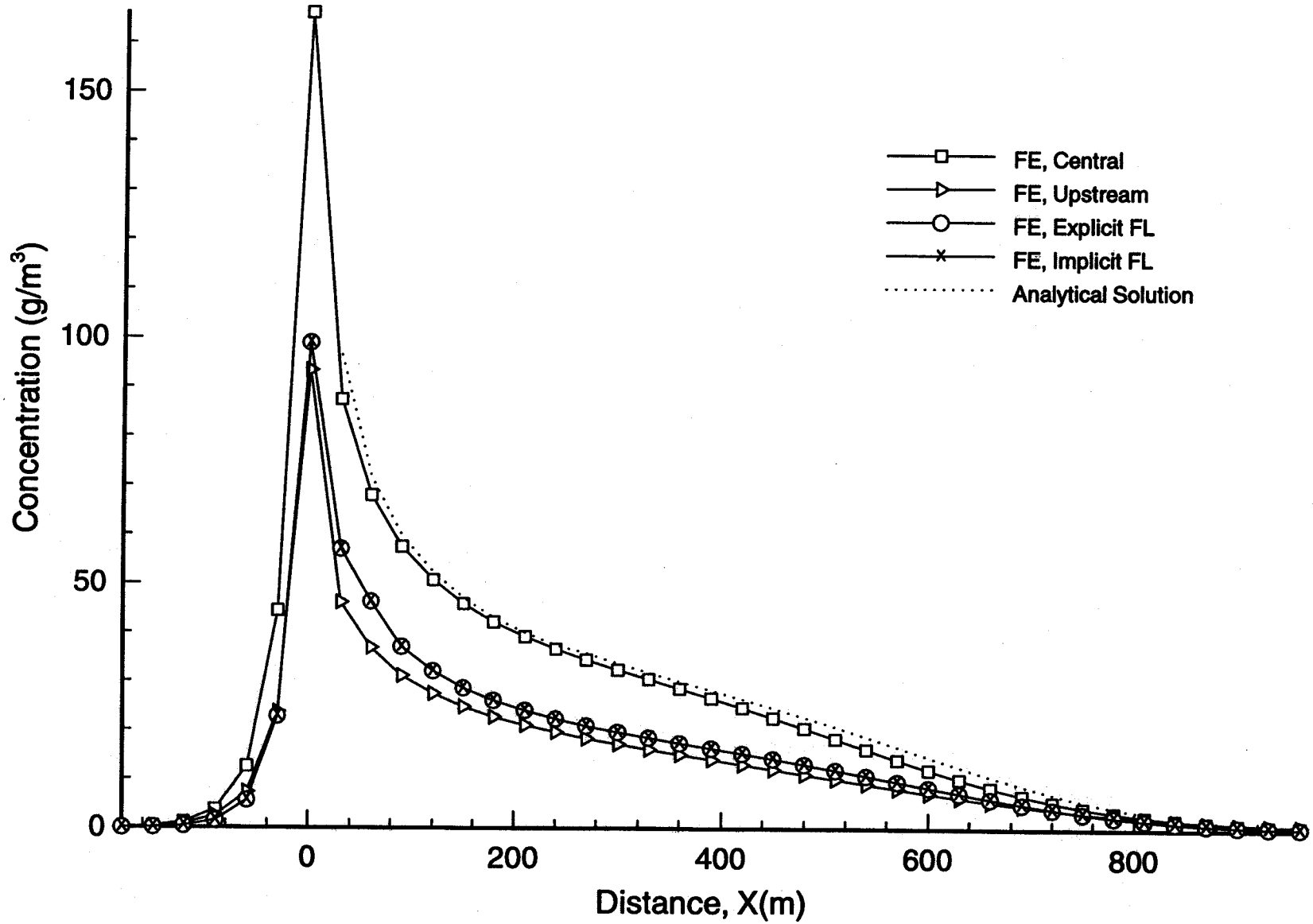

Figure 5.8 Finite Element Results (parallel flow).

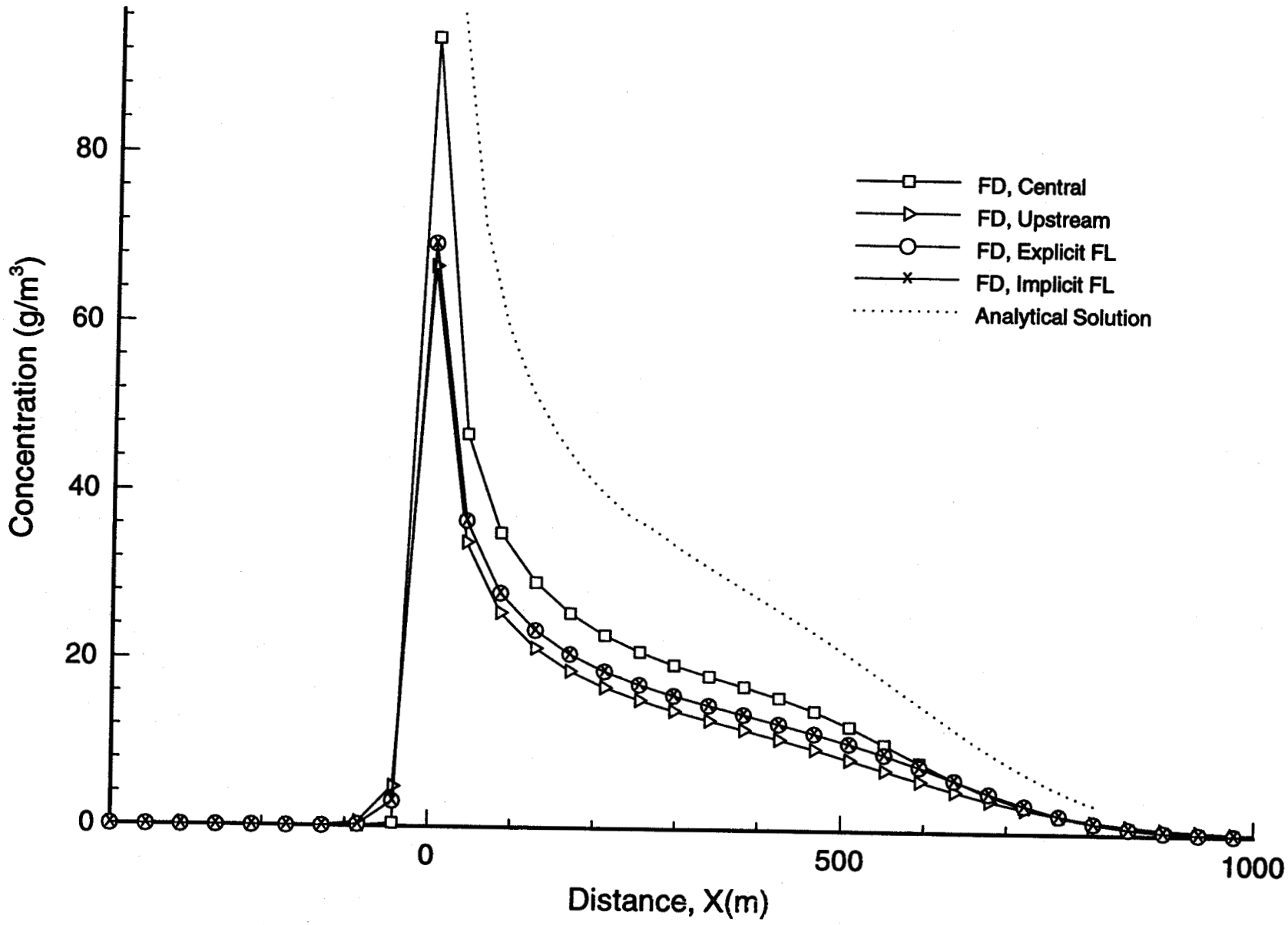

Figure 5.9 Finite Difference Results (diagonal flow).

000087

1768

0000088

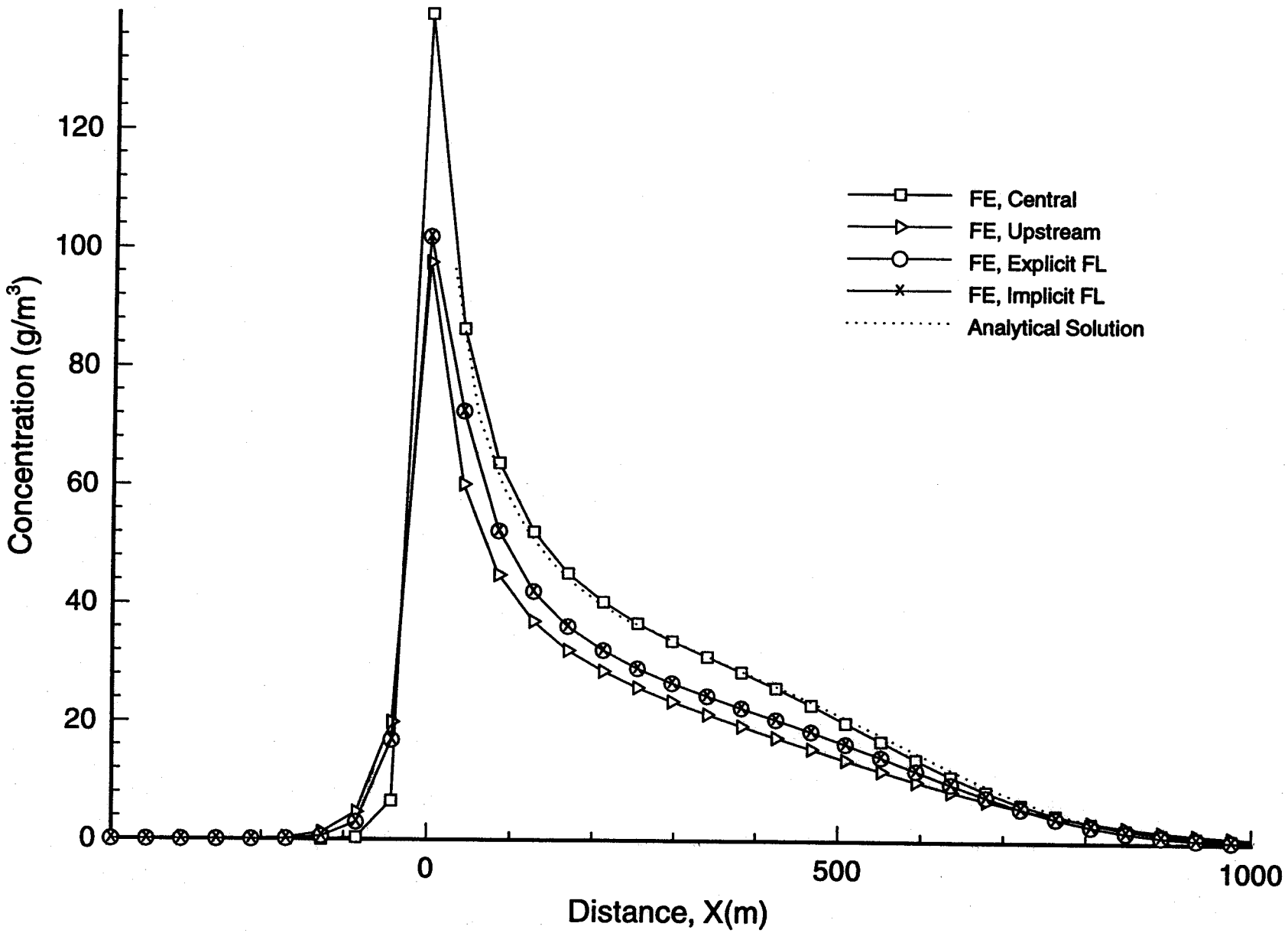

Figure 5.10 Finite Element Results (diagonal flow).

6.0 GENERAL MODEL APPLICATION PROCESS

6.1 MODEL BOUNDARY AND GRID

6.1.1 Specification of Mesh Parameters For Rectangular Grid

The rectangular mesh used by VAM3DF is generated as follows. If a fully three-dimensional analysis of the problem is required, the coordinate axes of the grid must be oriented such that the convention of a right hand cartesian system is followed and either y or z axis points in the upward vertical direction. If a two-dimensional analysis of the problem is required, the x and y axes need to be in the plane where spatial variation of the unknown dependent variable occurs. If an axisymmetric analysis is required, the x and y axes are oriented to correspond to the radial and vertical axes, respectively, of the cylindrical coordinate system.

Mesh specification parameters for a rectangular grid are listed in Appendix A, User's Guide.

The element topology (incidence matrix) is always generated for a rectangular mesh. Node numbering sequence of the grid starts from the first x-y plane (or slice). A parameter called ISWAP is used to indicate whether the numbering is along y or x axis (see Figures 6.1 and 6.2). The purpose of ISWAP is to achieve a smaller bandwidth in a case where 2-D or axisymmetric analysis is performed with the use of a direct banded matrix solver. For the 3-D simulation, ISWAP provides alternatives for input of data related to element indexing of material formations.

Even with the use of a rectangular mesh, the code allows an irregular region to be treated in a convenient manner. The user needs to overlay the selected rectangular grid and the modeled region. Elements that are outside the interested region can then be blocked out by zeroing components of the property array IPROP that correspond to such elements.

6.1.2 Specification of Mesh Parameters For Curvilinear Grid

The curvilinear mesh of VAM3DF should be used when the nodal coordinates within the domain do not lie on a rectangular grid system. This option for data input is required when transition elements are utilized in discretizing the domain. The curvilinear grid is also useful for irregular domain geometries or formation layering. Examples of the use of a curvilinear grid and transition elements are shown in Figure 6.3. Orthogonality of the curvilinear grid should be maintained as much as possible, for accuracy in element matrix computation. If a fully three-dimensional analysis of the problem is required, the coordinate axis of the grid must be oriented such that a right handed coordinate system is followed with either y or z axis pointing in the upward vertical direction. If a two-dimensional analysis of the problem is required, the x and y axis need to be in the plane of solution of the dependent variable. For an axisymmetric analysis, the x and y axes correspond to the radial and vertical axes of the cylindrical coordinate system.

Several options have been provided to simplify data input for curvilinear grid systems. General mesh generation control for the curvilinear grid is provided by record set 14a (see Appendix A).

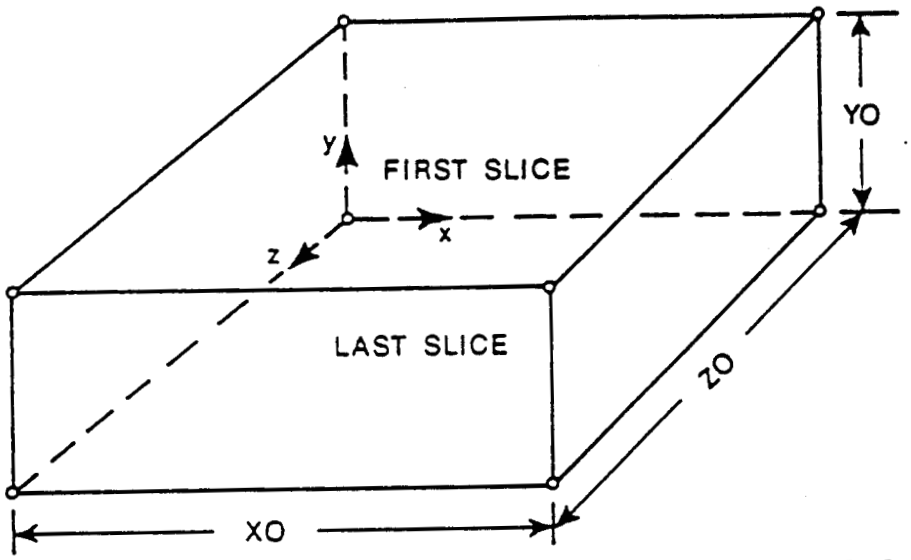

NROWS = 4, NCOLS =5, DX =25, DY =17.

XSTART = YSTART = 0., XO = 100., YO = 51.

SCFX = SCFY = 1., DXMAX = 25., DYMAX = 17.

SCFX = $\Delta x_i / \Delta x_{i-1}$, SCFY = $\Delta y_j / \Delta y_{j-1}$.

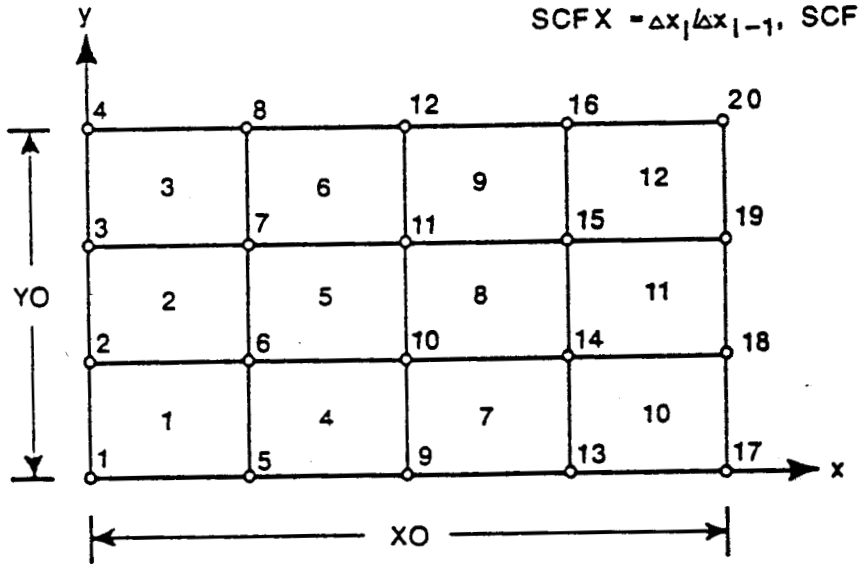

Figure 6.1 **Automatic discretization of flow region using the vertical slicing approach (y-axis vertically upward), and ISWAP=0.**

000090

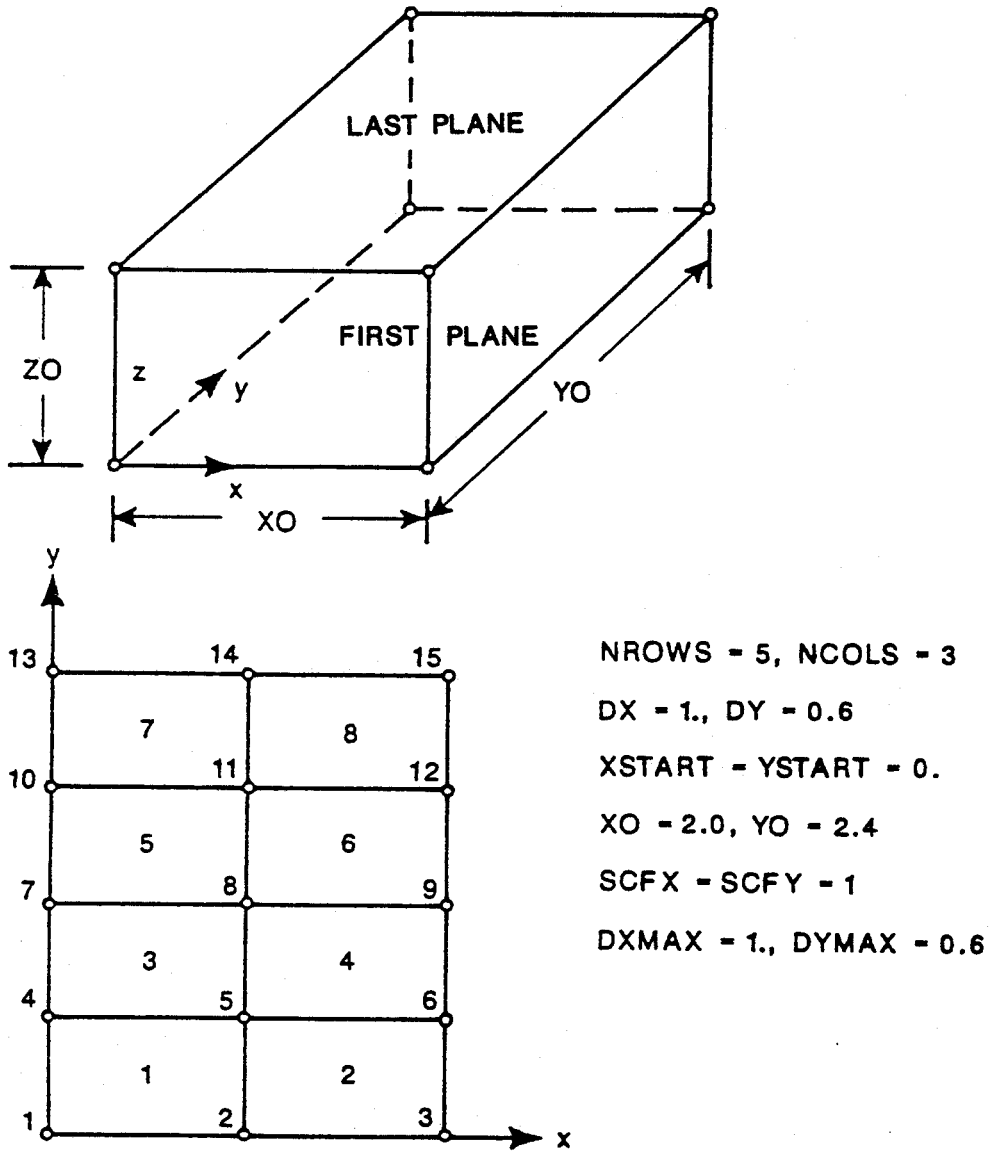

Figure 6.2 **Automatic discretion of flow region using the horizontal sectioning approach, with ISWAP=1.**

If transition elements are used in discretizing the domain (IPNCH=1), the elemental topology of the discretized domain needs to be input. VAM3DF allows the grid to be graded in the x or y directions, but not across planes in the z-direction. Hence, the nodal connectivities of only the first nodal slice are required as input (see group 14e of Appendix A), and the incidence matrix of the entire discretized 3-D domain is internally generated. Identification of the transition element, its pinch node (in the first gridding plane) and the location of the pinch are also required. The incidence of the corner nodes of all elements (in the first gridding surface) are first input through the first record subset in group 14e. The transition elements, their pinch node's number, and the location of the pinch are then identified via the second, third and fourth subsets of group 14e.

If there are no transition nodes in the modeled system (IPNCH=0), the elemental topology is generated by the code. Node numbering sequence of the grid starts from first x-y plane (or slice). The parameter ISWAP determines whether the numbering is first along the y or x direction (see Figures 6.1 and 6.2, respectively). The purpose of ISWAP is to achieve a smaller bandwidth for the 2-D or axisymmetric analysis, where the direct banded matrix solver is used. For the 3-D simulation, ISWAP provides flexibility in element indexing of materials of layered systems.

6.1.3 Initial and Boundary Condition Specifications

To perform a transient flow or transport analysis or a steady-state flow analysis, an initial distribution of the dependent variable to be solved must be supplied to the code. If the initial distribution is uniform, it is sufficient to supply constant default values of head and/or concentration to the code. The default initial head may be specified in terms of either the pressure head (ψ_o) or hydraulic head (h_o). If the hydraulic head h_o is specified and the pressure head (ψ) is the chosen dependent variable (or vice versa), the user needs to tell the code to convert the specified head to its dependent variable value using the input control parameter INTSPC (record group 3 in Appendix A).

In a case of a nonuniform initial distribution of heads or concentrations, it is necessary to supply initial nodal values to the code. If only a few of the nodes in the domain have initial values that differ from the default value, the non-uniformity index NONU (group 3, Appendix A) is set to 1, and the initial values for these NPIN nodes are input from the main data file, in record group 19, Appendix A. If most of the domain has non-uniform initial conditions, NONU can be set equal to 2 and the initial values of the dependent variable for all nodes are input via a separate data file.

Boundary conditions can be given in terms of either the pressure (or hydraulic) head (depending on which is the primary variable) or concentration at boundary nodes, or in terms of the fluid or solute flux at boundary nodes. Specification of a first-type boundary condition is very straight-forward and requires no further explanation. Specifying the nodal boundary condition values in the case of a flux-type boundary condition is more involved. The procedure is explained below by means of an example.

Suppose we wish to perform a two-dimensional cross-sectional analysis of migration of a contaminant through the unsaturated zone, where the contaminant originates from a leaky

container placed on the soil surface. A close-up of the finite element grid just below the container is shown in Figure 6.4. The boundary nodes that are in contact with the container are represented with the solid circles and are arbitrarily labeled i,j...m. Other nodes are represented by open circles. Nodal spacings between the boundary nodes in the horizontal direction are Δx_a, Δx_b,..Δx_d. Let's further assume that the container loses liquid at a rate of Q cubic meters per day. The liquid is distributed uniformly over the area (S,m^2) of the container which is in contact with the soil. The so-called *distributed liquid flux* is then $q = (Q/S)$ m/d. The contaminant concentration in the liquid is c_o mg/ℓ. The *distributed solute flux* is thus $(q \bullet c_o)$ gr/(m^2/d).

We must now translate this distributed flux into the correct flux boundary conditions at the boundary nodes. Starting at node i, the procedure is as follows: The total liquid flux applied over the boundary segment between nodes i and j is $q \bullet \Delta x_a$. One-half of this is a apportioned to node i and one-half to node j. In addition, node j receives one-half of the flux entering through the segment between nodes j and k. The resulting nodal flux values are called *integrated* (or concentrated) flux boundary conditions. For the current example, the integrated nodal fluid and solute flux boundary conditions are:

node	nodal fluid flux	nodal solute flux
i	$\frac{1}{2}q\Delta x_a$	$\frac{1}{2}qc_o\Delta x_a$
j	$\frac{1}{2}q(\Delta x_a + \Delta x_b)$	$\frac{1}{2}qc_o(\Delta x_a + \Delta x_b)$
k	$\frac{1}{2}q(\Delta x_b + \Delta x_c)$	$\frac{1}{2}qc_o(\Delta x_b + \Delta x_c)$
l	$\frac{1}{2}q(\Delta x_c + \Delta x_d)$	$\frac{1}{2}qc_o(\Delta x_c + \Delta x_d)$
m	$\frac{1}{2}q\Delta x_d$	$\frac{1}{2}qc_o\Delta x_d$

In general, the integrated nodal fluxes (for a flow or transport analysis) are obtained by multiplying the areally distributed flux by the effective nodal length. The example also illustrates that in a two-dimensional analysis the nodal fluid flux has dimensions of length * length/time = L^2/T (i.e., the simulation considers a unit width in the z-direction).

In a axisymmetric analysis, the nodal (integrated) fluid flux has dimensions of L^3/T. The area of flow of a rectangular prism element receiving the flux is computed by multiplying the nodal incremental length by $2\pi\bar{r}$, where $\bar{r}$ is the centroidal radius of the element. In a fully three-dimensional analysis, the effective flow area of a flux node of the element is computed as shown in Figure 6.4.

000094

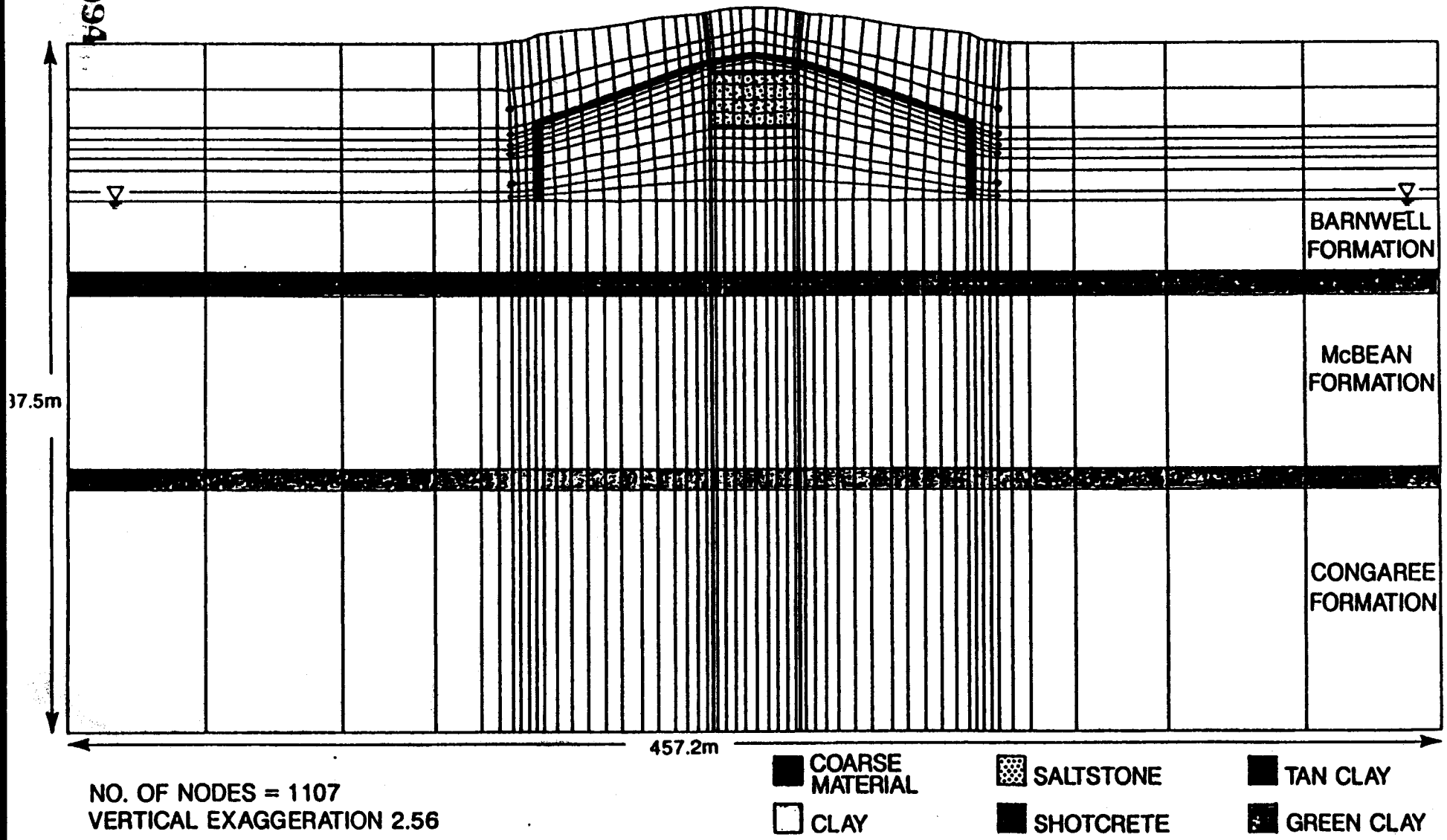

Figure 6.3 Discretization of a domain using a curvilinear grid and transition elements.

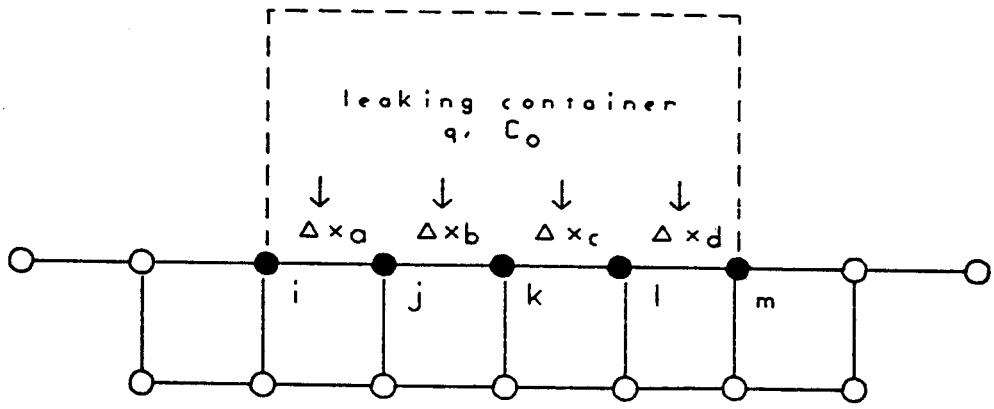

Figure 6.4 **Example illustrating calculation of integrated nodal fluxes for a two-dimensional cross-sectional analysis. Closed dots represent nodes along boundary segment receiving flux. Open dots represent remaining nodes.**

Steady-state boundary conditions for flow/transport are handled simply by specifying the node numbers and prescribed head/concentration or solute mass flux/fluid flux values. Transient boundary conditions are also handled in a convenient manner by specifying the node numbers and relationships of time versus head/concentration or flux values. The code admits both continuous and discontinuous temporal variations. A continuous variation is represented using the piecewise linear approximation passing through a number of control points. A discontinuous variation is represented using a stepped approximation passing through control points. The total number of control points is equal to the number of steps plus one.

6.2 PARAMETER ESTIMATION

After the conceptual model is complete and the system geometry has been discretized, information that is needed for estimation is assembled about calibration parameters. The parameters to be estimated can include:

- Transport properties such as dispersivities and kinetic mass transfer parameters.
- Flow hydraulic and storage properties and recharge rates.
- Boundary and initial conditions.

Transport calibration parameters are described in Sections 3.5 and 4.6. Groundwater flow parameters for the FEMP site can be updated in local areas based on new groundwater data. Boundary and initial condition parameters can also be updated.

DFM has the flexibility to view flow and transport parameters as constants over the model domain, constants within zones, or as heterogeneous parameters having geostatistical variation. Geostatistical variation can be viewed as a polynominal trend plus a spatially correlated process with a correlation distance and a standard deviation. Calibration parameters are a combination of constants, zonal constants, trend coefficients, and values of the spatially correlated process. Guidance for determining prior information about calibration parameter estimates and uncertainties can be obtained from previous data, data analysis, and the literature.

There are enough data for unique calibration when the number of data points over time that are available for calibration targets are considered. Consequently, DFM will allow for realistic transport dispersion and kinetic mass behavior with updated local flow parameters while still achieving a unique model.

6.3 INPUT FILE DEVELOPMENT

The general procedure for using VAM3DF to simulate water flow and/or solute transport in subsurface systems is outlined below.

- Prepare a diagrammatic description of the problem. The diagram should depict the solution region together with a description of the zones of different material properties and boundary conditions.

- Prepare a list of material numbers and properties to be supplied to the code.

- Design a finite-element grid for the domain with due consideration given to domain geometry, grid spacing requirements, available computing power, and simplicity of input data preparation. The complexity of the grid structure should be only as much as the problem demands.

- Prepare a sketch of the discretized region showing the orientation of the coordinate axes as well as sequential numbers of all nodes and elements in the first *x-y* plane of the simulation (Figures 6.1 and 6.2). Note that the node and element numbering order in the x-y plane can be selected using the ISWAP option, when automatic element topology generation is used (i.e., when there are no transition elements in the simulation domain).

- If a curvilinear grid is used, the *x-y* and *z* coordinates of all nodal points will need to be input. The areal *x-y* grid may be automatically generated using conformal mapping procedures, or may be prepared by creating flow-nets over the simulation domain and digitizing the flow-net element structure. Contours of depth to various layers may then be digitized and interpolated onto the *x-y* grid structure to provide the *z*-coordinate values of the nodes. Alternatively, an automatic orthogonal curvilinear grid generator for three-dimensional regions may be used. Several nodal-coordinate input options are provided to alleviate the difficulties in preparing 3-D data files for rectangular and curvilinear grids.

- Prepare steady-state boundary condition data. These data are classified into two sets. The first set consists of global node numbers and prescribed values of dependent variables to be determined. The second set consists of global node numbers and prescribed values of integrated nodal fluxes. If there are no steady-state boundary conditions, this step of the simulation procedure may be omitted.

- Prepare transient boundary condition data. The data are also classified into two sets. The first set consists of global node numbers and the time graph of prescribed values of dependent variables to be determined. The second set consists of global node numbers and the time graph of prescribed values of integrated nodal fluxes.

- Follow the input data preparation instructions given in Appendix A and supply the required input to the code.

- Run the code and interpret the output (a guide is provided in Chapter 9 of HydroGeoLogic, 1995).

VAM3DF is designed to analyze one problem or several consecutive problems in a single computer run. The code can perform the following types of simulations: (1) water flow in variably or wholly saturated porous media (IMODL=1), (2) solute transport (IMODL=0), and (3) combined flow and transport (IMODL=2) simulation.

Selection of the finite element grid and the various simulation options discussed in section 6.1 should take into consideration the required accuracy of the simulation, the available computing power, and simplicity of input data preparation. If a rectangular mesh is selected, the mesh and grid-co-ordinate data required for the simulation are automatically generated as discussed in

Section 6.1.1. Curvilinear meshes require coordinate input of the grid as discussed in section 6.1.2. A mesh containing transition elements further requires element topology input. Initial and boundary condition input is discussed in Section 6.1.3.

6.3.1 Required Input Data

Input data for variably saturated flow simulations include the following (see Appendix A for details of data file construction):

(1) System Geometry

- Horizontal and vertical dimensions including layering and other heterogeneities (L)

(2) Porous Medium Properties

- Horizontal longitudinal and transverse components of saturated hydraulic conductivity, K_{hL} and K_{hT} (LT^{-1})
- Vertical component of saturated hydraulic conductivity, K_v (LT^{-1})
- Specific storage, S_s (L^{-1})
- Saturated water content, θ_s

(3) Constitutive Relationships for Variably Saturated Flow

- Parameter n of the Brooks-Corey relation (2.9).
- Air-entry pressure head, ψ_a
- Parameters α, β and γ of the van Genuchten relations (2.10) and (2.11) (α has dimensions of L^{-1}).

000098

(4) Initial and Boundary Conditions

- Initial distribution of pressure head, ψ_o (L)
- Prescribed values of pressure head, $\bar{\psi}$ (L)
- Prescribed values of nodal fluid flux, Q (Q has dimensions of L^2T^{-1} for a cross-sectional simulation and L^3T^{-1} for an axisymmetric or a fully three-dimensional simulation)
- Other boundary conditions such as evaporation, infiltration and plant root uptake.

Input data for the transport model include the following:

(1) System Geometry

- Horizontal and vertical dimensions including layering and other heterogeneities (L)

(2) Porous Medium Properties

- Dispersivities α_{LH}, α_{LV}, α_{TH}, α_{TV} (see Section 3.0) (L)
- Free-water molecular diffusion coefficient, D_o (L^2T^{-1})
- Effective porosity, ϕ
- Bulk density, ρ_B (ML^{-3})

(3) Properties of Solute Species

- Decay coefficient, λ (T^{-1})
- Distribution coefficient, k_d (L^3M^{-1})
- Desorption rate coefficient, α_d (T^{-1})
- Chemisorption rate coefficient, α_c (T^{-1})
- Precipitation rate constants, α_p (T^{-1})
- Zeroth order dissolution rate constant, α_s ($ML^{-3}\ T^{-1}$)
- Solubility limits, S_L

(4) Darcy velocity components of the fluid phase considered, v_1, v_2 (and v_3 for fully 3-D) (LT^{-1})

(5) Saturation of the fluid phase considered, S_w

(6) Initial and boundary conditions

- Initial distribution of concentration, c_o (ML^{-3})
- Prescribed values of concentration, $\tilde{c}$ (ML^{-3})
- Prescribed values of solute flux, $\dot{m}$ ($\dot{m}$ has dimensions of $ML^{-1}T^{-1}$ and MT^{-1} for cross-sectional and axisymmetric analyses, respectively).

(7) Boundary geometry and fluid flux data at the boundary nodes.

000100

6.4 CALIBRATION

It is envisioned that a calibration and prediction code will be delivered in a Phase 2 effort. The calibration and prediction will be based on Data Fusion Modeling (DFM) described in Data Fusion Modeling for Groundwater Systems (Porter et al., 1996).

Calibration and prediction are driven by what model outputs with what statistical confidence are needed to meet regulatory requirements. The effort begins by defining the VAM3DF model parameters needed to predict what is wanted. Section 6.2 describes candidate parameters for calibration. With DFM, the parameters may be viewed as deterministic constants throughout the model domain, as deterministic constants defined in zones, or as heterogeneous parameters having geostatistical variation. Then previous data, data analysis, and experience at similar sites are reduced to prior parameter estimates and estimate uncertainties for deterministic and geostatistical parameters.

Calibration targets are selected from the existing time-history of measured data. Then DFM can be run in estimation mode to calibrate parameters, predict model outputs, and compute the statistical prediction error variances. Calibration targets can also be selected from candidates for new monitoring data. Then DFM can be run in covariance simulation (DOE, 1997) mode to determine the reduction in prediction error variances that would result if the data were acquired. This allows what-if analyses to optimize monitoring well locations and sampling frequencies to achieve the best tradeoff between plume prediction confidence and monitoring cost.

As described in the Hydrologic Data Fusion (DOE, 1997), DOE invested in VAM3DF implemented with DFM for the express purpose of providing a software platform that could be customized to handle the wide range of problems encountered at waste sites such as Fernald. DFM provides a Bayesian least squares estimate of calibration parameters. The nonlinear least squares solution is provided by Gauss-Newton methods that replace the nonlinear problem with iteration of a sequence of linear problems. The linear problems can be solved with Square Root Information Filter (SRIF) (Bierman, 1977) methods or by a fast solver using conjugate gradient methods. The SRIF method can be modified for efficiency to have separate grids for the numerical models and geostatistical models for heterogeneous parameters. Then the numerical model grid is selected based on the physical processes and the geostatistical grid is selected based on the degree of heterogeneity.

Based on the above, calibration and prediction code using DFM may be carried out by performing the following:

- Determine what VAM3DF outputs with what statistical confidence are required to meet regulatory requirements.
- Determine the calibration parameters and the type of prior information that are needed for constant, zonal, and geostatistical parameters.
- Select the type of calibration targets that will be used from the existing data and from candidate new monitoring data.
- Customize the software interface between VAM3DF and DFM.
- Customize DFM to provide both estimation and covariance simulation modes.

- Test and verify all code.

6.5 MODEL OUTPUT

Line printer output from VAM3DF is organized for each problem into categories of information. These categories are summarized as follows:

- Listing of general control input data supplied to the code by the user.
- Listing of the generated mesh data or user supplied mesh data.
- Listing of boundary condition data.
- Listing of initial condition data.
- Listing of user-supplied steady-state values of element velocities and saturation.
- Listing of user-supplied data pertaining to the nonzero flux nodes and flux values.
- Listing of element numbers and centroidal coordinates.
- Listing of the input data supplied from TAPE 9 for each time step.
- Listing of information pertaining to the computation of element matrices and incorporation of boundary conditions performed by the code.
- Listing of node numbers and values of head or concentration computed by the code. This listing is given for every *n*-th time step, where *n* is the value of NSTEP.
- Listing of element numbers and water saturation values for the elements that became unsaturated. This listing is given for every *n*-th time step, where *n* is the value of NSTEP.
- Listing of element numbers and the *x*, *y* and *z* components of Darcy velocity. This listing is given for every *n*-th time step, where *n* is the value of NVPR.
- Global mass balance information

6.5.1 Output Control

Output streams are controlled by several control parameters, the values of which must be supplied to the code. Record Group 5 (see Appendix A) lists the procedures used to control various categories of line printer output. The user should decide how much printed output is really needed for the problem simulated. For example, the mesh data and the boundary conditions are normally not needed in the restart run of the same problem.

000102

7.0 SITE SIMULATION

7.1 BACKGROUND INFORMATION

The VAM3DF model discussed earlier was used to simulate flow and Uranium transport in the Great Miami Aquifer (GMA) at Fernald. The site was the subject of several modeling studies using the Sandia Waste Isolation Flow and Transport (SWIFT III) code. Detailed description of the SWIFT GMA model can be found in DOE (1994). The SWIFT GMA model was also used to study the proposed remediation scenarios for aquifer restoration (DOE, 1997). The geochemical processes that affect the fate and transport of uranium were modeled in the SWIFT GMA model using the equilibrium-partitioning coefficient K_d. Implications of the underlying simplifying assumptions, implied in using the partitioning coefficient K_d, are discussed in Appendix A of the Baseline Remedial Strategy Report (DOE, 1997). The kinetic contaminant mass transfer module discussed in Section 4 was used to improve on these simplifying assumptions.

A three-dimensional (3-D) ground water model was developed using VAM3DF to simulate flow and mass transport in the GMA. The SWIFT GMA model grid, boundary and initial conditions, and input parameters were used directly in the VAM3DF GMA model. Owing to some differences in the formulation (VAM3DF is mesh-centered, while SWIFT is block-centered), the vertical discretization of the aquifer was modified to preserve the distinction between different hydrogeologic layers and the distribution of hydrogeologic properties of each layer. The simulations presented in the following sections can be grouped into four main sets of simulation runs. The main purpose of the first set was to ensure that the VAM3DF GMA model is capable of reproducing the same flow field predicted by the SWIFT GMA model. In the second set of simulations, the uranium plume migration was simulated using the transition K_d to compare the results with SWIFT GMA model results. In the third set of simulations, the kinetic module was used to simulate the migration of the uranium plume and to examine the sensitivity of the model to the variations in the kinetic parameters. For comparison purposes, the same flow and transport parameters, used in SWIFT GMA model, were used in the first three sets. In the last set of simulation runs, some reasonable transport parameters were used to examine the performance of the kinetic module in distributing the uranium mass between the different phases within the site during the 10-year period of the proposed remediation scenario. Also chemisorption influence on the transport of uranium was examined in the last set of simulation runs.

7.2 MODEL SCENARIOS SCENARIOS

The SWIFT GMA model grid contains 120 by 112 cells. Each cell is square and has a side length of 125 ft. The grid covers an area of 15,000 ft by 14,000 ft. Being a block-centered model, the first node is located in the center of the first block at a distance of 62.5 feet from the model edge in the x and y directions. To discretize the same domain using the mesh-centered grid utilized in VAM3DF, the first node should be placed at the corner of the model and the domain will require 121 by 113 nodes. To avoid shifting the nodes, the model nodes where placed at the same location as those of the SWIFT GMA model. As a result, the actual extent of the VAM3DF GMA model was reduced to 14,875 ft by 13,875 feet using 120 by 112 nodes. Figure 7.1 shows the extent of the model grid with respect to the site.

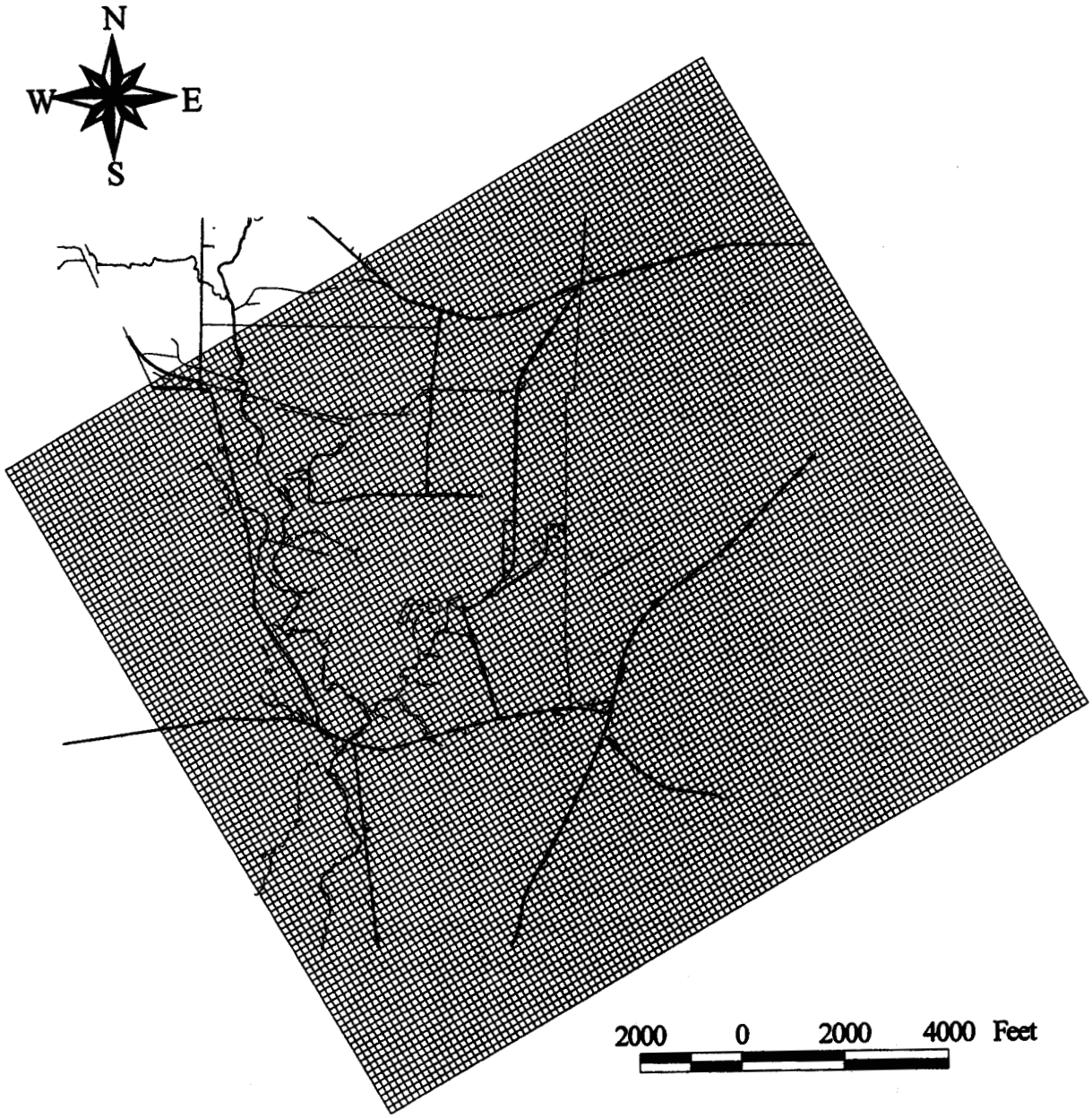

Figure 7.1 VAM3DF GMA Model Mesh with Respect to Fernald Site.

In addition, the SWIFT GMA model consisted of six layers. The SWIFT GMA nodes are located at the center of each layer (Figure 7.2). To preserve the distinct hydrogeologic layers, 12 nodes were used to discretize the aquifer in the vertical direction. The first node was placed at the upper boundary while the last node was placed at the lower boundary of the aquifer. Intermediate nodes were distributed such that each layer is represented by two nodes. One node was placed below the top boundary while the other was placed above the bottom boundary of the hydrogeologic layer. Nodes located on either side of a boundary between two layers were placed at an equal distance from the common boundary as shown in Figure 7.2. The nodes were located such that the distance between a node and the closest boundary is one third the thickness of the current layer or one third the thickness of the layer that share the common boundary, whichever is smaller. Such discretization allows direct comparison between the SWIFT GMA and the VAM3DF GMA models.

In SWIFT GMA model the uranium source loading is applied to the upper layer of the model, which is partially saturated. The upper layer was discretized using two nodes. The upper node is placed on the upper boundary of the aquifer. To avoid placing the source loading on the upper boundary of the aquifer, the source loading is applied at the lower node of Layer 1 instead. Such an approach was necessary to avoid applying the source loading on the unsaturated part of the aquifer and is more conservative. In the following discussion, Layer 1 had the highest uranium concentration among the model layers and the concentration distribution in the lower node of Layer 1 was used to represent the highest concentration in the site.

As mentioned above, the simulation runs are grouped in four main sets; Set A, Set B, Set C, and Set D. The conditions and parameters used in each set are listed in Tables 7.1 and 7.2, and summarized below.

1. Set A involves simulating the flow field during the four stress periods of the 10-year remedial scenario (DOE, 1997). Three simulation runs were carried out for the following conditions:
   - pre-pumping conditions (Run A1).
   - 10-year scenario under the old pumping rates at the Southwestern Ohio Water Company (SOWC) wells (10 mgpd and 8 mgpd) (Run A2).
   - 10-year scenario under the new pumping rates at the SOWC wells (12 mgpd and 6 mgpd) (Run A3).
2. Set B involves simulating the transport of the uranium plume during the 10-year pumping scenario. Adsorption/desorption was assumed to follow the equilibrium model with transitional K_d (as in SWIFT GMA model) (Run B1).
3. Set C involves simulating the transport of the uranium plume during the 10-year pumping scenario. Adsorption/desorption was represented using the kinetic module. Five simulation runs were carried out (C1 though C5) with different adsorption/desorption parameters as shown in Table 7.2.

4. Set D involves simulating the transport of the uranium plume during the 10-year pumping scenario. In addition to adsorption and desorption, chemisorption was considered in this set. Three simulation runs were carried out with different chemisorption rates.

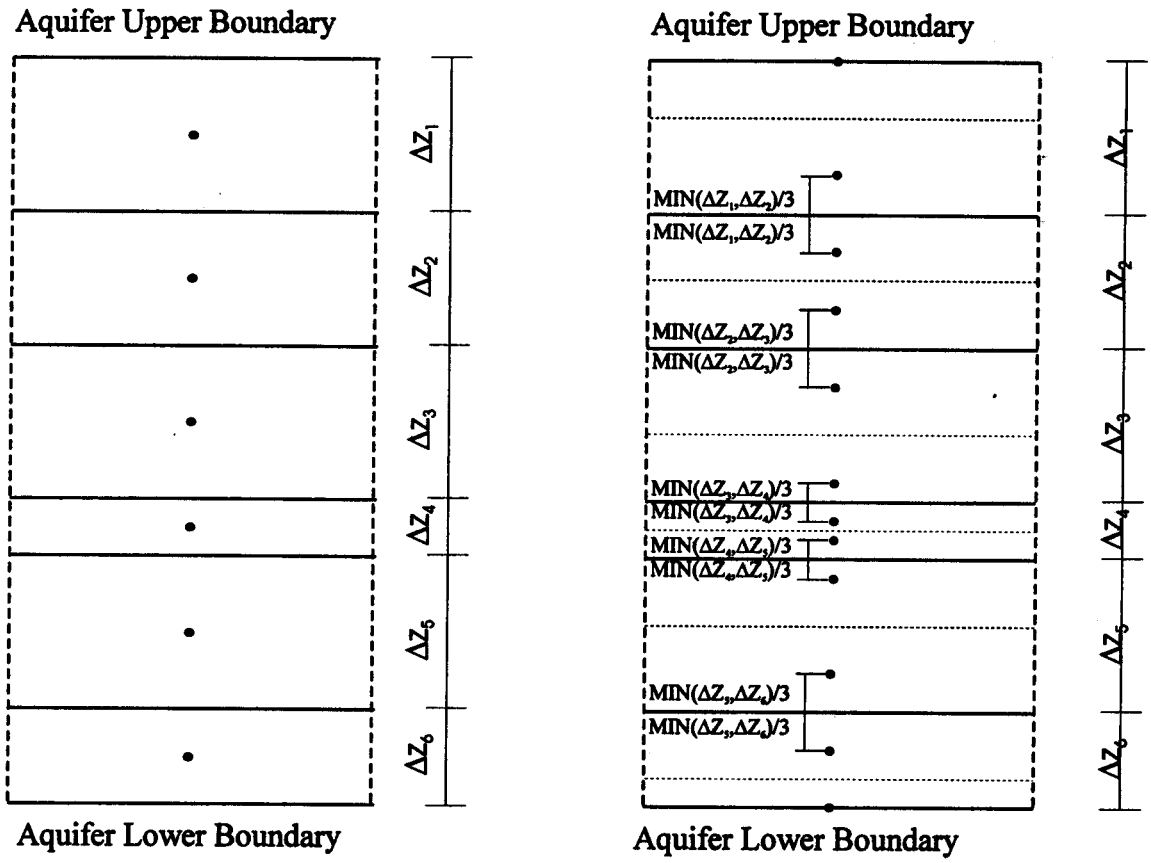

Figure 7.2 Discretization of the Hydrogeologic Layers in SWIFT and VAM3DF GMA Models.

000106

Table 7.1
Pumping stress and boundary conditions used in the flow simulations

Simulation Run	On site pumping wells	SOWC well 1, mgpd	SOWC well 2, mgpd	Eastern Boundary Condition	Results
A1	Inactive	8	10	Constant Head	Figure 7.3
A2	Active	8	10	Constant Head	Figures 7.4 through 7.11
A2	Active	6	12	Head-dependent Flux	Figures 7.12 through 7.15

Table 7.2
Parameters used in the transport simulations

Simulation Run	α_L, ft	α_T, ft	α_V, ft	α_d, 1/day	K_d, L/kg	α_c, 1/day	Results
B1[1]	100	0.1	0.1	0	1.78/17.8	0	Figures 7.16 through 7.19
C1	100	0.1	0.1	0.01	17.8	0	Figures 7.21 through 7.24
C2	100	0.1	0.1	0.01	1.78	0	Figures 7.25 through 7.28
C3	100	0.1	0.1	0.1	1.78	0	Figures 7.29 through 7.32
C4	100	0.1	0.1	0.5	1.78	0	Figures 7.33 through 7.36
C5[2]	100	0.1	0.1	0.1	1.78	0	Figures 7.37 through 7.40
D1	100	10.0	1.0	0.01	1.78	0.001	Figures 7.41 through 7.47
D2	100	10.0	1.0	0.01	1.78	0.0001	Figures 7.48 through 7.52
D3[3]	100	10.0	1.0	0.01	Tabular Relation	0.0004	Figures 7.53 through 7.57

[1] Simulation was performed using transitional K_d.
[2] Simulation was performed using initial zero solid phase concentration.
[3] A tabular equilibrium (piecewise linear) C_w/C_s was used in the simulation.

The values of the desorption rate, α_d, in Table 7.2 are intended to reflect a range of slow-to-fast reactions. There are no experimental data to assist in estimating the parameter. However, equilibrium batch experiments have shown that equilibrium is attained in a short period of time, in the order of hours-to-days. As a result, the half-live for the desorption process is likely to be of the same order, (hours-to-days) which support the choice of values in Table 7.2.

In Run A1, a steady state simulation prior to the installation of remediation wells was carried out. The results were compared to water levels produced from geostatistical analyses of measured water levels (DOE, 1994). Results of the simulated heads are presented in Section 7.3.

The VAM3DF GMA model was then used to simulate the flow fields during the 10-year remedial scenario chosen for the aquifer restoration (Run A2). The scenario consists of four stress periods, namely; 1997, 1998, 1999 through 2003, and 2004 through 2006. The

extraction/injection schedule used in the simulation is described in Table 5-1 of the Baseline Remedial Strategy Report (DOE, 1997). Similar to the approach used in the SWIFT GMA model, groundwater flow was assumed to be steady-state within each stress period. The boundary conditions and recharge rates used in Run A2 were similar to those used in SWIFT GMA model. The results of the Run A2 are compared to the SWIFT GMA model in Section 7.3.

One distinct feature of the flow field at the site is the influence of the Southwestern Ohio Water Company (SOWC) collector wells. The pumping rates of these wells have been changed from those rates used in the SWIFT GMA simulations (White, personal communication 1998). Pumping rates from collector well 2, which is located to the north of the Big Bend of the Miami River, was increased from 10 mgpd to 12 mgpd. While pumping rate from collector well 1, located to the south of the bend, was reduced from 8 mgpd to 6 mgpd. These wells are located close to the eastern boundary of the model. The influence of the changes in the pumping rates is expected to extend beyond the model eastern boundary. To simulate the impact the change has on the flow field; the eastern boundary of the model was converted from a constant head boundary (Run A2) to a head-dependent flux boundary (Run A3). Formulation and implementation of the head-dependent flux boundary in VAM3DF is discussed in HydroGeoLogic (1995). The governing equation for the flux across a head-dependent boundary conditions is given in VAM3DF by:

$$Q_I = A_I \ (K/b)_{bed} \ (h_T - h_I) \tag{7.1}$$

where A_I is the effective flow area of node I, K is the hydraulic conductivity, b is the distance between the specified head, h_T, and node I where the head is h_I. The specified head h_T was chosen from a larger model of the study area (DOE, 1993). Head values at column 49 of the IT Model (DOE, 1993) are located at a distance of about one mile from the VAM3DF eastern boundary and were used as the specified head h_T. The term $A_I(K/b)_{bed}$ represents the conductance of the head-dependent boundary. The whole term was estimated in the following manner. Flux across the eastern boundary was calculated during Run A2. The conductance was then calculated from Equation 7.1 using the head h_I from Run A2. The values of the conductance estimated in this manner were then used in Run A3 with the new pumping rates at the collector wells of the SOWC.

Simulation runs of uranium plume migration (simulation sets B, C and D) were performed using the steady state velocity field for each stress period from Run A2 (with the old SOWC wells pumping rates). Also in all three sets of simulations, the source loading and initial concentration distribution were taken directly from SWIFT GMA model. As mentioned earlier, the source loading was applied to the lower nodes of Layer 1 in all three sets of simulations. In the SWIFT GMA model, the geochemical processes affecting the migration of the uranium plume were simplified using the assumption of equilibrium partitioning between the aqueous and the solid phases. Two phases of transport were considered. During the first phase, adsorption controls the migration of uranium and the adsorption partitioning coefficient K_d = 1.78 L/kg was used. The second phase was dominated by desorption and started after the removal of the dissolved plume and source loading. A partitioning coefficient, K_d = 17.8 L/kg, was used during the second phase. Details of the modeling approach with K_d transition are presented in Appendix A of the Baseline Remedial Strategy Report (DOE, 1997). The simplifying assumption of equilibrium sorption with transitional K_d, used in the SWIFT GMA model, was used in the first group of

VAM3DF GMA (Run B1). Transport parameters used in Run B1 are shown in Table 7.2. For comparison, SWIFT GMA model transport parameters were used in Run B1.

The kinetic module discussed in Chapter 4 was then used to simulate the geochemical processes affecting the fate and transport of uranium. The simulations were performed over the four stress periods. In simulation Set C (Runs C1 through C5), the kinetic behavior of adsorption/desorption processes was modeled using the adsorption and desorption rate constants α_a and α_d, respectively. Such an approach accounts for the delay in mass transfer between the aqueous and solid phases as opposed to the instantaneous mass transfer implied in the equilibrium models (as in Run B1). However, in Run C1 through C5, the process is still fully reversible and all the adsorbed mass is always available for desorption. The initial solid-phase concentration was assumed to be in equilibrium with the initial aqueous phase concentration in Runs C1 through C4. In Run C5, the initial adsorbed mass was assumed to be zero. Such a condition was used to examine the influence of the initial condition on the simulation. The results of the simulation Set C are discussed in Section 7.3.

In simulation Set D, the irreversible process of chemisorption is incorporated in the VAM3DF GMA model. The difference between the "apparent" adsorption and desorption equilibrium partitioning coefficient K_d estimated experimentally was attributed to the irreversible process of chemisorption (DOE, 1997). A detailed discussion of the geochemical processes involved and the implications on the "apparent" K_d is given in Appendix A of the Base Line Remedial Strategy Report (DOE, 1997). Simulation set D (Run D1 through Run D3) was used to examine the effect of chemisorption on the fate and transport of uranium. In Run D1, a high chemisorption rate was used while a low chemisorption rate was used in Run D2. Mass balance analysis of Runs D1 and D2, showed that the initial uranium mass on the solid phase may be overestimated because of the use of a linear sorption isotherm. It is known that the adsorption ability of the solid phase starts to decrease at higher concentrations, which leads to nonlinear equilibrium isotherms. To represent such a condition, a tabular equilibrium isotherm was used in Run D3. The isotherm was used for estimating the initial solid-phase concentration and for limiting the mass transfer to the solid phase at high concentrations (Run D3).

Simulation runs described above were carried out on a Personal Computer (PC) equipped with a 200 Mhz Pentium processor with 300 MByte Random Access Memory (RAM) and WindowsNT operating system. A number of factors may have affected the computer run time. External factors included delay caused by other jobs running on the same processor and network traffic since input and output files were placed on a central server. Simulation options such as size of time step, allowable tolerance, type of nonlinearity, and type of simulation (transient or steady state) also affected the run time. In Table 7.3, estimates of the total computer time required for the simulations are presented. No attempt was made to measure processor clock cycles during the simulations.

Table 7.3
Estimate of the computer run time for the 10-year scenario

Simulation Run	A1-A3	B1	C1-C5	D1-D2	D3
Run Time	20-40 minutes	0.5-2 hours	2-6 hours	2-6 hours	4-10 hours

7.3 VERIFICATION BASED ON THE EXISTING MODEL

Simulation Sets A and B are similar to the SWIFT GMA model simulations. For the flow simulations (Set A), the flow fields in different layers were quite similar to one another. Hence, the results presented here are limited to the upper hydrogeologic layer (Layer 1). As mentioned before, the uranium source loading was applied to the lower node of Layer 1. Also, Layer 1 had the highest initial uranium concentration in the model. Hence, lower node of Layer 1 was also chosen for presenting the uranium plume configuration. Concentrations in lower layers are lower than those in Layer 1 in all simulations.

The first simulation run (Run A1) was used to verify the model against measured water levels. Table 4.3.8, of the SWIFT Great Miami Aquifer Model Summary of Improvements Report (DOE, 1994), shows a comparison between the simulated heads using SWIFT and the water levels calculated from well measurements. Details of the water level measurements and the geostatistical method used to derive the head at the SWIFT GMA model nodes are discussed in DOE (1994). Figure 7.3 shows the simulated head contours for the lower node of Layer 1 using VAM3DF. The well locations are posted on the contour map for reference. Table 7.5 shows a comparison between the head estimated from the VAM3DF GMA model and the geostatistically estimated water levels. The model results seem to be in close agreement with the estimated water levels in most of the study area except in the vicinity of the SOWC collector wells. Similar results can be observed in Table 4.3.8 of the SWIFT Great Miami Aquifer Model Summary of Improvements Report. The largest residual in the case of SWIFT occurred also in the vicinity of the collector wells. As discussed in Section 7.2, the VAM3DF GMA model was then used to simulate the flow field during the four stress periods representing the 10-year remediation scenario (Run A2). Figures 7.3 through 7.6 show the head contours in Layer 1 for each stress period estimated using the VAM3DF and SWIFT GMA models for Run A2. The results of the simulations are compared directly to the SWIFT GMA model in Figures 7.4 through 7.7. Favorable agreement can be observed in the figures, despite the difference in vertical discretization between the two models. Similar agreement was observed when results from other hydrogeologic layers were compared. In Figures 7.8 through 7.11, the drawdown caused by the on-site pumping wells is shown for the four stress periods resulting from Run A2. The drawdown was calculated by performing two sets of simulations. In the first, on-site wells were turned off and the head was calculated using the VAM3DF GMA model. In the second, the wells were turned on (i.e. Run A2). The drawdown is calculated as the difference between the two sets of simulations. Figures 7.7 through 7.10 can be compared to Figures 5-7 though 5-10 of the Baseline Remedial Strategy Report (DOE, 1997). The difference in the drawdowns between the VAM3DF and SWIFT models result can be attributed to the difference in the choice of the starting head (head value when the pumping wells were turned off).

To account for differences in pumping rates at the SOWC collector wells, the eastern boundary of the model was transformed from a constant head boundary into a head-dependent flux boundary in Run A3. Formulation and implementation of the head-dependent flux boundary in VAM3DF is discussed in HydroGeoLogic (1995). The steady-state hydraulic head h_T (Equation 7.1) was estimated from a larger model of the study area, (the IT model discussed in DOE, 1993). Conductance of the head-dependent flux boundaries was represented by the term $A_I\ (K/b)_{bed}$ (Equation 7.1). Run A2, with the original collector wells pumping rates, was used to estimate the

000110

flux across the head-dependent flux boundary, and subsequently estimate the conductance of the boundary required for Run A3. The conductance ws then used to simulate the flow field under the new pumping conditions for Run A3. Figures 7.12 though 7.15 show the new groundwater elevations from Run A3 together with the groundwater elevations from Run A2. The figures show

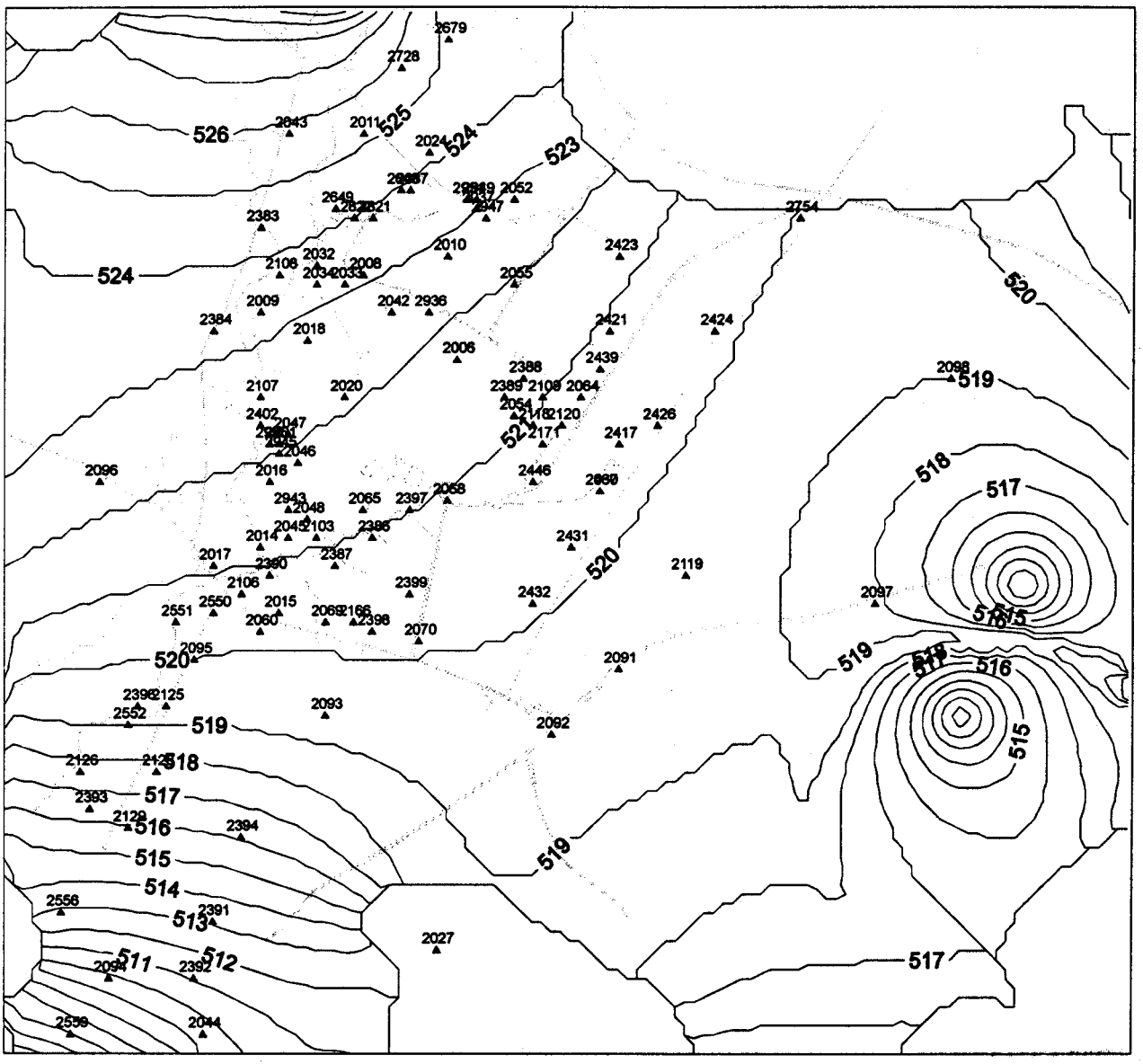

Figure 7.3 VAM3DF GMA Model Steady State Head Contours Prior to on-site Pumping Wells (Lower Node of Layer 1) (Run: A1).

000112

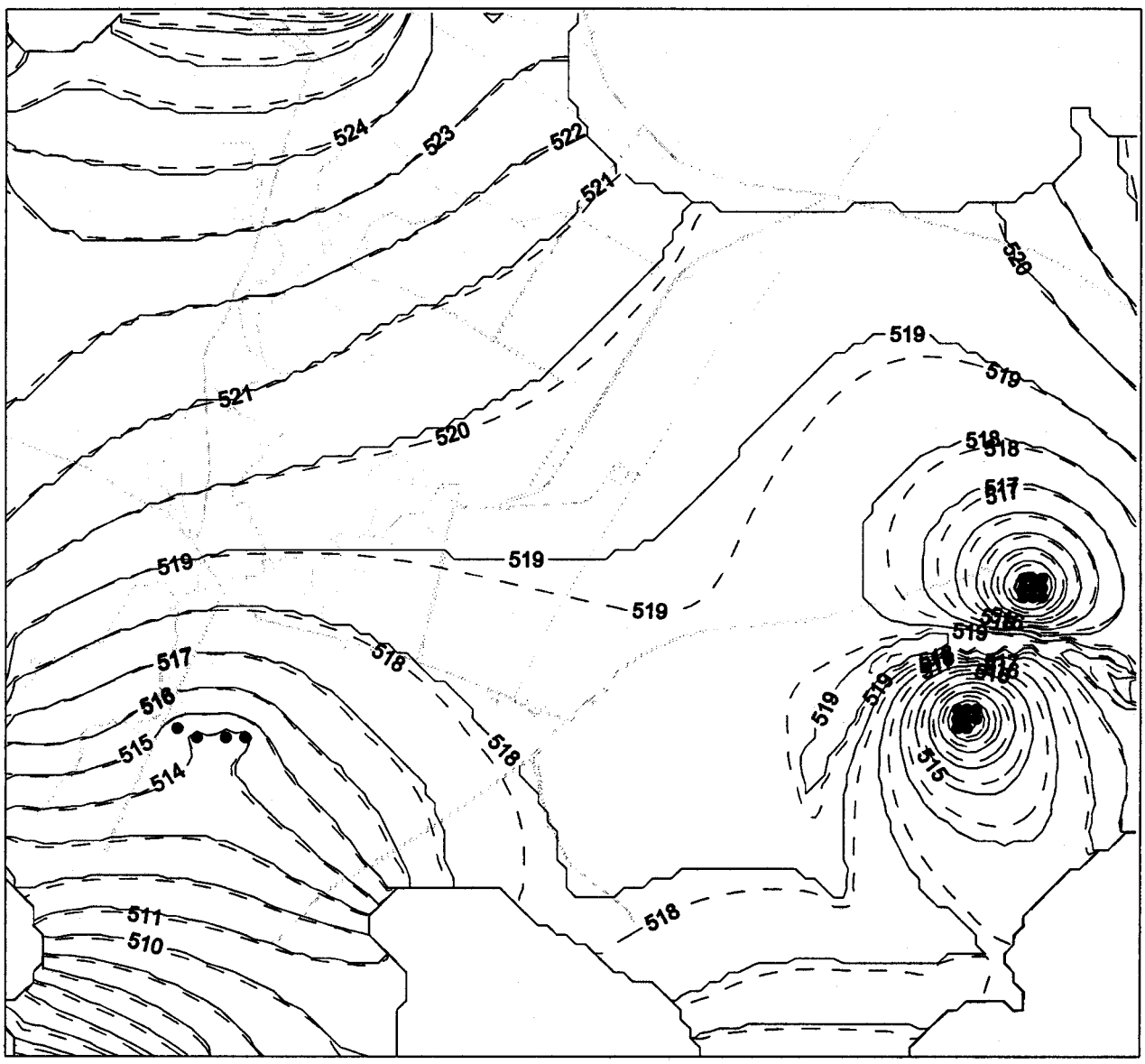

Head Contour in ft-MSL:

— 500 — VAM3DF

--- 500 --- SWIFT

• Well

2000 0 2000 4000 ft

Figure 7.4 Modeled Ground Water Elevations for 1997, for the 10-Year Scenario. Comparison between SWIFT (layer 1) and VAM3DF (lower node of layer 1) GMA Model (Run: A2).

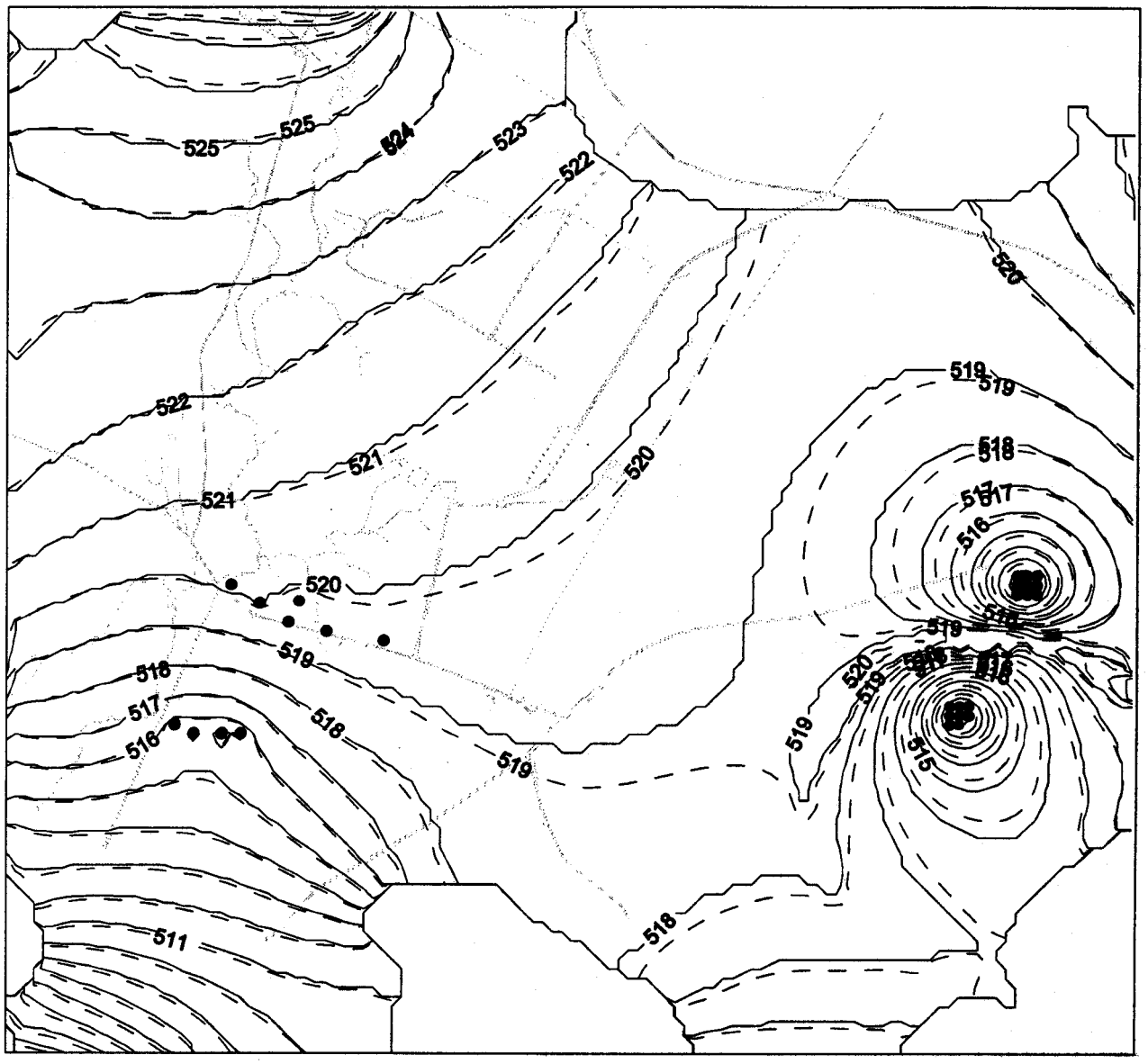

Head Contour in ft-MSL:

— 500 — VAM3DF

--- 500 --- SWIFT

● Well

2000 0 2000 4000 ft

Figure 7.5 Modeled Ground Water Elevations for 1998, for the 10-Year Scenario. Comparison between SWIFT (Layer 1) and VAM3DF (Lower Node of Layer 1) GMA Model (Run: A2).

000114

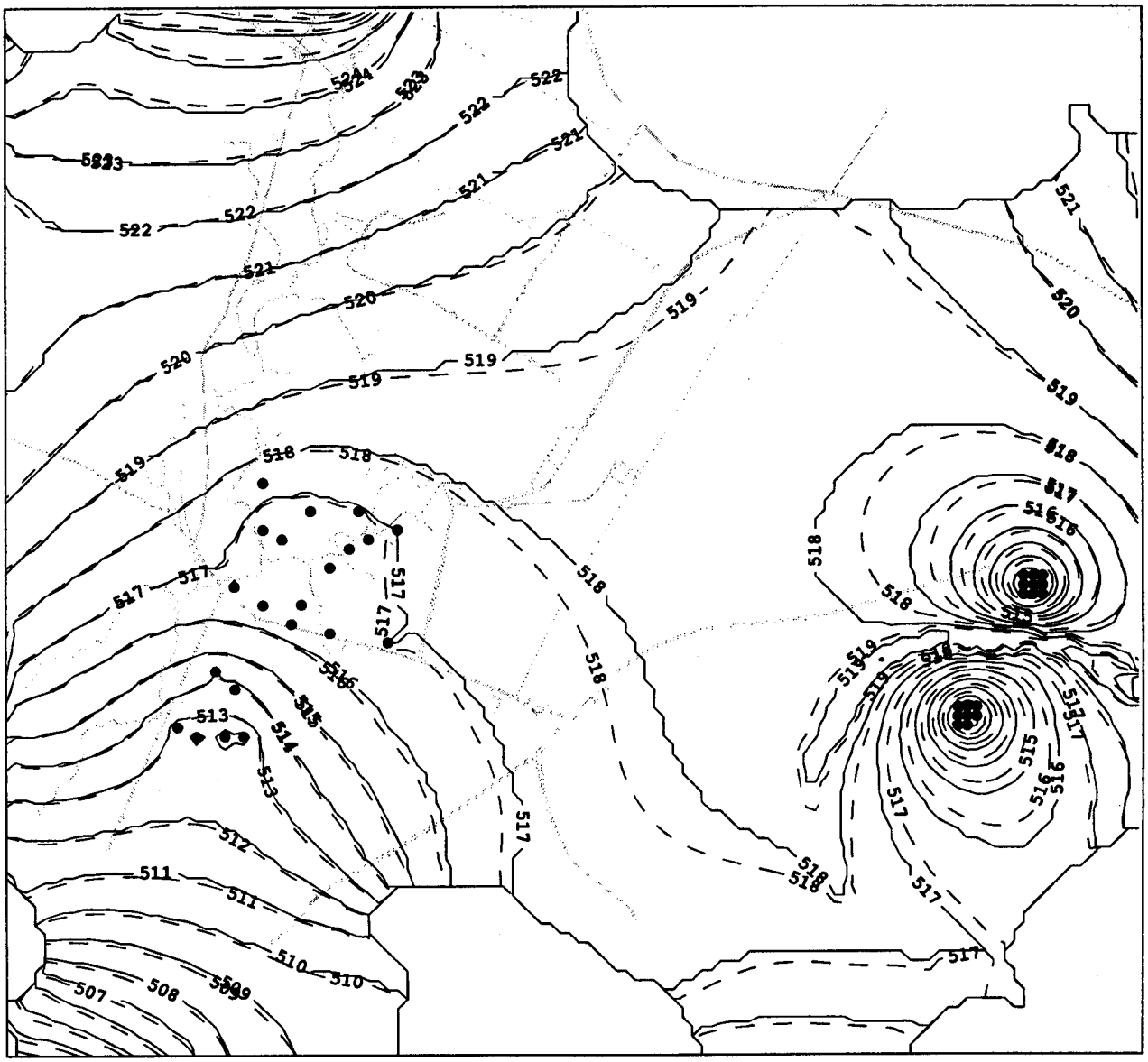

Head Contour in ft-MSL:

— 500 — VAM3DF

--- 500 ---- SWIFT

• Well

2000 0 2000 4000 ft

Figure 7.6 Modeled Ground Water Elevations for 1999 through 2003, for the 10-Year Scenario. Comparison between SWIFT (layer 1) and VAM3DF (Lower Node of Layer 1) GMA Model (Run: A2).

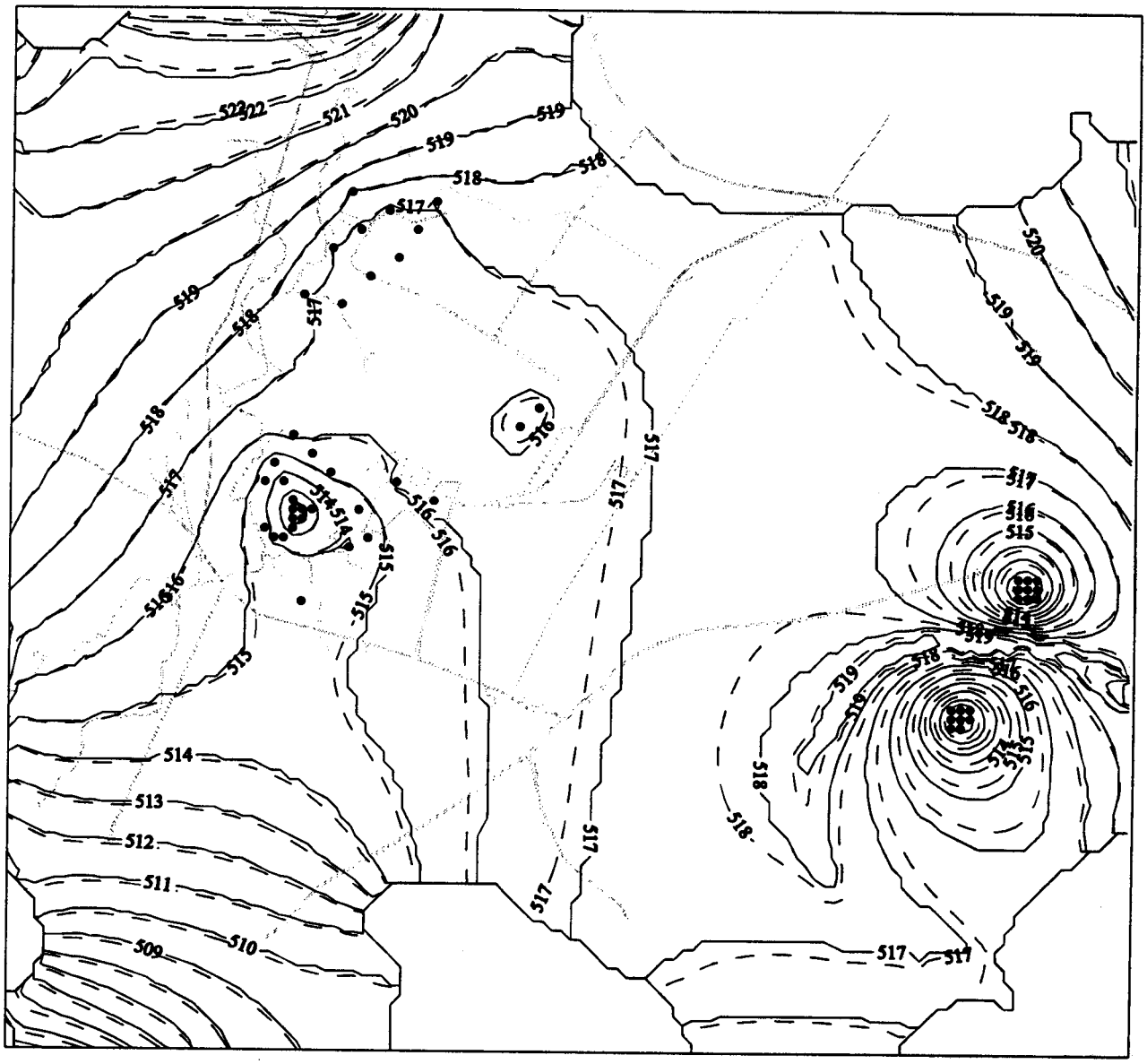

Head Contour in ft-MSL:

— 500 — VAM3DF

--- 500 --- SWIFT

• Well

2000 0 2000 4000 ft

Figure 7.7 Modeled Ground Water Elevations for 2004 through 2006, for the 10-Year Scenario. Comparison between SWIFT (Layer 1) and VAM3DF (Lower Node of Layer 1) GMA Models (Run: A2).

000116

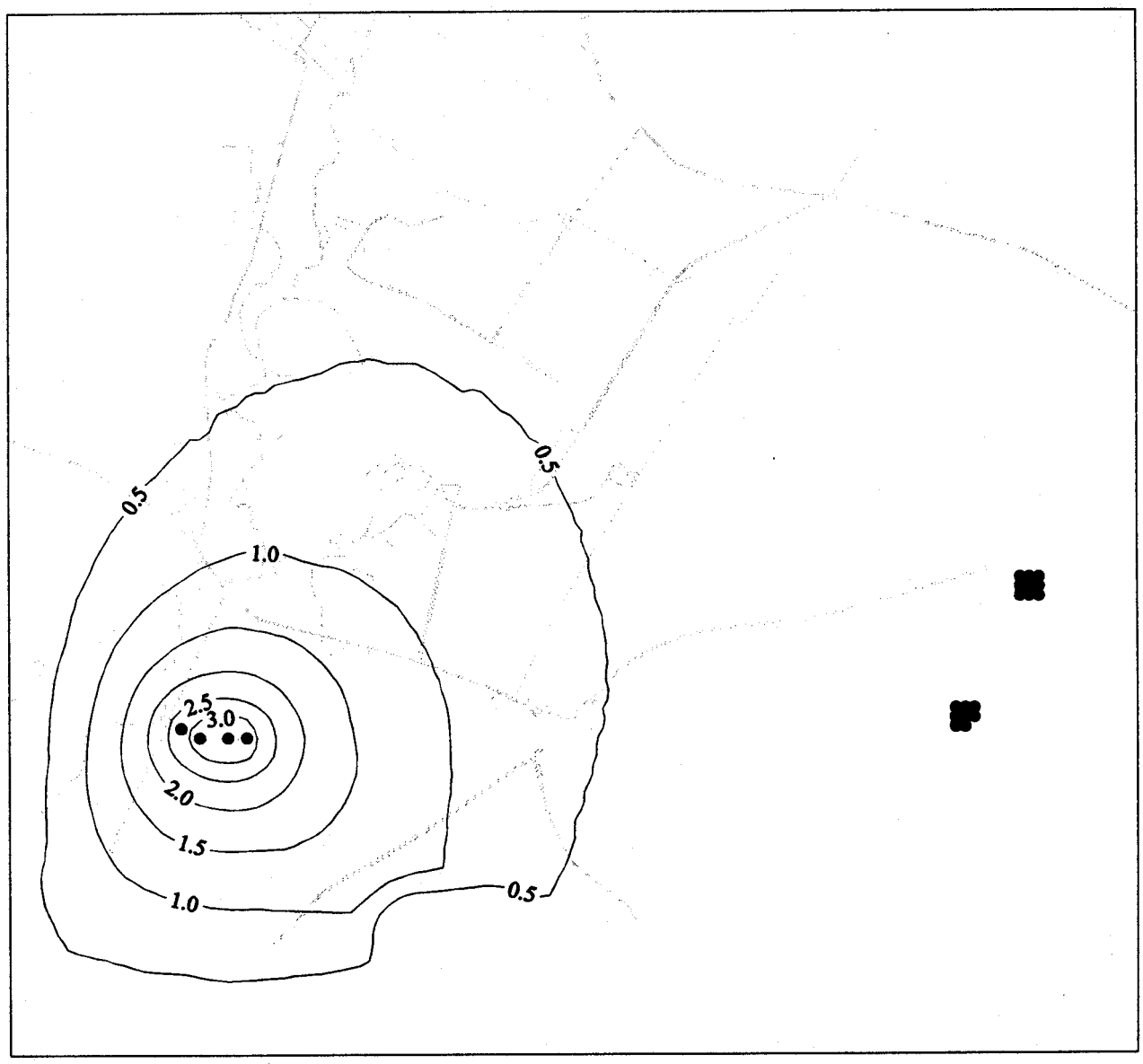

— 1.0 — Drawdown, ft.

• Well.

2000 0 2000 4000 ft

Figure 7.8 Ground Water Drawdown Contours for 1997 (Lower Node of Layer 1 in VAM3DF) (Run: A2).

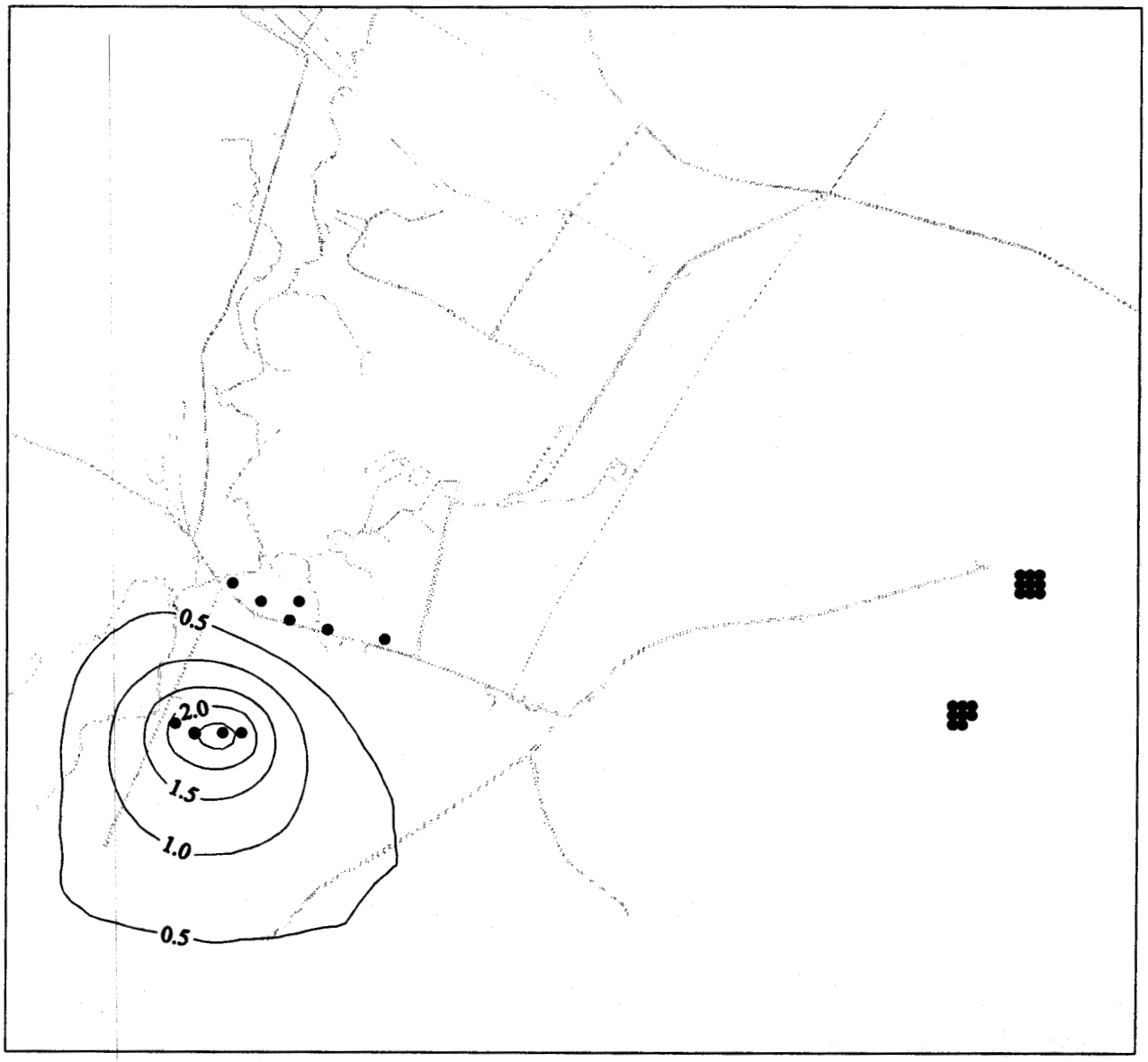

— 1.0 —Drawdown, ft.

• Well.

2000 0 2000 4000 ft

Figure 7.9 Ground Water Drawdown Contours for 1998 (Lower Node of Layer 1 in VAM3DF) (Run: A2).

000118

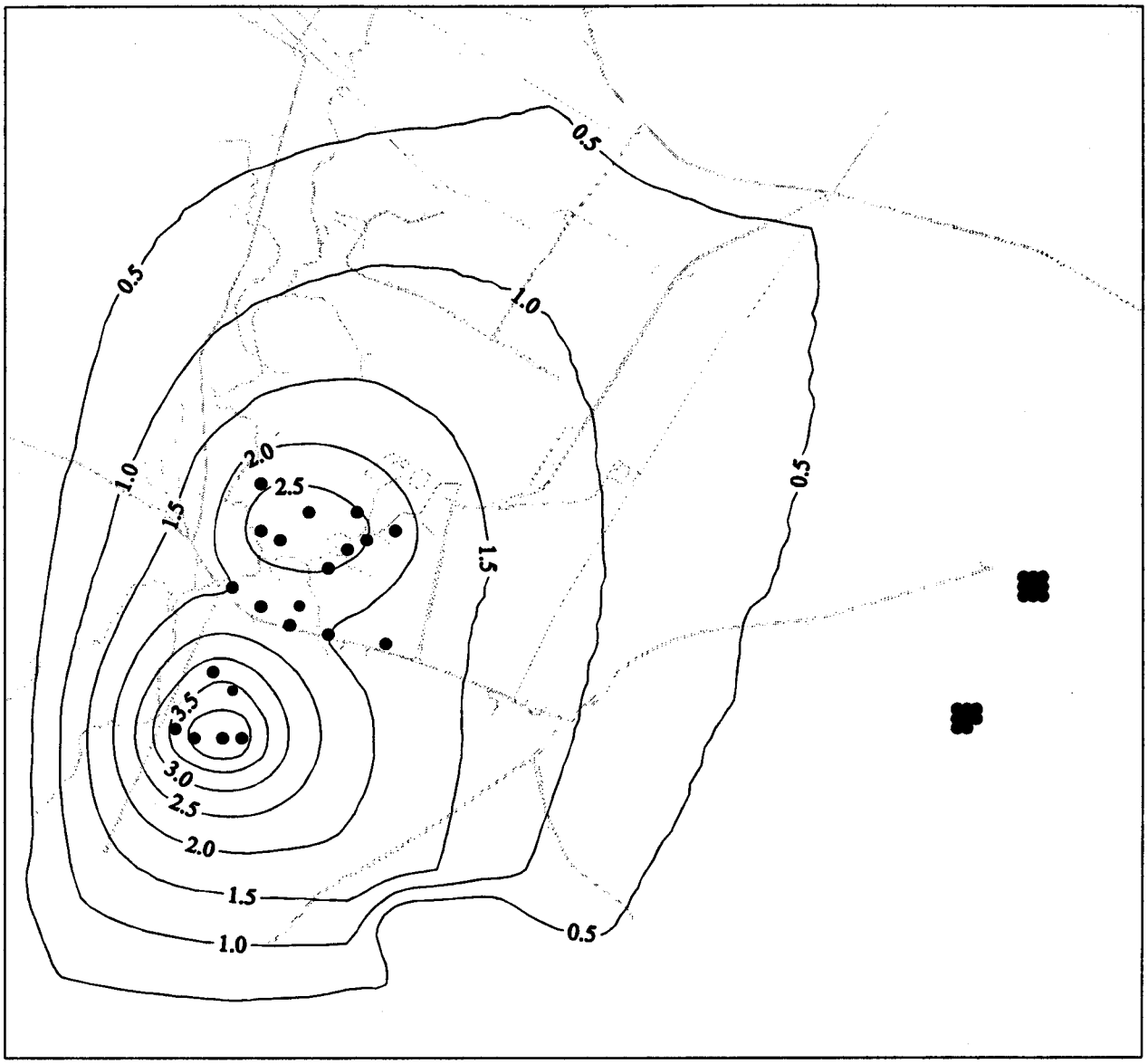

— 1.0 —Drawdown, ft.

• Well.

2000 0 2000 4000 ft

Figure 7.10 Ground Water Drawdown Contours for 1999 through 2003 (Lower Node of Layer 1 in VAM3DF) (Run: A2).

000119

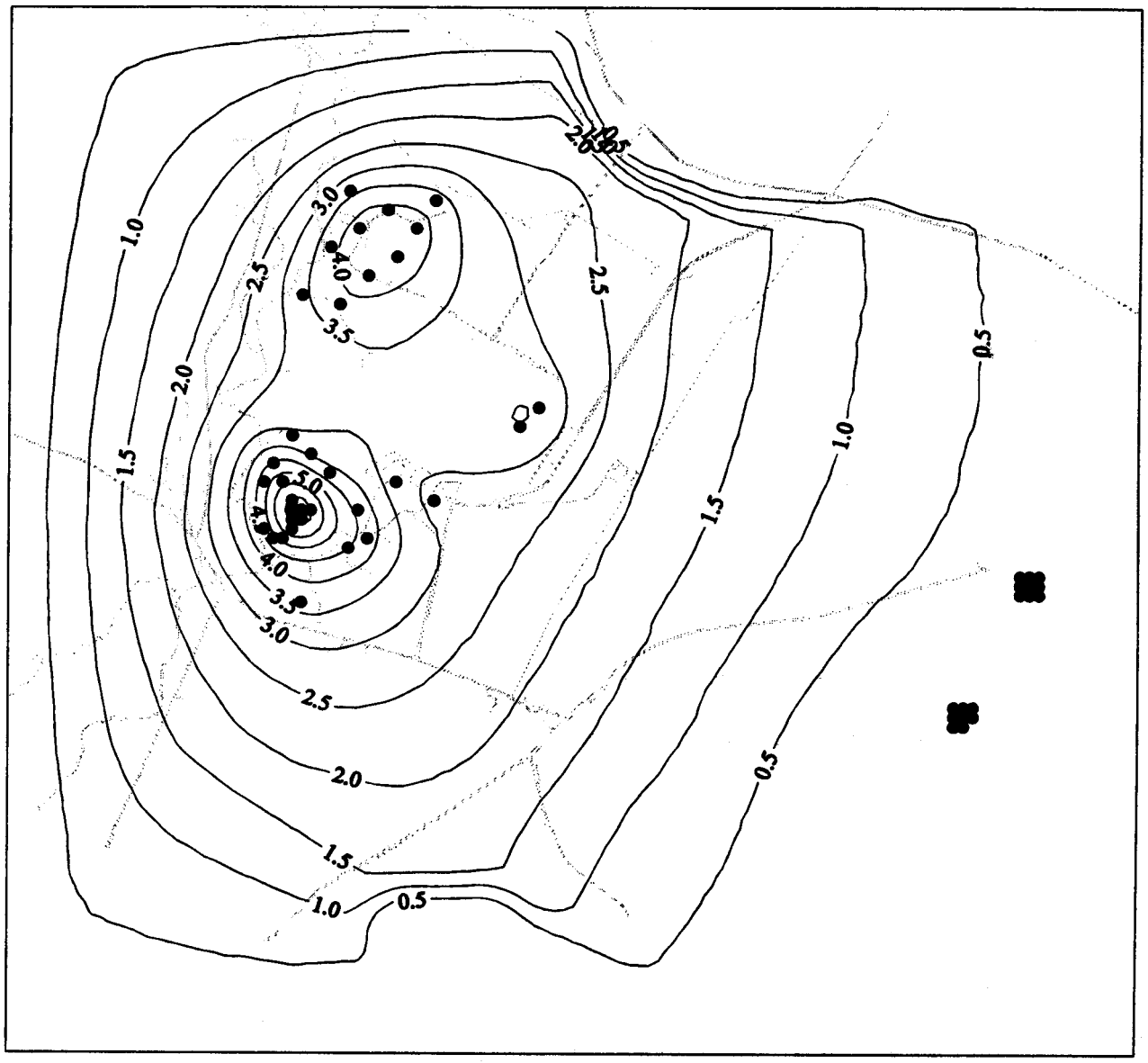

— 1.0 —Drawdown, ft.

● Well.

2000 0 2000 4000 ft

Figure 7.11 Ground Water Drawdown Contours for 2005 through 2007 (Lower Node of Layer 1 in VAM3DF) (Run: A2).

000120

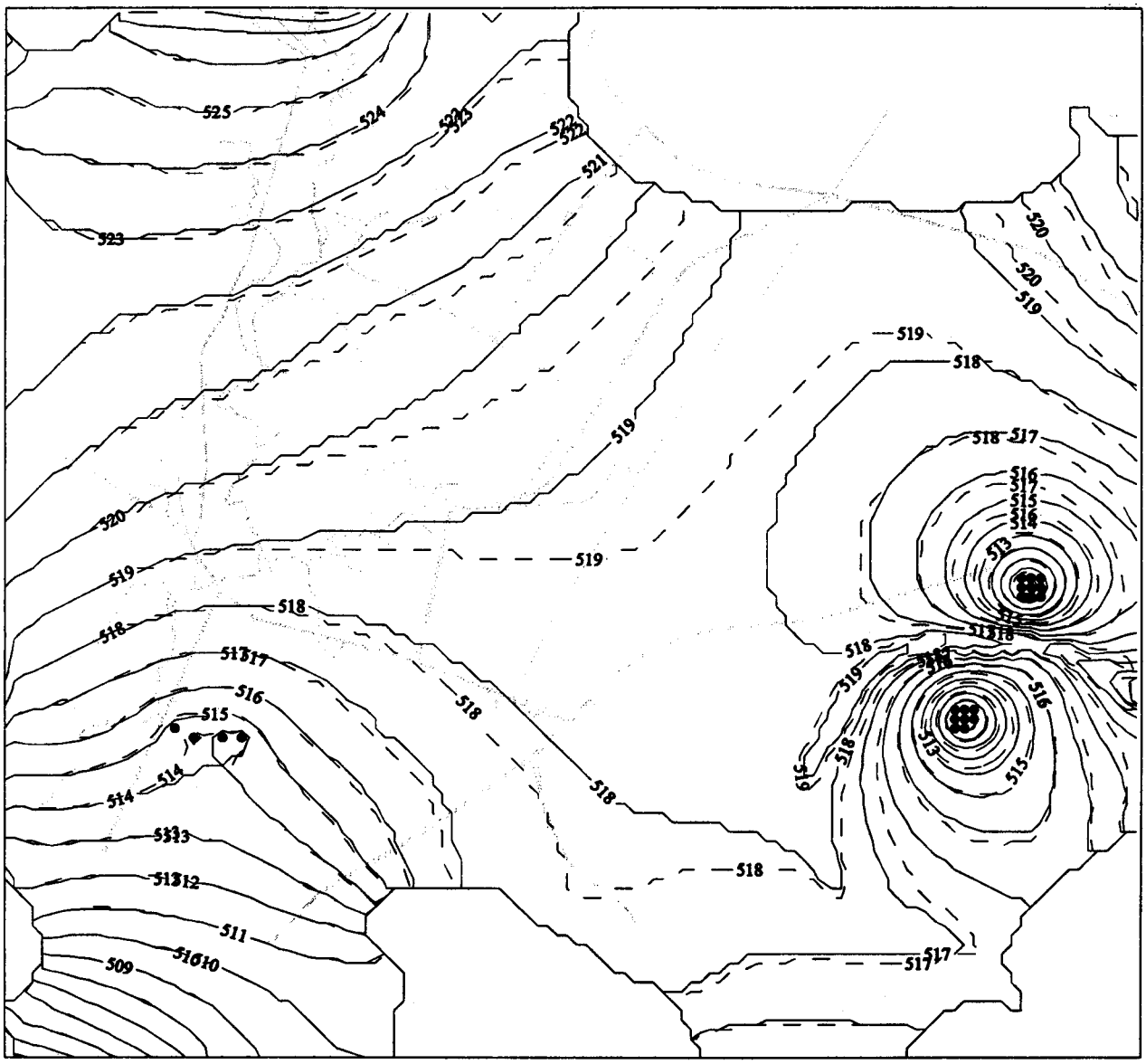

Head Contour in ft-MSL:

— 500 — New Pumping Rates

--- 500 --- Original Pumping Rates

• Well

2000 0 2000 4000 ft

Figure 7.12 Ground-Water Elevations under Different Pumping Rates at the SOWC Collector Wells for 1997 (VAM3DF GMA Model Results for the Lower Node of Layer 1) (Run: A3).

000121

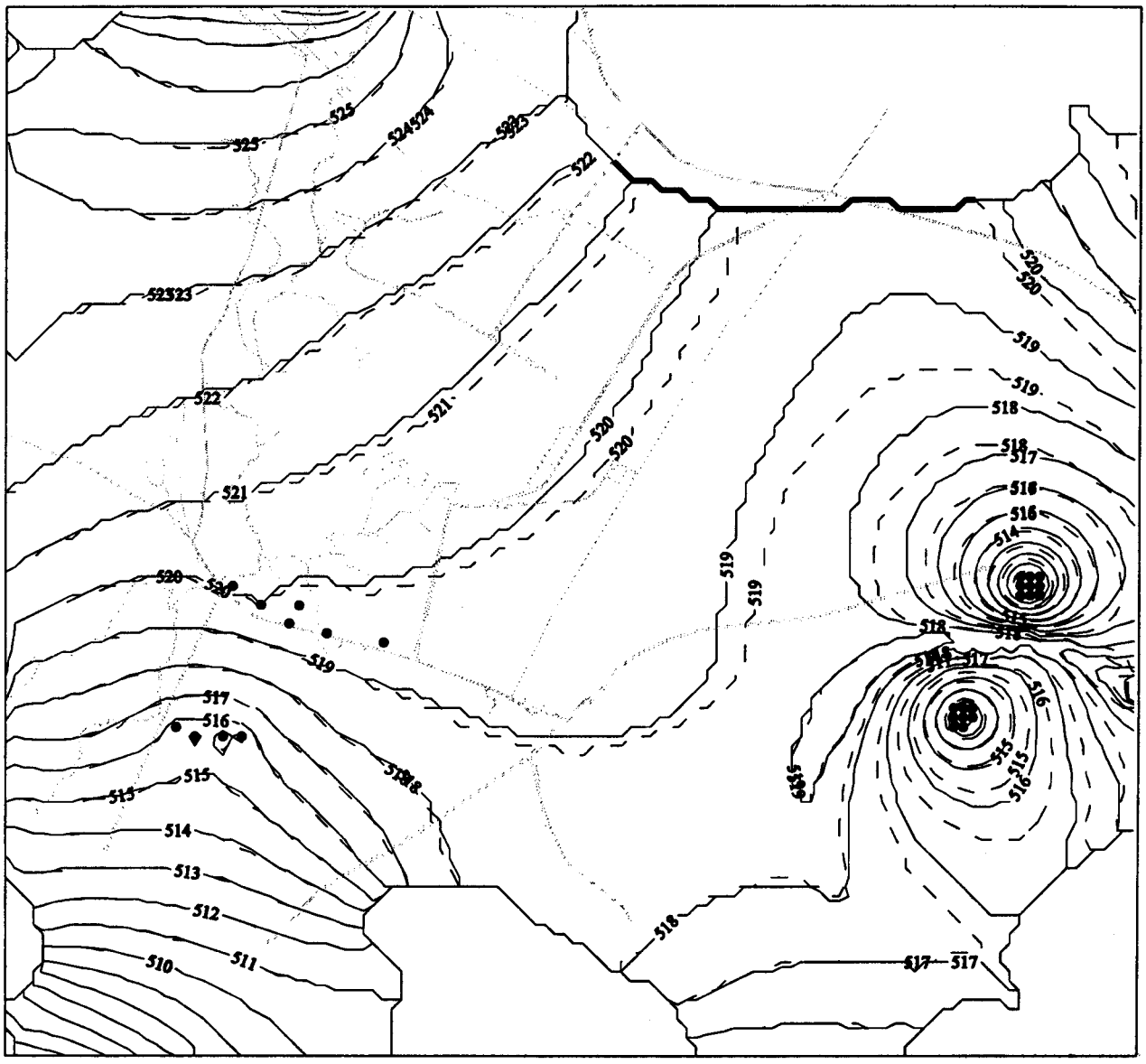

Head Contour in ft-MSL:

— 500 — New Pumping Rates

--- 500 --- Original Pumping Rates

• Well

2000 0 2000 4000 ft

Figure 7.13 Ground Water Elevations under Different Pumping Rates at the SOWC Collector Wells for 1998. (VAM3DF GMA Model Results for the Lower node of Layer 1) (Run: A3).

000122

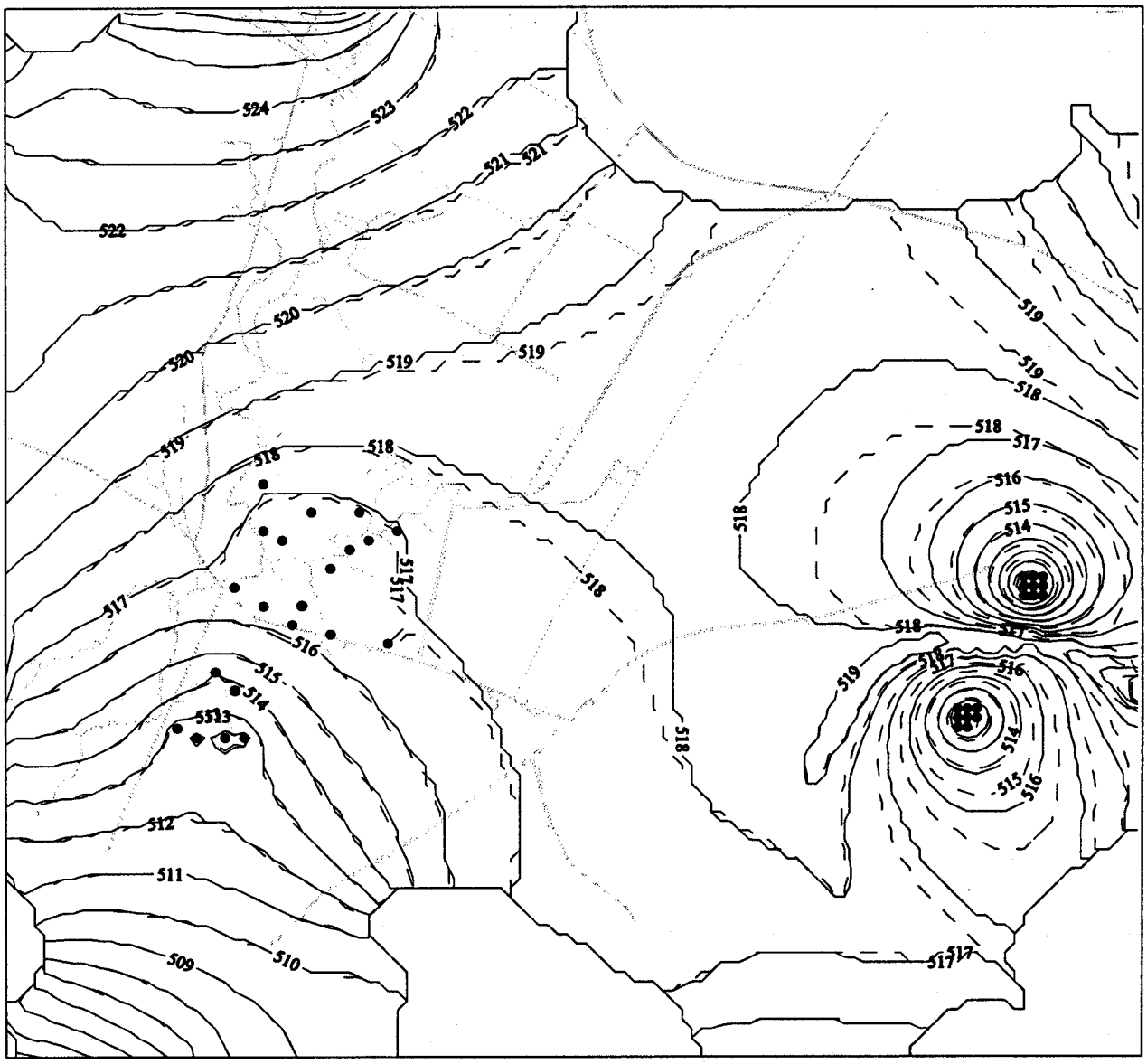

Head Contour in ft-MSL:

— 500 — New Pumping Rates

--- 500 --- Original Pumping Rates

• Well

2000 0 2000 4000 ft

Figure 7.14 Ground Water Elevations under Different Pumping Rates at the SOWC Collector Wells for 1999 though 2003. (VAM3DF GMA Model Results for the Lower node of Layer 1) (Run: A3).

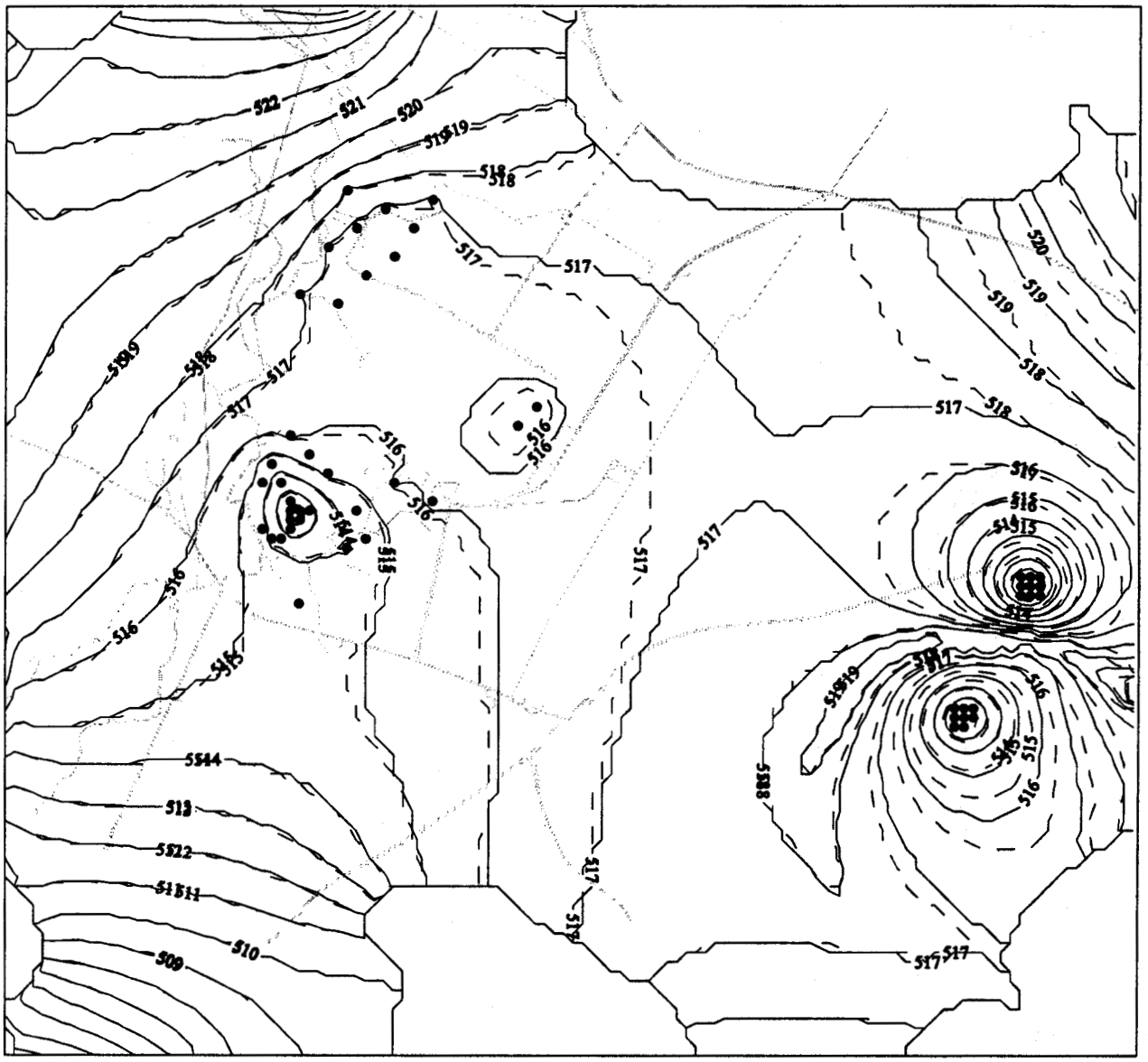

Head Contour in ft-MSL:

— 500 — New Pumping Rates

--- 500 --- Original Pumping Rates

● Well

2000 0 2000 4000 ft

Figure 7.15 Ground Water Elevation under Different Pumping Rates at the SOWC Collector Wells for 2003 though 2006 (VAM3DF GMA Model Results for the Lower node of Layer 1) (Run: A3).

000124

Table 7.4
Comparison between VAM3DF GMA Model Simulation and Water Levels

Well No.	X	Y	Z	Head (Geostat)	Std. (Geostat)	Head SWIFT	Head[1] VAM	Head[2] VAM	Residual[1] VAM-Geostat	Residual[2] VAM-Geostat	Abs.[1] Res.	Abs.[2] Res.
2556	812.50	1937.50	1	511.70	0.33	512.92	512.80	512.80	1.10	1.10	1.10	1.10
2559	937.50	312.50	1	504.80	0.32	506.19	505.90	505.90	1.10	1.10	1.10	1.10
2126	1062.50	3812.50	1	516.90	0.25	517.56	517.60	517.60	0.70	0.70	0.70	0.70
2393	1187.50	3312.50	1	516.10	0.40	516.41	516.40	516.40	0.30	0.30	0.30	0.30
4096	1312.50	7687.50	6	523.00	0.30	522.27	522.40	522.40	-0.60	-0.60	0.60	0.60
2096	1312.50	7687.50	1	523.00	0.30	522.27	522.40	522.40	-0.60	-0.60	0.60	0.60
3096	1312.50	7687.50	3	523.00	0.30	522.27	522.40	522.40	-0.60	-0.60	0.60	0.60
2094	1437.50	1062.50	1	507.80	0.32	509.9	509.80	509.80	2.00	2.00	2.00	2.00
3094	1437.50	1062.50	3	507.85	0.30	509.90	509.80	509.80	1.95	1.95	1.95	1.95
2129	1687.50	3062.50	1	515.60	0.38	515.89	515.90	515.90	0.30	0.30	0.30	0.30
3552	1687.50	4437.50	3	519.10	0.20	518.90	519.00	518.90	-0.10	-0.20	0.10	0.20
2552	1687.50	4437.50	1	519.08	0.24	518.92	519.00	519.00	-0.08	-0.08	0.08	0.08
2396	1812.50	4687.50	1	519.70	0.30	519.22	519.30	519.30	-0.40	-0.40	0.40	0.40
3396	1812.50	4687.50	3	519.70	0.20	519.22	519.30	519.30	-0.40	-0.40	0.40	0.40
2128	2062.50	3812.50	1	517.18	0.30	517.62	517.70	517.70	0.52	0.52	0.52	0.52
3128	2062.50	3812.50	3	516.75	0.23	517.61	517.70	517.7	0.95	0.95	0.95	0.95
2125	2187.50	4687.50	1	519.90	0.22	519.19	519.30	519.30	-0.60	-0.60	0.60	0.60
3125	2187.50	4687.50	3	519.90	0.20	519.19	519.30	519.30	-0.60	-0.60	0.60	0.60
4125	2187.50	4687.50	6	519.90	0.20	519.18	519.30	519.3	-0.60	-0.60	0.60	0.60
2551	2312.50	5812.50	1	521.60	0.31	520.38	520.50	520.50	-1.10	-1.10	1.10	1.1
3551	2312.50	5812.50	3	521.60	0.30	520.37	520.50	520.50	-1.10	-1.10	1.10	1.1
2392	2562.50	1062.50	1	510.77	0.40	511.13	511.10	511.10	0.33	0.33	0.33	0.33
3095	2562.50	5312.50	3	520.57	0.30	519.85	520.00	520.00	-0.57	-0.57	0.57	0.57
2095	2562.50	5312.50	1	520.81	0.33	519.85	520.00	520	-0.81	-0.81	0.81	0.81
3044	2687.50	8312.50	3	523.30	0.30	522.22	522.40	522.40	-0.90	-0.90	0.90	0.90
2044	2687.50	312.50	1	509.36	1.67	509.56	509.50	509.50	0.14	0.14	0.14	0.14
3017	2812.50	6562.50	3	522.30	0.40	520.94	521.10	521.10	-1.20	-1.20	1.20	1.20
3550	2812.50	5937.50	3	521.60	0.30	520.41	520.50	520.50	-1.10	-1.10	1.10	1.10
2550	2812.50	5937.50	1	521.60	0.36	520.41	520.50	520.5	-1.10	-1.10	1.10	1.10

Table 7.4 (continued)
Comparison between VAM3DF GMA Model Simulation and Water Levels

Well No.	X	Y	Z	Head (Geostat)	Std. (Geostat)	Head SWIFT	Head[1] VAM	Head[2] VAM	Residual[1] VAM-Geostat	Residual[2] VAM-Geostat	Abs.[1] Res.	Abs.[2] Res.
2017	2812.50	6562.50	1	522.40	0.40	520.94	521.10	521.10	-1.30	-1.30	1.30	1.30
2391	2812.50	1812.50	1	513.30	0.27	513.16	513.10	513.10	-0.20	-0.20	0.20	0.20
3391	2812.50	1812.50	3	513.30	0.20	513.14	513.10	513.1	-0.20	-0.20	0.20	0.20
2384	2812.50	9687.50	1	523.90	0.40	523.90	523.20	523.20	-0.70	-0.70	0.70	0.70
2394	3187.50	2937.50	1	516.70	0.38	516.70	516.10	516.1	-0.60	-0.60	0.60	0.60
3106	3187.50	6187.50	3	521.90	0.30	521.90	520.70	520.70	-1.20	-1.20	1.20	1.20
2106	3187.50	6187.50	1	521.90	0.33	521.90	520.70	520.70	-1.20	-1.20	1.20	1.20
2402	3437.50	8437.50	1	522.74	0.40	522.74	522.30	522.30	-0.44	-0.44	0.44	0.44
3107	3437.50	8812.50	3	523.70	0.20	523.70	522.50	522.50	-1.20	-1.20	1.20	1.20
2383	3437.50	11062.50	1	524.00	0.25	524.00	524.40	524.40	0.40	0.40	0.40	0.40
2060	3437.50	5687.50	1	521.40	0.40	521.40	520.30	520.30	-1.10	-1.10	1.10	1.10
4014	3437.50	6812.50	6	522.40	0.30	522.40	521.10	521.10	-1.30	-1.30	1.30	1.30
2014	3437.50	6812.50	1	522.40	0.34	522.40	521.20	521.20	-1.20	-1.20	1.20	1.20
2107	3437.50	8812.50	1	523.60	0.25	523.60	522.50	522.5	-1.10	-1.10	1.10	1.10
3402	3437.50	8312.50	3	523.10	0.40	523.10	522.20	522.20	-0.90	-0.90	0.90	0.9
3014	3437.50	6812.50	3	522.40	0.30	522.40	521.20	521.20	-1.20	-1.20	1.20	1.2
2009	3437.50	9937.50	1	524.10	0.32	524.10	523.30	523.30	-0.80	-0.80	0.80	0.8
3390	3562.50	6437.50	3	522.20	0.30	522.20	520.90	520.80	-1.30	-1.40	1.30	1.40
3016	3562.50	7687.50	3	522.70	0.20	522.70	521.80	521.80	-0.90	-0.90	0.90	0.9
3009	3562.50	9937.50	3	524.23	0.30	523.04	523.20	523.20	-1.03	-1.03	1.03	1.03
2955	3562.50	8187.50	1	523.10	0.23	521.88	522.10	522.10	-1.00	-1.00	1.00	1
2016	3562.50	7687.50	1	522.73	0.27	521.56	521.80	521.80	-0.93	-0.93	0.93	0.93
2390	3562.50	6437.50	1	522.20	0.31	520.71	520.90	520.90	-1.30	-1.30	1.30	1.30
4016	3562.50	7687.50	6	522.60	0.30	521.50	521.70	521.70	-0.90	-0.90	0.90	0.9
3108	3687.50	10437.50	3	523.85	0.20	523.56	523.70	523.70	-0.15	-0.15	0.15	0.15
3015	3687.50	5937.50	3	521.70	0.30	520.32	520.40	520.40	-1.30	-1.30	1.30	1.30
2015	3687.50	5937.50	1	521.70	0.30	520.31	520.40	520.40	-1.30	-1.30	1.30	1.30
2945	3687.50	8062.50	1	522.95	0.20	521.76	522.00	522.00	-0.95	-0.95	0.95	0.95
2401	3687.50	8187.50	1	523.07	0.20	521.84	522.00	522.00	-1.07	-1.07	1.07	1.07

Table 7.4 (continued)
Comparison between VAM3DF GMA Model Simulation and Water Levels

Well No.	X	Y	Z	Head (Geostat)	Std. (Geostat)	Head SWIFT	Head[1] VAM	Head[2] VAM	Residual[1] VAM-Geostat	Residual[2] VAM-Geostat	Abs.[1] Res.	Abs.[2] Res.
2108	3687.50	10437.50	1	524.17	0.25	523.56	523.70	523.70	-0.47	-0.47	0.47	0.47
2043	3812.50	12312.50	1	523.57	0.30	526.05	525.80	525.80	2.23	2.23	2.23	2.23
3043	3812.50	12312.50	3	523.50	0.30	526.03	525.80	525.70	2.30	2.20	2.30	2.20
2047	3812.50	8312.50	1	522.70	0.31	521.88	522.10	522.10	-0.60	-0.60	0.60	0.60
2045	3812.50	6937.50	1	522.30	0.26	521.01	521.20	521.20	-1.10	-1.10	1.10	1.10
2943	3812.50	7312.50	1	522.40	0.30	521.25	521.40	521.40	-1.00	-1.00	1.00	1.00
3045	3812.50	6937.50	3	522.30	0.20	521.01	521.20	521.20	-1.10	-1.10	1.10	1.10
2046	3937.50	7937.50	1	521.81	0.26	521.61	521.80	521.80	-0.01	-0.01	0.01	0.01
3046	3937.50	7937.50	3	522.23	0.23	521.61	521.80	521.8	-0.43	-0.43	0.43	0.43
3049	4062.50	6687.50	3	522.00	0.30	520.79	520.90	520.9	-1.10	-1.10	1.10	1.10
3018	4062.50	9562.50	3	526.93	0.30	522.54	522.70	522.70	-4.23	-4.23	4.23	4.23
2018	4062.50	9562.50	1	524.87	0.33	522.54	522.70	522.70	-2.17	-2.17	2.17	2.17
2048	4062.50	7187.50	1	522.30	0.25	521.11	521.30	521.30	-1.00	-1.00	1.00	1.00
2034	4187.50	10312.50	1	523.90	0.23	523.20	523.30	523.30	-0.60	-0.60	0.60	0.6
3034	4187.50	10312.50	3	523.90	0.20	523.19	523.30	523.30	-0.60	-0.60	0.60	0.6
3032	4187.50	10562.50	3	524.10	0.30	523.49	523.60	523.60	-0.50	-0.50	0.50	0.50
2103	4187.50	6937.50	1	522.00	0.40	520.93	521.10	521.10	-0.90	-0.90	0.90	0.90
2032	4187.50	10562.50	1	524.10	0.30	523.50	523.60	523.60	-0.50	-0.50	0.50	0.50
3385	4312.50	7562.50	3	522.20	0.30	521.27	521.40	521.40	-0.80	-0.80	0.80	0.80
3069	4312.50	5812.50	3	521.40	0.40	520.18	520.30	520.30	-1.10	-1.10	1.10	1.10
2069	4312.50	5812.50	1	521.50	0.40	520.18	520.30	520.30	-1.20	-1.20	1.20	1.20
3004	4312.50	11562.50	3	523.70	0.38	524.72	524.60	524.60	0.90	0.90	0.90	0.90
3093	4312.50	4562.50	3	520.50	0.20	519.30	519.40	519.40	-1.10	-1.10	1.10	1.1
2093	4312.50	4562.50	1	520.57	0.23	519.31	519.40	519.40	-1.17	-1.17	1.17	1.17
2387	4437.50	6562.50	1	521.80	0.40	520.65	520.80	520.80	-1.00	-1.00	1.00	1.00
3387	4437.50	6562.50	3	521.82	0.30	520.65	520.80	520.80	-1.02	-1.02	1.02	1.02
2649	4437.50	11312.50	1	523.90	0.30	524.30	524.30	524.30	0.40	0.40	0.40	0.4
2020	4562.50	8812.50	1	522.57	0.37	521.91	522.10	522.10	-0.47	-0.47	0.47	0.47
2033	4562.50	10312.50	1	523.50	0.30	523.01	523.10	523.10	-0.40	-0.40	0.40	0.4

Table 7.4 (continued)
Comparison between VAM3DF GMA Model Simulation and Water Levels

Well No.	X	Y	Z	Head (Geostat)	Std. (Geostat)	Head SWIFT	Head[1] VAM	Head[2] VAM	Residual[1] VAM-Geostat	Residual[2] VAM-Geostat	Abs.[1] Res.	Abs.[2] Res.
3020	4687.50	8812.50	3	522.45	0.40	521.86	522.00	522.00	-0.45	-0.45	0.45	0.45
2822	4687.50	11187.50	1	523.60	0.37	523.98	524.00	524.00	0.40	0.40	0.40	0.4
3065	4687.50	7312.50	3	522.10	0.30	521.03	521.20	521.20	-0.90	-0.90	0.90	0.9
2166	4687.50	5812.50	1	521.40	0.32	520.16	520.30	520.30	-1.10	-1.10	1.10	1.1
2008	4812.50	10437.50	1	523.10	0.25	523.03	523.10	523.10	0.00	0.00	0.00	0.00
4011	4812.50	12312.50	6	523.10	0.20	525.25	525.10	525.10	2.00	2.00	2.00	2
2011	4812.50	12312.50	1	523.10	0.40	525.42	525.20	525.20	2.10	2.10	2.10	2.1
2065	4812.50	7312.50	1	522.30	0.40	521.00	521.20	521.20	-1.10	-1.10	1.10	1.1
3011	4812.50	12312.50	3	523.10	0.20	525.42	525.20	525.20	2.10	2.10	2.10	2.1
2386	4937.50	6937.50	1	521.90	0.30	520.77	520.90	520.90	-1.00	-1.00	1.00	1.00
3821	4937.50	11187.50	3	523.30	0.20	523.81	523.80	523.80	0.50	0.50	0.50	0.50
2398	4937.50	5687.50	1	521.20	0.29	520.08	520.20	520.20	-1.00	-1.00	1.00	1.00
3398	4937.50	5687.50	3	521.30	0.20	520.08	520.20	520.20	-1.10	-1.10	1.10	1.1
2821	4937.50	11187.50	1	523.30	0.20	523.82	523.80	523.80	0.50	0.50	0.50	0.50
4398	4937.50	5687.50	6	521.30	0.30	520.08	520.20	520.20	-1.10	-1.10	1.10	1.1
4008	5062.50	10312.50	6	522.40	0.30	522.65	523.00	523.00	0.60	0.60	0.60	0.60
4001	5062.50	11062.50	6	522.70	0.30	523.61	523.70	523.70	1.00	1.00	1.00	1
3008	5062.50	10312.50	3	522.10	0.20	522.77	522.90	522.90	0.80	0.80	0.80	0.8
2042	5187.50	9937.50	1	522.41	0.40	522.32	522.50	522.50	0.09	0.09	0.09	0.09
2643	5312.50	11562.50	1	523.00	0.30	524.00	523.90	523.90	0.90	0.90	0.90	0.9
2728	5312.50	13187.50	1	523.25	0.30	525.95	525.70	525.70	2.45	2.45	2.45	2.45
3084	5437.50	11562.50	3	522.90	0.30	523.90	523.80	523.80	0.90	0.90	0.90	0.90
3397	5437.50	7312.50	3	521.80	0.20	520.85	521.00	521.00	-0.80	-0.80	0.80	0.8
2397	5437.50	7312.50	1	521.80	0.25	520.85	521.00	521.00	-0.80	-0.80	0.80	0.80
2399	5437.50	6187.50	1	521.20	0.30	520.30	520.40	520.40	-0.80	-0.80	0.80	0.80
2087	5437.50	11562.50	1	522.90	0.30	523.91	523.90	523.90	1.00	1.00	1.00	1.00
3070	5562.50	5562.50	3	520.90	0.30	519.99	520.10	520.10	-0.80	-0.80	0.80	0.80
2070	5562.50	5562.50	1	521.00	0.39	519.99	520.10	520.10	-0.90	-0.90	0.90	0.90
2936	5687.50	9937.50	1	522.30	0.30	522.10	522.20	522.20	-0.10	-0.10	0.10	0.10

Table 7.4 (continued)
Comparison between VAM3DF GMA Model Simulation and Water Levels

Well No.	X	Y	Z	Head (Geostat)	Std. (Geostat)	Head SWIFT	Head[1] VAM	Head[2] VAM	Residual[1] VAM-Geostat	Residual[2] VAM-Geostat	Abs.[1] Res.	Abs.[2] Res.
3024	5687.50	12062.50	3	523.00	0.30	524.28	524.20	524.20	1.20	1.20	1.20	1.20
2024	5687.50	12062.50	1	523.00	0.30	524.28	524.20	524.20	1.20	1.20	1.20	1.2
2027	5812.50	1437.50	1	522.60	0.31	523.50	-9999.00	-9999.00		No flow		
2010	5937.50	10687.50	1	522.49	0.36	522.70	522.70	522.70	0.21	0.21	0.21	0.21
2679	5937.50	13562.50	1	522.90	0.30	525.08	524.90	524.90	2.00	2.00	2.00	2.00
2068	5937.50	7437.50	1	521.60	0.40	520.78	520.90	520.90	-0.70	-0.70	0.70	0.7
3068	5937.50	7437.50	3	521.60	0.30	520.78	520.90	520.90	-0.70	-0.70	0.70	0.7
3452	5937.50	11812.50	3	523.00	0.30	523.80	523.70	523.70	0.70	0.70	0.70	0.70
4010	5937.50	10687.50	6	522.50	0.30	522.59	522.80	522.80	0.30	0.30	0.30	0.30
3679	5937.50	13562.50	3	522.80	0.30	525.08	524.90	524.90	2.10	2.10	2.10	2.10
2006	6062.50	9312.50	1	521.82	0.40	521.61	521.70	521.70	-0.12	-0.12	0.12	0.12
3010	6062.50	10812.50	3	522.30	0.20	522.74	522.80	522.80	0.50	0.50	0.50	0.50
2951	6187.50	11437.50	1	522.30	0.30	523.27	523.20	523.2	0.9	0.9	0.9	0.9
2949	6312.50	11437.50	1	522.31	0.30	523.16	523.10	523.1	0.79	0.79	0.79	0.79
3037	6312.50	11312.50	3	522.30	0.20	523.04	523.00	523	0.70	0.70	0.70	0.70
2037	6312.50	11312.50	1	522.30	0.24	523.04	523.00	523	0.70	0.70	0.70	0.7
2947	6437.50	11187.50	1	522.30	0.25	522.85	522.80	522.8	0.5	0.50	0.50	0.5
3733	6687.50	5187.50	3	520.75	0.30	519.78	519.80	519.8	-0.95	-0.95	0.95	0.95
2389	6687.50	8812.50	1	521.90	0.24	521.15	521.20	521.20	-0.70	-0.70	0.70	0.7
2055	6812.50	10312.50	1	522.00	0.30	521.90	521.90	521.90	-0.10	-0.10	0.10	0.1
2052	6812.50	11437.50	1	522.30	0.23	522.81	522.80	522.80	0.50	0.50	0.50	0.5
2054	6812.50	8562.50	1	521.60	0.30	521.00	521.10	521.10	-0.50	-0.50	0.50	0.5
2388	6937.50	9062.50	1	521.80	0.30	521.16	521.20	521.20	-0.60	-0.60	0.60	0.6
2446	7062.50	7687.50	1	521.50	0.26	520.58	520.60	520.60	-0.90	-0.90	0.90	0.9
2432	7062.50	6062.50	1	520.66	0.30	520.02	520.10	520.10	-0.56	-0.56	0.56	0.56
2432	7062.50	6062.50	3	520.13	0.30	520.02	520.10	520.10	-0.03	-0.03	0.03	0.03
4446	7062.50	7687.50	6	521.40	0.20	520.55	520.60	520.60	-0.80	-0.80	0.80	0.8
2118	7062.50	8437.50	1	521.40	0.30	520.87	520.90	520.90	-0.50	-0.50	0.50	0.5
2171	7187.50	8187.50	1	521.60	0.30	520.73	520.80	520.80	-0.80	-0.80	0.80	0.8

Table 7.4 (continued)
Comparison between VAM3DF GMA Model Simulation and Water Levels

Well No.	X	Y	Z	Head (Geostat)	Std. (Geostat)	Head SWIFT	Head[1] VAM	Head[2] VAM	Residual[1] VAM-Geostat	Residual[2] VAM-Geostat	Abs.[1] Res.	Abs.[2] Res.
2109	7187.50	8812.50	1	521.40	0.40	520.97	521.00	521.00	-0.40	-0.40	0.40	0.4
4432	7187.50	6062.50	6	518.70	0.30	519.99	520.00	520.00	1.30	1.30	1.30	1.3
3120	7312.50	8437.50	3	521.50	0.20	520.78	520.80	520.80	-0.70	-0.70	0.70	0.70
2092	7312.50	4312.50	1	520.44	0.36	519.47	519.50	519.50	-0.94	-0.94	0.94	0.94
2120	7437.50	8437.50	1	521.40	0.33	520.74	520.80	520.80	-0.60	-0.60	0.60	0.6
3092	7437.50	4312.50	3	520.40	0.35	519.45	519.50	519.50	-0.90	-0.90	0.90	0.9
3431	7562.50	6812.50	3	520.90	0.20	520.14	520.20	520.20	-0.70	-0.70	0.70	0.70
2431	7562.50	6812.50	1	520.99	0.24	520.14	520.20	520.20	-0.79	-0.79	0.79	0.79
3064	7687.50	8812.50	3	521.40	0.30	520.78	520.80	520.80	-0.60	-0.60	0.60	0.6
2064	7687.5	8812.50	1	521.50	0.30	520.79	520.80	520.80	-0.70	-0.70	0.70	0.70
4064	7687.50	8812.50	6	521.40	0.30	520.68	520.70	520.70	-0.70	-0.70	0.70	0.70
3678	7812.50	11562.50	3	521.90	0.40	522.07	522.00	522.00	0.10	0.10	0.10	0.10
4067	7937.50	7687.50	6	521.00	0.30	520.29	520.30	520.30	-0.70	-0.70	0.70	0.70
3067	7937.50	7687.50	3	521.00	0.30	520.30	520.30	520.30	-0.70	-0.70	0.70	0.70
4439	7937.50	9187.50	6	521.80	1.05	520.70	520.70	520.70	-1.10	-1.10	1.10	1.10
2067	7937.50	7562.50	1	521.00	0.33	520.26	520.30	520.30	-0.70	-0.70	0.70	0.70
2439	7937.50	9187.50	1	521.50	0.30	520.82	520.80	520.80	-0.70	-0.70	0.70	0.70
2430	7937.50	7562.50	1	521.00	0.33	520.26	520.30	520.30	-0.70	-0.70	0.70	0.70
4013	8062.50	9812.50	6	522.18	1.31	520.86	520.80	520.80	-1.38	-1.38	1.38	1.38
2421	8062.50	9687.50	1	521.70	0.29	520.93	520.90	520.90	-0.80	-0.80	0.80	0.80
3421	8062.50	9687.50	3	521.50	0.23	520.92	520.90	520.90	-0.60	-0.60	0.60	0.60
3417	8187.50	8062.50	3	520.45	0.40	520.32	520.30	520.30	-0.15	-0.15	0.15	0.15
4091	8187.50	5187.50	6	520.30	0.30	519.55	519.50	519.50	-0.80	-0.80	0.80	0.80
3423	8187.50	10687.50	3	521.70	0.30	521.32	521.20	521.20	-0.50	-0.50	0.50	0.5
2417	8187.50	8187.50	1	521.01	0.40	520.38	520.30	520.30	-0.71	-0.71	0.71	0.71
2091	8187.50	5187.50	1	520.39	0.31	519.57	519.60	519.60	-0.79	-0.79	0.79	0.79
3091	8187.50	5187.50	3	520.35	0.30	519.55	519.50	519.50	-0.85	-0.85	0.85	0.85
2423	8187.50	10687.50	1	521.70	0.40	521.24	521.20	521.20	-0.50	-0.50	0.50	0.5
3426	8687.50	8437.50	3	521.00	0.30	520.26	520.20	520.20	-0.80	-0.80	0.80	0.80

Table 7.4 (continued)
Comparison between VAM3DF GMA Model Simulation and Water Levels

Well No.	X	Y	Z	Head (Geostat)	Std. (Geostat)	Head SWIFT	Head[1] VAM	Head[2] VAM	Residual[1] VAM-Geostat	Residual[2] VAM-Geostat	Abs.[1] Res.	Abs.[2] Res.
4426	8687.50	8437.50	6	520.90	0.30	520.25	520.20	520.20	-0.70	-0.70	0.70	0.70
2426	8687.50	8437.50	1	520.90	0.33	520.27	520.20	520.20	-0.70	-0.70	0.70	0.7
2119	9062.50	6437.50	1	519.91	0.23	519.62	519.6	519.60	-0.31	-0.31	0.31	0.31
3051	9062.50	9062.50	3	519.60	0.21	620.31	520.20	520.20	0.60	0.60	0.60	0.60
2424	9437.50	9687.50	1	521.10	0.30	520.34	520.10	520.10	-1.00	-1.00	1.00	1.00
3424	9437.50	9687.50	3	521.10	0.30	520.33	520.10	520.10	-1.00	-1.00	1.00	1.00
4424	9437.50	9687.50	6	522.02	1.63	520.33	520.10	520.10	-1.92	-1.92	1.92	1.92
2754	10562.50	11187.50	1	521.50	0.36	520.36	519.90	519.90	-1.60	-1.60	1.60	1.60
3097	11562.50	6062.50	3	518.70	0.30	518.27	518.10	518.10	-0.60	-0.60	0.60	0.60
2097	11562.50	6062.50	1	518.70	0.36	518.30	518.20	518.20	-0.50	-0.50	0.50	0.50
4097	11562.50	6062.50	6	518.70	0.40	518.24	518.10	518.10	-0.60	-0.60	0.60	0.60
3098	12562.50	9062.50	3	519.97	0.30	519.48	519.00	519.00	-0.97	-0.97	0.97	0.97
2098	12562.50	9062.50	1	520.33	0.40	519.48	519.00	519.00	-1.33	-1.33	1.33	1.33
SW2D	12562.50	4562.50	5	501.50	0.22	500.53	506.90	506.20	5.40	4.70	5.40	4.70
COLL1	12687.50	4562.50	5	499.39	0.33	492.35	502.20	501.20	2.81	1.81	2.81	1.81
H-2	13062.50	2937.50	3	516.90	0.40	515.15	516.00	516.00	-0.90	-0.90	0.90	0.90
R6	13187.50	5062.50	2	515.38	0.33	513.94	514.80	514.70	-0.58	-0.68	0.58	0.68
SWIRR	13312.50	3562.50	3	512.63	0.30	514.01	515.20	515.20	2.57	2.57	2.57	2.57
COLL3	13437.50	3312.50	2	517.25	0.38	514.62	515.70	515.60	-1.55	-1.65	1.55	1.65
COLL2	13562.50	6312.50	5	501.20	0.30	501.77	504.20	503.20	3.00	2.00	3.00	2
K5	13687.50	6312.50	2	506.02	0.24	511.87	511.40	509.90	5.38	3.88	5.38	3.88
H-4	14437.50	6937.50	3	518.67	0.4	516.94	516.60	516.60	-2.07	-2.07	2.07	2.07

[1] Upper Node of VAM3DF Model Hydrogeologic Layer.
[2] Lower Node of VAM3DF Model Hydrogeologic Layer.

that the new pumping rate causes the general direction of flow to rotate slightly towards the east. However, that effect associated with the new pumping rate was limited to the northern part of the Fernald Site. To the south, the flow field was not affected.

Transport of uranium at the end of each stress period was simulated using the VAM3DF GMA model. The same approach used in the SWIFT GMA model, which is based on using K_d transition was implemented in simulation Run B1. Details of the approach used and the timing of the transition can be found in the Baseline Remedial Strategy Report (DOE, 1997). The same initial concentration distribution of the first stress period, used in the SWIFT GMA model, was used in Run B1. Also, the mass loading rates applied to the first layer of the SWIFT GMA model are applied to the lower nodes of the first layer of VAM3DF GMA model. Transport parameters used in Run B1 are shown in Table 7.2. Figures 7.16 though 7.19 show the uranium concentration distribution in the site at the end of each stress period for Run B1. It should be noted that the concentrations of the aqueous phase shown in Figure 7.19 are adjusted to account for the change in the partitioning coefficient K_d. When compared to Figures 5.11, 5.12 and 5.13 of the Baseline Remedial Strategy Report (DOE 1997), Run B1 predicted higher concentration and less dispersed uranium plume. In general, the VAM3DF GMA model results (Run B1) agree favorably with the SWIFT GMA results.

7.4 SENSITIVITY ANALYSIS BASED ON THE NEW KINETIC MODULES

The kinetic mass transfer module discussed in Section 4 was applied to the VAM3DF GMA site model in simulation Set C. The adsorption/desorption component of the model was used to simulate the transport of the uranium plume during the four stress periods, described in Section 7.3. Similar to the approach used in simulation Run B1, the flow fields during the different stress periods were assumed to be at steady state. Adsorption/desorption parameters were used directly in simulation Sets C and D, instead of using a transition distribution coefficient, K_d, as in the SWIFT GMA model and Run B1. These parameters included desorption rate constant, α_d, the distribution coefficient, K_d, and chemisorption rate, α_c. Note that the adsorption rate constant, α_a, is calculated internally in the code, since α_a is a function of α_d, K_d, and the solid phase concentration C_s (see Equation 4.10). At equilibrium, the adsorption and desorption rates were assumed to follow a linear isotherm. Hence, the Freundlich exponent, n = 1, was used in all runs of simulation Set C. In Runs C1 through C4, the initial solid phase concentration was assumed to be in equilibrium with the initial aqueous phase concentration ($C_s = K_d\ C_w$). In Run C5, the initial solid phase concentration was assumed to be zero to examine the effect of the initial conditions on the simulation results. Other initial and boundary conditions were identical to those used in the SWIFT GMA model (DOE, 1997). A list of the parameters used in the simulation Sets C and D are shown in Tables 7.5 and 7.6, respectively.

7.4.1 Fully Reversible Sorption

In simulation Set C, the parameters controlling the adsorption/desorption rates were varied to examine the sensitivity of the model to uncertainty in these parameters. The two parameters, α_d, and α_a (through K_d) control the rate of desorption, and the rate of adsorption (see Equation 4.10), respectively. Five test runs (Runs C1 through C4) were carried out with different parameters. The values of parameters used in these simulations are summarized in Table 7.5.

000132

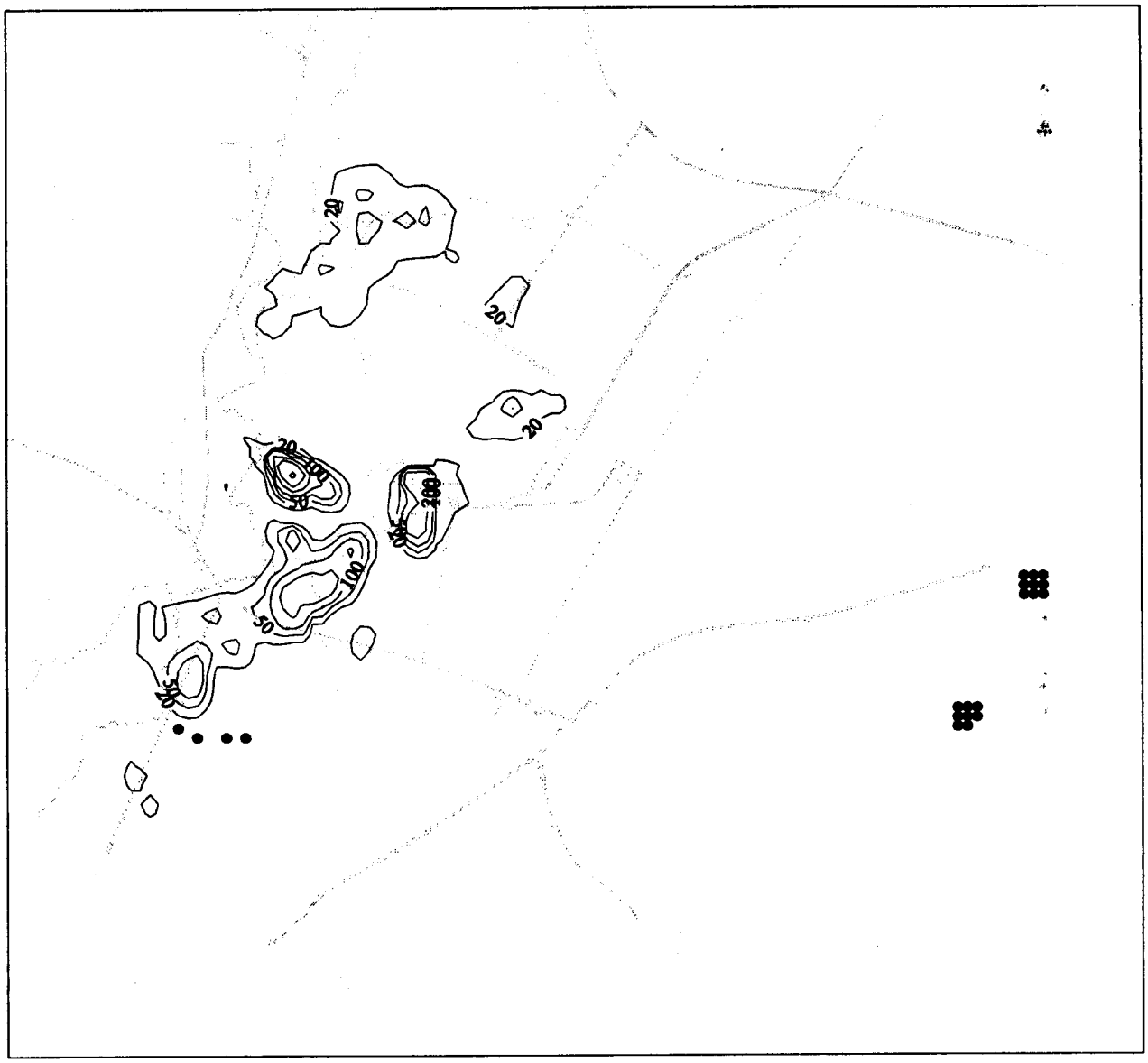

— 20 — Concentration in ppb.

• Well.

2000 0 2000 4000 ft

Figure 7.16 Projected Uranium Concentration Contours for 1997 (Run: B1).

— 20 — Concentration in ppb.

• Well.

2000 0 2000 4000 ft

Figure 7.17 Projected Uranium Concentration Contours for 1998 (Run: B1).

000134

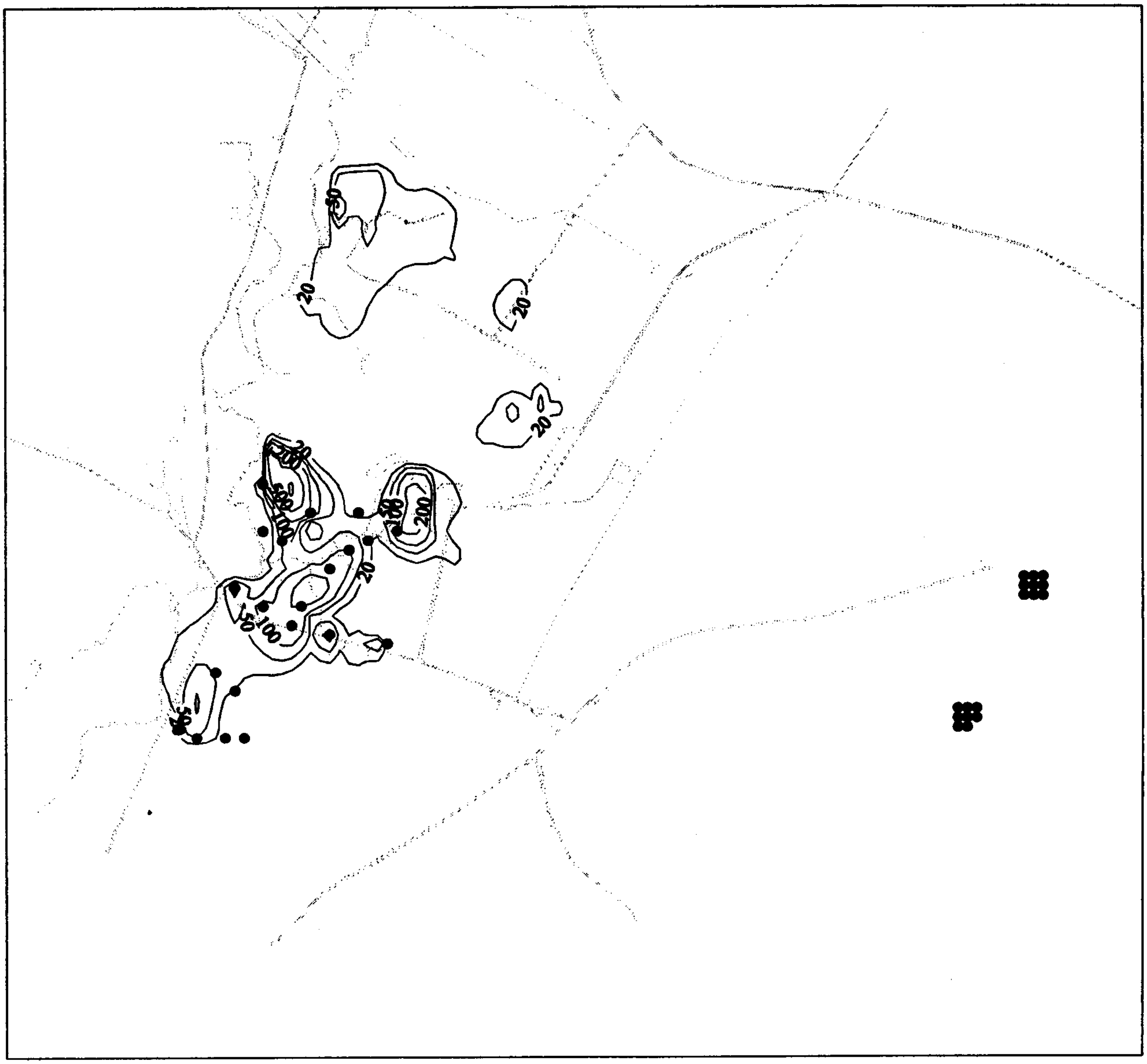

— 20 — Concentration in ppb.

• Well.

2000 0 2000 4000 ft

Figure 7.18 Projected Uranium Concentration Contours for 2003 (Run: B1).

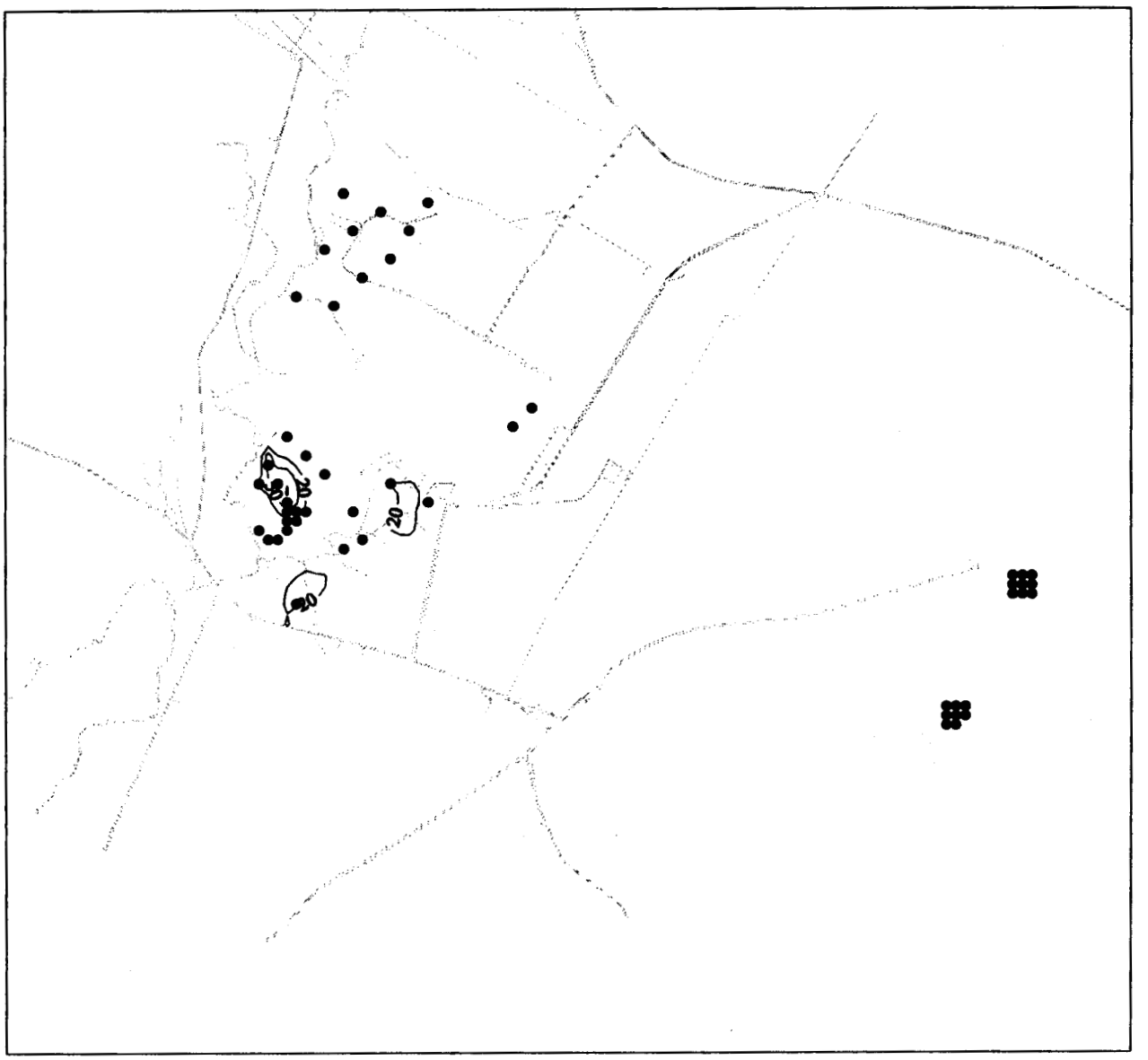

— 20 — Concentration in ppb.

• Well.

2000 0 2000 4000 ft

Figure 7.19 Projected Uranium Concentration Contours for 2006 (Run: B1).

000136

Figure 7.20 shows the initial uranium plume distribution. Figures 7.21 though 7.40 show the extent of the uranium plume (aqueous phase) at the end of the respective stress periods.

Table 7.5
Values of Sorption Parameters used for the Simulations with the Kinetic Module

Run	α_L, ft	α_T, ft	α_V, ft	K_d	α_d	α_c	Results
C1	100	0.1	0.1	17.80	0.01	0.0	Figures 7.21 through 7.24
C2	100	0.1	0.1	1.78	0.01	0.0	Figures 7.25 through 7.28
C3	100	0.1	0.1	1.78	0.1	0.0	Figures 7.29 through 7.32
C4	100	0.1	0.1	1.78	0.5	0.0	Figures 7.33 through 7.36
C5[1]	100	0.1	0.1	1.78	0.1	0.0	Figures 7.37 through 7.40

[1]Zero initial solid phase concentration.

The difference between Run C1 and Run C2 is in K_d, which controls the adsorption rate, α_a, and the initial solid phase concentration, C_s. In Run C1, the rate of adsorption is higher than that in Run C2. However, the initial mass adsorbed on the aquifer solids is 10 times higher in Run C1 compared to Run C2. As a result, more mass was available for desorption at the end of the simulation. Runs C2, C3 and C4 have the same K_d but different α_d. Hence the initial adsorbed mass on solids was the same for the three runs. Increasing the desorption rate, α_d, also increased the sorption rate, a_a. The results shown in Figures 7.25 through 7.36 suggest that the model is not very sensitive to changes in adsorption/desorption rates. The plume configurations and extent change slightly as a result of varying α_d. However, the use of the kinetic module was essential for modeling processes such as chemisorption as discussed below. Note that, in comparing the aqueous uranium concentration contours shown in Figures 7.24, 7.28, 7.32, and 7.36 with those in Figure 7.19, the final uranium concentrations resulting from transport with kinetic sorption tend to be greater than those resulting from transport with instantaneous sorption. To examine the effect the initial solid phase concentration has on the plume distribution, simulation Run C5 was carried out with zero initial solid phase concentrations. Figures 7.37 through 7.40 show that most of the dissolved mass is removed within the first stress period. After the initial removal of the dissolved mass by sorption, the change in dissolved plume becomes slower as can be seen in Figures 7.38, 7.39, and 7.40. Such a condition is less likely to happen at the site since the uranium plume has been in the aquifer for a long period of time, and the equilibrium condition may have been attained.

7.4.2 Simulations with Chemisorption

Simulation Set D was intended to examine the effect of chemisorption, a process believed to be responsible for the difference in the "apparent" K_d during adsorption and desorption. Parameter values used for simulation Runs D1, D2, and D3 are shown in Table 7.6. In the following discussion, two different solid phases are considered. The adsorbed phase concentration, C_s, refers to the uranium contaminants that are adsorbed to the solid phase and

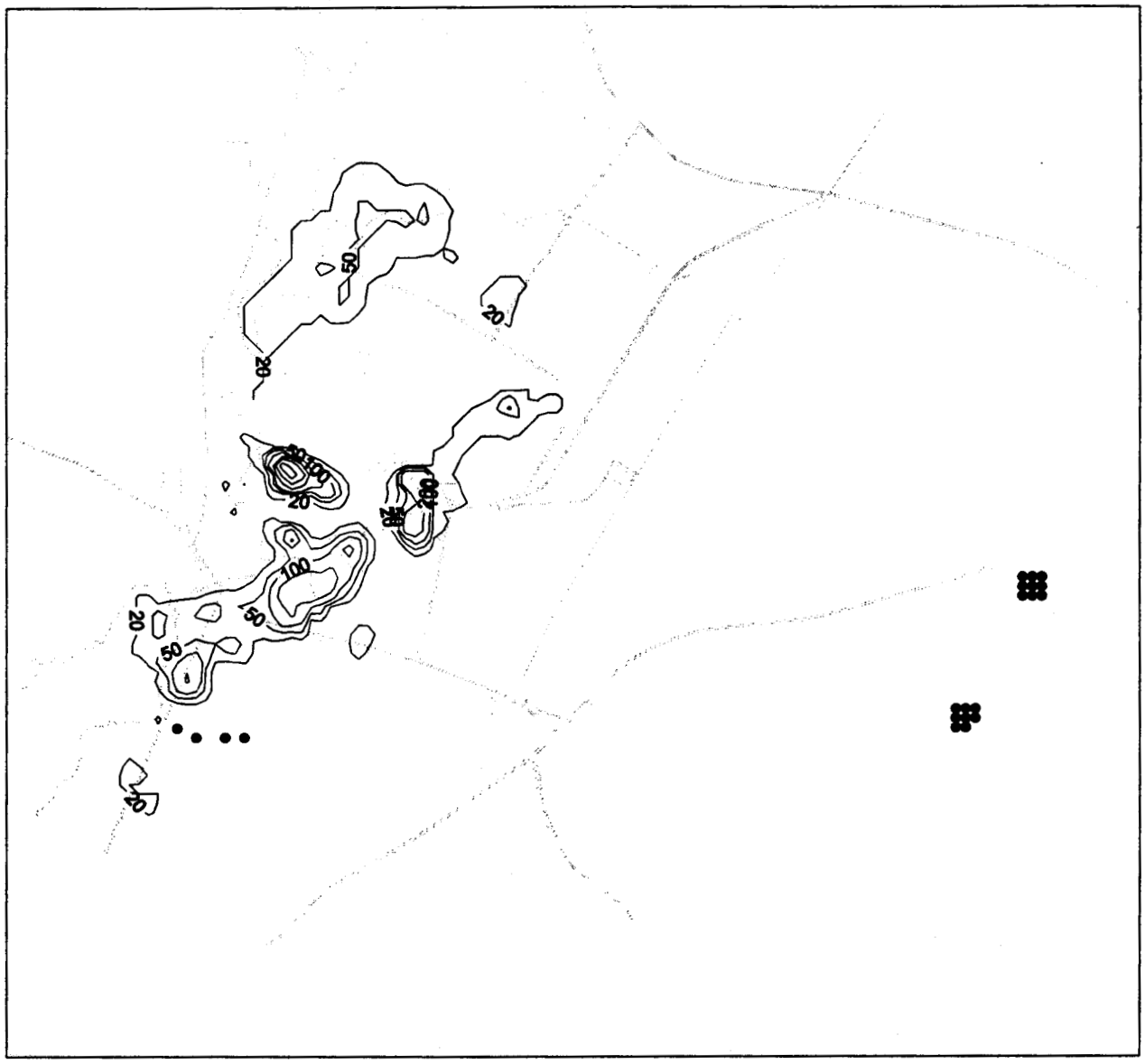

— 20 — Concentration in ppb.

• Well.

2000 0 2000 4000 ft

Figure 7.20 Initial Uranium Concentration Contours.

000138

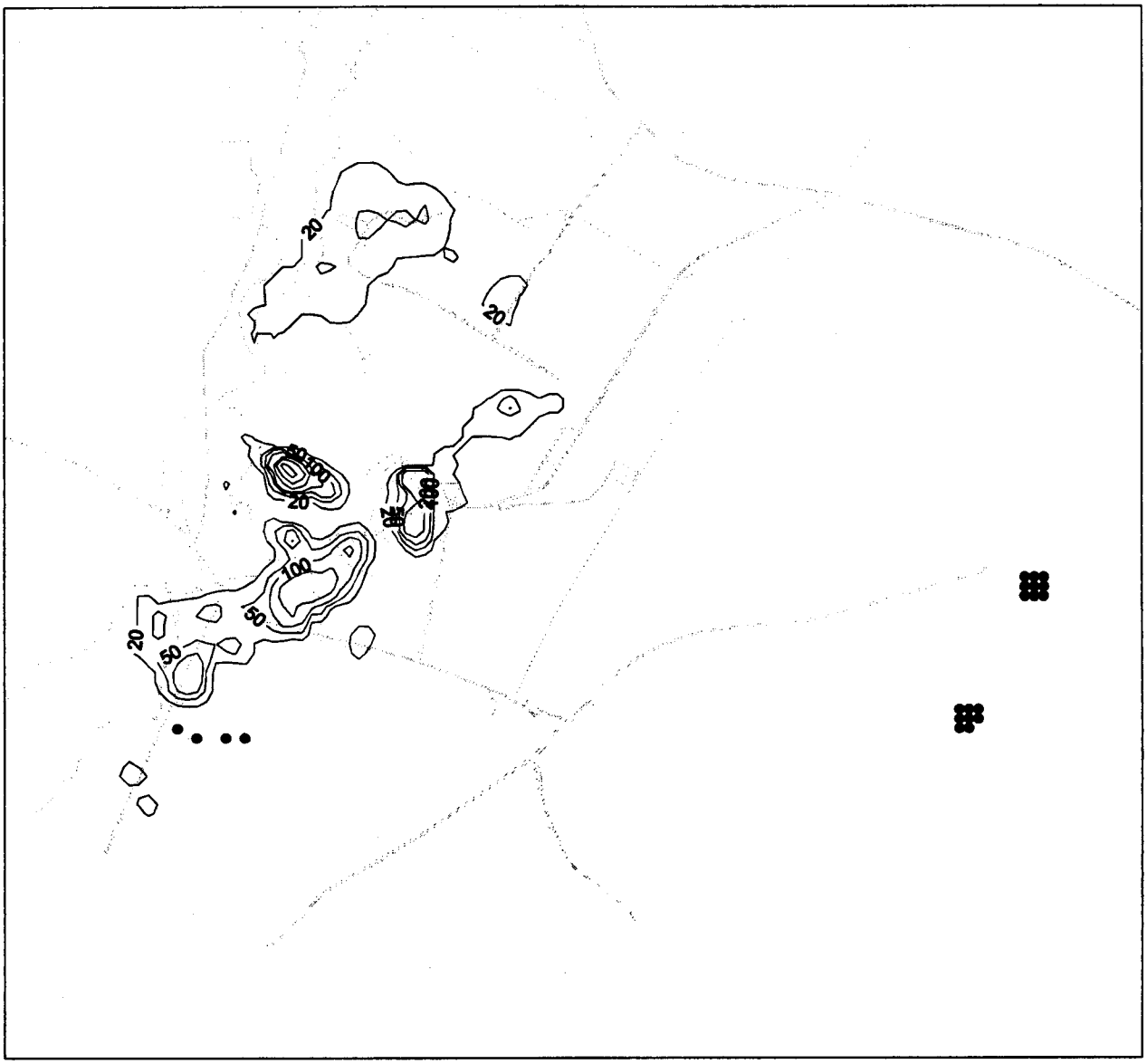

Figure 7.21 Projected Uranium Concentration Contours for 1997 Using the Kinetic Model. (Run: C1)

000139

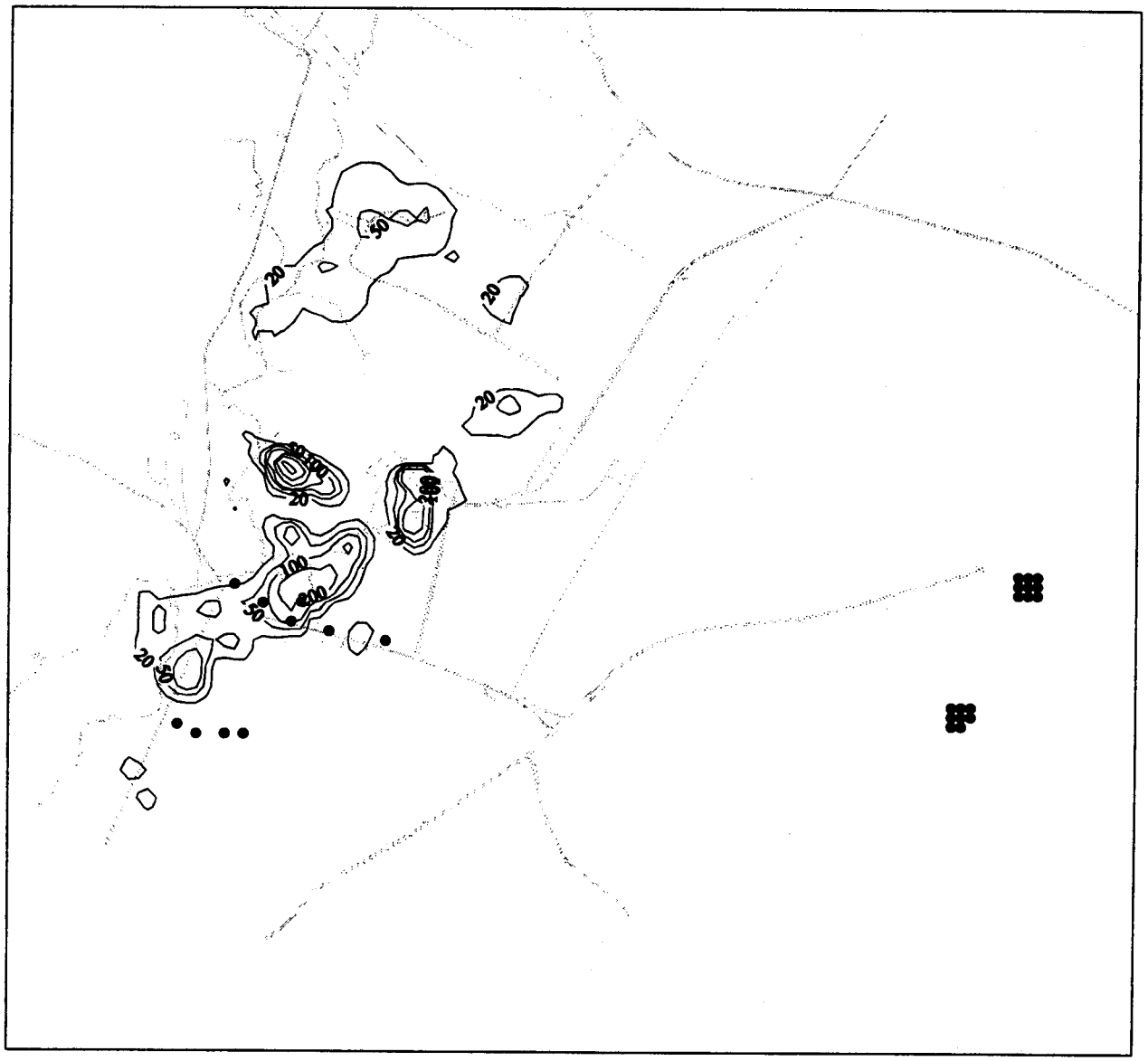

— 20 — Concentration in ppb.

● Well.

2000 0 2000 4000 ft

Figure 7.22 Projected Uranium Concentration Contours for 1998 Using the Kinetic Model (Run: C1).

000140

— 20 — Concentration in ppb.

• Well.

2000 0 2000 4000 ft

Figure 7.23 Projected Uranium Concentration Contours for 2003, Using the Kinetic Model (Run: C1).

000141

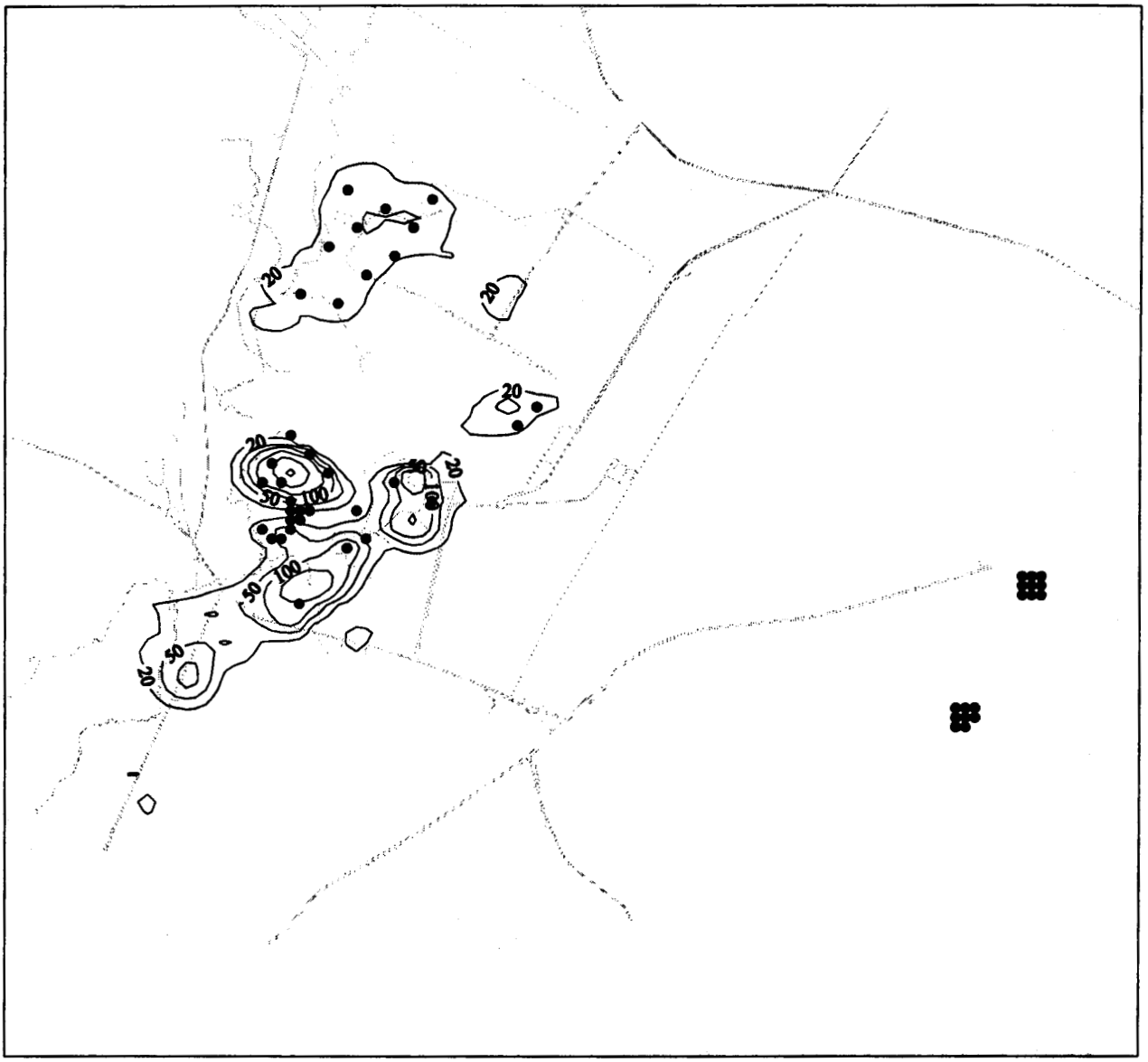

— 20 — Concentration in ppb.

• Well.

2000 0 2000 4000 ft

Figure 7.24 Projected Uranium Concentration Contours for 2006, Using the Kinetic Model (Run: C1).

000142

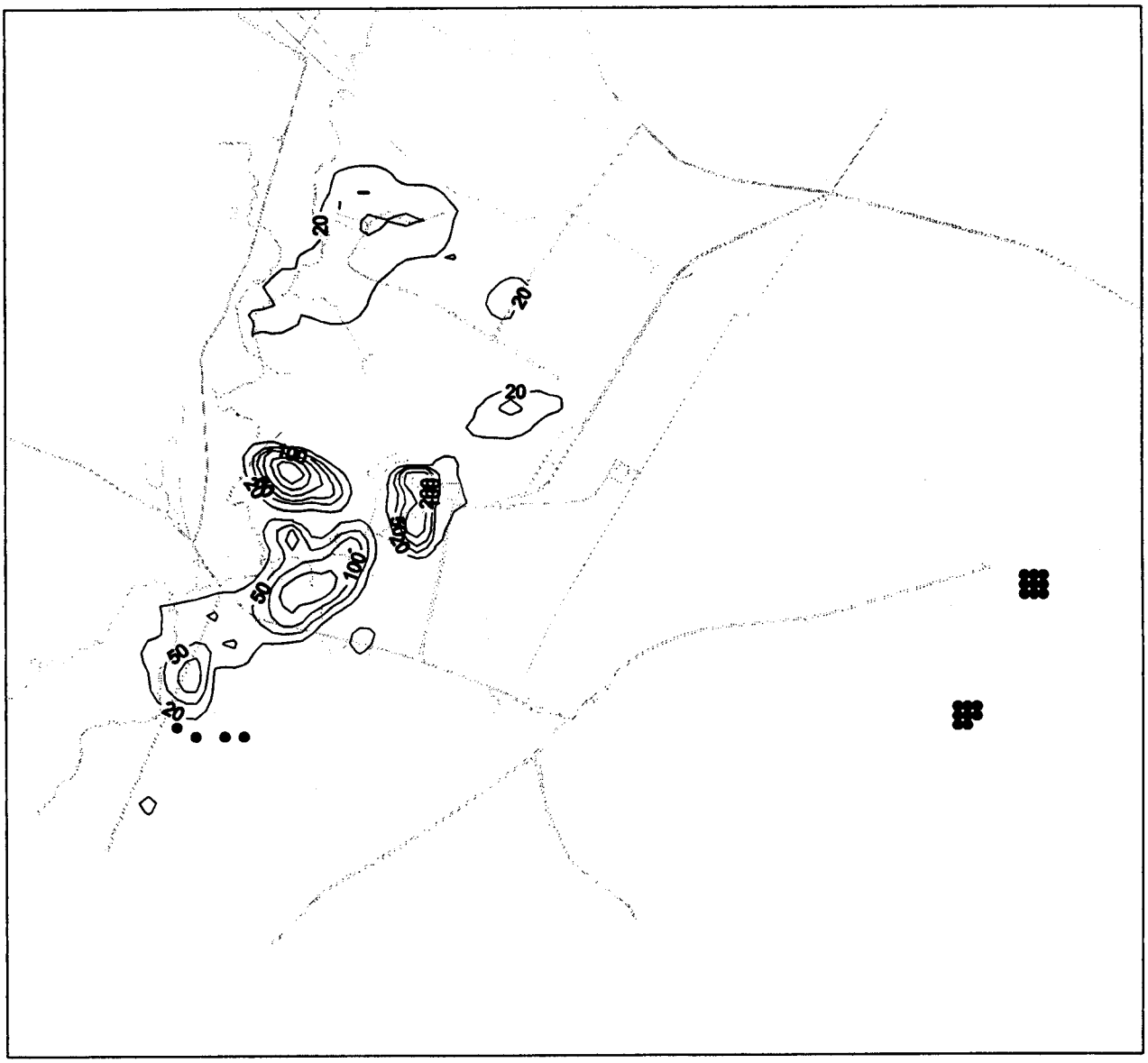

— 20 — Concentration in ppb.

• Well.

2000 0 2000 4000 ft

Figure 7.25 Projected Uranium Concentration Contours for 1997, Using the Kinetic Model (Run: C2).

000143

— 20 — Concentration in ppb.

• Well.

2000 0 2000 4000 ft

Figure 7.26 Projected Uranium Concentration Contours for 1998, Using the Kinetic Model (Run: C2).

000144

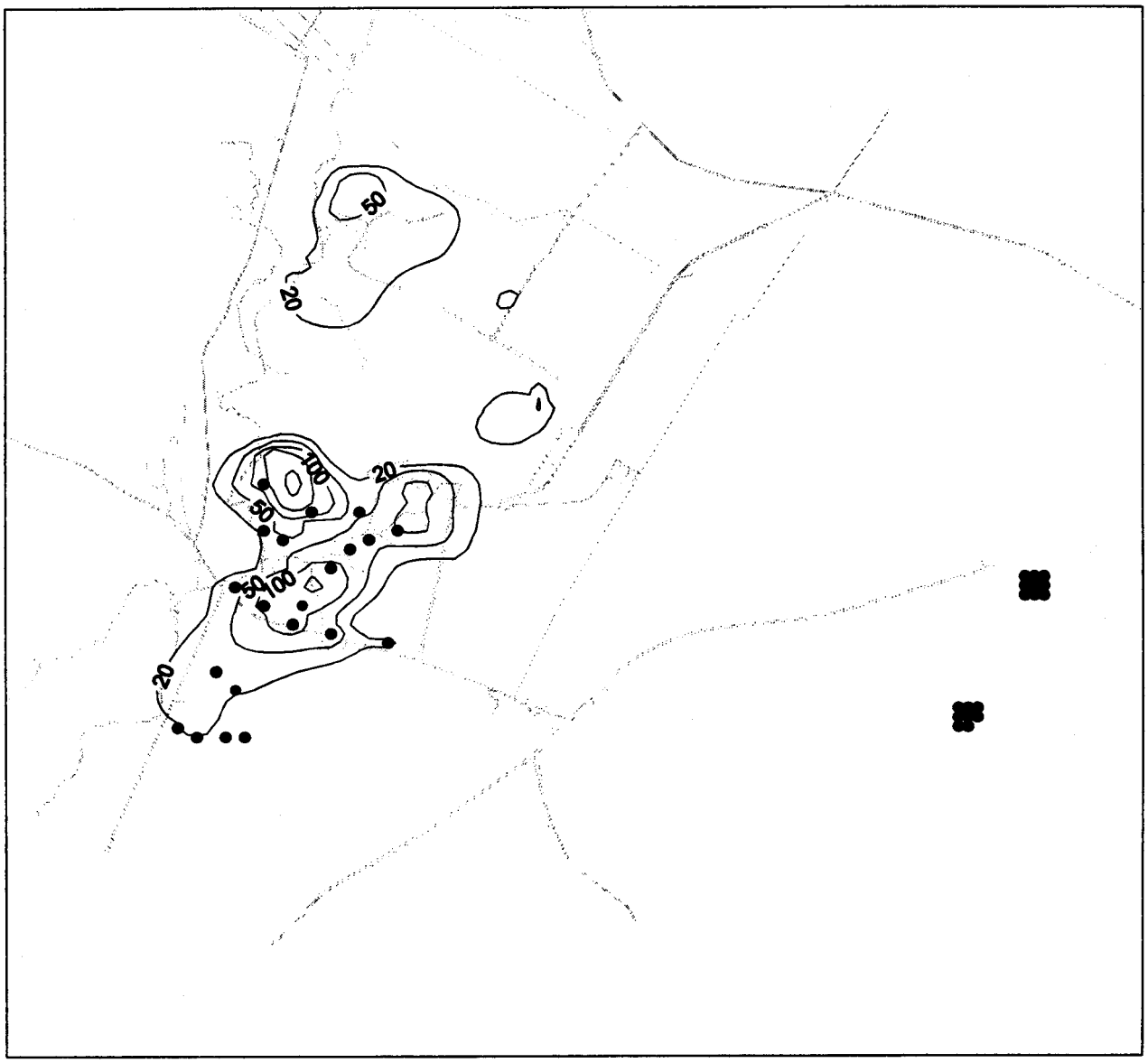

— 20 — Concentration in ppb.

• Well.

2000 0 2000 4000 ft

Figure 7.27 Projected Uranium Concentration Contours for 2003, Using the Kinetic Model (Run: C2).

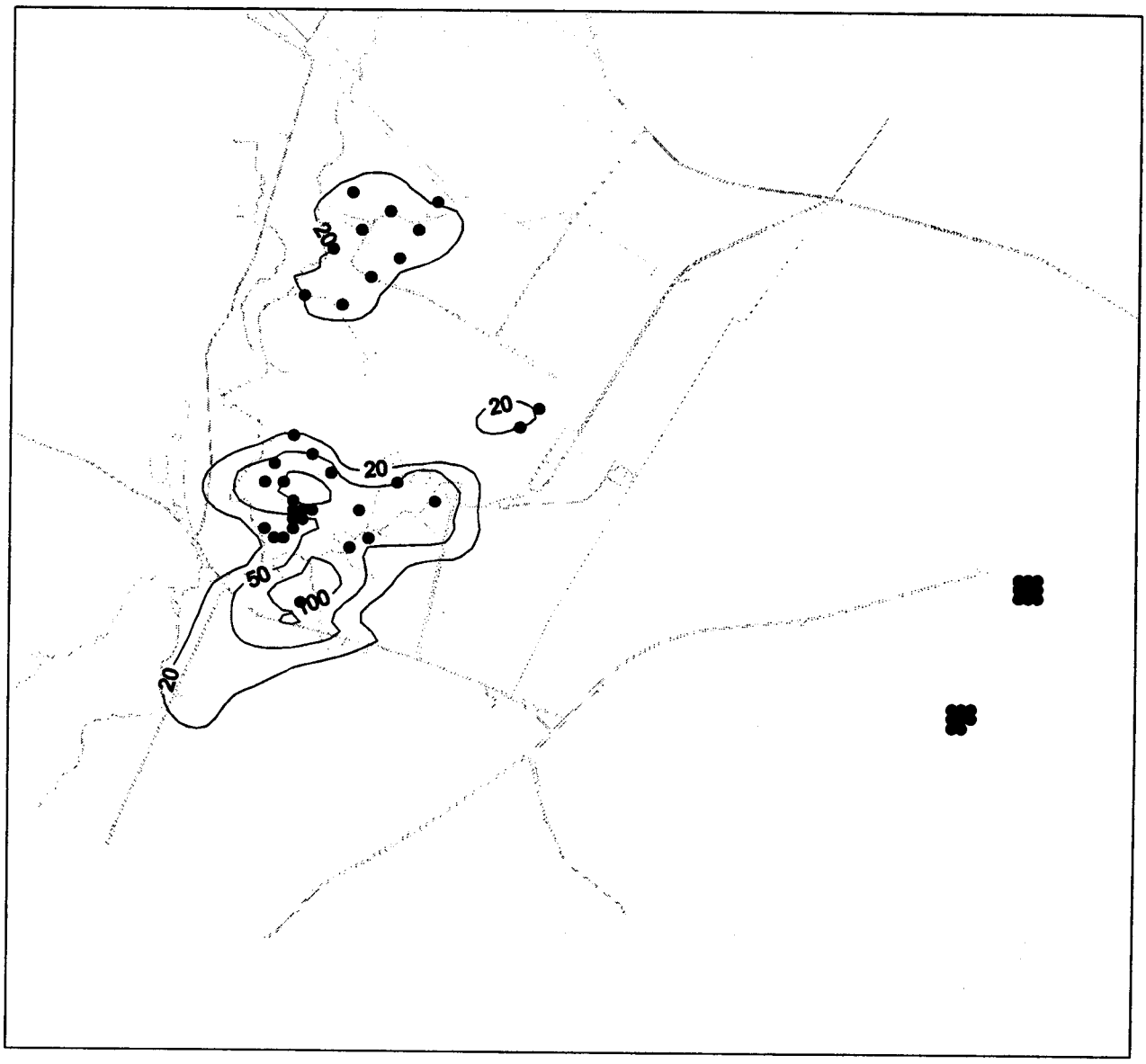

— 20 — Concentration in ppb.

• Well.

2000 0 2000 4000 ft

Figure 7.28 Projected Uranium Concentration Contours for 2006, Using the Kinetic Model. (Run: C2).

000146

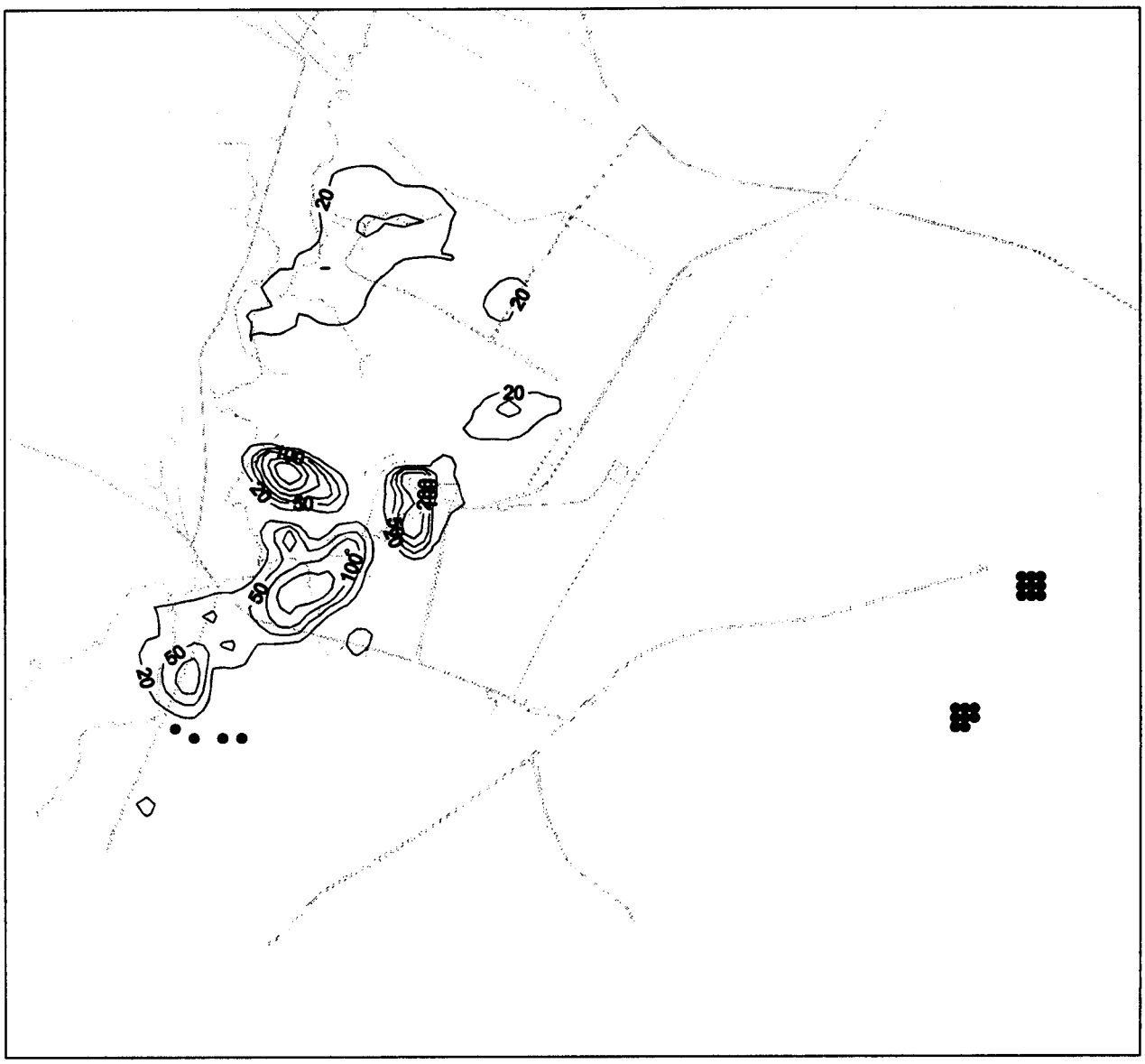

— 20 — Concentration in ppb.

• Well.

2000 0 2000 4000 ft

Figure 7.29 Projected Uranium Concentration Contours for 1997, Using the Kinetic Model (Run: C3

000147

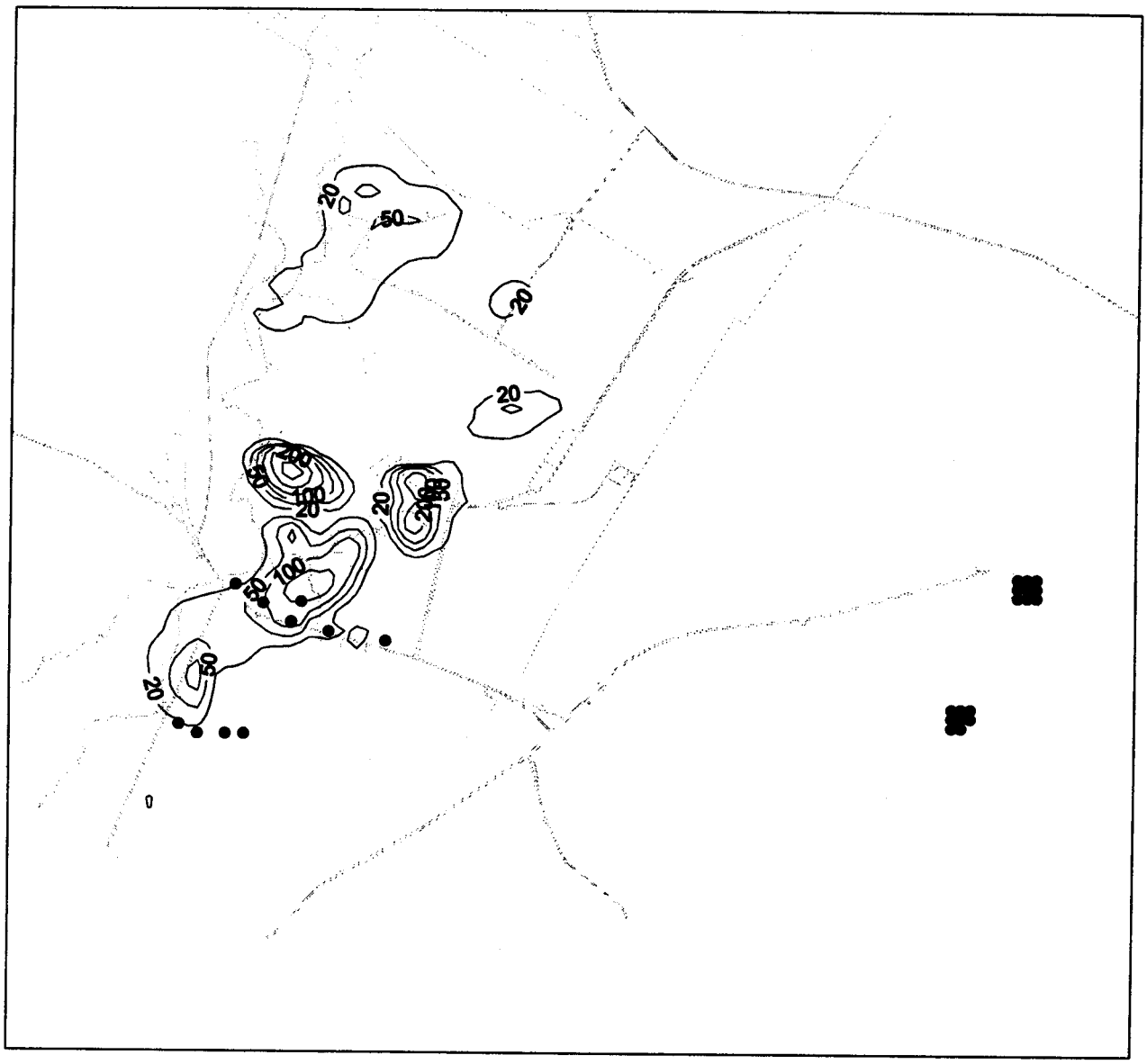

— 20 — Concentration in ppb.

● Well.

2000 0 2000 4000 ft

Figure 7.30 Projected Uranium Concentration Contours for 1998, Using the Kinetic Model (Run: C3

000148

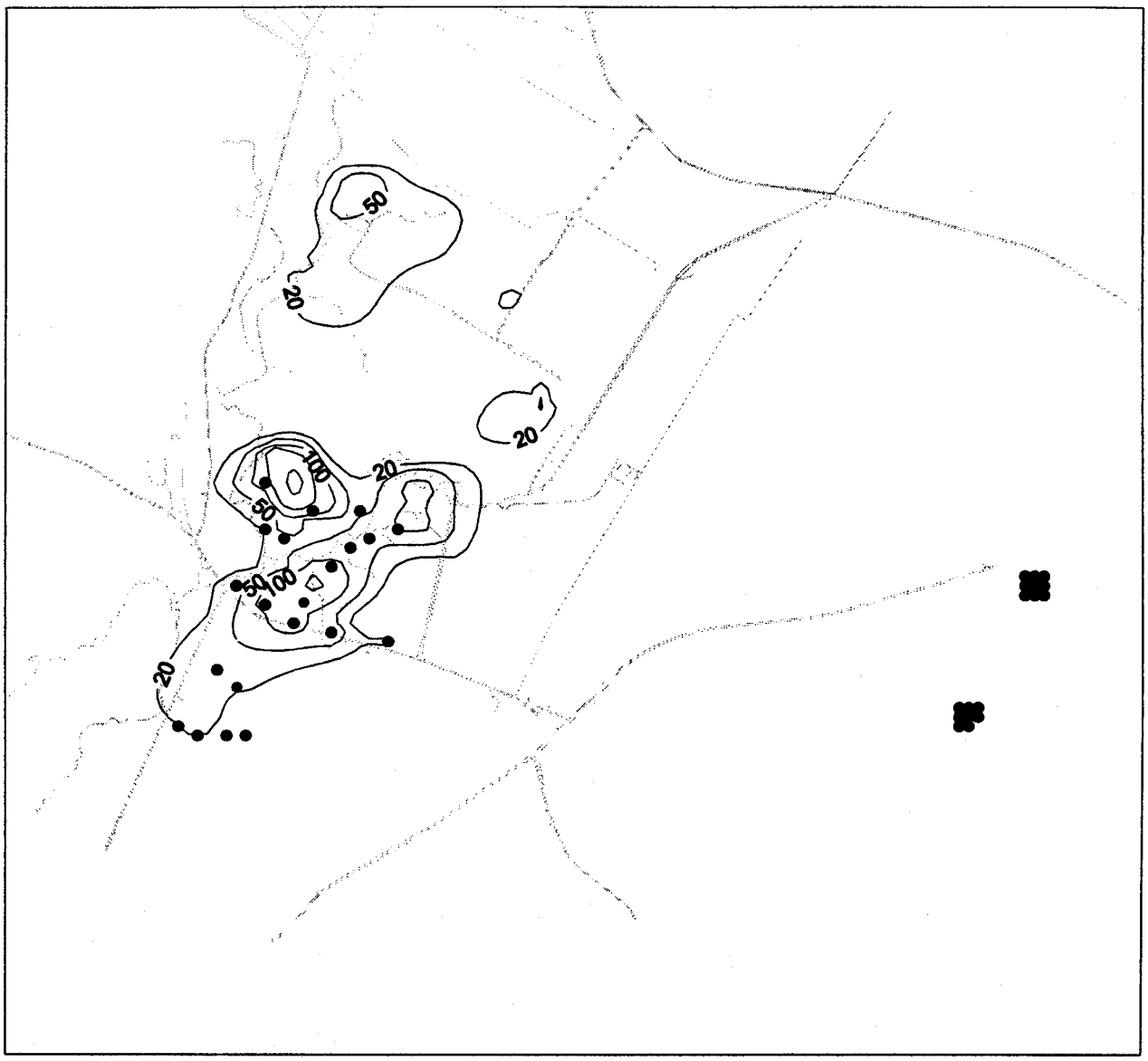

— 20 — Concentration in ppb.

• Well.

2000 0 2000 4000 ft

Figure 7.31 Projected Uranium Concentration Contours for 2003, Using the Kinetic Model (Run: C3).

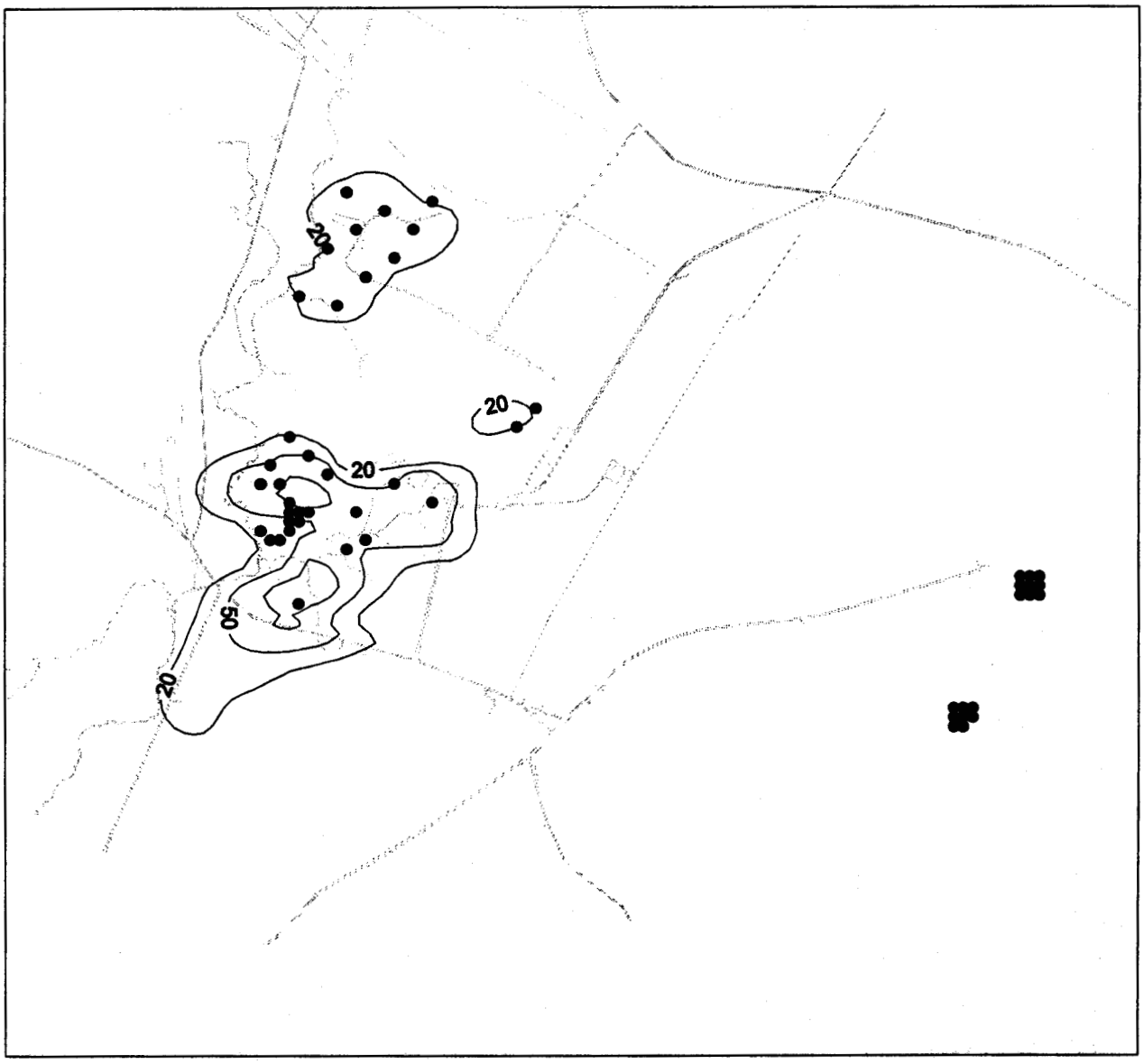

— 20 — Concentration in ppb.

• Well.

2000 0 2000 4000 ft

Figure 7.32 Projected Uranium Concentration Contours for 2006, Using the Kinetic Model (Run: C3

000150

— 20 — Concentration in ppb.

• Well.

2000 0 2000 4000 ft

Figure 7.33 Projected Uranium Concentration Contours for 1997, Using the Kinetic Model (Run: C4).

000151

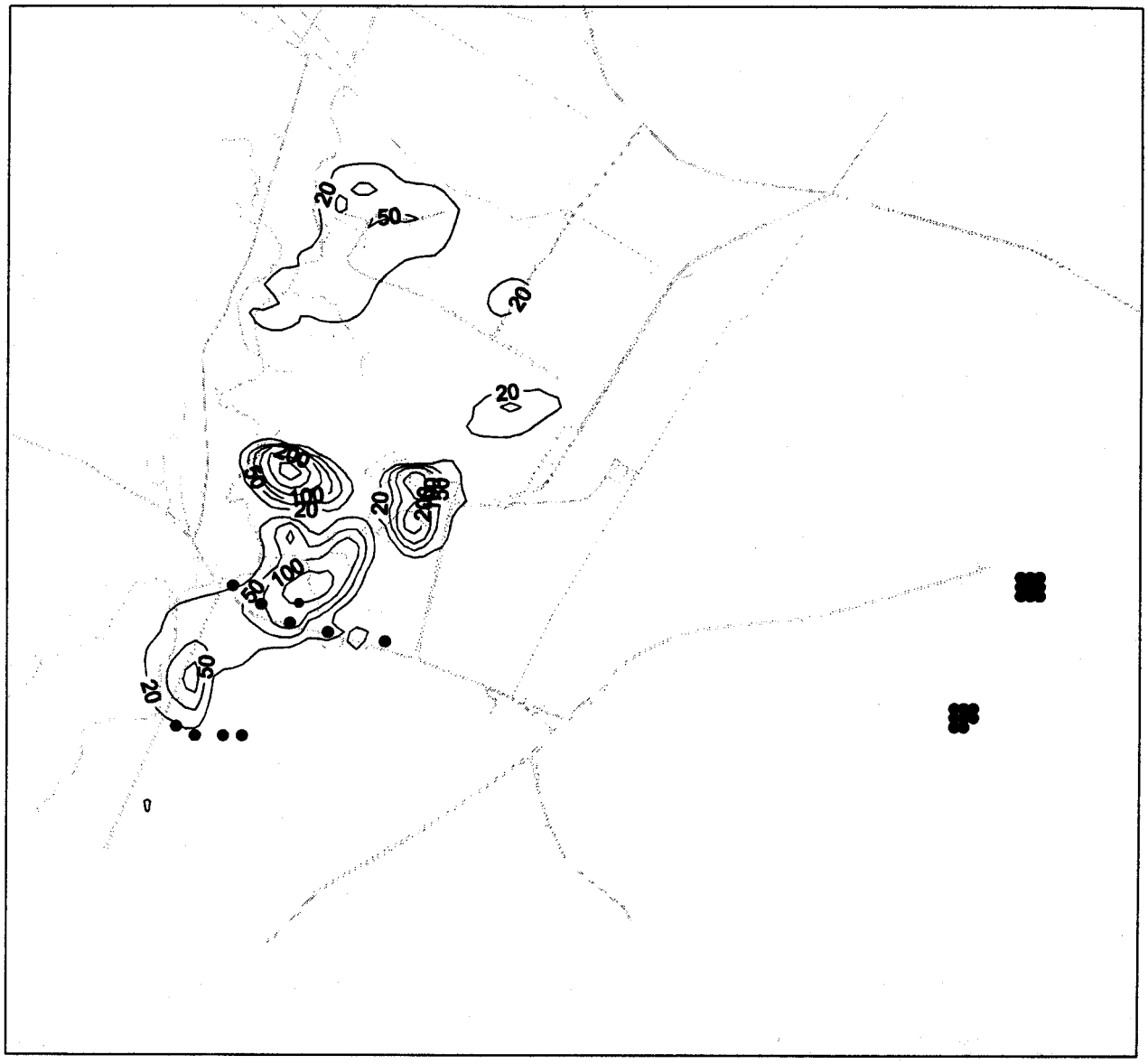

— 20 — Concentration in ppb.

• Well.

2000 0 2000 4000 ft

Figure 7.34 Projected Uranium Concentration Contours for 1998, Using the Kinetic Model (Run: C4)

000152

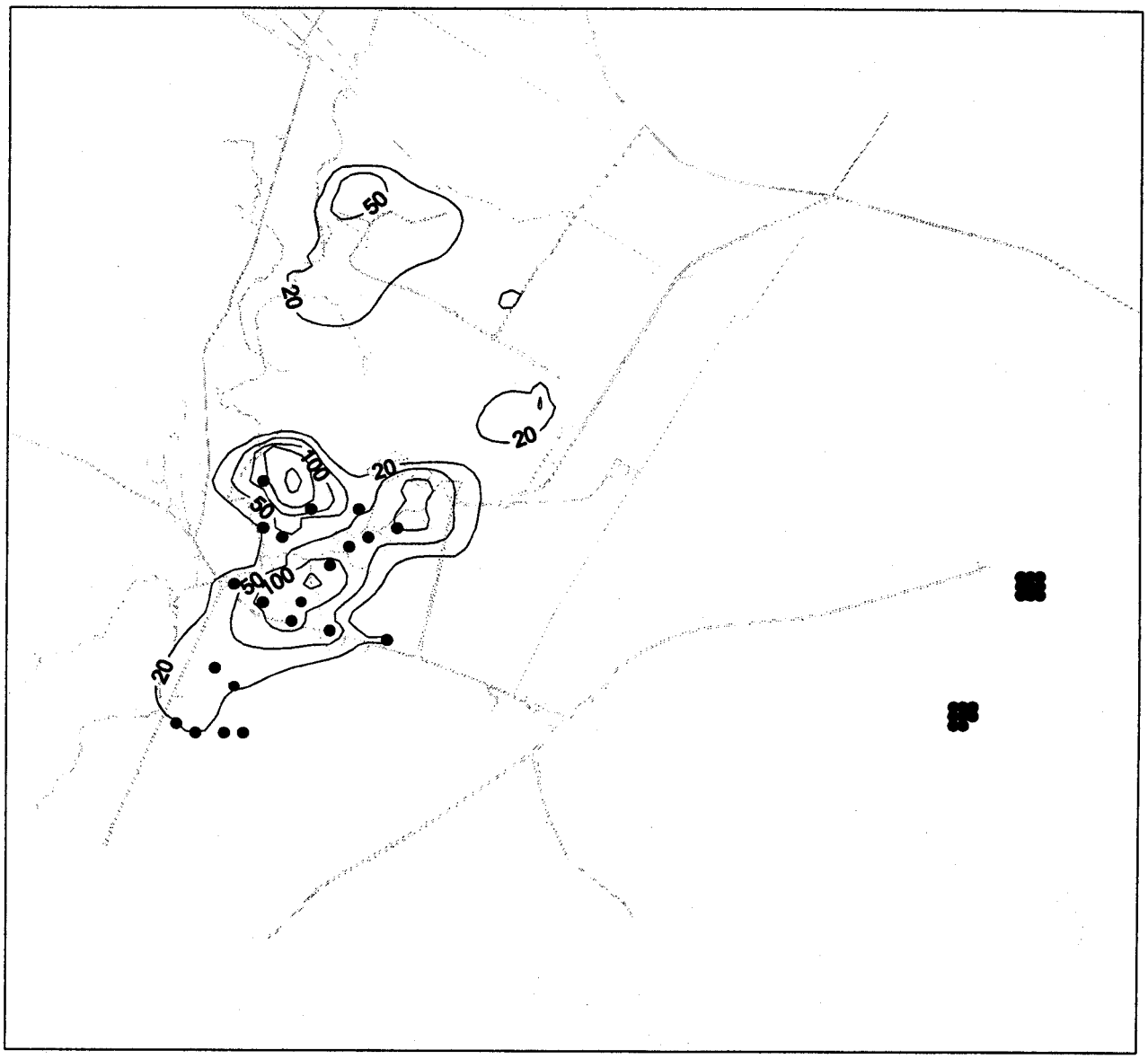

— 20 — Concentration in ppb.

● Well.

2000 0 2000 4000 ft

Figure 7.35 Projected Uranium Concentration Contours for 2003, Using the Kinetic Model (Run: C4)

000153

— 20 — Concentration in ppb.

• Well.

2000 0 2000 4000 ft

Figure 7.36 Projected Uranium Concentration Contours for 2006, Using the Kinetic Model (Run: C4

000154

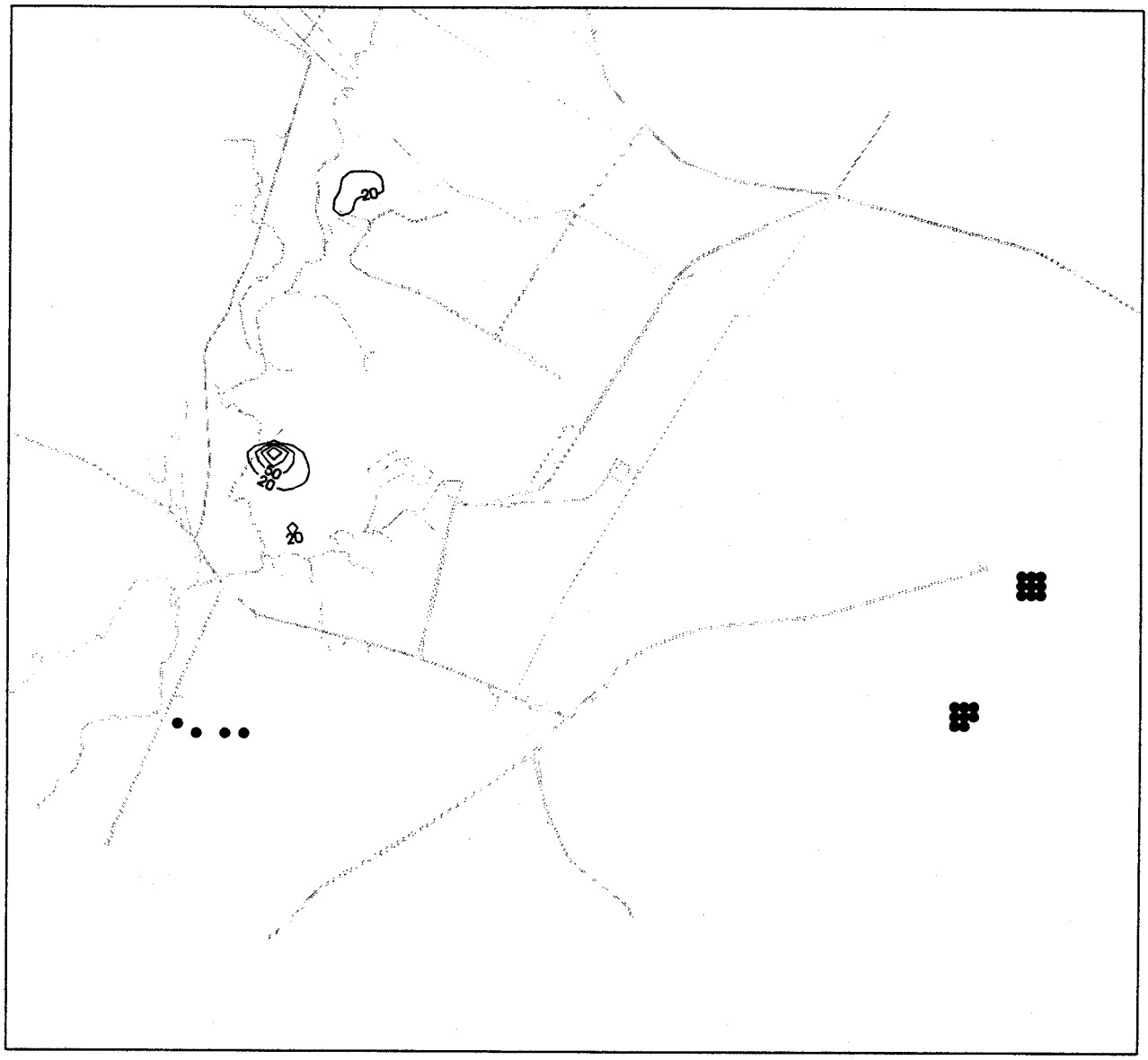

— 20 — Concentration in ppb.

• Well.

2000 0 2000 4000 ft

Figure 7.37 Projected Uranium Concentration Contours for 1997, Using the Kinetic Model (Run: C5).

000155

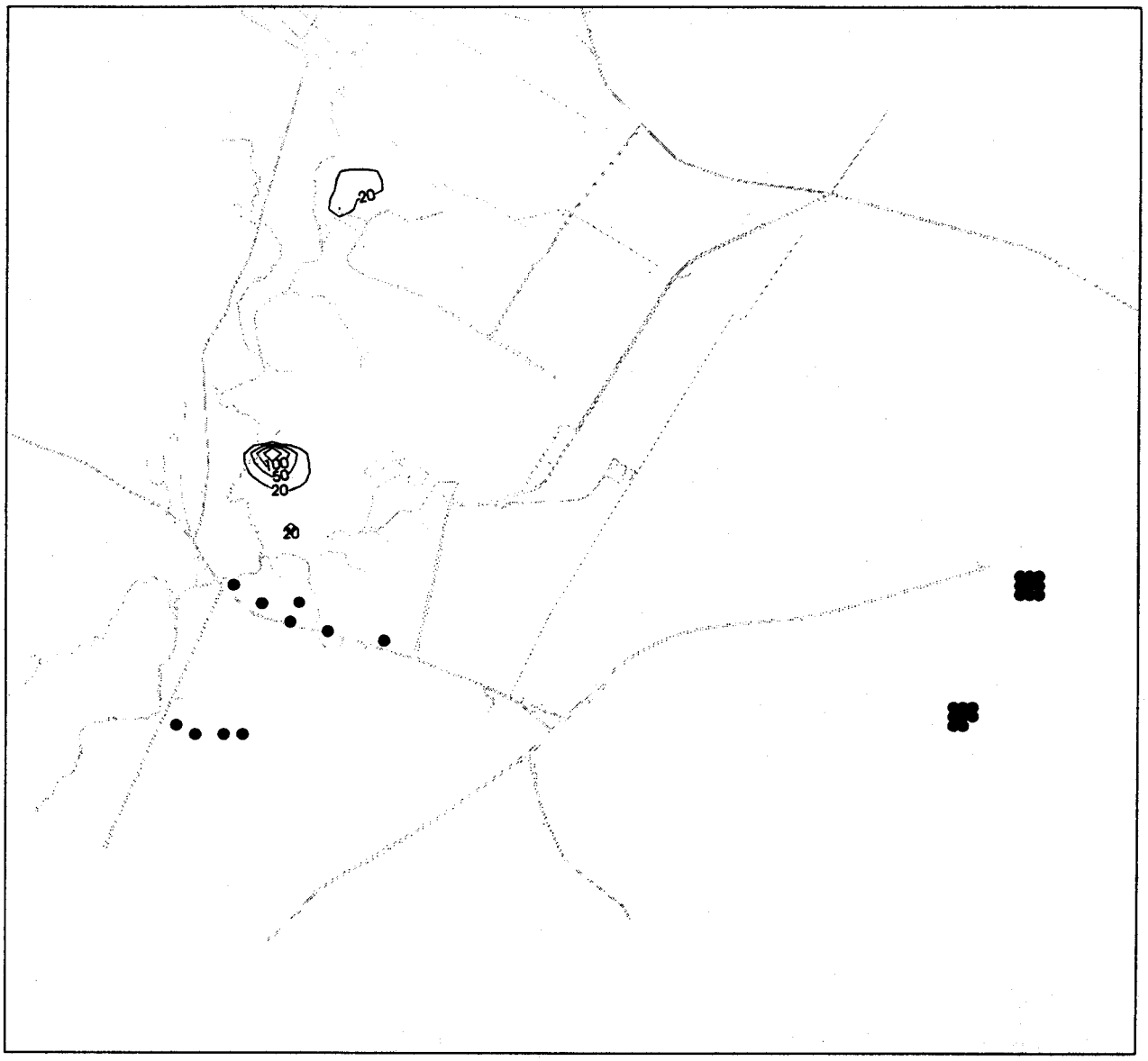

— 20 — Concentration in ppb.

● Well.

2000 0 2000 4000 ft

Figure 7.38 Projected Uranium Concentration Contours for 1998, Using the Kinetic Model (Run: C5).

000156

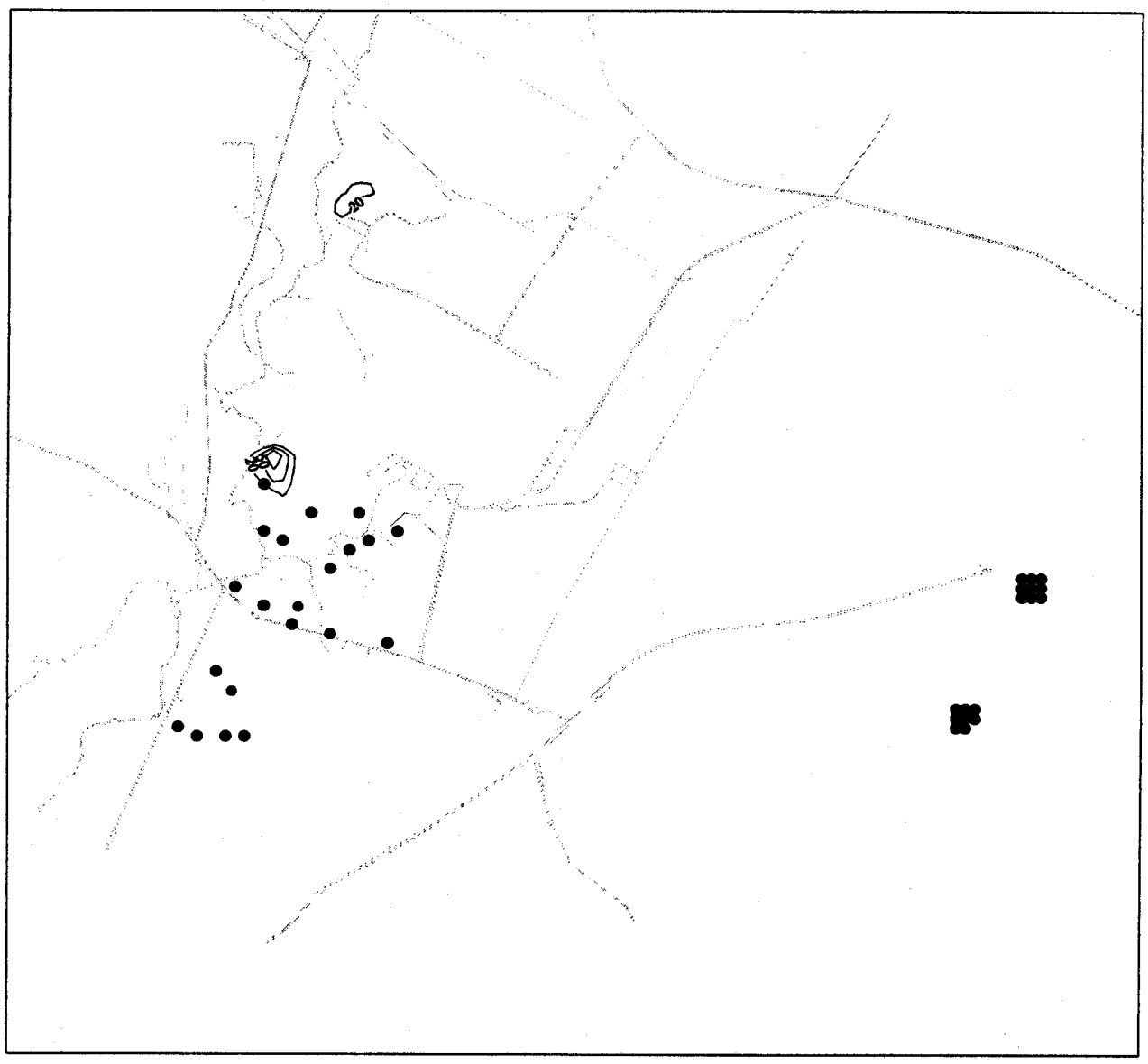

— 20 — Concentration in ppb.

• Well.

2000 0 2000 4000 ft

Figure 7.39 Projected Uranium Concentration Contours for 2003, Using the Kinetic Model (Run: C5).

— 20 — Concentration in ppb.

• Well.

2000 0 2000 4000 ft

Figure 7.40 Projected Uranium Concentration Contours for 2006, Using the Kinetic Model (Run: C5).

000158

always available for desorption. The chemisorbed phase concentration, C_{Cs}, is the uranium mass permanently adsorbed to the aquifer material and is not available for desorption. The initial solid phase concentration was assumed to be adsorbed uranium available for desorption and was calculated as $C_s = K_d C_w$ at time $t=0$. The initial chemisorption concentration was assumed to be zero in Runs D1, D2, and D3. Simulation Set D is the most realistic since it incorporates all the processes that are expected to affect the uranium plume. In addition, dispersivity values considered to be more realistic were used (see Table 7.6).

Table 7.6
Values of Sorption Parameters Used for the Simulations with the Kinetic Module

Run n	$\alpha_{L,x}$ ft	$\alpha_{L,y}$ ft	$\alpha_{L,z}$ ft	K_d	α_d	α_c	Results
D1	100	10.0	1.0	1.78	0.01	0.001	Figures 7.41 through 7.45
D2	100	10.0	1.0	1.78	0.5	0.0001	Figures 7.48 through 7.51
D3	100	10.0	1.0	Tabulated[1]	0.1	0.0004	Figures 7.54 through 7.57

[1] The tabulated equilibrium curve is shown in Figure 7.53.

Figures 7.41 through 7.45 show the aqueous-phase uranium concentrations distribution for the four pumping stress periods in Run D1. The chemisorption rate, α_c, used in Run D1 was one order of magnitude smaller than desorption rate α_d. There were no experimental data to guide the choice of α_c. Desorption batch experiments have shown that a considerable portion of uranium mass remained in the solid phase after reaching equilibrium. A simple calculation of the chemisorbed mass since the beginning of mass loading indicated that the chemisorption rate is on the order of 0.001 to 0.0001 1/day. The values assigned to Set D were intended to cover this range. However, chemisorption had a profound impact on the concentration distribution. Compared to the simulation runs that involved reversible sorption, the predicted plume is much smaller and the dissolved concentrations fall below 20 ppb by the end of Stress Period 4.

The distribution of mass between the dissolved, adsorbed, and chemisorbed phases at a location of high initial aqueous concentration can be seen in Figure 7.45. The dimensions of the grid block, in which the mass balances calculation was conducted, are 125 ft x 125 ft x 29 ft. The initial dissolved concentration was 2,300 ppb and the corresponding adsorbed concentration was 4,094 μg/kg. As mentioned above, the initial chemisorbed concentration was assumed to be zero. Note that the initial chemisorbed concentration does not affect the mass transfer process. The initial uranium masses, referred to in Figure 7.45, were calculated by integrating the uranium concentrations over the volume of one model cell. An initial decrease in the dissolved mass can be seen at the start of the simulation. The equilibrium model would have predicted an instantaneous decrease in the adsorbed phase. The kinetic module predicted a delayed response in the adsorbed mass. The increase in the chemisorbed mass can be seen in Figure 7.45. Over the period of the simulation, chemisorption removed mass from the adsorbed phase into a chemisorbed phase preventing the uranium from desorbing back to the water when concentration drops. It should be noted that, some of the initial mass has been transported outside the model cell under consideration. Figure 7.46 shows the mass distribution at a model cell where the pumping well

RW-2 (Well 25 in DOE, 1997) is located. At this location the initial concentrations were low. The dimensions of this grid block are 125 ft x 125 ft x 23.8 ft. As the uranium was transported towards the well, the dissolved, as well as the adsorbed, mass started to increase. As noted

000160

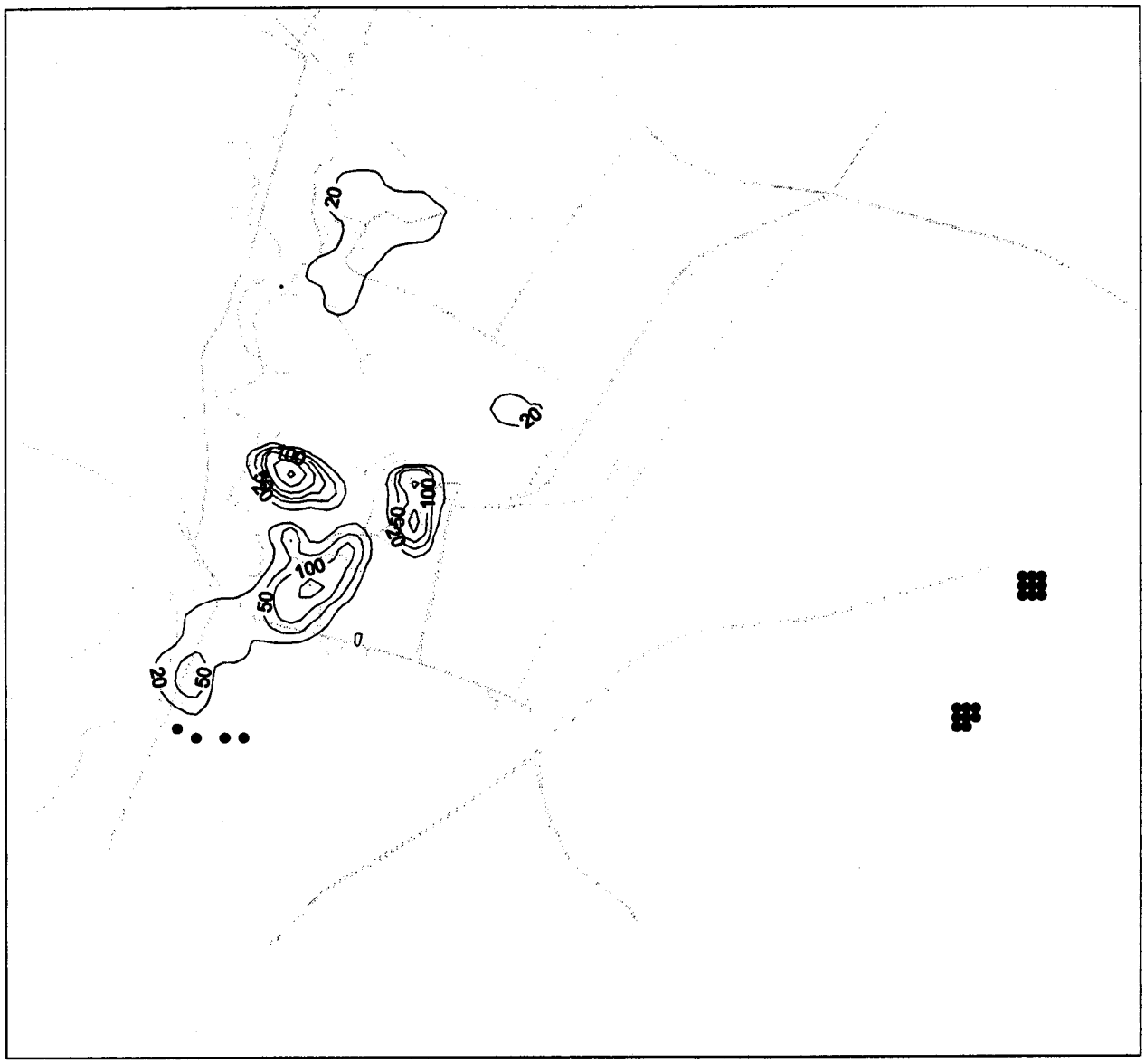

— 20 — Concentration in ppb.

• Well.

2000 0 2000 4000 ft

Figure 7.41 Projected Uranium Concentration Contours for 1997, Using the Kinetic Model (Run: D1).

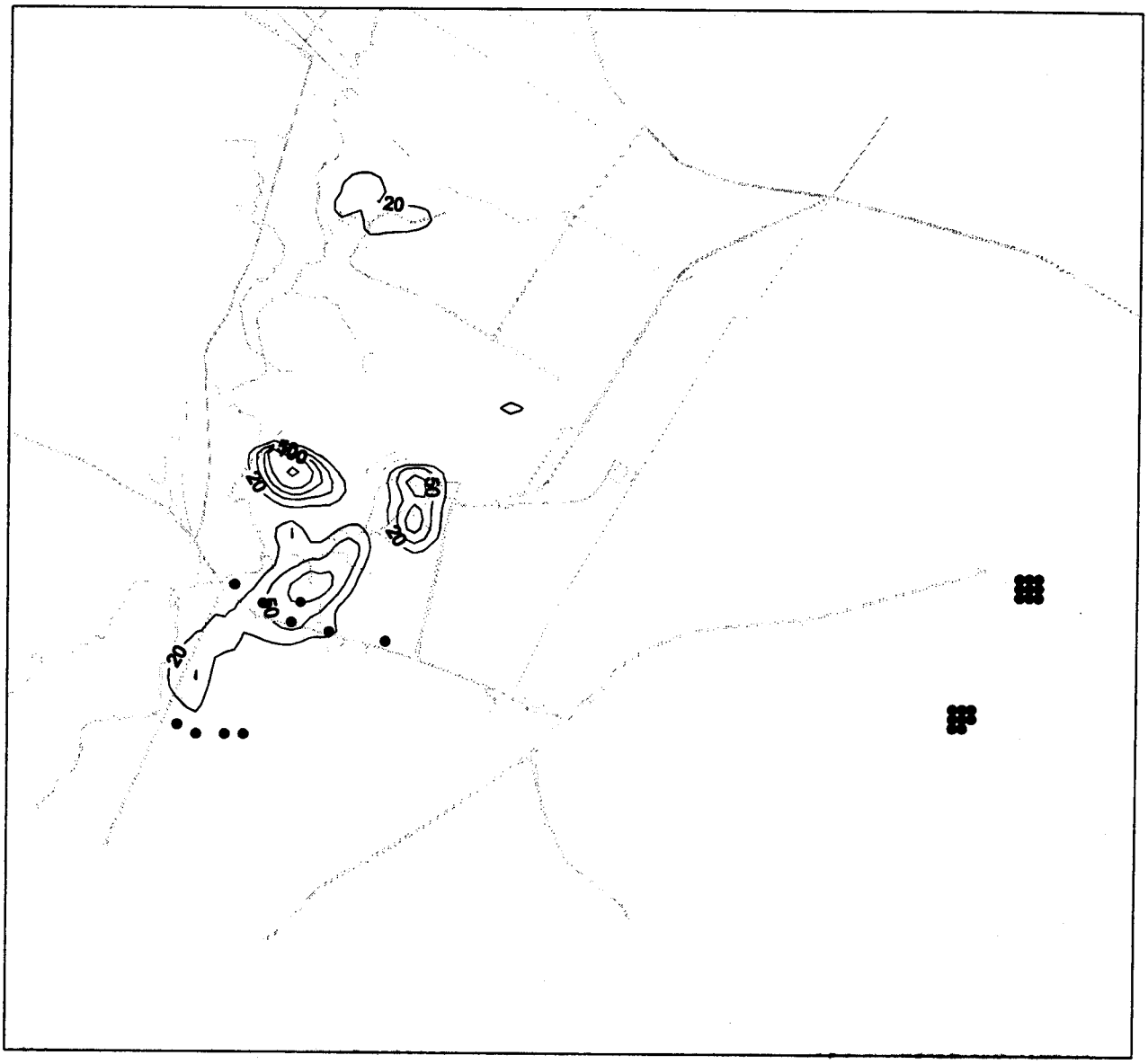

— 20 — Concentration in ppb.

• Well.

2000 0 2000 4000 ft

Figure 7.42 Projected Uranium Concentration Contours for 1998, Using the Kinetic Model (Run: D1).

000162

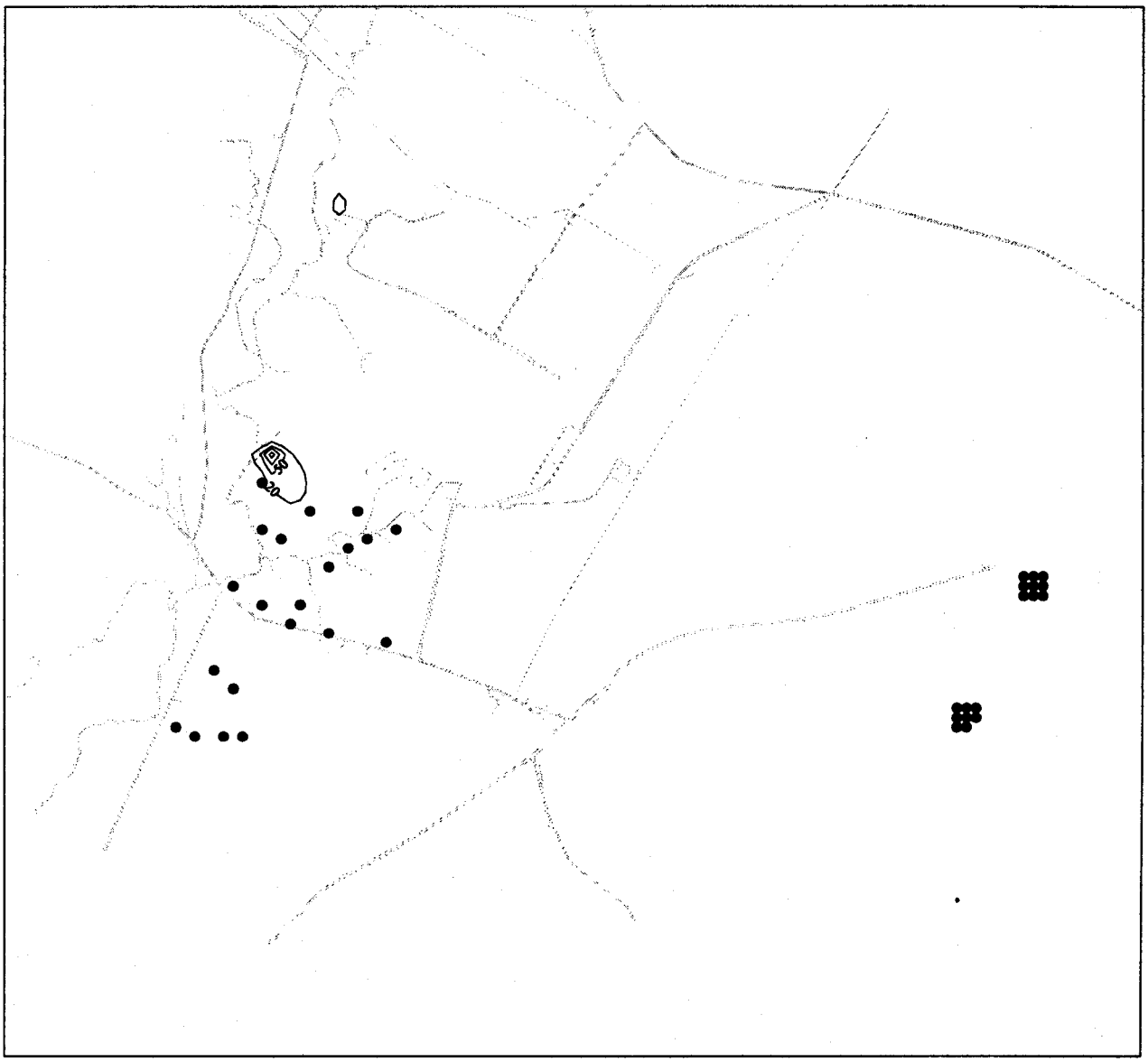

— 20 — Concentration in ppb.

• Well.

2000 0 2000 4000 ft

Figure 7.43 Projected Uranium Concentration Contours for 2003, Using the Kinetic Model (Run: D1).

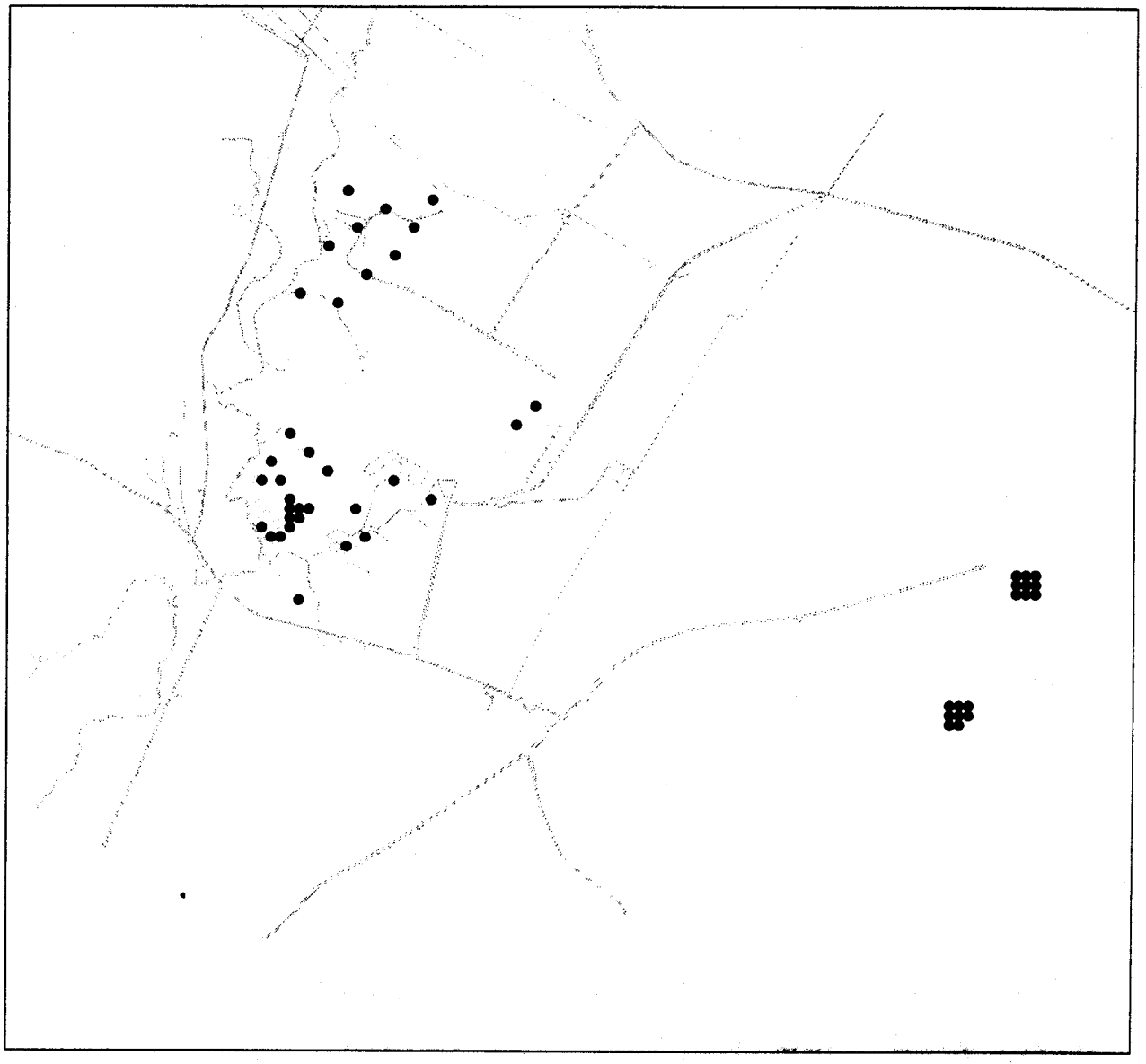

— 20 — Concentration in ppb.

• Well.

2000 0 2000 4000 ft

Figure 7.44 Projected Uranium Concentration Contours for 2006, Using the Kinetic Model (Run: D1).

000164

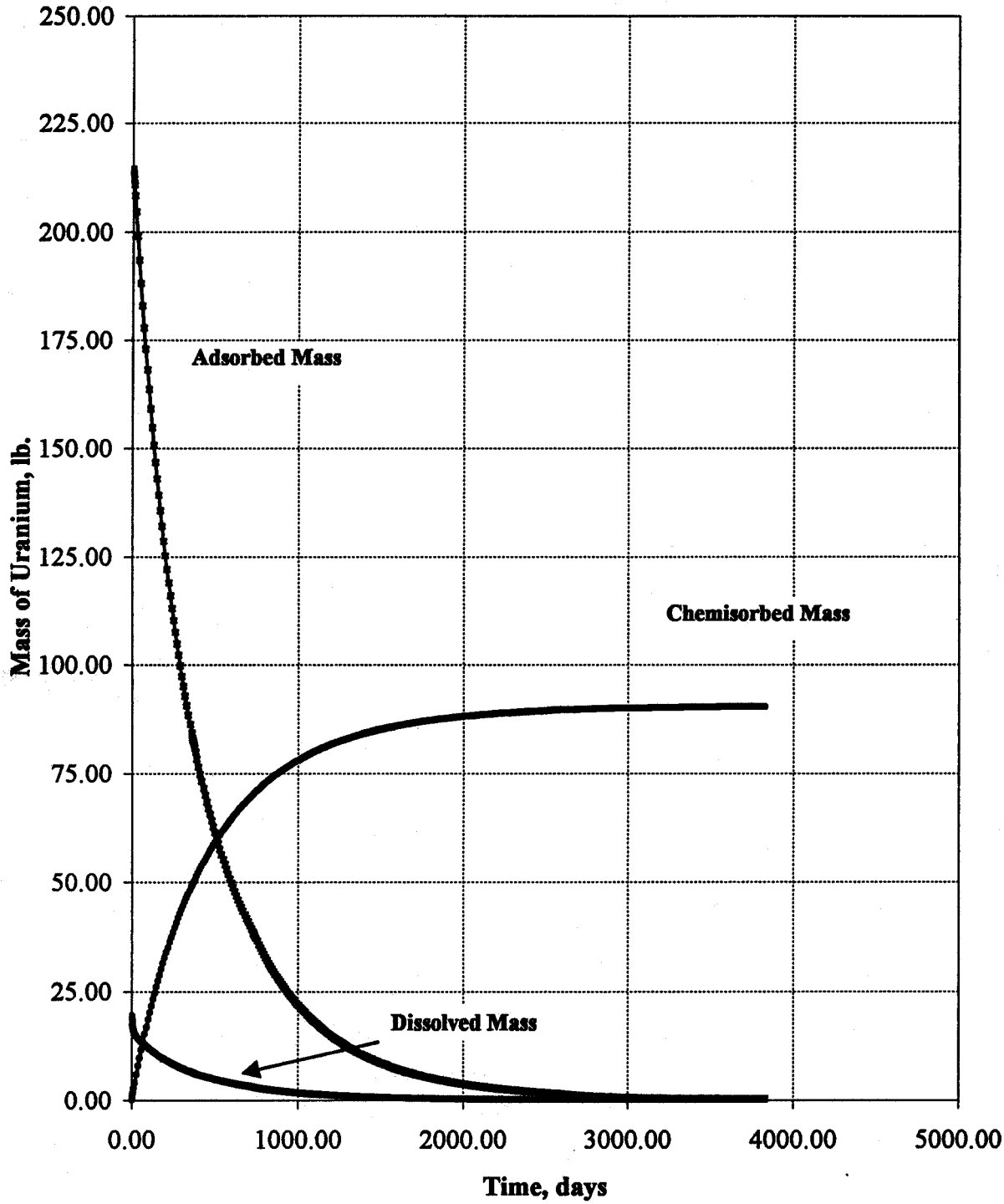

Figuer 7.45 Mass Distribution at a Location with High Initial Aqueous Phase Concentration (Run: D1).

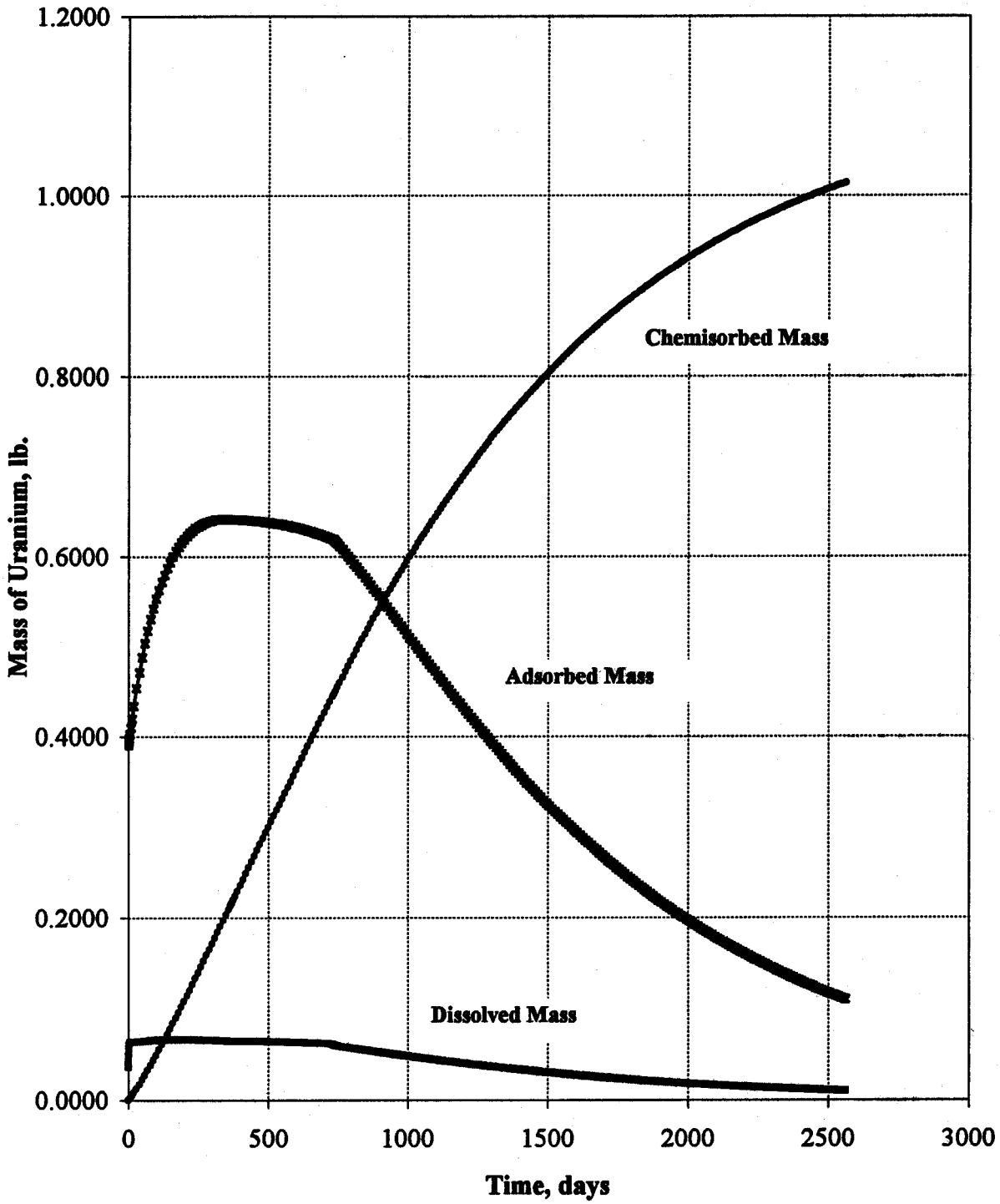

Figure 7.46 Mass Distribution at Pumping Well RW-2 (Run: D1).

000166

before, a delayed increase in the sorbed concentration can be observed as the dissolved concentration increase. Chemisorption continuously removes mass causing the dissolved and sorbed mass to decrease.

A mass balance calculation that accounts for the total mass distribution over the domain provided more insight into the partitioning of uranium between the dissolved, sorbed, and chemisorbed phases. Figure 7.47 shows the partition of the total uranium mass between the different phases over the site. The source mass loading indicated in Figure 7.47 is only attributed to additional mass loading during the simulation period (10 years) which was added to the initial mass already in the system at the start of the simulation. At any specific time, the sum of mass loading plus the initial mass (cumulative mass loading after time 0 plus initial sorbed and dissolved mass) is equal to the sum of the masses currently in the system plus mass removed by pumping (cumulative chemisorbed mass and cumulative mass loss due to pumping). The results show that most of the mass was transferred to the chemisorbed phase by the end of the simulation. However, the rate of accumulation of chemisorbed mass decreases as the sorbed and dissolved masses decrease. Figure 7.47 shows also that the initial adsorbed mass was large and might be overestimated due to the use of a linear sorption isotherm. Simulation Run D2 is similar to Run D1. However, a much lower chemisorption rate was used (α_c = 0.0001 1/day). As a result, chemisorption did not remove the dissolved plume as much as in Run D1 (see Figures 7.48 through 7.51). However, the size of the plume was much smaller than the corresponding plumes in simulations in Set C (with fully reversible sorption). An account of the total mass in the system at each time step is shown in Figure 7.52. The change in adsorbed mass and dissolved mass was much smaller than in Run D1. However, the mass removed by pumping increased considerably from Run D1 to Run D2. Figure 7.52 also shows that the mass removed by pumping is larger than the initial dissolved plume. It is also evident from the figures that the estimate of the initial adsorbed mass is considerably large and might be overestimated.

The sorption capability of the aquifer sediment is known to decrease at higher concentrations giving rise to a nonlinear isotherm. In Run D3, the linear equilibrium isotherm, which is implied in using a fixed K_d, was replaced by a nonlinear isotherm. Figure 7.53 shows the relationship between the dissolved versus adsorbed concentration at equilibrium. As shown in Figure 7.53, the relation is piecewise linear and was input in a tabular form. The relationship was chosen to ensure that the sorption capacity of the aquifer material decreases as the dissolved uranium concentration increases. This is to reflect what is known in the literature that the sorption capacity of the aquifer material is usually limited. Similar to Runs D1 and D2, the initial adsorbed concentration was calculated based on the equilibrium assumption. However, the estimated adsorbed mass was lower than Run D1 and D2 since the equilibrium isotherm shown in Figure 7.53 was used in calculating the initial adsorbed mass. Initial chemisorbed mass was assumed to be zero. The chemisorption rate used in Run D3 was lower than that in Run D1 (α_c = 0.0004 1/day). Figures 7.54 through 7.57 show that the concentration was reduced to below 20 ppb by the end of the simulation period and the uranium plume has been effectively remediated by the end of the 10 years.

In summary, results from simulation Sets C and D show that chemisorption plays an important role in the fate and transport of uranium at the site. The kinetic module was capable of capturing two main aspects of the adsorption/desorption process. The first aspect was the lag

in the response of the adsorbed concentration to changes in the dissolved concentration. However, the ranges of the adsorption rate, α_a, and desorption rate, α_d, used in the simulation were fast compared to the duration of the simulation (10 years). As a result, the model was not very sensitive to the variation in α_a and α_d. However, the use of these rates, as opposed to using equilibrium K_d, is essential to capture the physics involved in the mass transfer between the different phases, and to simulate other processes such as chemisorption. The second aspect of the adsorption/desorption process was the impact of chemisorption on the fate and transport of the uranium plume. In simulation Set D, a wide range of chemisorption rates was used. In all runs,

000168

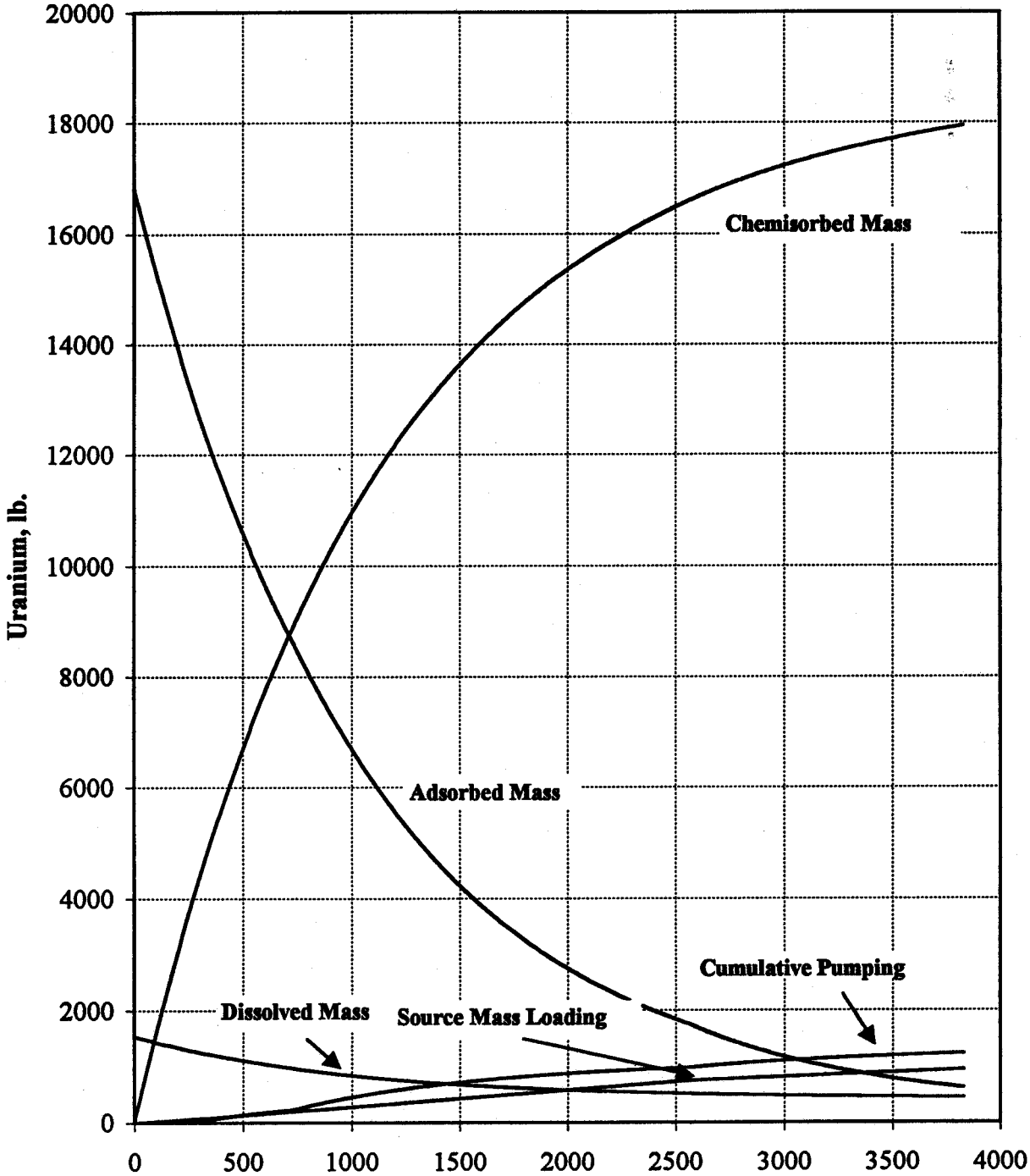

Figure 7.47 Distribution of the Total Uranium Mass over the Site (Run: D1).

000169

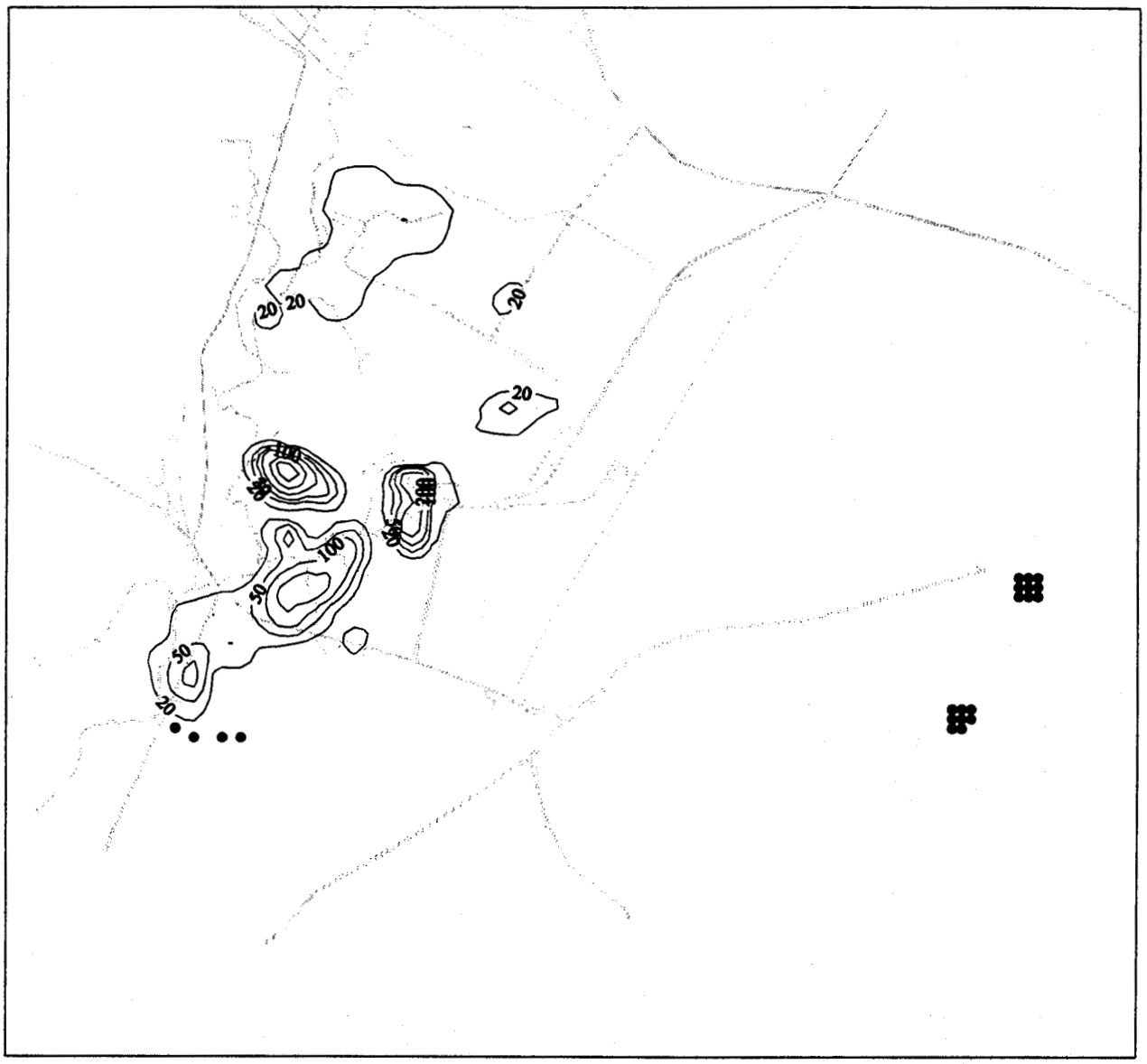

— 20 — Concentration in ppb.

● Well.

2000 0 2000 4000 ft

Figure 7.48 Projected Uranium Concentration Contours for 1997, Using the Kinetic Model (Run: D2).

000170

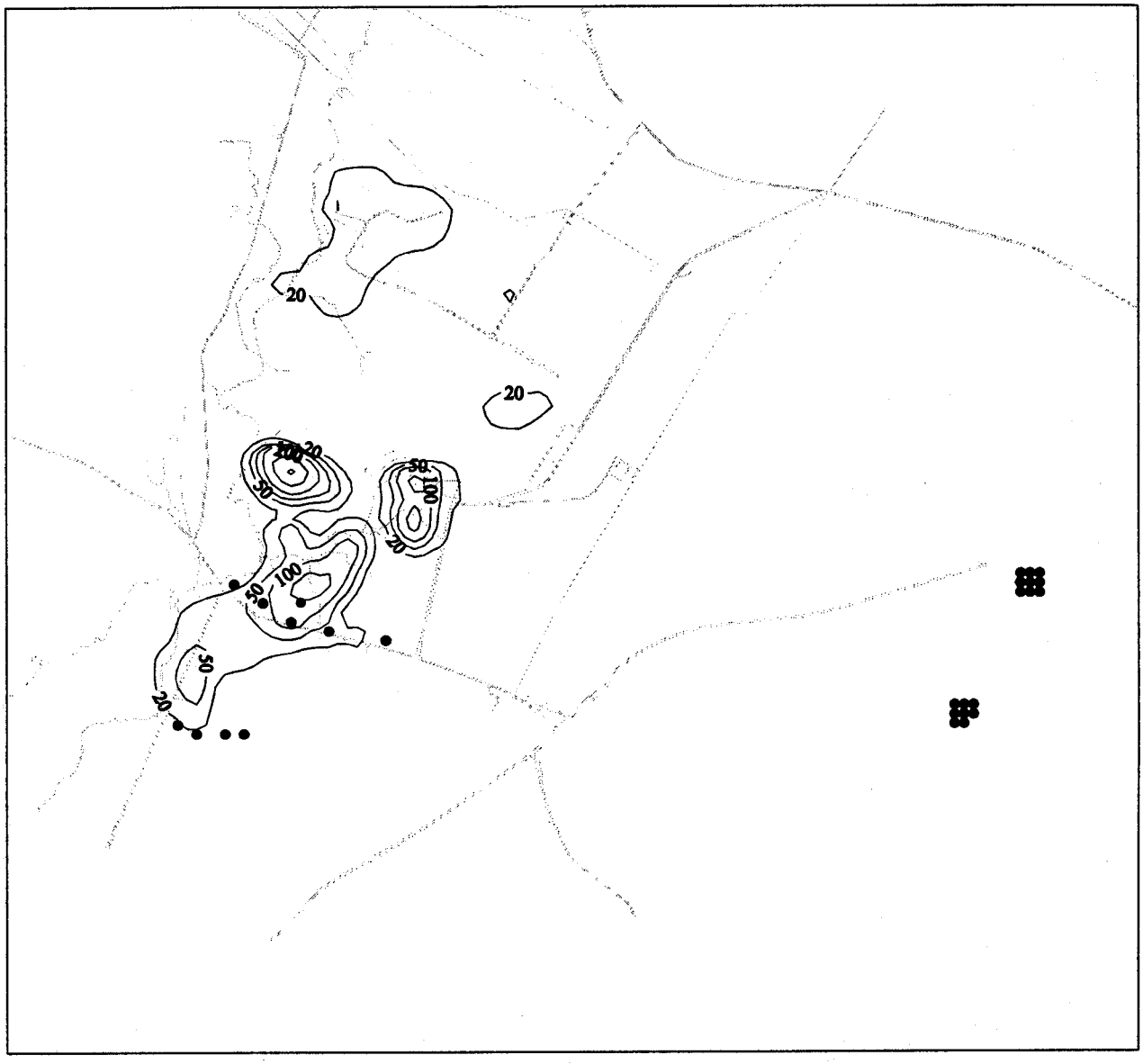

— 20 — Concentration in ppb.

• Well.

2000 0 2000 4000 ft

Figure 7.49 Projected Uranium Concentration Contours for 1998, Using the Kinetic Model (Run: D2).

000474

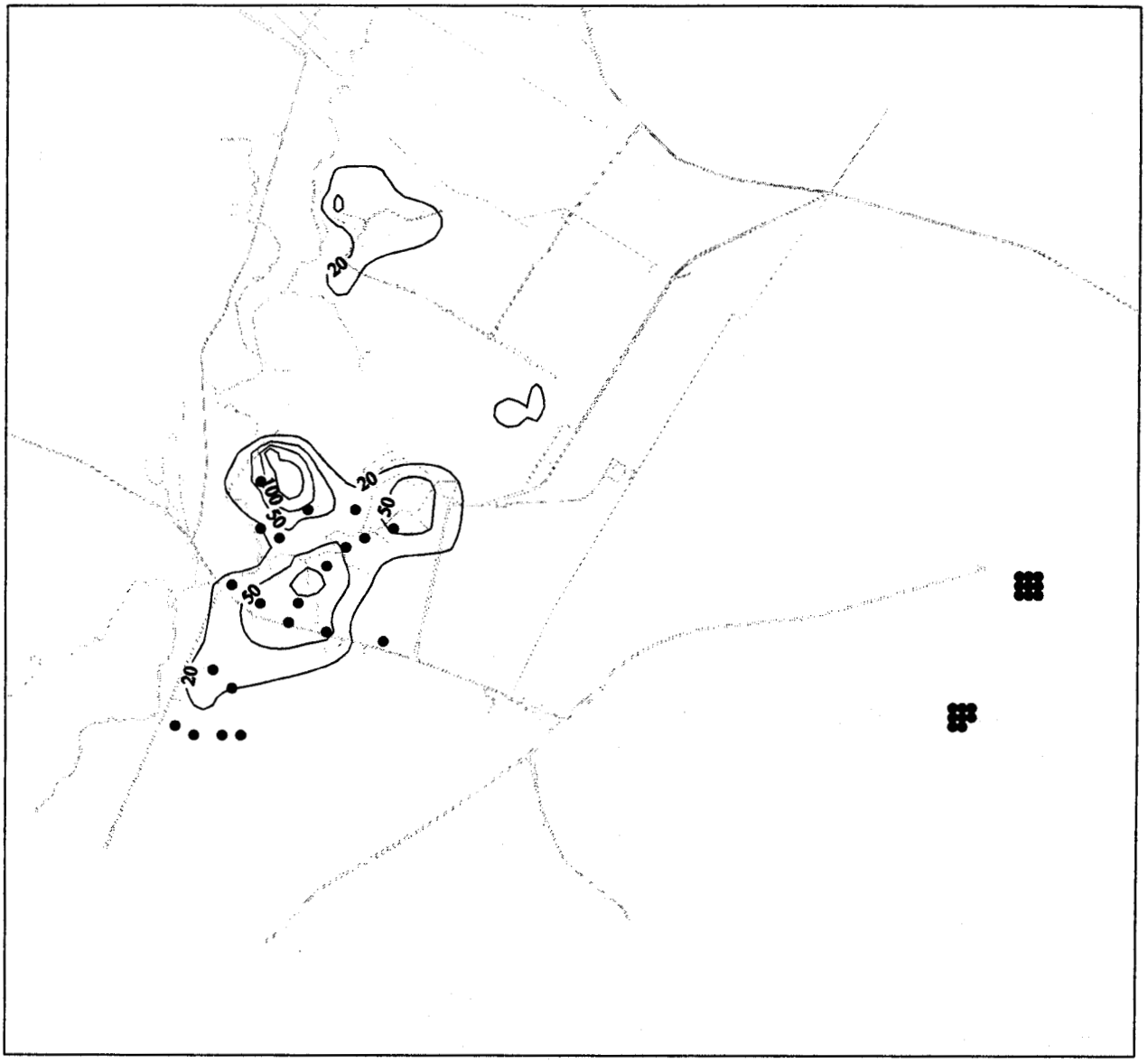

— 20 — Concentration in ppb.

● Well.

2000 0 2000 4000 ft

Figure 7.50 Projected Uranium Concentration Contours for 2003, U sing the Kinetic Model (Run: D2).

000172

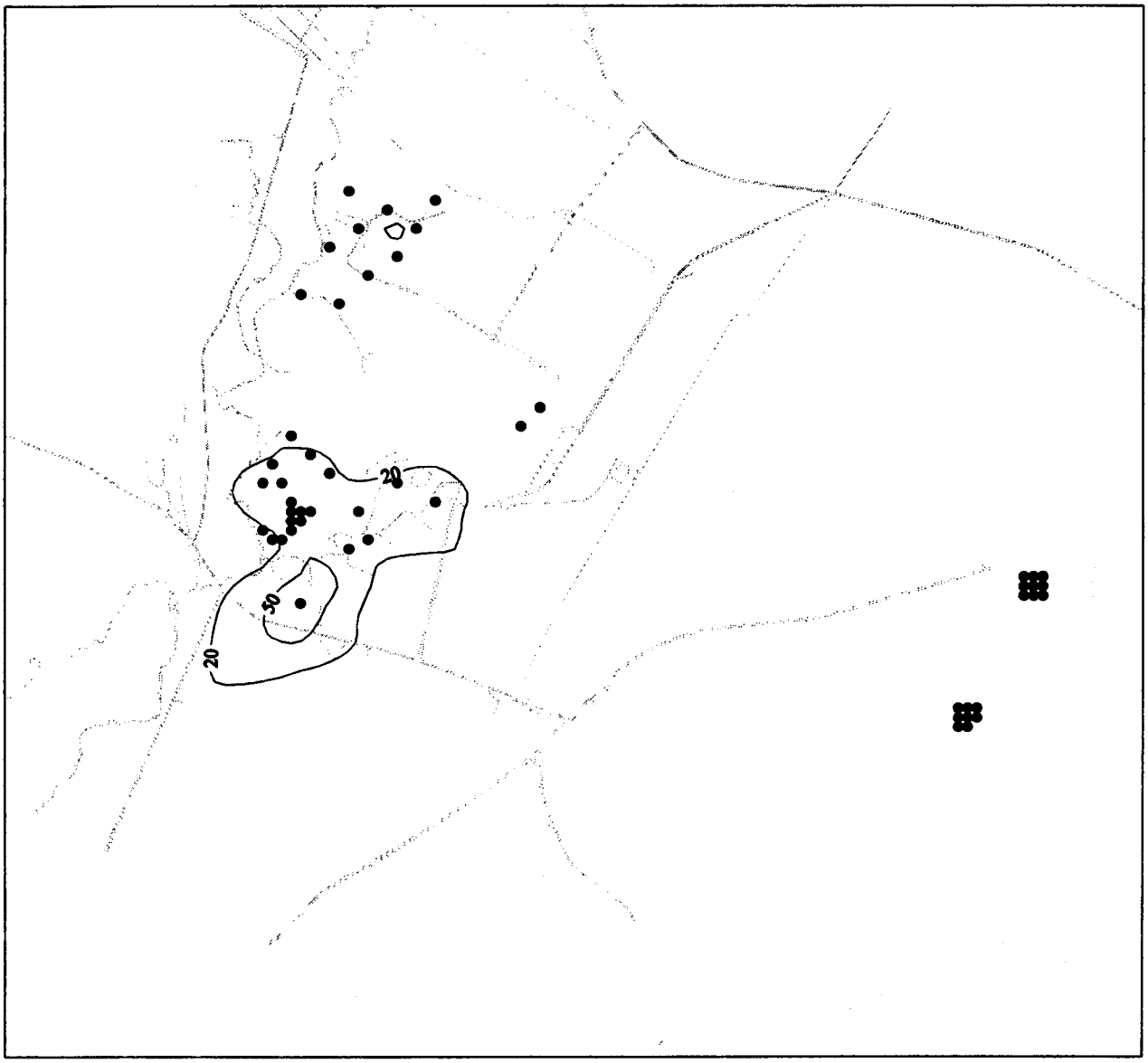

— 20 — Concentration in ppb.

• Well.

2000 0 2000 4000 ft

Figure 7.51 Projected Uranium Concentration Contours for 2006, Using the Kinetic Model (Run: D2).

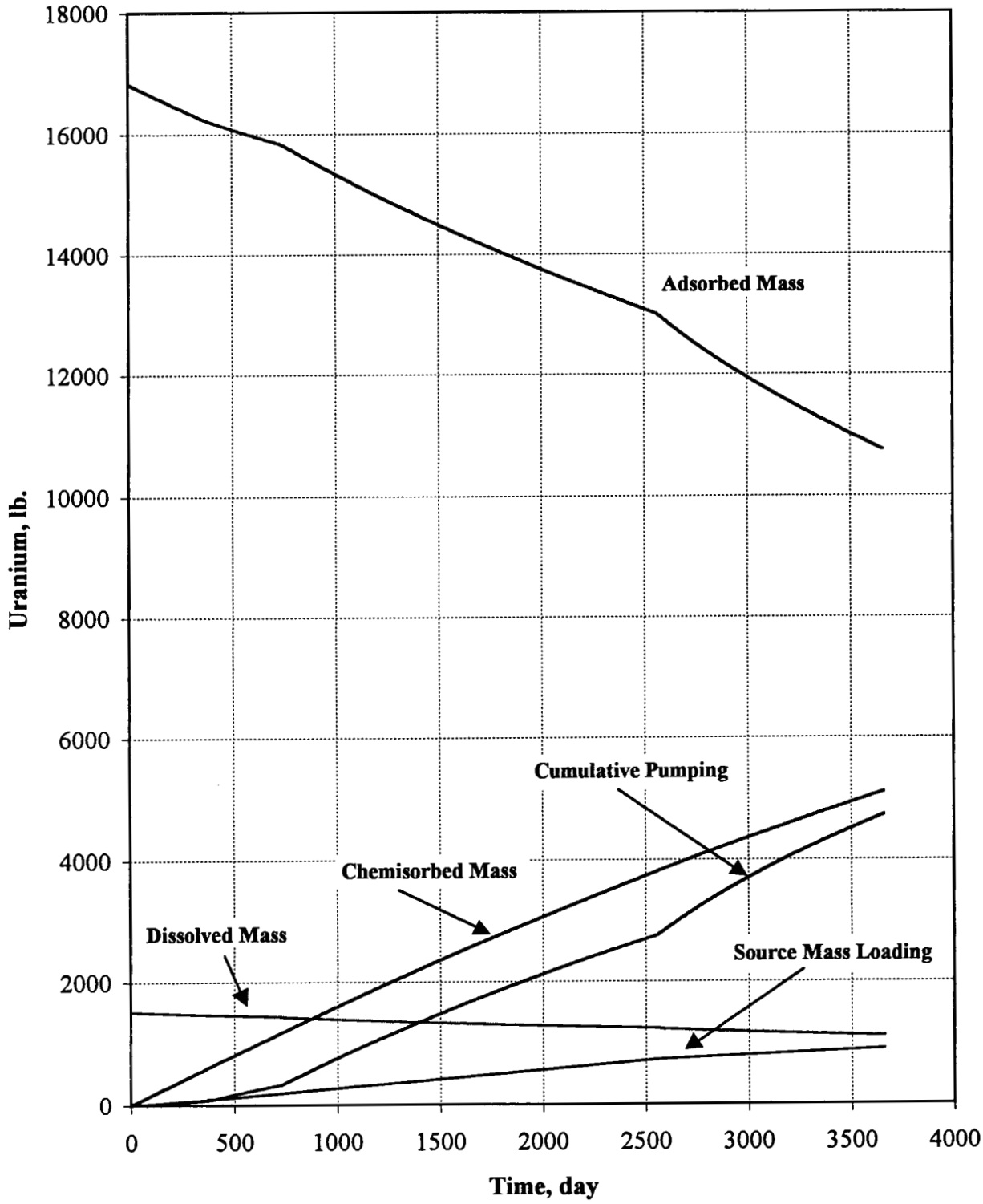

Figure 7.52 Distribution of the Total Uranium Mass over the Site (Run: D2).

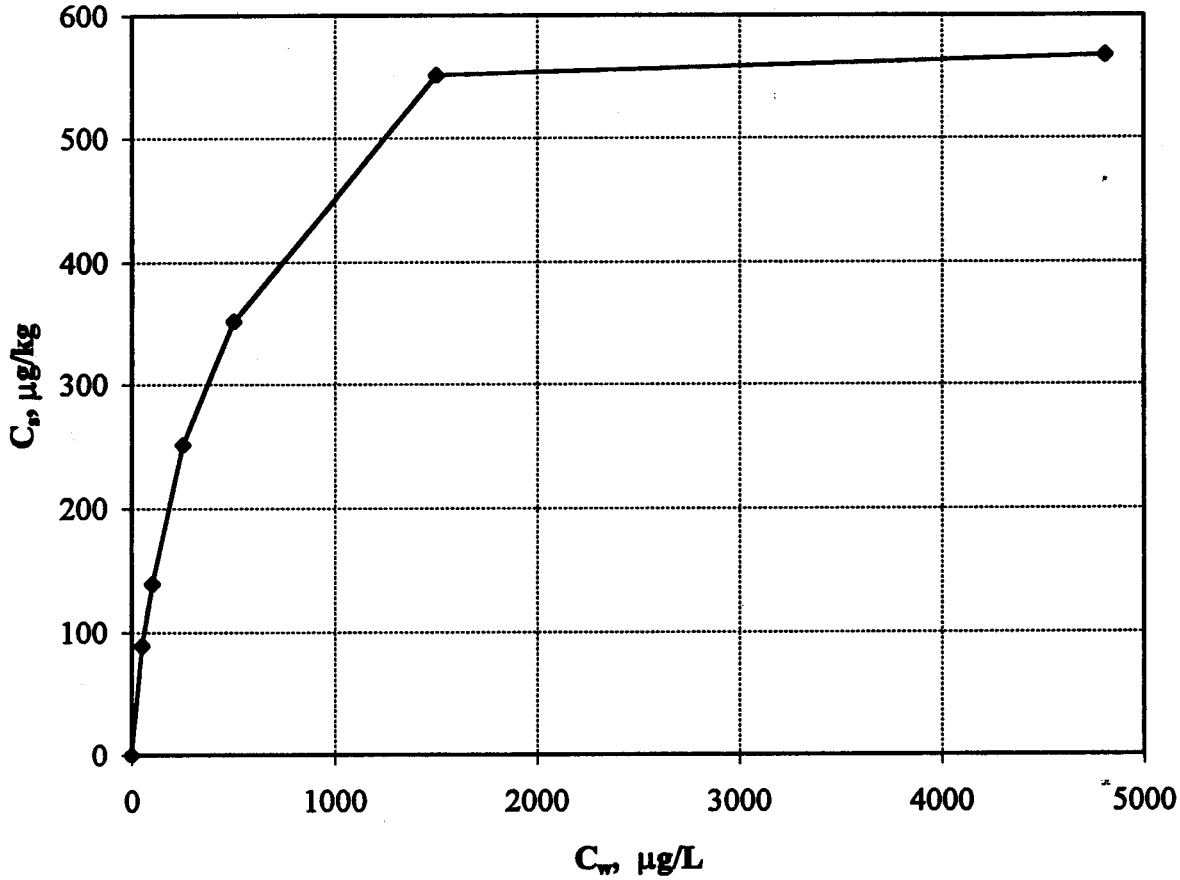

Figure 7.53 Equilibrium Isotherm Used for Run D3.

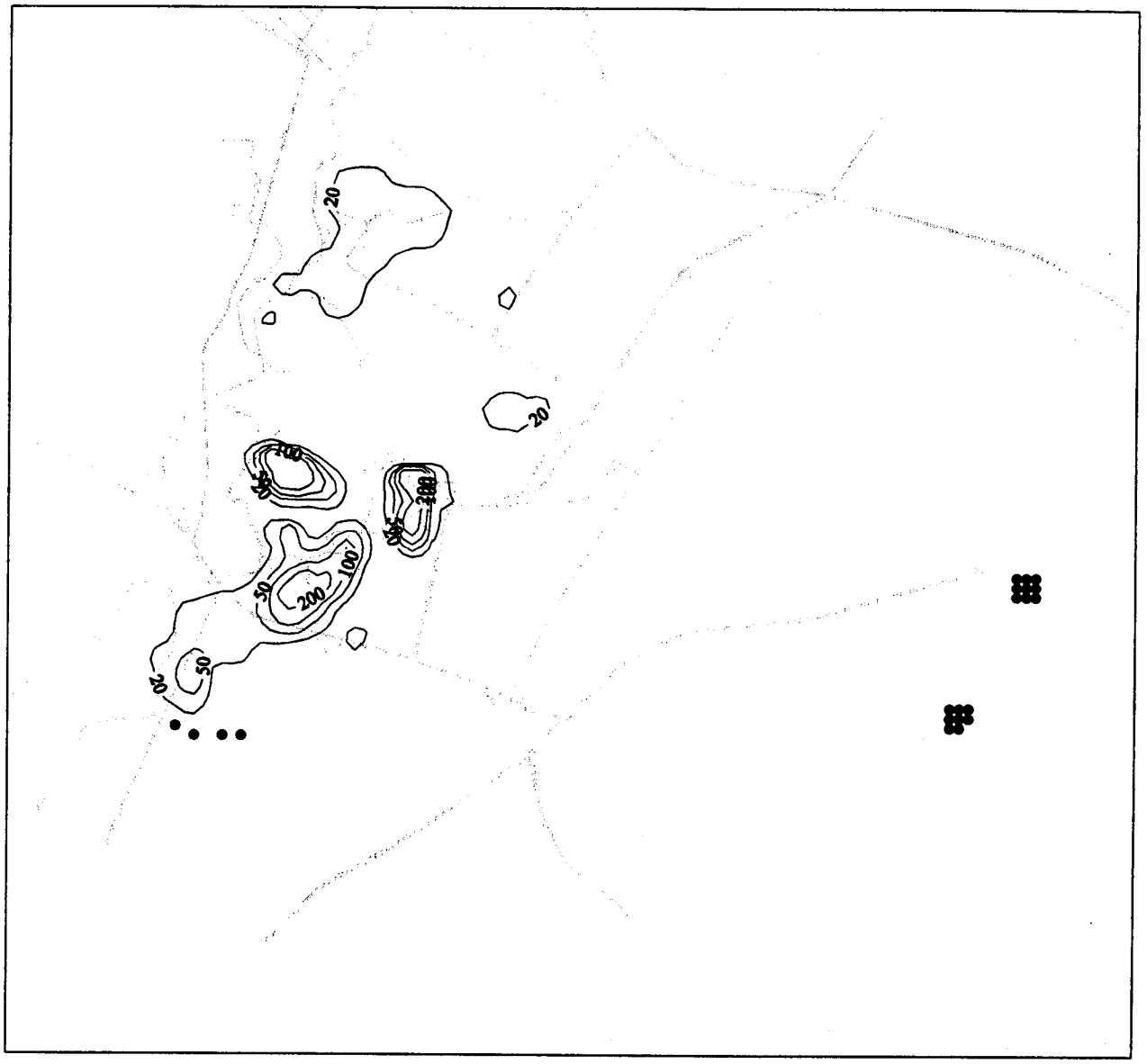

— 20 — Concentration in ppb.

• Well.

2000 0 2000 4000 ft

Figure 7.54 Projected Uranium Concentration Contours for 1997, Using the Kinetic Model (Run: D3).

000176

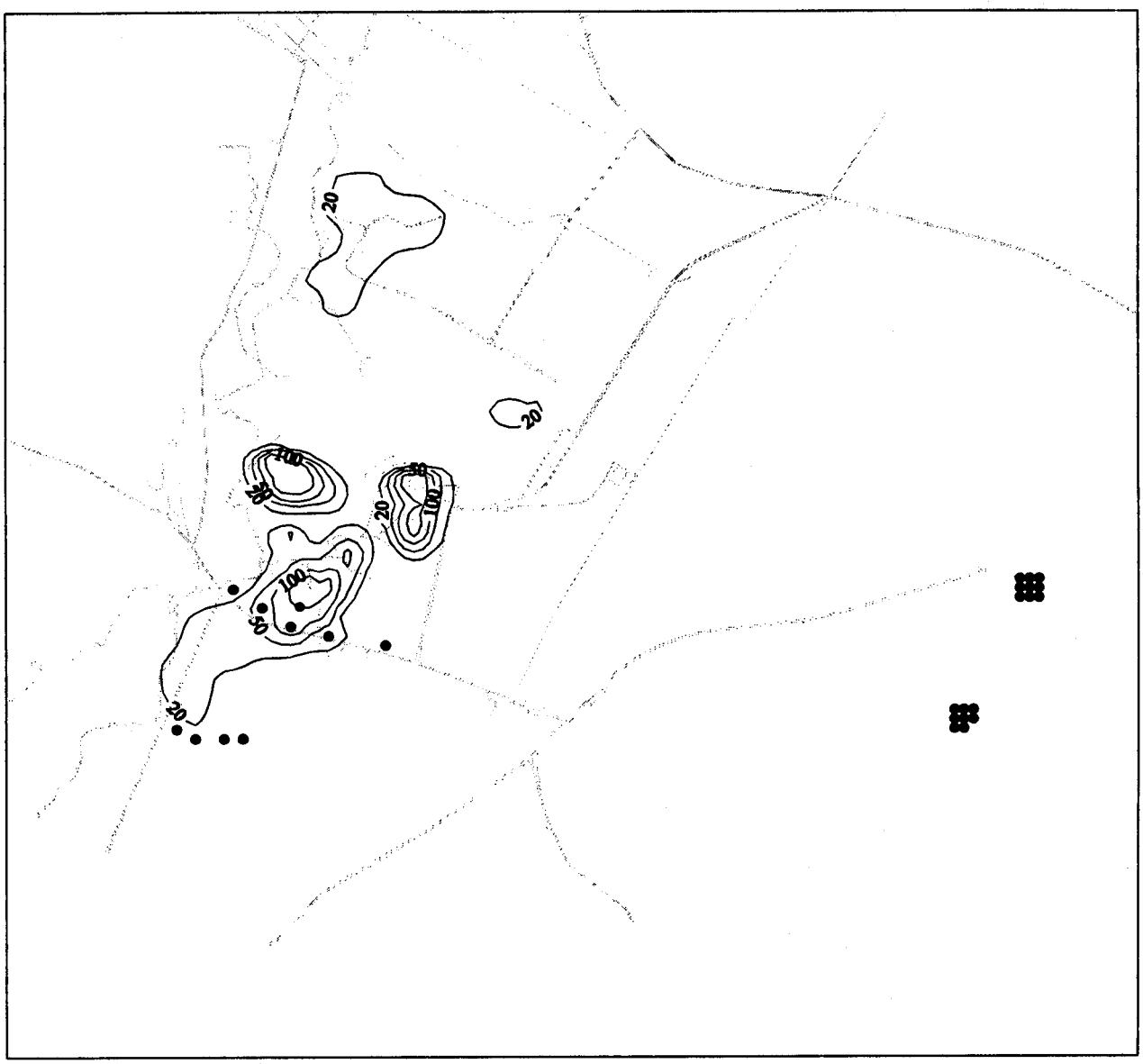

— 20 — Concentration in ppb.

• Well.

2000 0 2000 4000 ft

Figure 7.55 Projected Uranium Concentration Contours for 1998, Using the Kinetic Model (Run: D3).

000177

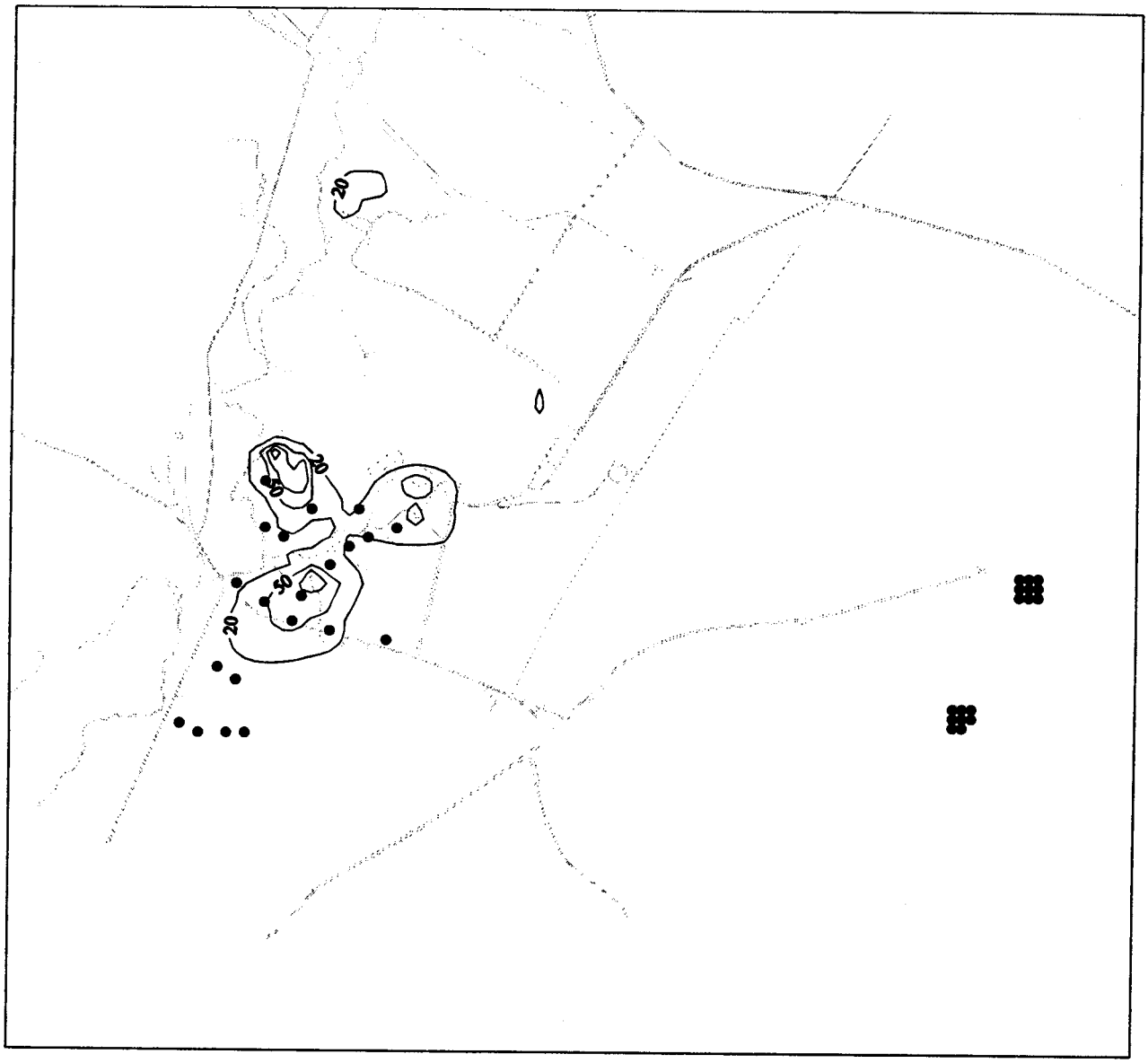

— 20 — Concentration in ppb.

• Well.

2000 0 2000 4000 ft

Figure 7.56 Projected Uranium Concentration Contours for 2003, Using the Kinetic Model (Run: D3).

000178

— 20 — Concentration in ppb.

• Well.

2000 0 2000 4000 ft

Figure 7.57 Projected Uranium Concentration Contours for 2006, Using the Kinetic Model (Run: D3).

chemisorption had a profound impact on the uranium plume. Within the range of rates used in Runs D1 and D3, the simulation results suggest that the site can be remediated within 10 years. It should be noted however, that in the case of a high chemisorption rate, the extraction wells were less effective in removing the uranium mass from the aquifer.

000180

8.0 SUMMARY, CONCLUSIONS, AND RECOMMENDATIONS

8.1 SUMMARY AND CONCLUSIONS

The major accomplishments of the current Phase I work are summarized below:

a. Development and implementation of the kinetic contaminant mass transfer module. A kinetic mass transfer module was developed and incorporated into the existing VAM3DF code. The module has the capability of simulating the following kinetic processes: adsorption, desorption, precipitation, and chemisorption. These kinetic processes, with the exception of precipitation, are anticipated to play a major role in the transport of sorptive contaminants at the site. Components within the kinetic module were verified against available analytical solutions. A systematic sensitivity analysis was conducted to assess the effects due to the variation of kinetic parameters. With the new kinetic module, it is possible to simulate a wide range of kinetic sorptive behaviors, including precipitation and irreversible chemisorption, which may occur during the aquifer restoration activities.

b. Development and implementation of the multi-dispersivity module. A new multi-dispersivity module was developed and incorporated into the existing VAM3DF code. In the new module, up to four dispersivities are available. The module can generate the hydrodynamic dispersion coefficients that are based on an assumption of isotropy (two dispersivities), or transverse anisotropy (three dispersivities without significant vertical groundwater movement, or four dispersivities with significant vertical groundwater movement). Components within the module were verified against available analytical solutions. A sensitivity analysis was conducted to compare the effects due to the various types of hydrodynamic dispersion based on two, three, and four dispersivity components. Results indicate that when the vertical groundwater velocity component is significant, the four-dispersivity option leads to a more realistic mass distribution in the vertical direction.

c. Development and implementation of the Total Variation Diminishing (TVD) solution scheme for the transport equation. A new solution scheme based on the TVD technique was implemented in the transport module within the existing VAM3DF code. The TVD scheme allows the transport simulation to be conducted without the serious discretization restrictions (grid Péclet number and grid Courant number). The TVD scheme was incorporated into both the finite-difference and finite-element solution options. The new transport module was verified against available analytical solutions. Oscillation due to high grid Péclet and Courant numbers is suppressed, while excellent mass balance is maintained.

d. Preliminary Simulation of groundwater flow and radionuclide transport in the Great Miami Aquifer (GMA). In order to ensure that the customized VAM3DF code can be used to reliably simulate the groundwater flow and chemical transport at the site, the code was utilized to simulate the groundwater flow and uranium transport, and then compared with modeling results from the existing calibrated GMA SWIFT model (DOE, 1994). The SWIFT data files, translated for VAM3DF, were used to simulate a number of

groundwater flow and uranium transport scenarios, with the assumption of geochemical equilibrium. Good agreement was achieved between the simulation results generated by the calibrated GMA SWIFT model and those generated by VAM3DF using the identical data set. The predicted aqueous uranium concentrations in 2006, based on the transport with kinetic, tend to be somewhat greater than those based on the equilibrium sorption model. A sensitivity analysis was conducted to assess the potential impact of kinetic-module parameters on the groundwater remediation period. The results suggested that the adsorption and desorption rates did not have significant impact on the distribution of the dissolved uranium plume. However, it was found that chemisorption caused the dissolved uranium concentration to decrease significantly during the 10-year simulation period.

8.2 RECOMMENDATIONS

Specific recommendations are as follows:

Work for future parameter estimation, remediation, and monitoring programs. The customized VAM3DF code may be used as the main computational kernel for automated parameter estimation through the Data Fusion Method (DFM), remedial optimization through nonlinear programming or the simulated annealing method, and monitoring optimization through an efficient method such as the Kalman filtering technique. It is recommended that the DFM phase of the work now be conducted. As part of the DFM phase, the following needs to be done in close cooperation with site groundwater management group.

- Review of the existing data to determine potential zones for kinetic parameters, and local heterogeneity for parameter estimation purposes.
- Determine types of prior information that will be required and that will be available.

000182

9.0 REFERENCES

Anderson, D.V., 1983. ILUCG3: Subprograms for the solution of a linear asymmetric matrix equation arising from a 7, 15, 19 or 27 point 3D discretization, Computer Physics Communications, 30, pp. 43-49.

Anderson, D.V., 1983. ICG3: Subprograms for the solution of a linear symmetric matrix equation arising from a 7, 15, 19 or 27 point 3D discretization, Computer Physics Communications, 30, 51-57.

Bear, J., 1979. *Hydraulics of Groundwater*, McGraw-Hill, New York, 569 pp.

Bear, J., 1972. *Dynamics of Fluids in Porous Media*. New York: American Elsevier.

Behie, G.A. and P.K.W. Vinsome, 1982. Block iterative methods for fully implicit reservoir simulation, Soc. Petrol. Engr. J., Oct., pp. 658-668.

Bierman, G.J. Factorization Methods for Discrete Sequential Estimation, Academic Press, New York, 1977.

Brooks, R.H., and A.T. Corey, 1966. Properties of porous media affecting fluid flow, ASCE J. Irrig. Drain. Div., 92(IR2):61-88.

Burnett, R.D., and E.O. Frind, 1987. Simulation of contaminant transport in three dimensions 2. Dimensionality Effects, Water Resour. Res., v. 23, no. 4, pp. 695-705.

Carsel, R.F., Mulkey, L.A., Lorber, M.N., and Baskin, L.B. 1985. The pesticide root zone model (PRZM): A procedure for evaluating pesticide leaching threats to groundwater. *Ecological Modelling*, 30:49-69.

Chiaramonte, G.R., C.W. Denslow, A.J. Knepp, R.D. Landon, S. Panday, 1997. Hanford Sitewide Groundwater Remediation Strategy - Groundwater Contaminant Predictions. Bechtel Hanford, Inc., Richland, WA.

Coleman Research Corporation, 1994. PARAGON Development Plan. CMR/94-360.

Cooley, R.L., 1983. Some new procedures for numerical solution of variably saturated flow problems, Water Resour. Res., v. 19, no. 5, pp. 1271-1285.

Cooley, R.L., 1971. A finite difference method for unsteady flow in variably saturated porous media: Application to a single pumping well, Water Resour. Res., v. 7, no. 6, pp. 1607-1625.

Davis, L.A., and S.P. Neuman, 1983. Documentation and User's Guide: UNSAT2-Variably Saturated Flow Model, U.S. Nuclear Regulatory Commission, NUREG/CR-3390, Washington, D.C.

Department of Energy, 1997. Hydrologic Data Fusion. Innovative Technology Summary Report, December.

Domenico, P.A, 1987. *An Analytical Model for Multidimensional Transport of a Decaying Contaminant Species*. J. Hydrology, V. 91, No. 1, pp. 49-58.

Duguid, J., and M. Reeves, 1976. Material transport in porous media: A finite element Galerkin model, Rep. ORNL-4928, Oak Ridge National Lab., Oak Ridge, Tennessee.

Feddes, R.A., E. Bresler, and S.P. Neuman, 1974. Field test of a modified numerical model for water uptake by root systems, Water Resour. Res., v. 10, no. 6, pp. 1199-1206.

Flach, G. P., L. L. Hamm, M. K. Harris, P. A. Thayer, J. S. Haselow and A. D. Smits, 1995, "Characterizing hydrogeologic heterogeneity using lithologic data", draft.

Frind, E.O., R.W. Gillham, and J.F. Pickens, 1977. Application of unsaturated flow properties in the design of geologic environments for radioactive waste storage facilities, Finite Elements in Water Resources, edited by W.G. Gray, G.F. Pinder, and C.A. Brebbia, Pentech Press, Plymouth, England, pp. 3.133-3.163.

Gambolati, G., F. Sartoretto, and F. Uliana, 1986. A conjugate gradient finite element model of flow for large multiaquifer systems, Water Resour. Res., vol. 22, no. 7, pp. 1003-1015.

Gambolati, G., 1980. Fast solution to finite element flow equations by Newton iteration and modified conjugate gradient method, Int. J. Numer. Meth. Engng., vol. 15, pp. 661-675.

Gillham, R.W., A. Klute, and D.F. Heermann, 1979. Measurement and numerical simulation of hysteretic flow in a heterogeneous porous medium, Soil Sci. Soc. Am. J., v. 43, pp. 1061-1067.

Guvanasen, V. 1998. A New Multiple-Parameter Dispersion Coefficient Tensor for Transversely Anisotropic Porous Media. In preparation for submission to Water Resources Research.

Hanks, R.J., A. Klute, and E. Bresler, 1969. A numeric method for estimating infiltration, redistribution, drainage, and evaporation of water from soil, Water Resour. Res., v. 5, no. 5, pp. 1064-1069.

Harten, A. 1983. High resolution schemes for hyperbolic conservation laws. *Journal of Computational Physics*, 49:357-393.

000184

Huyakorn, P.S., P.F. Andersen, J.W. Mercer, and H.O. White, Jr., 1987. Saltwater intrusion in aqufiers: development and testing of a three-dimensional finite element model, Water Resources Research, 23, 2, 293-312.

Huyakorn, P.S., J.B. Kool, and Y.S. Wu, 1991. VAM2D - Variably saturated analysis model in two dimensions, Version 5.2, Report No. NUREG/CR-5352, U.S. Nuclear Regulatory Commission, Washington, D.C.

Huyakorn, P.S., and S. Panday, 1990. VAM3D-CG: Variably Saturated Analysis Model in Three-Dimensions with Preconditioned Conjugate Gradient Matrix Solvers, Code Documentation, and User's Guide, HydroGeoLogic's technical report submitted to Westinghouse Savannah River Site, Aiken, South Carolina.

Huyakorn, P.S., J.B. Kool, and J.B. Robertson, 1989. VAM2D-Variably Saturated Analysis Model in Two Dimensions: Version 5.0 with Hysteresis and Chained Decay Transport, U.S. Nuclear Regulatory Commission, NUREG/CR-5352.

Huyakorn, P.S., E.P. Springer, V. Guvanasen, and T.D. Wadsworth, 1986. A three-dimensional finite-element model for simulation of water flow in variably-saturated porous media. Water Resources Research, Vol. 22, no.12, pp.1790-1808.

Huyakorn, P.S., J.W. Mercer, and D.S. Ward, 1985. Finite element matrix and mass balance computational schemes for transport in variably-saturated porous media. Water Resources Research, Vol. 21, no.3, pp. 346-358.

Huyakorn, P.S., S.D. Thomas, and B.M. Thompson, 1984. Techniques for making finite elements competitive in modeling flow in variably saturated porous media, Water Resour. Res., v. 20, no. 8, pp. 1099-1115.

Huyakorn, P.S., Kretschek, A.G., Broome, R.W., Mercer, J.W., and Lester, B.H., 1984. Testing and Validation of Models for Simulating Solute Transport in Groundwater. Development, Evaluation, and Comparison of Benchmark Techniques. International Ground Water Modeling Center. HRI Report No. 35, Nov. 1984.

Huyakorn, P.S., and G.F. Pinder, 1983. Computational Methods in Subsurface Flow, Academic Press, Orlando, Florida, 474 pp.

Huyakorn, P.S., and K. Nilkuha, 1979. Solution of transient transport equation using an upstream finite element scheme, Applied Mathematical Model, v. 3, pp. 7-17.

HydroGeoLogic, Inc., 1996. Development of a Fully Three-Dimensional Groundwater Flow Model for the A/M Area Using Data Fusion. Prepared for Westinghouse Savannah River Company.

HydroGeoLogic, Inc., 1995. VAM3DF: Varaibly Saturated Analysis Model in Three-Dimensions for the Data Fusion System: Documentation and User's Guide, Version 1.0, 278p. Prepared for the DOE Office of Technology Development PARAGON Project.

Jury, W.A., W.F. Spencer, and W.J. Farmer, 1983. Behavior assessment model for trace organics in soil: 1. Model description, J. Environ. Qual., v. 12, no. 4, pp. 558-564.

Kalf, F.R.P., 1988. A variably saturated finite element model for three-dimensional seepage face problems, Ph.D. Thesis, the Univ. of New South Wales, Sydney, Australia, 339 pp.

Kershaw, D.S., 1978. The incomplete Cholesky-conjugate gradient method for the iterative solution of systems of linear equations, J. Comp. Physics, 26, pp. 43-65.

Kool, J.B., and Y.S. Wu, 1991a. Groundwater Flow and Transport Modeling of the NRC-Licensed Waste Disposal Facility, West Valley, New York. U.S. Nuclear Regulatory Commission, NUREG/CR-5794.

Kool, J.B. and Y.S. Wu, 1991b. Validation and testing of the VAM2D computer code, Report No. NUREG/CR-5795, U.S. Nuclear Regulatory Commission, Washington, D.C.

Kool, J.B., P.S. Huyakorn, and P.J. Wierenga, 1990. Model calibration and simulation of flow in a heterogeneous soil. Presented at International Conference on Calibration and Reliability in Groundwater Modeling, The Hague, The Netherlands, September 3-6.

Kool, J.B., and J.C. Parker, 1987. Development and evaluation of closed-form expressions for hysteretic soil hydraulic properties, Water Resour. Res., v. 23, pp. 105-114.

Kuiper, L.K., 1987. A comparison of iterative methods as applied to the solution of the nonlinear three-dimensional groundwater flow equation, SIAM J. Sci. Stat. Comput., vol. 8, no. 4, pp. 521-528.

Kuiper, L.K., 1981. A comparison of the incomplete Cholesky-conjugate gradient method with the strongly implicit method as applied to the solution of two-dimensional groundwater flow equations, Water Resour. Res., v. 17, no. 4, pp. 1082-1086.

Law, A., S. Panday, C. Denslow, K. Fecht, and A. Knepp, 1997. Hanford Sitewide Groundwater Flow and Transport Model Calibration Report. Bechtel Hanford, Inc., Richland, WA.

McCord, J.T., D.B. Stephens, and J.L. Wilson, 1988. Field experiments and numerical simulations of unsaturated flow and transport: The roles of hysteresis and state-dependent anisotropy. Proc. Nato Advanced Study Institute on Recent Advances in Modeling Hydrologic Systems, Sintra, Portugal, July 9-23.

Meijerink, J.A. and H.A. van der Vorst, 1977. An iterative solution method for linear systems of which the coefficient matrix is a symmetric M-Matrix, Math. of Comp., v. 31, no. 137,

000186

pp. 148-162.

Meyer, P.D., A.J. Valocchi, S.F. Ashby, and P.E. Saylor, 1989. A numerical investigation of the conjugate gradient method as applied to three-dimensional groundwater flow problems in randomly heterogeneous porous media, in press, Water Resour. Res., Technical Note.

Millington, R.J., and J.M. Quirk, 1961. Permeability of porous solids. Trans. Faraday Society, 57: 1200-1207.

Montaglou, A., and L.W. Gelhar, 1987. Effective hydraulic conductivities of transient unsaturated flow in stratified soils, Water Resour. Res., v. 23, pp. 57-68.

Mualem, Y., 1976. A new model for predicting the hydraulic conductivity of unsaturated porous media, Water Resour. Res., v. 12, no. 3, pp. 513-522.

Neuman, S.P., R.A. Feddes, and E. Bresler, 1974. Finite element simulation of flow in saturated-unsaturated soils considering water uptake by plants, Hydrodynamics and Hydraulic Engineering Laboratory Report for Project No. ALO-SWC-77, Haifa, Israel.

Ogata, A., and Banks, R.B., 1961. A Solution of the Differential Equation of Longitudinal Dispersion in Porous Media, U.S. Geological Survey Professional Paper No. 411-A.

Panday, S., P.S. Huyakorn, R.Therrien, and R.L. Nichols, 1993. Improved three-dimensional finite-element techniques for field simulation of variably saturated flow and transport. J. Contaminant Hydrology, Vol. 12, no. 1, pp. 3-33.

Perlmutter, N.M., and Lieber, M., 1970. Dispersal of Plating Wastes and Sewage Contaminants in Groundwater and Surface Water, South Famingdale-Massapequa Area, Nassau County, New York, U.S. Geological Survey Water Supply Paper 1879-G.

Porter, D.W., B.P. Gibbs, W.P. Jones, P.S. Huyakorn, L.L. Hamm, G.P. Flach, 1996. Data fusion modeling for groundwater systems. Proceedings of the Advanced Simulation of Subsurface Flow and Contaminant Transport Conference, Research Triangle Park, NC, December (also submitted to Journal of Contaminant Hydrology).

Reeves, M. Ward, D.S., Johns N.D., and Cranwell, R.M., 1986, Theory and Implementation for SWIFT II: The Sandia Waste-Isolation Flow and Transport Model for Fractured Media, Release 4.84, prepared for the U.S. Nuclear Regulatory Commission, Sandia National Laboratory, Albuquerque, New Mexico.

Reeves, M., and R.M. Cranwell, 1981. User's manual for the Sandia-waste isolation flow and transport model (SWIFT) 4-81, NUREG/CR-2324, U.S. Nuclear Regulatory Commission, 145 pp.

Rubin, J., 1968. Theoretical analysis of two-dimensional transient flow of water in unsaturated and partly unsaturated soils, Soil Sci. Soc. Am. Proc., v. 32, no. 5, pp. 607-615.

Scheidegger, A.E., 1961. General theory of dispersion in porous media, J. Geophys. Res., v. 66, pp. 3273-3278.

Treybal, R.E., 1986. *Mass-Transfer Operations*, third edition, 9th printing, McGraw Hill, Singapore.

U.S. Department of Energy, 1997. Hydrologic Data Fusion. Innovative Technology Summary Report, December.

U.S. Department of Energy, 1997, Baseline remedial strategy report: Remedial design for aquifer restoration (Task 1), Fernald Environmental Management Project, DOE, Fernald Area Office, Cincinnati, OH.

U.S. Department of Energy, 1995, Remedial Investigation Report for Operable Unit 5, Final, Fernald Environmental Management Project, DOE, Fernald Area Office, Cincinnati, OH.

U.S. Department of Energy, 1994, SWIFT Great Miami Aquifer model - summary of improvements, report, Fernald Environmental Management Project, DOE, Fernald Area Office, Cincinnati, OH.

U.S. Department of Energy, 1993, Ground water modeling project - summary of model development, Fernald Environmental Management Project, DOE, Fernald Area Office, Cincinnati, OH.

van Genuchten, M.Th., and W.J. Alves, 1982. Analytical Solutions of the one-dimensional convective-dispersive solute transport equation. U.S. Department of Agriculture, Tech. Bull. No. 1661, 151 p.

van Genuchten, M.Th., 1980. A closed-form equation for predicting the hydraulic conductivity of unsaturated soils. Soil Science Soc. of Am. Journal 44:892-898.

van Genuchten, M.Th., G.F. Pinder, and W.P. Saukin, 1977. Modeling of leachate and soil interactions in an aquifer, Management of Gas and Leachate in Landfills, U.S. Environmental Protection Agency, Rep. EPA-600/9-77-026, pp. 95-103.

van Leer, B. 1977. Towards the ultimate conservative difference scheme. IV. A new approach to numerical convection. Journal of Computational Physics, 23: 276-299.

Voss, C.I., SUTRA, A finite-element simulation model for saturated-unsaturated fluid-density-dependent groundwater flow with energy transport or chemically-reactive single species solute transport, *US Geological Survey Water-Resources Investigations Report 84-4369*, 1984.

Wilson, J.L., and Miller, P.J., 1979. Two-dimensional plume in uniform ground-water flow, *Journal of the Hydraulics Division, ASCE*, 104(HY4):503-514.

000188

Yeh, T.-C. J., L.W. Gelhar, and A.L. Gutjahr, 1985. Stochastic analysis of unsaturated flow in heterogeneous soils 2. Statistically anisotropic media with variable α, Water Resour. Res., v. 21, pp. 457-464.2

Yeh, G.T., and D.S. Ward, 1981, FEMWASTE: A finite-element model of waste transport through saturated-unsaturated porous media, Rep. ORNL-5601, Oak Ridge National Lab., Oak Ridge, Tennessee, 137 pp.

Yeh, G.T., 1981. AT123D: Analytical transient one-, two- and three-dimensional simulation of transport in the aquifer system, Oak Ridge National Lab., Tennessee, Report no. ORNL-5602.

APPENDIX A

USER'S GUIDE

A.1 DATA FILE DESCRIPTIONS

There are six data files associated with VAM3DF. These are described as follows.

1. File 1 (unit number 5). This is the major input file containing the essential input data for each run of the code. The contents of this file as well as the description of input variables and their formats are provided in Section A.2, which deals with input data.

2. File 2 (Unit number 6). This is the output file containing the line printer output from the code. The details of this file as well as the description of output variables are provided in (HydroGeoLogic, 1995).

3. File 3 (Unit number 8). This is the output file containing nodal values of the dependent variables which correspond to the final time step of the current run. Information in this file can be used as the initial condition for the next restart run. File number 8 is written in ASCII when the control input variable NOWRIT is set equal to 1 and in binary when NOWRIT is set equal to -1. This file (TAPE 8) contains the following information:

- Title Heading giving final time value; written in the FORMAT (20A4).
- List of Nodal Values of the unknown function (head and/or concentration, depending on whether one is dealing with flow or transport) at the final time level. For a hysteretic flow simulation, the element values of water saturation and wetting-drying index are also written to the file on unit 8. These values are written in FORMAT (8E10.3).

The nodal values in TAPE 8 can be used as an initial condition for the next flow or transport restart run (not flow to transport). To do this, the user should make the TAPE 8 file accessible to the simulation by setting the parameter NONU=2 or -2 (record group 3, col. 56-60). Note that if NOWRIT=1 or -1, the file on TAPE 8 will be overwritten by information from this simulation.

4. File 4 (Unit number 9). This file is written when the flow simulation is performed and the value of the output control parameter NVWRIT is greater than 0. For each user-selected time step of the flow simulation, this output file (TAPE 9) contains the following information, written in binary format:

- Title heading, giving the time value.
- List of element values of the x, y, and z components of Darcy velocity.
- List of element water saturation values.
- List of storage capacity values at the nodes. This information is written only when the mass balance calculation option, IMBAL, is set equal to 1.

- List of boundary node fluxes. This information is written only when the output flux calculation option IOUTLT is set equal to 1.

The output file TAPE 9 from the flow simulation can be used as a direct input into the subsequent transport simulation. To do this, the user should proceed by editing the input file on unit 5 as follows:

- Set the control parameter NVREAD (group 5, cols. 1-5) equal to 2. This directs the code to read velocity and saturation data from TAPE 9.

- Make sure that IMBAL (record group 5, col. 46-50) on TAPE 5 is set to the value used in the flow simulation, and that IOUTLT and NBOUT (number of boundary nodes for flux calculations) are also set to the same value used in the flow simulation. Further, the sequence of boundary nodes NDOUT(I), I=1, NBOUT should also be the same as in the flow simulation. This is necessary to insure compatibility of FORMAT and avoid I/O format error.

5. File 5 (Unit number 10). This file is written when the value of the plotting control parameter NPLOT (record group 5, col. 31-35) is not equal to zero.

For NPLOT=n, the output file on unit 10 contains the following data in ASCII format:

a. Simulation day, time, title, IMODL, NP, NE.
b. Nodal x, y, and z coordinates and nodal values of initial heads and/or concentrations.
c. Heading, giving the time step value and time value.
d. Nodal x, y, and z coordinates and the nodal values of the dependent variables pressure head and/or concentration, written in FORMAT 4E15.8.

Note: Records c and d are written every NPLOT = n-th time step.

For NPLOT = -n, the output file on unit 10 contains the following data in binary format:

a. Simulation day, time, title, IMODL, NP, NE.
b. Heading and nodal coordinates.
c. Initial head and/or concentrations along with the respective headings.
d. Heading and nodal corner connectivities.
e. Time step number and time value.
f. Nodal heads and/or concentrations for the time value in record e.

Note: Records e and f are written every NPLOT = n-th time step.

6. File 6 (Unit number 11). This file is written when a flow simulation is performed, IMODL = 1 or 2 (group 3, col. 1-5) and NPLOT is not equal to zero.

For NPLOT = n the file on unit 11 contains the following data for each n-th time step in ASCII format:

a. Simulation day, time, title, IMODL, NE.
b. Material type index heading and IPROP(I), I=1, NE.
c. Heading, giving the time step value, time step size, and IVSTED.
d. Coordinates of the element centroids and element water saturation and components of the Darcy velocity, written in FORMAT 7E14.7.

Note: Records c and d are written every NPLOT = n-th time step.

For NPLOT = -n the file on unit 11 contains the following data for each n-th time step in binary format.

a. Simulation day, time, title, IMODL, NE.
b. Heading and element centroidal coordinates.
c. Heading and nodal corner connectivities.
d. Heading and material property indices IPROP(I), I<1, NE.
e. Heading giving the time step value, the time value.
f. Elemental saturation, and velocity components for the time value in record e for all elements.

Note: Records e and f are written every NPLOT = n-th time step.

A.2 INPUT RECORDS

The main stream of input data is to be supplied from input file unit 5. The VAM3DF code simulates three-dimensional water flow and solute transport in a partially or wholly saturated medium. The program can solve the following problems: (1) variably-saturated water flow; (2) transport of single component or multi-component chain in a variably saturated porous medium; and (3) combined flow and transport. The main stream of input data is to be supplied from input file unit 5. To facilitate data entry, the input data is divided into 28 groups, arranged as follows:

1. Number of problems to be solved

2. Problem title

3. Simulation control parameters

4. Time stepping and iteration control parameters

5. Input and output control parameters

6. Temporal discretization data

7. Default initial values

8. Node property numbers

9. Hydraulic parameters of soil

10. Soil moisture retention parameters

11. Soil-solute transport parameters

12. Rectangular mesh parameter specification

13. Rectangular mesh data

14. Curvilinear mesh parameter specification and data

15. Boundary condition data

16. Transient dirichlet boundary conditions

17. Transient flux boundary conditions

18. Concentration-dependent boundary condition data

19. Initial nodal value data

20. Defauult parameters for transport simulation

21. Element Darcy velocity data for transport simulation

22. Element water saturation data for transport simulation

23. Boundary nodal data

24. Evaporation and infiltration control data

25. Plant species data

26. Root zone element node data

27. Observation node data

28. Velocity file output time specification data

29. Output time specification data

30. Solver setup parameters

31. Recharge/drain boundary condition data

000194

32. Head-dependent source bed data

The above sequence must be strictly followed when entering data into the program. Following are descriptions of the input variables and data formats.

GROUP 1. Number of problems (3I6)

One record.

Col.	1-6	NPROB:	Number of problems to be solved in this run.
	7-12	ISCDP:	Parameter requesting screen communication indicating that the code is running. = 0 if no screen indication is required. = 1 if screen indication is required.
	13-18	IPFSPAR:	Parameter indicating if solver options are to be input = 1 if yes, use Group 30, = 0 if no, use set defaults.

*** The following record groups are to be repeated for each problem.

GROUP 2. Problem title (A80)

One record.

Col.	1-80	TITLE:	Title of problem

GROUP 3. Simulation control parameters (16I6)

One record.

Col.	1-6	IMODL:	Parameter indicating the type of modeling required; = 0 for solute transport modeling, = 1 for water flow modeling, = 2 for simultaneous flow and transport modeling. Flow specific parameters are input via groups 9 and 10. Transport specific parameters are input via groups 11, 17d, 18, 20, 21, and 23c.
	7-12	MARK:	Parameter indicating if gravity terms are to be included in the flow equation;

000195

= -1 if yes and y corresponds to the upward vertical coordinate,
= 0 if no,
= 1 if yes and z corresponds to the upward vertical coordinate.

Note: the gravity terms need to be considered if the formulation of the water flow equation is in terms of pressure head (ITOTHD, col. 85-90 of this record = 0).

13-18 INTSPC: Parameter specifying if initial head values supplied to the code by the user are to be converted to initial pressure head values or vice versa;

= 1 if convert the given total hydraulic head to pressure head;
= -1 if convert the given pressure head to total hydraulic head.
= 0 if do not convert.

Set INTSPC = 0 if dealing with the transport equation (IMODL = 0).

19-24 ISSTA: Parameter indicating if a steady-state analysis of the problem is required;
= 1 if yes,
= 0 if no.

25-30 ITSGN: Parameter indicating if simulation time values are to be generated by the code;
= 0 if no (time values are to be input from record group 6b),
= 1 if yes and time values are to be computed using time steps generated from parameters in group 6a,
= 2 if yes and time values are to be computed using specific time step values as indicated in record group 6c.
= 3 if automatic time-step control is desired.

31-36 NTS: Number of simulation time steps. Set = 1 if a steady-state analysis of the problem is required.

37-42 NP: Total number of nodal points in the finite element grid.

000196

GROUP 3 continued.

43-48	NE:	Total number of elements in the finite element grid.
49-54	ISWAP:	Parameter indicating the number of nodes in each gridding plane (x-y) of the rectangular mesh; = 1 if the nodes are sequentially numbered in the x-direction, = 0 if the nodes are sequentially numbered in the y-direction.
55-60	IAXSYM:	Parameter indicating if the problem is axisymmetric with x and y corresponding to radial and vertical coordinates respectively; = 1 if yes, = 0 if no.
61-66	NMAT:	Number of different active soil materials. Material indentification numbers are input via group 8.
67-72	NONU:	Parameter indicating if initial condition values are nonuniform; = 0 if no, default values of group 7 occur throughout the domain, = 1 if yes and initial condition data are to be input as part of this input file (see group 19), = 2 if yes and initial condition data are to be supplied by reading from an ASCII file on unit 8. =-2 if yes and initial condition data are to be supplied by reading from a binary file on unit 8.
73-78	NEIEVP:	Number of elements of the grid that are subject to infiltration or evaporation (see group 24).
79-84	NPLANT:	Number of different plant species (see groups 25 and 26).
85-90	ITOTHD:	Parameter indicating how the water flow equation is formulated; = 0 if pressure head is used as the dependent variable,

000197

= 1 if hydraulic head is used.

91-96 ICURVL: Parameter indicating if orthogonal curvilinear coordinates are used in setting up the finite element grid;
= 1 if yes, use groups 14 for input of grid data,
= 0 if no, use groups 12 and 13 for input of grid data.

Note: In a case where the curvilinear grid is used (ICURVL=1) the value of ITOTHD must be set equal to 1, and the problem setup including boundary condition must be in terms of hydraulic head.

GROUP 4. Time stepping and iteration control parameters (5I6,2E10.3,3I6,E10.3,2I6)
One record.

Col. 1-6 IKALL: Parameter indicating the time stepping scheme required for the transport simulation;
= 1 for backward difference scheme,
= 0 for central difference scheme.
Note IKALL is automatically set to 1 if steady-state analysis is required.

7-12 INEWT: Parameter indicating the type of iterative procedure to be used in solving the variably-saturated flow equation.
= 0 for Picard procedure
= 1 for Newton-Raphson procedure
Note: Set INEWT = 0 if dealing with the transport model (i.e., if IMODL = 0).

13-18 NITMAX: Maximum number of non-linear iterations allowed. If only solute transport is required (IMODL = 0), NITMAX is set equal to 1.
Otherwise set NITMAX equal to the desired maximum number of iterations. A recommended value of NITMAX is between 10 and 20 depending on the degree of nonlinearity of the flow problem.

19-24 IRESOL: Maximum number of refinements of time steps allowed if the nonlinear iterative solution of the variably-saturated flow equation does not converge (recommended value is 3 or 4). Leave blank if transport simulation only is required (IMODL = 0). Use a negative number if solution is to proceed

000198

GROUP 4 continued.

without time refinements, even if convergence is not attained for that time step.

25-30	ILUMP:	Parameter indicating if mass lumping procedure is to be applied in formulating the element matrix of the flow equation; = 2 if full lumping is to be applied, = 1 if partial lumping is done, = 0 if no lumping.
31-40	HTOL:	Head tolerance for the nonlinear solution of the variably-saturated flow problem. For a transport simulation, HTOL is automatically set = 0.0.
41-50	HWWT:	Parameter indicating cord-slope evaluation of saturation derivative with respect to pressure head. = 1.0 for cord-slope evaluation. = 0.0 for tangent-slope evaluation.

Note: Cord-slope is incorporated for non-upstream relative permeability solution.

51-56	IUPSTR:	Upstream weighting control parameter for relative permeability; = 1 if upstream weighting is required; = 0 otherwise.
57-62	INSTOC:	Parameter indicating the procedure to be used in computing the storage term of the Newton-Raphson formulation of the flow problem (leave blank if not used); = 0 if water storage computed in terms of the product of moisture capacity and the rate of change in pressure head, $(dS_w/d\psi)\ \partial\psi/\partial t$, = 1 if computed directly from the rate of change of water saturation, $\partial S_w/\partial t$.
63-68	ISELSC:	Parameter indicating if a combined use of Newton-Raphson and Picard nonlinear schemes is to be made in the transient simulation of the flow problem; = 1 if yes, 6d(i) and 6d(ii) are used to input the switching parameters for the schemes, = 0 if no.

000199

67-78	CTOL:	Concentration tolerance to be used in the matrix solution of 3-D transport problem using PCG or ORTHOMIN scheme.
79-84	IFDM:	Parameter indicating matrix connectivity = 0 for finite element connectivity, = 1 for finite element connectivity for transport and finite difference connectivity for flow, =2 for finite difference connectivity.
85-90	IHYST:	Parameter indicating if hysteresis is to be included in flow simulation; = 1 if yes. Group 7b will be read for uniform initial saturation conditions, group 19c for non-uniform initial saturation input, and group 10b for hysteretic wetting curve parameters, = 0 if no. (Set IHYST = 0 if IMODL = 0).

GROUP 5. Input and output control parameters (16I6)

One record.

Col.	1-6	NVREAD:	Parameter specifying if element velocity and water saturation data are to be input; = 0 if only uniform velocity and saturation input are needed via group 20 (this option is used for a flow simulation or for transport simulation involving uniform flow), = 1 if nonuniform velocity and saturation data are to be included via overriding the group 20 data with groups 21 and 22 (this option is used for a transport run), = 2 if velocity and satruation data are to be input using a separate data file unit number 9. Note: NVREAD is set to 0 if IMODL = 1 or 2.
	7-12	IOUTLT:	Parameter indicating if boundary node data (see group 23) are to be read in; = 1 if yes, = 0 if no.

000200

GROUP 5 continued.

13-18	NPIN:	Number of nodes for which initial nodal values to be input as part of this input file via group 19. NPIN is automatically set = 0 unless NONU = 1. IF NPIN < NP, the default values of primary variables group 7 are overridden by the values supplied in group 19a. If NPIN = NP, initial values of primary variables for all nodes are input via group 19b.
19-24	IPRD:	Parameter indicating output requirement; = 0 if complete mesh data printout is required, = 1 if element connection data printout is not needed, = 2 if the whole mesh data printout is not needed, = 3 if mesh and initial condition data printouts are not needed. = 4 if material properties and boundary conditions printouts are not needed.
25-30	NVWRIT:	Parameter specifying if computed values of element velocities and water saturation are to be written on file unit 9; = 0 if no, = 1 if yes and output is to be written for each time step; = 2 if yes and output is to be written for selected time steps as specified in record group 28. Note: NVWRIT is set to 0 if IMODL = 2.
31-36	NVPR:	Parameter controlling printout of computed element velocities and water saturation; = 0 if no output is to be written, = n if the output is to be written for each nth time step.
37-42	NPLOT:	Parameter indicating if time and computed nodal values of the variables concerned (head or concentration) are to be written on file unit 10 for use in subsequent plotting; = 0 if no output is to be written,

000201

= n if the output is to be written for each nth time step in ASCII format as discussed in Section A.1.

=-n if output is to be written each nth time step in binary format as discussed in Chapter 7.

For flow simulation (IMODL = 1 or 2) values of saturation and velocity components at element centroids are also written on file unit 11.

43-48 NSTEP: Parameter controlling printout of computed nodal values;

= 0 if no output is to be written,

= n if the output is to be written for each nth time step.

49-54 IOBSND: Parameter indicating if values at some specified nodes are to be recorded for all time steps (see group 27);

= 1 if yes,

= 0 if no.

55-60 IMBAL: Parameter specifying if mass balance calculation is required,

= 1 if yes,

= 0 if no.

Note: If IMBAL = 1 then IOUTLT (group 5, col. 7-12) should be set equal to one to identify boundary nodes in group 23.

61-66 NOWRIT: Parameter indicating if computed values of head or concentration at the final time level are to be written on file unit 8;

= 1 if yes, write and ASCII file,

= 0 if no,

=-1 if yes, write a binary file.

67-72 IPRCHK: Print check debugging option parameter;

= 1 if element matrix and boundary condition print check is required,

= 0 if no print check is required.

000202

73-78 NHIS_FLG: Parameter indicating if separate time history file for water contents is needed as discussed in

GROUP 5 continued.

		Section 8.4; = 0 if no, = 1 if yes.
79-84	NHIS_FLG2:	Parameter indicating if separate time history file for concentrations is needed as discussed in Section 8.4; = 0 if no, = 1 if yes.
85-90	IWATP:	Code for indicating if pseudo-soil functions are to be used for water-table conditions; = 0 if no, = 1 if yes.
91-96	IKNTIC:	Code for indicating kinetic phase transfer = 0 if no, = 1 if yes.

GROUP 6. Temporal discretization data

(a) Time discretization parameters (7E10.3, 2I6)

One record.

Col. 1-10	TIMA:	Initial time value.
11-20	TIN:	Initial time step size.
21-30	TFAC:	Time step multiplier.
31-40	TMAX:	Maximum value of time step allowed.
41-50	TMIN:	Minimum value of time step during automatic time step selection.
51-60	TEND:	Final simulation time value.
61-70	TRED:	Reduction factor for time step size, if failure of outer iteration occurs.

000203

71-76	ITVD:	Code for indicating if TVD scheme is to be used for transport. = 0 if no, = 1 if yes.
77-82	ICROSS:	Code for indicating if cross dispersion terms are to be included when a finite difference scheme is used for transport. = 0 if no, = 1 if yes. Note: Finite element schemes always include the cross dispersion terms.

Note: if ITSGN = 0 or 2 (group 3, col. 21-25), TIN and TFAC are not used. Their values may be left blank or set = 0.0 TMIN and TEND are used only for ITSGN = 3, and may be left blank or set equal to zero otherwise.

(b) <u>Time values</u> (8E10.3)

*** Omit if ITSGN (group 3, col. 25-30) is equal or greater than 1.

Number of records = (NTS+7)/8.

Col. 1-10	TMVEC(I):	Time values at the end of time steps 1 through
11-20	1=1,	NTS.
etc.		NTS

(c) <u>Time discretization parameters</u> (3E10.3,I6)

*** Omit <u>unless</u> ITSGN (group 3, col. 25-30) = 2.

Number of records = as many as needed.

Each record contains the following information:

Col. 1-10	TMST:	Starting time value.
11-20	TMEND:	Ending time value.
21-30	DTS:	Time step used between TMST and TMEND.

000204

GROUP 6 continued.

31-36	IPAUSE:	Parameter indicating if this is the last record for subgroup 6c; = 1 if yes, = 0 if no.

(d) Nonlinear Scheme Selection Parameters

*** Omit if ISELSC (group 4, col. 67-72) = 0.

(i) Control record (2I6)

Col. 1-6	ISWICH:	Parameter indicating whether a switch from the Picard to Newton-Raphson scheme is to be made if convergence difficulty occurs; = 1 if yes, = 0 if no.
7-12	ENRFAC:	Relaxation factor used to reduce the degree of nonlinearity when convergence difficulty occurs. Suggested value of ENRFAC lies between 0.75 and 1. If no reduction of the degree of nonlinearity is required set ENRFAC = 1. In any case, ENRFAC must not be greater than 1.

(ii) Nonlinear scheme selection records (4I6)

Number of records = as many as needed.

Col. 1-6	ISC:	Nonlinear scheme indicator; = 1 for Newton-Raphson, = 0 for Picard scheme.
7-12	ITST:	Starting time step number when the specified value of ISC (the selected nonlinear scheme) is to be applied.
13-18	ITEND:	Ending time step number when the specified value of ISC is to be applied.
19-24	IPAUSE:	Parameter indicating if this is the last record of subgroup 6d; = 1 if yes, = 0 if no.

000205

GROUP 7. Default initial values

(a) Dependent variables (2E10.3)

One record.

Col. 1-10	HEADI:	Default initial value of the pressure head (or hydraulic head if INTSPC = 1, (L). Leave blank if dealing with transport simulation only (IMODL = 0).
11-20	CONCI:	Default initial value of the solute concentration (M/L^3). Leave blank if dealing with flow simulation only (IMODL = 1).
21-30	CSI:	Default initial value of the solid (adsorbed) phase concentration (M/M). Leave blank if dealing with water phase only (IKNTIC = 0). Give negative value if starting at equilibrium (CSCI = 0 and EMPI = 0 in this case).
31-40	CSCI:	Default initial value of chemisorbed concentration (M/M). Leave blank if dealing with water phase only (IKNTIC = 0).
41-50	EMPI:	Default initial value of precipitated mass. Leave blank if dealing with water phase only (IKNTIC = 0).

(b) Water saturation (E10.3,I6)

***Omit if IHYST (group 4, col. 75-80) = 0.

One record.

Col. 1-10	SWND(1):	Default initial value of saturation.
11-16	KHYST(1):	Default initial value of the hysteresis index, =-1 if initial condition is drying, =+1 if initial condition wetting. Note: If the saturation value is left blank, the saturation will be computed from the initial pressure head value, using parameters for the main drying retention curve if KHYST(1) = -1, or the main wetting curve if KHYST(1) = +1.

000206

GROUP 8. Node property numbers (16I6)

*** Omit this group if NMAT (group 3, col. 51-55) = 1. Supply node identification index as zero for inactive nodes in the gridded domain.

Number of records = (NP+15)/16.

Col.	1-6	IPROP(J):	Material number specification for nodes
	7-12	J=1, NP	1 through NP.
	etc.		

GROUP 9. Hydraulic properties of soil

*** Omit this group if IMODL (group 3, col. 1-6) = 0.

Number of records = NMAT (group 3, col. 60-66).

a) Saturated properties values (7E10.3)

Col.	1-10	PROP(I,1):	Principal component K_{xx} of saturated hydraulic conductivity tensor.
	11-20	PROP(I,2):	Principal component K_{yy} of saturated hydraulic conductivity tensor.
	21-30	PROP(I,3):	Principal component K_{zz} of hydraulic conductivity tensor.
	31-40	PROP(I,4):	Specific storage, S_s.
	41-50	PROP(I,5):	Saturated water content, θ_{sat}.
	51-60	PROP(I,6):	Air entry pressure head value, ψ_a (set 0 if IWATP = 1).
	61-70	SANGLE(I):	Angle (in degrees) of inclination of the surface of the soil material zone. If the zonal surface is horizontal, set this angle to zero.

GROUP 10. Soil moisture functional parameters

*** Omit this group if IMODL (group 3, col. 1-6) = 0, or if IWATP (group 5, col. 85-90) = 1.

Number of records = NMAT (group 3, col. 61-66 or NMAT x 2 if IHYST (group 4, col. 91-96) = 1.

000207

(a) <u>Parameters for main drying curve</u> (5E10.3)

Col. 1-10	PROP(I,7):	Residual saturation of (S_{wr}) of material number I.
11-20	PROP(I,8):	Control parameter (n) of the Brooks-Corey relative permeability versus saturation relationship, $k_{rw} = (S_w-S_{wr})^n/(1-S_{wr})^n$. Set PROP(I,8) = 0 if the van Genuchten k_{rw} versus S_w is to be used instead of the Brooks-Corey relationship.
21-30	PROP(I,9):	Leading coefficient (α^d) of the van Genuchten saturation versus capillary head relationship, (1/L), $(S_w-S_{wr}) = (1-S_{wr})/[1+(\alpha\|\psi-\psi_a\|)^\beta]^\gamma$.
31-40	PROP(I,10):	Power index (β^d) of the saturation versus capillary head relationship.
41-50	PROP(I,11):	Power index (γ^d) of the saturation versus capillary head relationship. If PROP(I,11) is left blank, the code then assumes that $\gamma^d = 1-1/\beta^d$.

(b) <u>Parameters for main wetting curve</u> (4E10.3)

***Omit if IHYST (group 3, col. 6-10) = 0.

Col. 1-10	PROP(I,12):	Maximum wetting saturation (S_{ws}) of material number I. Default value is $S_{ws} = 1$.
11-20	PROP(I,13):	Leading coefficient (α^w) of the saturation versus capillary head relationship (1/L). Default is $\alpha^w = \alpha^d$.
21-30	PROP(I,14):	Power index (β^w) of the saturation versus capillary head relationship. Default if $\beta^w = \beta^d$.
31-40	PROP(I,15):	Power index (γ^w) of the saturation versus capillary head relationship. If PROP(I,15) is left blank, the code assumes that $\gamma^w = 1-1/\beta^w$.

000208

GROUP 10 continued.

Note: If a non-hysteretic simulation is performed (IHYST=0), only group 10a is read. If a hysteretic simulation is performed (IHYST=1), the parameters for the main drying curve are given in group 10a and the parameters for the main wetting curve are given in group 10b.

GROUP 11. Soil-solute transport parameters

*** Omit this group if IMODL (group 3, col. 1-6) = 1.

(a) Soil transport parameters (9E10.3)

Number of records = NMAT (group 3, col. 61-66).

Col.	1-10	PROPJ(I,1):	Longitudinal dispersivity, α_L (or α_{LH}).
	11-20	PROPJ(I,2):	Transverse dispersivity, α_T (or α_{TH}).
	21-30	PROPJ(I,3):	Apparent molecular diffusion coefficient, D^o ($D^o = \tau\phi D^*$, where D^* is the free-water molecular diffusion, ϕ is porosity, and τ is tortuosity). Note: τ may be estimated from $\tau = \phi^{1/3}$ where ϕ is the effective porosity.
	31-40	PROPJ(I,4):	Exponent of the Freundlich sorption isotherm. Set = 1 if linear isotherm is used.
	41-50	PROPJ(I,5):	Effective porosity, ϕ.
	51-60	PROPJ(I,6):	Bulk density, ρ_b.
	61-70	PROPJ(I,7):	Exponent m of the equation used to compute effective molecular diffusion in unsaturated porous media ($D_u = S^m D_o$); = 0 for no variation with saturation, = 1 for linear dependency of D_u on saturation, =3.333 for nonlinear dependency according to Millington-Quirk constitutive relation (see Jury et. al., 1983).
	71-80	PROPJ(I,8):	α_{TV} vertical transverse dispersivity.

000209

81-90	PROPJ(I,9):	α_{LV} vertical longtudinal dispersivity.

(b) Soil-solute transport parameters (2E10.3)

Number of records = NMAT (group 3, col. 61-66).

Col. 1-10	RPROP(I,1):	Decay coefficient, λ. For a conservative solute species set RPROP(I,1) = 0.0. Note $\lambda = \ln 2/t_{1/2}$, where $t_{1/2}$ = half life.
11-20	RPROP(I,2):	Distribution coefficient, k_d. Note: the unit for k_d must be the reciprocal of the unit for bulk density. For a unretarded solute species set RPROP(I,2) = 0.0.

(c) Kinetic parameters (5F10.3, 2I6)

*** Omit this group if IKNTIC (group 5, col. 91-96) = 0.

Number of records = NMAT (group 3, col. 61-66). For every material type (I=1, . . . NMAT) supply subgroup i, ii, and iii.

(i) Functional parameter set

Col. 1-10	RPROP (I,3):	α_d, desorption rate coefficient (t^{-1})
11-20	RPROP (I,4):	α_c, chemisorption rate coefficient (t^{-1})
21-30	RPROP (I,5):	α_p, precipitation rate constant (t^{-1})
31-40	RPROP (I,6):	α_s, zeroeth order dissolution rate constant ($ML^{-3}\ t^{-1}$)
41-50	RPROP (I,7):	solubility limit (ML^{-3})
51-56	IKMTAB(I):	Parameter indicating if tabular or functional form of equilibrium curve is supplied. = 0 if use equilibrium curve, = 1 if read in tabular form.
57-62	NTABPTS(I):	number of control points in a tabulated equilibrium curve.

000210

GROUP 11 continued.

(ii) Tabulated kinetic parameters (water concentration) (8E10.3)

*** Omit this group if IKMTAB(I) = 0

Col. 1-10	CWTAB(I,J):	Tabulated equilibrium curve water concentration.
11-20	J=1,	(ML^{-3})
etc.	NTABPTS(I)	

(iii) Tabulated kinetic parameters (soil concentration) (8E10.3)

*** Omit this group if IKMTAB(I) = 0

Col. 1-10	CSTAB(I,J):	Tabulated equilibrium curve soil concentrations.
11-20	J=1,	(MM^{-1})
etc.	NTABPTS(I)	

GROUP 12. Rectangular mesh parameter specification (4I6, 3F10.3,2I5)

***Omit this group if ICURVL (group 3, col. 91-96) = 1.

One record.

Col. 1-6	NROWS:	Number of grid lines parallel to the x-direction.
7-12	NCOLS:	Number of grid lines parallel to the y-direction.
13-18	NPLANE:	Number of gridding surfaces (or planes) to be used in the 3-D mesh generation. NPLANE must not be less than 2.
19-24	IFSTPL:	Parameter indicating if the problem to be solved can be reduced to or treated as a two-dimensional or axisymmetric problem; = 1 if yes, = 0 if no.
25-34	DXMAX:	Maximum value of spatial increment allowed in the x-direction.
35-44	DYMAX:	Maximum value of spatial increment allowed in the y-direction.
45-54	DZMAX:	Maximum value of spatial increment allowed in the z-direction.

55-61	IXYZRD:	Parameter indicating if x, y, and z coordinates of the grid lines are to be input or generated by the code; = 0 if coordinates are to be computed using generated values of spatial increments, use group 13b, = 1 if coordinate input is needed, use group 13a, = 2 if coordinates are to be computed using specified values of spatial increments, use groups 13b and 13c.
62-66	ICOORD:	Parameter indicating the vertical coordinate orientation; = 3 for y is vertically upward, = 2 for z is vertically upward.

GROUP 13. Rectangular mesh data

*** Omit this group if ICURVL (group 3, col. 91-96) = 1

(a) Grid line x-coordinates

***Omit this subset if IXYZRD (group 12, col. 55-60) = 0 or 2.

(i) Grid line x-coordinates (8F10.4)

Number of records = (NCOLS+7)/8 (group 11, col. 7-12).

Col. 1-10	XW(J):	x-coordinates of grid lines 1 through NCOLS.
11-20	J=1,	
etc.	NCOLS	

(ii) Grid line y-coordinates (8F10.4)

Number of records = (NROWS+7)/8 (group 12, col. 1-6).

Col. 1-10	YW(J):	x-coordinates of grid lines 1 through NCOLS.
11-20	I=1,	
etc.	NROWS	

(iii) Grid line z-coordinates (8F10.4)

Number of records = (NPLANE+7)/8 (group 12, col. 13-18).

000212

GROUP 13 continued.

Col. 1-10	ZW(K):	z-coordinates of gridding planes 1 through
11-20	K=1,	NPLANE.
	etc.	NPLANE

(b) Mesh generation data

***Omit this subset if IXYZRD (group 12, col. 51-55) = 1.

(i) x-y coordinate parameters (8F10.4)

Col. 1-10	DX:	Nodal spacing in the x-direction of the first grid block.
11-20	DY:	Nodal spacing in the y-direction of the first grid block.
21-30	XO:	Maximum value of x-coordinate.
31-40	YO:	Maximum value of y-coordinate.
41-50	SCFX:	Mesh grading factor in the x-direction.
51-60	SCFY:	Mesh grading factor in the y-direction.
61-70	XSTART:	Minimum value of x-coordinate.
71-80	YSTART:	Minimum value of y-coordinate.

(ii) z-direction coordinate parameters (4F10.4)

Col. 1-10	DZ:	Nodal spacing in the z-direction of the first grid block.
11-20	ZO:	Maximum value of z-coordinate.
21-30	SCFZ:	Mesh grading factor in the z-direction.
31-40	ZSTART:	Minimum value of z-coordinate.

(c) Spatial increment data (F10.2,3I6)

***Omit unless IXYZRD = 2.

Number of records = as many as needed.

000213

(i) First record set

Each record contains the following information:

Col. 1-10	DELTAX:	Spatial increment in the x-direction.
11-16	ISTC:	Starting element column number.
17-22	IENDC:	Ending element column number.
23-28	IPAUSE:	Parameter indicating if this is the last record in this record set; = 1 if yes; = 0 if no.

(ii) Second record set

Each record contains the following information:

Col. 1-10	DELTAY:	Spatial increment in the y-direction.
11-16	ISTR:	Starting element row number.
17-22	IENDR:	Ending element row number.
23-28	IPAUSE:	Parameter indicating if this is the last record in this record set; = 1 if yes, = 0 if no.

(iii) Third record set

Each record contains the following information:

Col. 1-10	DELTAZ:	Spatial increment in the z-direction.
11-16	ISTB:	Starting element block number.
17-22	IENDB:	Ending element block number.
23-28	IPAUSE:	Parameter indicating if this is the last record in this record set; = 1 if yes, = 0 if no.

000214

GROUP 13 continued.

Note: (1) the last values of IENDC, IENDR, and IENDB must be equal to NCOLS-1, NROWS-1, and NPLANE-1, respectively;
(2) the sum of DELTAX*(IENDC-ISTC+1) must be equal to XO-XSTART;
(3) the sum of DELTAY*(IENDR-ISTR+1) must be equal to YO-YSTART; and
(4) the sum of DELTAZ*(IENDB-ISTB+1) must be equal to ZO-ZSTART.

GROUP 14. Curvilinear mesh data

***Omit this group (14a-14d) if ICURVL (group 3, col. 76-80) = 0.

(14A) Mesh control record (8I6)

One record

Col.	1-6	ICOORD:	Parameter indicating the vertical coordinate; = 3 for z-vertical, = 2 for y-vertical.
	7-12	NPLANE:	Number of gridding surfaces to be used in 3-D mesh. NPLANE must not be less than 2.
	13-18	IFSTPL:	Parameter indicating if problem to be solved can be reduced to, or treated as two-dimensional, or axisymmetric; = 1 if yes, = 0 if no.
	19-24	IXYCOM:	Parameter indicating if the x-y mesh coordinates are the same for all gridding surfaces; = 1 if yes, use group 14Ba for simplified x-y data input, = 0 if no, use group 14Bb.
	25-30	IZCOM:	Parameter indicating if gridding surfaces are all planar and parallel to the x-y plane. = 1 if yes, use the third subset of groups 14Ba and 14Bb for simplified z-data input, = 0 if no, use the fourth subset of groups 14Ba and 14Bb.

31-36	IPNCH:	Parameter indicating if pinch nodes exist: = 1 if yes, read group 14D for connectivity information within a slice or gridding surface, = 0 if no, read group 14C for gridding slice information.
37-42	IEXEC:	Parameter indicating if the code is to be fully executed after the problem is set up; = 1 if yes, execute, = 0 if no, print all data and stop.

(14B) Coordinate Data

(14Ba) Coordinate data for cases where (x,y) coordinates are located in an identical manner for all gridding surfaces

***Omit if IXYCOM (group 14a, col. 19-24) = 0

There are four record subsets in group 14b.

(i) First subset (8F10.6)

Number of records = (NNDSL+7)/8 where NNDSL = number of nodes per gridding surface.

Col. 1-10	XCVR(I):	x-coordinates of curvilinear mesh nodal points
11-20	I=1,	in the first gridding surface.
etc.	NNDSL:	

(ii) Second subset (8F10.6)

Number of records = (NNDSL+7)/8 or 1 where NNDSL = number of nodes per gridding surface.

Col. 1-10	YCVR(I):	y-coordinates of curvilinear mesh nodal points
11-20	I=1,	in the first gridding surface.
etc.	NNDSL:	

(iii) Third subset (8F10.6)

***Omit this subset if IZCOM (group 14A, col. 25-30) = 0. In this case gridding surfaces correspond to x-y planes.

000216

GROUP 14 continued.

Number of records = (NPLANE+7)/8 where NPLANE = number of gridding surfaces assumed to x-y planes.

Col. 1-10	ZCR(I):	z-coordinates of all gridding planes (for planar
11-20	I=1,	where all x-y surfaces are planes).
etc.	NPLANE:	

(iv) Fourth subset (8F10.6)

***Omit this subset if IZCOM = 1. In this case gridding surfaces are nonplanar and z-coordinates need to be input for all nodes.

Number of records = (NP+7)/8 where NP = total number of nodes.

Col. 1-10	CORD(I,3):	z-coordinates for nodal points 1 through NP.
11-20	I=1,	
etc.	NP:	

(14Bb) Coordinate data for cases where (x,y) coordinate patterns are different for different gridding surfaces

***Omit if IXYCOM (group 14a, col. 19-24) = 1.

Number of records sets = NPLANE (group 14a, col. 6-10), one for each gridding plane. These record sets are to be entered sequentially from the first through the last gridding surfaces. Each record set consists of 4 subsets described as follows:

(i) First subset (8F10.6)

Number of records = (NNDSL+7)/8 where NNDSL = number of nodes per gridding surface.

Col. 1-10	CORD(I,1):	x-coordinates of all nodes that lie in a gridding
11-20	I = IREF,	surface. In a particular gridding surface number,
etc.	IEND	the values of IREF and IEND are determined by the code.

(ii) Second subset (8F10.6)

Number of records = (NNDSL+7)/8.

Col. 1-10	CORD(I,2):	y-coordinates of all nodes that lie in the gridding
11-20	I=IREF,	surface.
etc.	IEND	

000217

(iii) Third subset (F10.6)

***Omit IZCOM (group 14a, col. 25-30) = 0. In this case, all gridding surfaces are parallel x-y planes.

One record.

Col. 1-10	ZCVR(NS):	z-coordinate value of the gridding plane.

(iv) Fourth subset (8F10.6)

***Omit IZCOM = 1.

Number of records = (NNDSL+7)/8.

Col. 1-10 11-20 etc.	CORD(I,3): I=IREF, IEND	z-coordinates of all nodes that lie in the gridding surface.

Note: Subsets (i) through (iv) of group 14Bb) are repeated for all gridding surfaces.

(14C) Regular grid parameters (2I6)

***Omit if IPNCH = 1 (group 14a, col. 31-36).

One record.

Col. 1-6	NROWS:	Number of rows of grid lines along the x-axis.
7-12	NCOLS:	Number of columns of grid lines along the y-axis.

Note: NNDSL = NROWS*NCOLS, where NNDSL is the number of nodes per slice.

(14D) Element nodal connection data

(14Da) Corner node data (5I6)

***Omit if IPNCH = 0 (group 14a, col. 31-36).

Number of records = NESL where NESL is the number of elements per gridding surface.

000218

GROUP 14 continued.

Col. 1-6	N:	Element number for which nodal connectivities in the first gridding surface are sought.
7-12	NOP(N,1):	Nodal connectivity of element N in
13-18	NOP(N,2):	in the first gridding surface.
19-24	NOP(N,3):	(Connectivity is counterclockwise).
25-30	NOP(N,4):	

(14Db) Transition element nodal data

***Omit this group if IPNCH (group 14a, 31-36) = 0

(i) First subset (I6)

Number of records = 1.

Col. 1-6	NPND:	Number of transition elements used in the first slice of the modeled domain.

(ii) Second subset (16I6)

Number of records = (NPND+15)/16.

Col. 1-6	NODPNC(I,1):	Element number of transition element I in the first slice of the grid.
7-12	I=1, NPND	(This data should be input in increasing order of element numbers).
etc.		

(iii) Third subset (16I6)

Number of records = (NPND+15)/16.

Col. 1-6	NODPNC(I,2):	Node number of pinch node I in the first slice of the grid.
7-12	I=1, NPDND	
etc.		

(iv) Fourth subset (16I5)

Number of records = (NPND+15)/16.

000219

Col. 1-6	NODPNC(1,3):	Code for indicating location of pinch node I.
7-12	I=1, NPND	
etc.		= 1 if pinch node is on right-y of element,
		= 2 if pinch node is on left-y of element,
		= 3 if pinch node is on bottom-x of element,
		= 4 if pinch node is on top-x of element.

The boundary conditions and initial condition (groups 15, 16, 17 and 18) are specified for the first and second dependent variables. The first dependent variable is either pressure head or hydraulic head if the flow simulation is performed (IMODL=1 or 2). In the case where only transport simulation is performed (IMODL=0), the first dependent variable corresponds to concentration. The second dependent variable is used only when a combined flow and transport simulation is performed (IMODL=2). In that case, concentration is the second dependent variable.

GROUP 15. Boundary condition data

(a) Boundary condition control record (8I6)

One record.

Col. 1-6	NBTO:	Number of steady-state Dirichlet (prescribed head or prescribed concentration) boundary conditions. These are input via group 15b.
7-12	NDFLUX:	Number of steady-state prescribed flux boundary conditions. Do not count the time-dependent flux boundary conditions when determining NDFLUX. These are input via group 15c.
13-18	NBHVAR:	Number of transient Dirichlet boundary conditions. These are input via group 16.
19-24	NBFVAR:	Number of transient flux boundary conditions (excluding those corresponding NDCS). These are input via group 17.
25-26	NDCS:	Number of nodes representing contaminant source boundary conditions having leachate fluxes that are concentration dependent. For IMODL = 1 (flow simulation only), the code automatically sets NDCS = 0. This input is provided via group 18 I.

000220

GROUP 15 continued.

27-36	NDVTBC:	Number of nodes representing contaminant flux boundary conditions with a constant concentration and time-varying flow field calculated from the flow problem. For IMODL = 1 (flow simulation only) the code automatically sets NDVTBC = 0. This input is provided via group 18 II.

Note: For NDVTBC ≠ 0, the parameter IOUTLT should be set equal to 1 for the corresponding flow run, and the respective nodes should be listed in group 23 to enable a fluid flux calculation, which may be used to perform solute flux calculations.

37-42	IRDBC:	Parameter indicating if recharge/drain boundary condition is to be used. = 1 if yes, = 0 if no.
43-48	NHDFSB:	Number of source beds with steady-state head-dependent fluxes.

(b) Dirichlet boundary condition data (2I6,E10.3)

*** Omit this record if NBTO (group 15, col. 1-5)=0.

Number of records = NBTO.

Col. 1-6	NODV(I):	Node number.
7-12	MDEGB(I):	Dependent variable number.
13-22	VALV(I):	Prescribed value of the dependent variable (head or concentration) at the boundary node.

(c) Flux boundary condition data (2I5, 2E10.3)

*** Omit this record if NDFLUX (group 15, col. 6-10) = 0.
Number of records = NDFLUX. Note that the outward flux is taken to be negative and the inward flux is taken to be positive.

Col. 1-6	NODF(I):	Node number.
7-12	MDEGF(I):	Dependent variable number.

000221

13-22	FLUXVO(I):	For the flow equation, FLUXVO(I) denotes fluid volumetric flux at the boundary node. It is to be left blank if the boundary condition at the node is time dependent. For the transport equation FLUXVO(I) corresponds to the solute mass flux prescribed at the node.
23-32	QVALV(I):	For the flow equation, QVALV(I) is to be left blank. For the transport equation, QVALV(I) corresponds to the fluid volumetric flux assigned to the boundary node.

GROUP 16. Transient Dirichlet boundary conditions

*** To be omitted if NBHVAR (group 15, col. 13-18) = 0.

Number of record sets = NBHVAR.

Each set contains the following records:

(a) Control record (4I6)

One record.

Col.	1-6	NDHVAR(I):	Node number of a time-dependent head or concentration boundary node.
	7-12	MDEGBT(I):	Dependent variable number.
	13-18	NTSNDH(I):	Number of control points on the time graph of the boundary condition at the node.
	19-24	ITVARH(I):	Parameter indicating variation of the prescribed dependent variable; = 0 for continuous variation; = 1 for discontinuous (stepped) variation.

(b) Time value records (8E10.3)

Number of records = (NTSNDH(I)+7)/8 (group 16a, col. 7-12).

Col.	1-10	TMHV(I,J):	Sequential time values corresponding to the control points on the time graph depicting temporal variation of the prescribed dependent variable.
	11-20	J=1,	
	etc.	NTSNDH(I)	

000222

GROUP 16 continued.

(c) Functional value records (8E10.3)

Number of records = NTSNDH(I)+7/8 + 0 or 1 (group 16a, col. 7-12).

Col.	1-10	HVTM(K,J):	Values of the dependent variable corresponding to TMHV(I,J).
	11-20	J=1,	
	etc.	NTSNDH(1)	

GROUP 17. Transient flux boundary conditions

*** Omit this record if NBFVAR (group 15a, col. 19-24) = 0.

Number of card sets = NBFVAR.

Each set contains the following cards:

(a) Control records (4I6)

Col.	1-6	NDFVAR(I):	Node number of a time-dependent flux boundary node.
	7-12	MDEGFT(I):	Dependent variable number corresponding to the governing equation being considered.
	13-18	NTSNDF(I):	Number of control points on the time graph of the flux boundary condition at the node.
	19-24	ITVARF(I):	Parameter indicating the time variation of the prescribed nodal flux data; = 0 for continuous variation, = 1 for stepped variation.

(b) Time value records (8E10.3)

Number of records = (NTSNDF(I)+7)/8 (group 17a, col. 7-12).

Col.	1-10	TMHF(I,J):	Sequential time values corresponding to the control points on the time graph depicting temporal variation of the flux boundary condition at the node.
	11-20	J=1,	
	etc.	NTSNDF(I)	

(c) Flux value cards (8E10.3)

Number of records = (NTSNDF(I)+7/8 (group 17a, col. 7-12).

000223

Col.	1-10	FVTM(I,J):	Nodal integrated volumetric fluid flux values (for flow or solute mass flux values (for transport) corresponding to TMHF(I,J).
	11-20	J=1,	
	etc.	NTSNDF(I)	

(d) Fluid flux value records (8E10.3)

*** Omitted if dealing with the flow equation. (IMODL = 1) (group 3, col. 1-6).

Number of records = (NTSNDF(I)+7)/8 (group 16a, col. 13-18).

Col.	1-10	QVTM(I,J):	Volumetric fluid flux values corresponding to TMHF(I,J).
	11-20	J=1,	
	etc.	NTSNDF(I)	

GROUP 18I. Concentration-dependent source boundary condition data

*** Omit if IMODL = 1 or NDCS = 0.

I(a) Source characteristic data

Control record (I6)

Col.	1-6	NDCSRC:	Number of sources to be considered. The correct value of NDCSRC must be greater than zero and less than equal to NDCS.

For each source, supply one record set containing the following information:

I(b) Leach time data (I6,E10.3)

Col.	1-6	ISC:	Source identification number.
	7-16	TLDCS(ISC):	Contaminant release time duration. For a case of continuous leaching source or step release, TLDCS(I) can be left blank or set to a very large value.

I(c) Source parameters (5E10.3)

For the saltstone source diffusion model, the source parameters required by the code are as follows:

Col.	1-10	SLPAR(ISC,1):	Initial concentration in the saltstone.

000224

GROUP 18I continued.

11-20	SLPAR(ISC,2):	Apparent diffusion coefficient of the saltstone.
21-30	SLPAR(ISC,3):	Apparent diffusion coefficient of the clay cap.
31-40	SLPAR(ISC,4):	Thickness of the clay cap.
41-50	SLPAR(ISC,5):	Solubility of contaminant in water (concentration units).

I(d) Source node data (3I6,E10.3)

One record set for each source node. Each set contains the following information:

Col.	1-6	NODCS(I):	Node number.
	7-12	IDCSNO(I):	Source identification number.
	13-18	IBDCS(I):	Boundary condition identifier; = 1 if initial concentration values are prescribed, = 2 if initial solute mass flux values are prescribed.
	19-28	QFLSN(I):	Net integrated (volumetric) fluid flux at the sour ce node.

GROUP 18 II. Time-varying contaminant flux condition with constant concentration inflows

***Omit this record if NDVTBD (group 15, col. 31-36) = 0. (2I6,E10.3)

Number of records = NDVTBC.

Col.	1-6	NODTF(I):	Node number.
	7-12	MDEGTF(I):	Dependent variable number.
	13-22	VALC(I):	Value of concentration of contaminant in inflowing fluid.

GROUP 19. Initial nodal value data of dependent variable

*** Omit if NONU (group 3, col. 56-60) = 0 or 2. Also omit if NPIN (group 5, col. 13-18) = 0.

000225

Supply these data to the code according to one of the following formats.

(a) Format type 1 (I6,2F10.5)

To be used only when NPIN (group 5, col. 13-18) is less than NP (group 3, col. 25-30).

(NOTE: NP = total number of nodes and NPIN = number of nodes for which initial nodal values are to be read).

Number of records to be supplied = NPIN (group 5, col. 13-18).

Col.	1-6	N:	Node number.
	7-16	HINT(N,1):	Initial value of the first dependent variable.
	17-26	HINT(N,2):	Initial value of the second dependent variable.
	27-36	CSINT(N):	Initial value of the solid phase concentration. Leave blank if dealing with water phase only (IKNTIC=0).
	37-46	CSCINT(N):	Initial value of chemisorbed concentration. Leave blank if dealing with water phase only (IKNTIC=0).
	47-56	MPINT(N):	Initial value of precipitated mass. Leave blank if dealing with water phase only (IKNTIC = 0).

(b) Format type 2 (8E10.4)

To be used when NPIN = NP. It may therefore be used for a restart run where initial values to be read correspond to the final set of nodal values obtained from a previous run. This set of nodal values can be obtained from file unit 8.

(i) First subset

Col.	1-10	HINT(I,1),	Initial value of first dependent variable for
	11-20	I=1, NP	all nodes.
	etc.		

(ii) Second subset

***Omit if solving for only one dependent variable i.e., omit if IMODL = 0 or 1.

Col.	1-10	HINT(I,2),	Initial value of second dependent variable for
	11-20	I,1, NP	all nodes.

000226

GROUP 19 continued.

(iii) Third subset

***Omit if solving for water phase only i.e., omit if IKNTIC = 0.
Omit if CSI (group 7, col. 27-30) is negative. Initial solid concentration becomes in equilibrium with water phase concentration.

Col.	1-10 11-20 etc.	CSINT(I), I,1, NP	Initial value of solid phase concentration for all nodes.

(iv)Fourth subset

***Omit if solving for water phase only i.e., omit if IKNTIC=0.
Omit if CSI (group 7, col. 21-30) is zero.

Col.	1-10 11-20 etc.	CSCINT(I), I=1, NP	Initial value of chemisorbed concentration for all nodes.

(v) Fifth subset
*** Omit if solving for water phase only.

Col.	1-10 11-20 etc.	MPINT(I), I=1, NP	Initial value of precipitated mass for all nodes.

(c) Initial element saturation data for hysteresis simulation

***Omit if IHYST (group 4, col. 75-80) = 0 or NONU (group 3, col. 56-60) = 0.

(i) Number of elements (I6)

One record.

Col. 1-6	NELS:	Number of elements for which initial saturation values are to be read.

(ii) Saturation and hysteresis data

Format Type 1 (2I6,E10.3)

Number of records = NELS

Col. 1-6	IL:	Element number.

000227

7-12	KHYST(IL):	Value of hysteresis index for element IL; = -1 for drying, = +1 for wetting.
13-22	SWINT(IL):	Saturation value for element IL.

GROUP 20. Default parameters for transport analysis (7F10.6,I6)

*** Omit if only flow modeling is required (i.e., if IMODL (group 3, col. 1-5)=1). One record.

Col.	1-10	VCX:	Default value of Darcy velocity component in the x-direction.
	11-20	VCY:	Default value of Darcy velocity component in the y-direction.
	21-30	VCZ:	Default value of Darcy velocity component in the z-direction.
	31-40	WFAC:	Default value of upstream weighting factor in x-direction. Leave blank if upstream weighting is not used.
	41-50	YFAC:	Default value of upstream weighting factor in y-direction. Leave blank if upstream weighting is not used.
	51-60	ZFAC:	Default value of upstream weighting factor in the z-direction. Leave blank if upstream weighting is not used.
	61-70	SWD:	Default value of initial saturation. Leave blank if not used.
	71-76	IVSTED:	Parameter indicating if the velocity field is steady-state; = 1 if yes, = 0 if no.

NOTE: If IMODL = 2 the velocity values of the flow simulation are used, and VCX, VCY and VCZ are ignored.

000228

GROUP 21. Element Darcy velocity data (2(I6,3E10.3)

*** This record type is to be omitted unless NVREAD (group 5, col. 1-5) is equal to 1.

Number of records = (NE+1)/2.

Each record contains 2 blocks of the following data:

Col.	1-6	I:	Element number.
	7-16	VELX(I):	Value of x-component of Darcy velocity at the element centroid.
	17-26	VELY(I):	Value of y-component of Darcy velocity at the element centroid.
	27-36	VELZ(I):	Value of z-component of Darcy velocity at the element centroid.

GROUP 22. Element water saturation data for transport analysis (8F10.6)

*** This record type is to be omitted unless variably-saturated transport analysis is to be performed, and NVREAD (group 5, col. 1-6) is equal to 1.

Number of records = (NE+7)/8.

Col.	1-10	SWND(I):	Values of saturation at centroids of elements 1 through NE.
	11-20	I=1,	
	etc.	NE	

GROUP 23. Boundary nodal data

*** This record type is to be omitted if IOUTLT (group 5, col. 6-10) = 0 and IMBAL (group 5, col. 55-60) = 0 (flux and mass balance calculations are not required).

(a) Control record (3I6)

One record.

Col.	1-6	NBOUT:	Number of nodes where nodal flux values are to be computed.
	7-12	NTSTB:	Number of time steps at which mass balance output is to be generated.

000229

13-18	NTSTF:	Number of time steps at which flux output is to be generated.

Note: If NTSTB and NTSTF are left blank, these outputs will be generated at every NSTEP time steps.

(b) Nodal numbers for flux computation (3I5)

*** Omit if NBOUT (group 23a, col. 1-6) = 0.

Number of records = (NBOUT+15)/16.

Col.	1-6	NDOUT(1):	Node numbers of the nodes for which through nodal fluid flux values are to be computed.
	7-12		
	etc.	NDOUT(NBOUT)	

Note: Every Dirichlet, flux or rechard node must be entered here only once if mass balance computations are required.

(c) Computed values of integrated fluid fluxes (8F10.3)

*** Omit this record set if only flow simulation is required (IMODL = 1 or 2). Also omit if NVREAD = 2.

Number of records = (NBOUT+7)/8.

Col.	1-10	QNDOUT(1):	Nodal values of integrated (volumetric) through fluid flux for the outlet boundary nodes.
	11-20		
	etc.	QNDOUT(NBOUT)	

GROUP 24. Evaporation and infiltration control data

*** Omit if NEIEVP (group 3, col. 73-78) = 0.

(a) Control record (4E10.3)

One record.

Col.	1-10	EIMAX:	Maximum value of potential infiltration flux per unit surface area (L/T).
	11-20	PSIMIN:	Minimum value of allowable pressure head at the soil surface (L).

000230

GROUP 24 continued.

21-30	EVMAX:	Maximum absolute value of potential evaporation flux per unit surface area (L/T).
31-40	FRACT:	Fraction of EIMAX and EVMAX to be imposed during the first iteration. Suggested value = 0.1. Note that FRACT must be greater than 0 and less than or equal to 1.

(b) Nodal infiltration or evaporation identification numbers (16I5)

Number of records = (NEIEVP+15)/16 (group 3, col. 73-78).

Col.	1-6 7-12 etc.	IELEVP(I): I=1, NEIEVP	Sequential number of elements that are subject to infiltration or evaporation. For those elements that are subject to evaporation, attach negative sign to their sequential elements numbers.

GROUP 25. Plant species data

*** Omit if NPLANT (group 3, col. 79-84) = 0.

(a) Wilting pressure head and potential transpiration (2(I6,2E10.3))

Number of records = (NPLANT+1)/2 (group 3, col. 66-70).

Col.	1-6	N:	Plant species number.
	7-16	PWILT(N):	Wilting pressure head for species N.
	17-26	TPOT(N): N=1, NPLANT	Absolute value of potential transpiration rate of species N.

(b) Control record (3I6)

One record.

Col.	1-6	NZRDF:	Number of z-coordinate values for which effective root function values are specified.
	7-12	NCOLPL:	Number of vertical nodal columns in the root zone.
	13-18	NEROOT:	Number of finite elements in the root zone.

000231

(c) Depth coordinate records (8E10.3)

Number of records = (NZRDF+7)/8 (group 25b, col. 1-6).

Col.	1-10	ZRDF(I):	Values of y-coordinate for which root
	11-20	I=1,	effectiveness function values are specified.
	etc.	NZRDF	

(d) Effective root function data (8E10.3)

Number of records for each plant = (NZRDF+7)/8 (group 25b, col. 1-6).

Col.	1-10	RDF(I,J):	Values of effective root function for plant
	11-20	I=1,	species J.
	etc.		

GROUP 26. Root zone element and node data

*** Omit if NPLANT (group 3, col. 79-84) = 0.

(a) Root zone element data (16I6)

Number of records = (NEROOT+15)/16 (group 25b, col. 13-18).

Col.	1-6	IEROOT(I):	Sequential numbers of the element that lie within
	7-12	I=1,	the root zone.
	etc.	NEROOT	

(b) Root zone nodal column data (5I5)

Number of records = NCOLPL (group 25b, col. 7-12).

Col.	1-5	I:	Nodal column number.
	6-10	INDRMN(I):	Lowest nodal sequential number for column I.
	11-15	INDRMX(I):	Highest nodal sequential number for column I.
	16-20	INDICR(I):	Nodal number increment for column I.
	21-25	IPLCOL(I):	Plant species number for column I.

Note: Elements and nodes that are at the soil surface should not be counted because they contribute only to direct evaporation and not to plant transpiration.

000232

GROUP 27. Observation node data (16I6)

*** Omit if IOBSND (group 5, col. 49-54) = 0.

Number of records = (NNOBS+15)/16, if more than 15 observation nodes (= 1 otherwise).

Col.	1-6	NNOBS:	Number of nodes for which time history of nodal values of dependent variable(s) is to be recorded.
	7-12	NDOBS(I):	Node numbers of observation nodes.
	etc.	I=1, NNOBS	

GROUP 28. Velocity file output time specification data (2E10.3,2I6)

*** Omit unless NVWRIT = 2.

Number of records = as many as needed.

Each record contains the following information:

Col.	1-10	TSTVOP:	Starting time value for writing the velocity output onto unit 9.
	11-20	DTVOP:	Time increment for velocity output.
	21-26	NDTVOP:	Number of increments with constant value of DTVOP.
	27-32	IPAUSE:	Parameter indicating if this is the last record in group 28; = 1 if yes, = 0 if no.

GROUP 29. Output time specification data

***Omit unless ITSGN (Group 3, col. 25-30) = 3.

(a) Control record (I5)

Col.	1-6	NPRCON:	Number of time values at which output is desired.

000233

(b) Output time value records (8E10.3)

Col.	1-10	TMPRC(I),:	Time values at which output is desired.
	11-20	I=1	
	etc.	NPRCON	

Note: This output is for primary variables, and mass balances, in the plot files and primary output file.

GROUP 30. Solver setup parameters (3I6)

***Omit this group if IPFSPAR (group 1, col. 13-18) = 0

Col.	1-6	INFOS:	Parameter indicating level of solver information that is output. = -2 no printing = -1 Error messages only = 0 Warnings and error messages = 1 The above, plus workspace usage and convergence history. (default)
	7-12	LEVELS:	Level of ILU decomposition of left hand side matrix (default = 1).
	13-18	IACCELS:	Type of acceleration method used for unsymmetric equations = 1 ORTHOMIN acceleration (default) = 2 CGS Conjugate Gradient Squared = 3 CGSTAB (stablized CGS) = 4 GMRES

GROUP 31. Recharge/drain boundary condition cards (2F10.6,4I6)

***Omit if IRDBC (group 15, col. 37-42) = 0.
Repeat Group 31 for all zones of recharge/drain.

Col.	1-10	RECHMAX:	Maximum recharge rate (L/T) for the recharge/drain zone.
	11-20	DRANCOEF:	Leakance coefficient of the drain (T^{-1}) for the recharge/drain zone.

000234

GROUP 31 continued.

21-26	NDST:	Lowest sequential global node number of top nodes receiving the assigned recharge/drain boundary condition.
27-32	NDEND:	Highest sequential global node of the top nodes receiving the assigned recharge/drain boundary condition.
33-38	NICR:	Nodal increment. NICR must be less than or equal to NDEND - NDST (default value = 1).
39-44	IREPET:	Index used to indicate if additional recharge/drain data will follow. = 1 if yes, = 0 if no.

GROUP 32. Head-dependent source bed data

***Omit if NHDFSB (group 15, col. 43-48) = 0.

Number of card sets = NHDFSB.
Each set contains the following cards:

(a) Control record (2I5,3E10.3)

Col.	1-6	IBDTYP(I):	Source bed type. = 0 for an aquitard source bed, = 1 for a river source bed, = 2 for a drain source bed, = 3 for a general source bed.
	7-12	NSBNDI(I):	Number of nodes having leakage flux interac tion with the source bed.
	13-22	SBDLKP(I):	Leakance coefficient of the source bed (T^{-1}).
	23-32	SBDBEL(I):	Elevation of the bottom of the source bed. (Not used when IBDTYP(I) = 2 or 3)
	33-42	SSHBD(I):	Steady-state hydraulic head at the top of the source bed.

000235

(b) Source bed nodes (16I6)

Number of records = (NSBNDI(I)+7)/8

Col.	1-6	INDSBD(J,I):	Node numbers of the source bed nodes.
	7-13	J=1,NSBNDI(I)	
	etc.		

(c) Source bed nodal flow areas (8E10.4)

*** Omit if IBDTYP(I) = 0.

Number of records = (NSBNDI(I)+7)/8

Col.	1-10	ANDSBD(J,I):	Effective flow areas of the source bed nodes.
	11-20	J=1,NSBNDI(I)	
	etc.		

A.3 INPUT PREPARATION CHECKLIST

To facilitate the preparation of input data for water flow and solute transport simulations, four checklists are provided in Tables A.1-A.4, respectively. These checklists should be used as a means for echo checking of the input data file (unit number 5).

000236

Table A.1 Checklist for Water Flow Simulation by VAM3DF

1. If there is only one set of material properties specified for the flow system, omit record group 8.

2. If boundary conditions are invariant with time, omit record group 16 and 17.

3. If initial conditions are uniform, omit record group 18.

4. Make sure that the setting of certain control parameters is performed as depicted in Table 8.3.

5. If time step values are to be automatically generated in VAM3DF (ITSGN = 1 or 2), omit record group 6b.

Table A.2 Checklist for Solute Transport Simulation by VAM3DF

1. Omit record group 9 and 10.

2. If there is only one set of material properties specified for the flow system, omit record group 8.

3. If boundary conditions are invariant with time, omit record group 16 and 17.

4. If initial conditions are uniform, omit record group 19.

5. Make sure that the setting of certain control parameters is performed as depicted in Table 8.4.

6. If time step values are to be automatically generated in VAM3DF (ITSGN = 1 or 2), omit record group 6b.

000238

Table A.3 Control Parameter Values Used by VAM3DF in the Transport Simulation

GROUP	COLUMN	VARIABLE	SET VALUE
3	1-5	IMODL	= 1
3	16-20	ISSTA	= 0 if transient analysis is to be performed = 1 if steady-state solution is desired
4	11-15	NITMAX	= 1 (for fully-saturated flow) > 1 (for variably-saturated flow)
4	21-25	ILUMP	= 0 for consistent storage matrix = 1 for partially lumped storage matrix = 2 for fully lumped storage matrix
4	46-50	IUPSTR	= 0 if upstream weighting of relative permeability is not to be performed = 1 if upstream weighting of relative permeability is desired
5	1-5	NVREAD	= 0

Table A.4 Control Parameter Values Used by VAM3DF in the Transport Simulations

GROUP	COLUMN	VARIABLE	SET VALUE
3	1-5	IMODL	=0
4	6-10	INEWT	=0
	11-15	NITMAX	=1
	16-20	IRESOL	=0
	21-25	ILUMP	=0
	26-35	HTOL	=0
5	26-30	NVPRNI	=0

000240